University of Copenhagen
Faculty of Science
The PhD School of Science
Niels Bohr Institute
Membrane Biophysics Group
Denmark

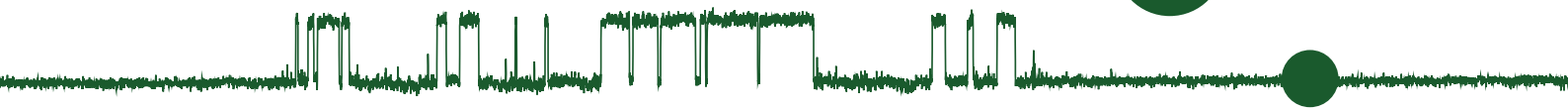

Electrical aspects of lipid membranes

PhD Thesis

Submitted
1 May 2011

Author
Andreas Blicher

Supervisor
Thomas Heimburg

Abstract

This thesis contains four studies of the electrical aspects of lipid membranes.

In the first study we present data of ion currents through planar lipid bilayers. We demonstrate that the conduction takes place via quantised events that under certain conditions exhibit a strong dependence on the applied electric potential. It is further demonstrated that both the life time of such events and the waiting time between them show a non-exponential distribution, which implies time-dependent transition rates between the open and closed states. Two independent measures suggest that the conductance steps in pure lipid bilayers are due to water-filled pores with a radius of up to few nanometers. Additionally, a number of other phenomenological findings are presented, and from these studies we conclude that the spontaneous lipid pores can exhibit the same characteristic gating behaviours as protein ion channels.

The second study investigate the influence of radio-frequency electromagnetic fields (RF EMF) from mobile phones on the spontaneous lipid pores. The study was complicated by the interference of the EMF with the experimental setup, but the data indicates that the influence of the mobile phone EMF on the membranes is small at normal levels.

In the third study we model how the head group tilt depends on the lipid state. It was found that the head groups become more parallel with the membrane surface in the dense gel phase. This, in turn, allows us to estimate how strongly a bilayer will react to a transmembrane electric potential under the assumption of a strong coupling between head group orientation and the phase state of the lipid. Even though the change in average tilt is slight ($\langle\theta\rangle_{gel} = 68.7^\circ$ versus $\langle\theta\rangle_{fluid} = 64.1^\circ$), this is enough to see a significant change in melting behaviour even at moderate voltages.

The final study deals with the analysis of the spontaneous action potentials from the motor nerve of the Australian red claw crayfish. It was found that the spontaneous action potentials are all of identical physical width, independent of the temperature and which neuron is firing. It was consistently found that the voltage amplitude of an action potential is strongly correlated with its propagation speed, and that the propagation speed goes down with decreasing temperature. Finally, we present data on the minimum-distance doublet and triplet pulses that are often found in these neurons. All results are then compared to the predictions of the soliton model.

Dansk resumé

Denne afhandling indeholder fire studier af membraners elektriske egenskaber.

I det første studie præsenterer vi ionstrømme gennem plane lipid dobbeltlag. Vi demonstrerer at dette sker i kvantiserede trin, der under visse omstændigheder kan udvise en stærk afhængighed af det påtrykte elektriske felt. Vi demonstrerer ydermere, at både varigheden af sådanne begivenheder og tiden imellem dem udviser en ikke-eksponentiel sandsyndlighedsfordeling. Dette indikerer at overgangsraten mellem åben og lukket tilstand er tidsafhængig. To uafhængige mål viser at de kvantiserede trin stammer fra vandfyldte pore i lipid dobbeltlaget. Et antal yderligere fænomenologiske observationer præsenteres, og fra disse studier konkluderer vi, at de spontane lipidpore kan udvise alle de samme karakteristiske egenskaber som protein ionkanaler.

I det andet studie undersøger vi hvordan elektromagnetisk stråling fra mobiltelefoner påvirker den spontane dannelse af lipidpore. Studiet blev vanskeliggjort af elektronisk interferens med måleudstyret, men vor data indikerer at påvirkningen af den elektromagnetiske stråling på membraner er lille ved normale strålings-niveauer.

I det tredje studie modellerede vi hvordan orienteringen af lipidernes hovedgrupper afhænger af lipidernes fasetilstand eller areal. Det blev fundet at hovedgrupperne bliver mere parallelle med membranens overflade i den kompakte gel-fase. Dette gjorde det muligt at estimere hvor stærkt membranen vil blive påvirket af et transmembrant elektrisk felt, under antagelsen af en stærk kobling mellem hovedgruppens orientering og lipidens fasetilstand. Selvom ændringen i orientering var begrænset (hhv. $\langle\theta\rangle_{gel} = 68.7°$ og $\langle\theta\rangle_{fluid} = 64.1°$), så er dette tilstrækkeligt til at se en betragtelig ændring i membranens smelteadfærd, selv ved moderate spændinger.

Det sidste studie omhandlede analyse af spontane aktionspotentialer i nerve fra krebs. Det blev fundet at de spontane aktionspotentialer alle har identisk fysisk bredde, uafhængigt af temperatur og hvilken neuron de stammede fra. Det blev konsekvent fundet at spændingsamplituden af aktionspotentialerne korrelerer stærkt med deres udbredelseshastighed, og at hastigheden falder med faldende temperatur. Til slut præsenterer vi data af minimumsafstand doublet og triplet pulser, som ofte kan observeres i denne slags neuroner. Alle resultaterne bliver derefter sammenlignet med solitonmodellens forudsigelser.

Contents

Preface

> *We analyze and interpret experimental data within the framework of paradigms. These paradigms give us the tools to understand the world. But when the paradigms do not match the world, then the paradigms prevent us from properly understanding the data. The assumptions of these paradigms are often so deep, and so accepted by mutual consent and repeated use, that we fail to see them.*
>
> – Liebovitch et al. (2001) paraphrasing T. S. Kuhn

The present thesis is a study of biological membranes, with a strong emphasis on the thermodynamics of these systems. One question that has received surprisingly little attention from the biomembrane community, is how the fundamental properties of the lipid membranes are influence by the strong, electric forces that are omnipresent in biology. This is most obvious in the context of nerves, where we find transient, but large, changes in the membrane potential – a fact that has formed the basis of the famous Hodgkin-Huxley model of action potential propagation. However, this model exclusively focussed on how this electric field interacted with proteins embedded in nerve membranes. Following its success, an entire field known as electrophysiology has sprung up, yet little attention is paid to the interaction of the electric field with the lipid membranes themselves.

The main project of this work was an experimental study of the various aspects of spontaneous pore formation in lipid membranes. This phenomenon has led to heated debates in the past (and present), due to its close resemblance to the signature evidence for protein ion channels. Hopefully, the present work will help shed some light on this topic.

Next, three related studies are presented. The first one was a spin-off from the main project, dealing with the influence of mobile phone radiation on the properties of cell membranes. My involvement with this project began after my supervisor met Dr. Salford of Lund University – a neurosurgeon who has studied the effects of electromagnetic fields

on the mammalian brains since 1988. Yet another topic that is rife with controversies, but holds great interest to many.

The third chapter is entirely uncontroversial, being a theoretical study of various aspects of the lipid membranes by use of computer simulations. Its purpose is to provide a bit more substance to some of the concepts and statements made in the theory sections in the first (main) chapter.

The fourth and final chapter deals with pulse propagation in nerves. In 2005 an alternative model was proposed – the soliton model – which was based on the thermodynamics of the system as a whole, and not on the specific properties of protein ion channels imbedded in the nerve membrane. I therefore found it an interesting question how the state of the membrane itself is affected by the action potential, since this had not been properly addressed in the soliton model. Also, at the time I started on my project no experiments had been performed on real, live nerves, with the intent to investigate the various aspects of the nervous impulse in the context of the soliton model. Everything before had been gathered from the literature, by different people, on different animals, using different methods. Consequently, I found it worthwhile to contribute to a new series of electrophysiological experiments performed in our laboratory, which were centred on investigating the various predictions of the soliton model in a systematic manner.

My interest in all of these topics was initially piqued by a number of findings that questioned some of the conventional wisdom in various fields. The thing with conventional wisdom, though, is that it is often more conventional than wise.

Acknowledgements

First I would like to thank all of the people who are not mentioned below – you know who you are, and you deserve my deepest gratitude.

Second, I want to thank my supervisor, Thomas Heimburg, for opening my eyes to the wonderful world of fluctuations and thermodynamics. I also wish to thank the other members of the NBI Membrane Biophysics Group for company in the lab, and in particular Katrine Rude Laub for helping developing the tip-dipping method and Rolf Justesen Pedersen for killing crayfish in the name of science. I would also like to thank Andrew D. Jackson for enthusiastic conversations about the various aspects of the soliton model.

Lastly, I would like to show my appreciation for the people of the BioComplexity Group at the Niels Bohr Institute. They have helped me hone my table football skills and made my long days at the institute much more enjoyable.

Publications

During my time as a Ph.D. student, the two following articles were written and published. While they are based on work performed as part of my master's thesis, they are closely related to the topics of this thesis and have therefore been included in the Appendix.

- **A. Blicher, K. Wodzinska, M. Fidorra, M. Winterhalter and T. Heimburg:** The temperature dependence of lipid membrane permeability, its quantized nature, and the influence of anesthetics. *Biophysical Journal, 2009, volume 96, pp. 4581–4591.*

- **K. Wodzinska, A. Blicher and T. Heimburg:** The thermodynamics of lipid ion channel formation in the absence and presence of anesthetics. BLM experiments and simulations. *Soft Matter, 2009, volume 5, 3319–3330.*

A note on figures

All of the figures in this thesis were made using

- IGOR Pro 6 (www.wavemetrics.com)
- Adobe Create Suite 5 (www.adobe.com)
- CorelDRAW X3 (www.corel.com)
- PyMOL (www.pymol.org)
- POVray (www.povray.org)

Unless explicitly noted otherwise, all figures were made by Andreas Blicher. Some figures have been adapted from other sources, meaning that the data was extracted from the original figure and then replotted.

Pore formation in membranes

1

1.1 Introduction

Lipid bilayers are found everywhere in the living world, with plasma membranes forming a 5nm thick skin around every eukaryotic and prokaryotic cell. Organelles and other intracellular structures such as the endoplasmic reticulum, the nucleus of eukaryotic cells, mitochondria, and the chloroplasts of green plant cells are all surrounded by lipid membranes, as are several animal and plant viruses.

Cell membranes are primarily constructed from lipids and proteins, and are generally arranged in topologically closed surfaces which physically separate the intracellular components from the extracellular environment. At the most fundamental level they function as selective barriers, which allow living cells to maintain an intracellular composition that is different from that of the extracellular solution. The barrier function is provided by the hydrophobic core of the lipid bilayer which has a very low dielectric constant compared to water (a factor of ~ 40). This results in a prohibitively large transfer energy for moving ions from the aqueous solution into the bilayer core (Paula et al. (1998)). Thus, it is possible to maintain different ion concentrations on the intracellular and extracellular sides of the membrane.

However, the plasma membranes of cells are not perfect insulators, as they contain channels and defects which make them permeable to certain ions, e.g. potassium. Thus, a membrane can possess a net voltage across the membrane, the so-called transmembrane potential. For neurons, typical values of the membrane resting potential is in the range of -70 to -80mV.[1] Changes in the membrane permeability, e.g. by the opening or closing of ion channels, will result in a departure from the resting potential, called a *depolarisation* if the voltage rises, or a *hyperpolarisation* if the voltage becomes more negative.

The membrane potential is considered to have two basic functions: Firstly, it allows a cell to function as a battery, providing energy to a variety of "molecular devices" embedded in the membrane. Secondly, in electrically excitable cells such as neurons, it is believed to transmit signals between different parts of the cell (Alberts et al. (2008)).

1.1.1 Motivation

The original motivation for this thesis came from a desire to get a better understanding of how electric fields interact with the lipid membranes themselves. The magnitude of the naturally occurring transmembrane electric fields are often in the range of 10 MV/m or more. To put this into perspective, this is roughly an order of magnitude larger than what is required to cause the dielectric breakdown of air. Obviously, such strong forces must have an influence on the properties of the cell membranes, yet the nature and extent of this has received surprisingly little attention by the biomembrane community.

In particular, even though the entire field of electrophysiology revolves around studying the electrical properties of biological cells and tissues, the focus seems to be almost exclusively on the function of the proteins that are embedded in the membranes, and not on the properties of the lipids themselves nor the system as a whole.

[1] Conventionally, the membrane potential is defined as the potential difference between the interior and exterior of the cell, i.e. $V_m \equiv V_{int} - V_{ext}$.

1.2 Biological membranes

Ever since Overton (1899) concluded that cells must be surrounded by a "fatty oil", there have been speculations on the structure and properties of the cell membranes. The first evidence of a bilayer structure was obtained by Gorter and Grendel (1925), who predicted and demonstrated that the lipid membrane was indeed a bilayer by comparing the surface area of different animal (and human) erythrocytes to the "surface occupied by all of the lipoids of the chromocytes" and found that they differed by a factor 2.

The first, commonly accepted, membrane model came ten years later. It was proposed by Danielli and Davson (1935), who suggested that cells must be surrounded by "lipoidal material" that was sandwiched in between two layers of proteins. The membrane itself was considered to be homogeneous and it could be either liquid or solid.

This model persisted for several decades, undergoing only some minor revisions with the introduction of the electron microscope studies, where Robertson (1957) observed a characteristic trilaminar appearance consisting of two darker outer lines and a lighter inner region. The interpretation was that all cell membranes must have a common

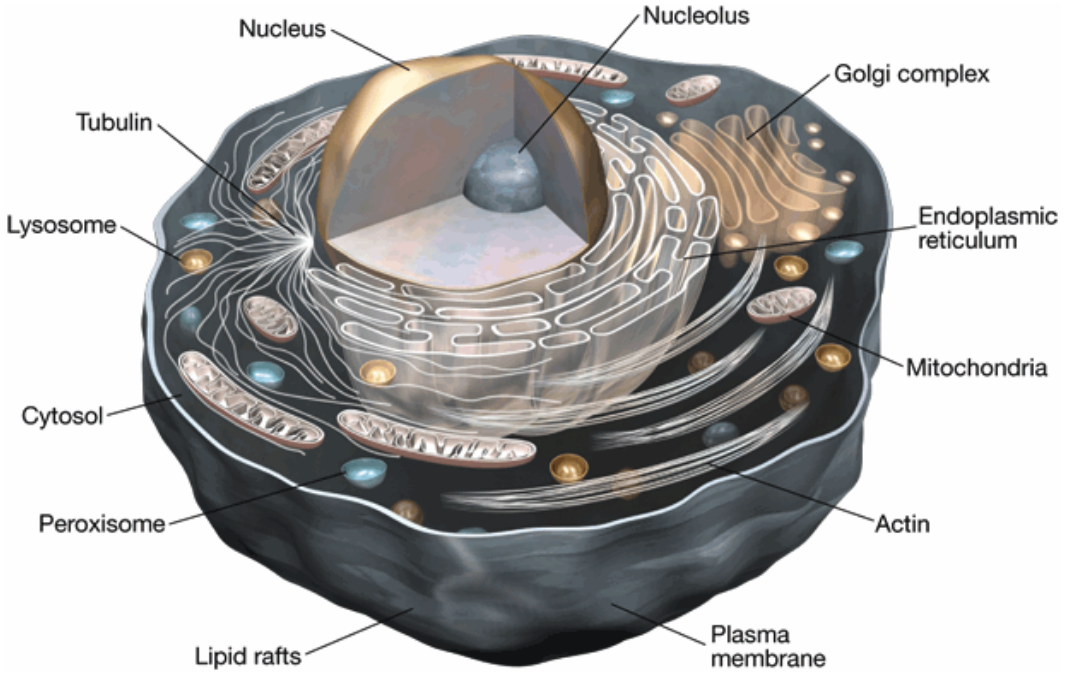

Fig. 1.1: Illustration of an idealised animal cell. The plasma membrane is a thin phospholipid bilayer that acts a selective barrier between the inner and outer part of the cell. Inside the cell itself, membranes also appear in different organelles like the endoplasmic reticulum, the Golgi complex and the mitochondria. The endoplasmic reticulum is involved in the synthesis of e.g. lipids, steroids and proteins. The Golgi complex is a network of flat membranous sacs that produce, change and store proteins, while the mitochondria are involved in cellular respiration and the production of ATP from nutrients. The picture was taken from www.probes.invitrogen.com.

structure (the "unit membrane"), where the darker lines were believed to be protein layers and the light region the lipid bilayer.

This model was eventually refined by Singer and Nicolson (1972), who proposed a fluid mosaic model for the gross organisation and structure of the proteins and lipids of biological membranes. In their model the lipids are arranged in the form of a bilayer, in which the proteins are embedded and are free to diffuse laterally (see Fig. 1.2).

Since its proposal this model has been subjected to further refinement to take into account that lipids and proteins may distribute inhomogeneously (Mouritsen and Bloom (1984); Jacobson et al. (1995)), and that domains rich in sphingolipids and cholesterol (so-called "rafts") may form in the membrane. This lateral heterogeneity has a strong influence on diffusion and directed transport in the membrane as well as signalling pathways (Simons and Ikonen (1997)).

The lipid and protein composition of the various membranes shows a large variation

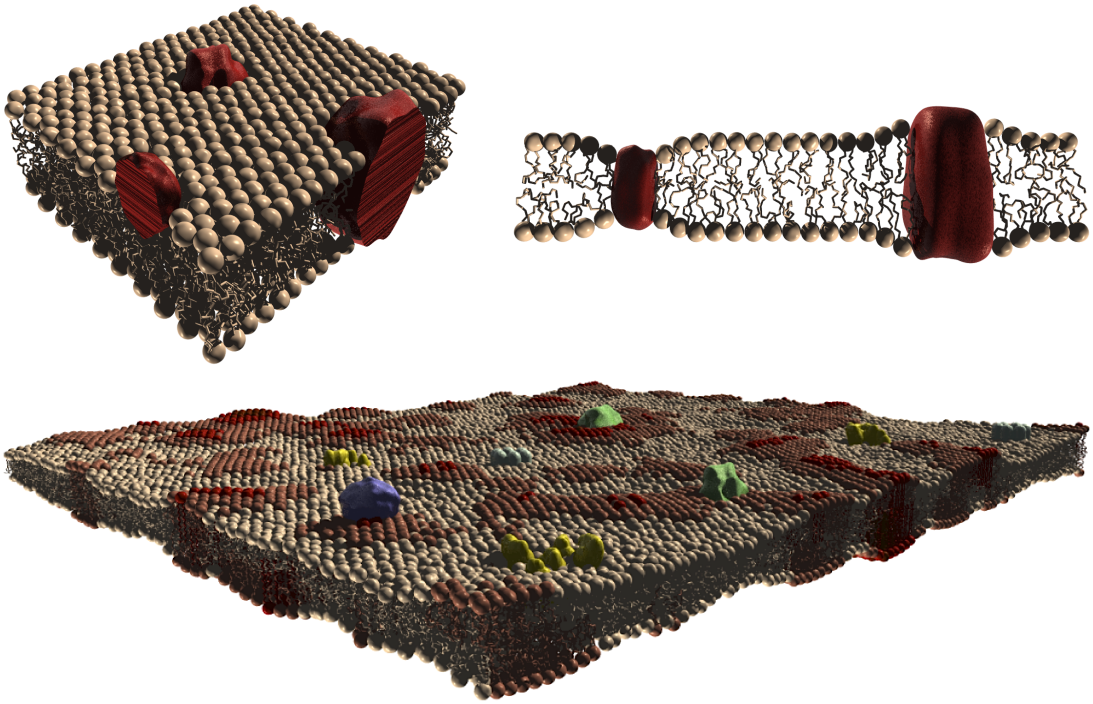

FIG. 1.2: Models for cell membranes. *Left:* The fluid mosaic model of Singer and Nicolson (1972). The phospholipids are arranged in a discontinuous bilayer with the polar head regions being exposed to the aqueous phases while the hydrocarbon tails are sequestered away. The proteins are partially or fully embedded in the fluid membrane and are largely randomly distributed, though they may locally form aggregates. *Right:* The mattress model of Mouritsen and Bloom (1984). Transmembrane proteins or polypeptides are located in an environment that is primarily determined by the mismatch in the hydrophobic regions of the lipids and the amphiphilic molecules. *Bottom:* Modern view of the membrane, where the system is a highly heterogenous and dynamic.

– in particular, the amount of unsaturated fatty acids as well the amount of charged lipids can vary substantially between different membranes (Heimburg (2007)). The reason behind this diversity in membrane composition still remains unresolved (Heimburg (2007)).

1.2.1 Fatty acids and phospholipids

Fatty acids are carboxylic acids of the form RCOOH, where the R represents a long hydrocarbon chain. They are usually not found in their free state in cells, but are instead components of covalently bonded molecules, such as phospholipids or triglycerides where two or three fatty acids are linked to a glycerol backbone. In the case of the phospholipids, the remaining -OH group in the glycerol is replaced by a phosphate group -PO_4 which, in turn, is linked to another group that is referred to as the polar head group.

Like all lipids in biological membranes, phospholipids are amphiphilic in nature (i.e. they have both a polar and a non-polar region). The length of the non-polar hydrocarbon chains lies in the range from 12 to 24 carbons with the typical value being 16 or 18 (Eisenberg and McLaughlin (1976); Heimburg (2007)).

The polar head groups of phospholipids may be chosen from a variety of organic compounds, such as choline, ethanolamine, serine and glycerol. Both serine and glycerol phospholipids have negative charge due to the phosphate group, while choline and ethanolamine are zwitterionic and hence have no net charge.

The naming convention for a phospholipid reflects, in part, its fatty acid composition. For example, a phospholipid containing two palmitic acids (16 carbons each) and a choline group is called dipalmitoyl phosphatidylcholine or DPPC for short. Common abbreviations include:

- phosphatidylcholine: PC
- phosphatidylethanolamine: PE
- phosphatidylserine: PS
- phosphatidylglycerol: PG

In many membranes the fraction of charged lipids is around 10–20%, though it can be as high as 40%, as is the case for mitochondria (Heimburg (2007)). This will of course have an influence on the electrostatic potential of the membranes.

While the phospholipids are major component of cellular membranes, there are other kinds of lipids present, such as glycolipids and cholesterol. Cholesterol is a member of the steroid family and is universally present in the plasma membranes of eukaryotic cells, in contrast to prokaryotic cells where it is universally absent (Mouritsen and Zuckermann (2004)). As an example, in erythrocytes the cholesterol content may be 20% or even higher (Parmahamsa et al. (2004); Heimburg (2007)).

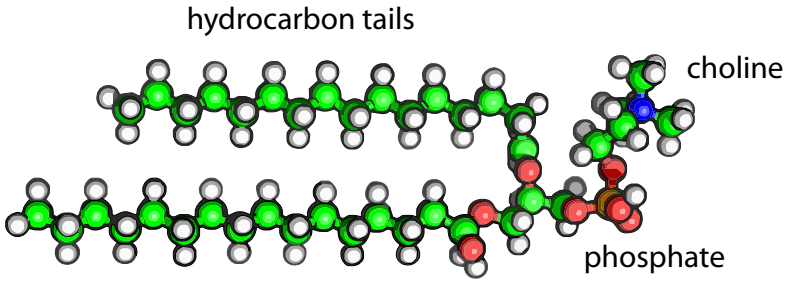

FIG. 1.3: Schematic drawing of 1,2-Dipalmitoyl-*sn*-Glycero-3-Phosphocholine (DPPC).

1.2.2 Membrane adaptation

When bacteria are grown under different environmental conditions (different temperature, pressure, salinity, pH), they display a different lipid composition (Hazel and Williams (1990); Heimburg (2007)). They can regulate the composition of their membranes by either changing the number of double bonds in the hydrocarbon chains, or by changing the chain lengths. Desaturases – i.e. enzymes that can introduce carbon-carbon double bonds – are normally synthesised by expression of the relevant genes when the temperature is lowered. At higher temperatures, a protein binds to the enzymes and thereby inactivates them (Jensen and Prentø (1994)). This ability to regulate the composition of the membranes to cope with the effects of different environmental conditions is known as homeoviscous adaptation (Marr and Ingraham (1962); Sinensky (1974)), and numerous examples of this phenomenon have been found (see MacDonald (1988) and the references therein).

The cells of eukaryotic organisms also make use of the regulation of the number of double bonds in the hydrocarbon chains as well as adjusting the concentration of cholesterol to control the state of the membranes. For instance, the number of double bonds and amount of cholesterol will increase with decreasing temperature for poikilothermic animals[2]. Similarly, it has been found that the cell membranes of deep sea fish also show homeoviscous adaptation to pressure[3] (MacDonald (1988); Hazel and Williams (1990)).

Another example can be found in trouts that have been raised at different temperatures. Here it has been found that the lipid composition of their livers changes with temperature. Likewise, it has been found that the brain synaptic membranes of teleost fish display different lipid compositions depending on whether their habitat is arctic, temperate, or tropical (Logue et al. (2000)). Arctic animals, such as seagulls and reindeer, also have high amounts of unsaturated lipids in the membranes near the feet/hooves, whereas membranes near the thigh have relatively few double bonds (Fox (1972); MacDonald (1988)). In fact, this adaptation can even be found in humans, where

[2]I.e. vertebrate animals, such as fish and reptiles, where the body temperature varies with the temperature of its surroundings.

[3]For lipid bilayers the transition temperature increases with pressure by 0.1–0.4°C/MPa, depending on the exact composition. For most phospholipids, this value lies in the vicinity of ≈ 0.23°C/MPa (Hazel and Williams (1990)).

it is a well-established fact that chronic alcoholics have higher amounts of saturated lipids and cholesterol in their red blood cells that compensate for the changes induced by the alcohol (Benedetti et al. (1987); Parmahamsa et al. (2004)).

A different – and still poorly understood – change in the membranes happens during anaesthesia. Anaesthesia occurs when the membranes of the nerve cells absorb certain hydrophobic compounds, which changes their state as a result. This change inhibits the cells' ability to receive and process signals. A couple of thermodynamically based explanations have been proposed. One theory is that the anaesthetic alter the transverse pressure profile of the membrane, thereby influencing the conformations and function of the embedded proteins (Cantor (1997a,b)). Another explanation has been proposed by Heimburg and Jackson (2005), who argue that the nerve signals are in fact a propagating density pulses (solitons). The effect of the anaesthetic would then solely be due to the induced melting point depression which alters the amount of free energy needed to generate a pulse. It thus predicts that anaesthesia can be reversed by adjusting e.g. the hydrostatic pressure, pH, or pCa, so that the free energy of the membrane returns to its original value (Heimburg and Jackson (2007a,b); Seeger et al. (2007)).

In conclusion, the composition and thermodynamic state of the lipid membranes must play an important role for biological function, as it would be rather easy to lower the melting temperature significantly by introducing unsaturated lipids or cholesterol, if only soft and fluid membranes were required.

1.3 An incomprehensive summary of previous permeability studies

Present theories of ion channel formation (whether in artificial bilayers or in cell membranes) favour the notion of ion channels being formed by specific proteins that are embedded in the membrane and provide pathways for fast and controlled flow of selected ions along their electrochemical gradients.

This activity is used to explain action potentials in nerves, muscles and other excitable cells, and is thought to form the basis of all movement, sensation and thought processes in living beings.

While it is well-known that certain proteins and peptides can create selective ion channels and thereby regulate the permeability of the membrane, it seems less well-known that pores can transiently form in protein-free membranes due to thermal fluctuations. This phenomenon can make permeation rates of water, ions, and even small molecules much higher than expected from the Arrhenius law, especially in states where there are strong lateral density fluctuations (Papahadjopoulos et al. (1973); Wu and McConnell (1973); Georgallas et al. (1987); Corvera et al. (1992); Jansen and Blume (1995); Sabra et al. (1996); Blicher et al. (2009)). An interesting feature of these spontaneously formed pores is that they exhibit features normally considered to be indicative of protein channels including stepwise conductance changes, flickering, ion selectivity, and inactivation (Woodbury (1989)).

While physiological studies provide detailed information about the functional properties of ion channels, there has been a notorious lack of structural knowledge about them. Even the famous potassium channel from the Hodgkin-Huxley theory was only crystallised in 1998 by Roderick MacKinnon (Doyle et al. (1998)) (who was awarded the Nobel Prize already in 2003 for this feat), even though the Hodgkin-Huxley theory was proposed almost 50 years earlier (Hodgkin and Huxley (1952)).

Prior to the publication of the first patch clamp studies of quantised currents through proteins, Yafuso et al. (1974) reported spontaneous conductance changes and multilevel conductance states in pure black lipid membranes made from oxidised cholesterol. While the exotic nature of the lipids used made it difficult to draw conclusions about biological membranes, this early experiment provided a proof-of-principle of that quantised conduction through membranes does not require the presence of specialised proteins or peptides.

Two years later Neher and Sakmann (1976) performed the first patch clamp experiments (which also won them the Nobel Prize in 1991). This was the first time single-channel currents were recorded in biological membranes. Since then an enormous number of patch clamp studies have been performed, so for a thorough discussion of this field see Hille (2001).

Despite the vital nature and omnipresence of lipid membranes in patch clamp experiments, most studies have for a long time tended to ignore them and simply consider them as being homogeneous and impermeable barriers without any noteworthy properties (Tien and Ottova-Leitmannova (2003)).

The fact that the membrane permeability increases strongly under certain conditions is unfortunately rarely considered when interpreting measurements from protein-channels. For instance, the simple act of applying suction or a transmembrane voltage in patch clamp experiments can induce a change in the state of the membrane, resulting in quantised lipid events that are disturbingly similar to the protein channel activity (Kaufmann et al. (1989b)).

Furthermore, even when some protein-channels are found to be influenced by the lipid membrane (Schmidt et al. (2006)), it is usually only specific interaction with proteins that is considered, and rarely the thermodynamics of the system as a whole. Consequently, the studies of pure lipid membrane systems are few and far between, though their importance is starting to dawn on the scientific community (Hilgemann (2003)).

However, in an early paper by Antonov et al. (1980) the electrical conductance of protein-free membranes made from synthetic DSPC was examined. It was discovered that at the fluid-gel transition temperature long-lived, quantised current fluctuations appeared. In this article they tentatively proposed that such channels could in fact conduct the known transmembrane ionic currents, without the direct involvement of protein-channels.

Five years later Antonov et al. (1985) (and also more recently, such as in Antonov et al. (2005)) followed up on their findings. The capacitive and ionic currents through bilayer lipid membranes formed from dipalmitoylphosphatidic acid were studied, and it was found that by causing a phase transition by introducing Ca^{2+} ions, they could observe single ion channel events in the bilayer lipid membranes.

Two years before that, Kaufmann and Silman (1983b) published a comprehensive study on how ion channels through lipid bilayer membranes could be induced by changes in the pH of the system. Specifically, they found that there was a certain threshold for the proton concentration at which otherwise stable lipid bilayers of very low conductivity would show resolved ion channels. Further acidification would reduce the permeability of the membrane to a much lower value, indicating that this was related to a transition in the membrane. The later monograph by Kaufmann et al. (1989b) also contained extensive studies of how ion channel fluctuations in pure lipid bilayer membranes could be controlled in a deterministic fashion by changing any of the intensive thermodynamic variables, such as voltage, surface pressure, and temperature. This led them to conclude that the reversible fluctuations in the membrane are responsible for the opening and closing of aqueous defects in the lipid bilayer.

Other groups have observed similar properties of protein-free phospholipid membranes. Boheim et al. (1980) and later on Yoshikawa et al. (1988); Blicher et al. (2009); Wunderlich et al. (2009) all verified that fluctuations and stepwise changes in the electrical current across a synthetic membrane could be induced by having the system near its phase transition temperature or when pure lipid vesicles are fused with a planar lipid bilayer (Woodbury (1989)).

More recently it has also been found that the membrane phospholipid composition and state affects the function (conductivity, opening and closing kinetics, midpoints of activation, etc.) of certain protein-channels (Turnheim et al. (1999); Schmidt et al.

(2006); Seeger et al. (2010a)). Furthermore, the various channel activity parameters even show a pronounced peak in the membrane's transition regime in some cases (Cannon et al. (2003); Seeger et al. (2010a)).

In summary, it has been found that

- The permeability and conductance of lipid membranes depends strongly on the temperature, with a pronounced peak at the phase transition temperature. (Papahadjopoulos et al. (1973); Wu and McConnell (1973); Georgallas et al. (1987); Corvera et al. (1992); Jansen and Blume (1995); Sabra et al. (1996); Blicher et al. (2009); Wunderlich et al. (2009)).

- Ion channels appear in any lipid bilayer even in the absence of any further membrane component, and they reversibly open and close. These fluctuating channels are thought to be due to structural changes (transient pores) in the lipid bilayer during the melting-transition of the phospholipids (Yafuso et al. (1974); Antonov et al. (1980); Boheim et al. (1980); Antonov et al. (1985); Yoshikawa et al. (1988); Woodbury (1989); Kaufmann et al. (1989b); Antonov et al. (2005)).

- The spontaneously formed pores exhibit stepwise conductance changes, flickering, ion selectivity, and inactivation (Woodbury (1989); Antonov et al. (2005); Wodzinska et al. (2009)).

- The probability of an event can be controlled by all of lipid variables, such as voltage, surface pressure, pH, pCa, and temperature (Antonov et al. (1980); Boheim et al. (1980); Kaufmann and Silman (1983a,b); Antonov et al. (1985); Kaufmann et al. (1989b); Antonov et al. (2005)).

- The typical time scales of ion channel opening and closing in both transient pores as well as in protein-channels are similar to the characteristic relaxation time of the membrane (Seeger et al. (2007, 2010a)).

- The function of certain protein-channels depends strongly on the composition and state of the lipid environment (Turnheim et al. (1999); Cannon et al. (2003); Schmidt et al. (2006); Lee (2006); Seeger et al. (2010a)).

1.4 The thermodynamics of membranes

Lipid membranes are fascinating systems to study in that – in addition to their obvious biological relevance – they have interesting thermodynamic properties of their own. These properties can be studied in detail by using model systems prepared from pure (synthetic) lipids, and has been done so extensively for the last four decades (Hinz and Sturtevant (1972); Heimburg (2007)). This section will introduce the basic theory of phase transitions in the context of lipid bilayers and the significance of transitions for biological membranes.

1.4.1 Phase transitions

Phase transitions occur when there is a singularity in a system's free energy or one of its derivatives. This can normally be observed as a sharp change in one or more of the properties of the system. There are many examples of this, such as the transition from solid to liquid, from paramagnet to ferromagnet, or from normal conductivity to superconductivity.

Another example is, of course, amphiphilic molecules in solution, which can exhibit fairly exotic behaviour. As previously mentioned, these molecules have a hydrophilic polar head group and two hydrophobic hydrocarbon tails. This means that in an aqueous system the polar heads of the lipids will be orientated towards the polar, aqueous environment, while the hydrophobic tails seek to minimise their contact with the water as shown in Fig. 1.4. If there is a surface they will migrate there and as a result lower the surface tension – hence their use as soaps.

The phase diagrams of lipid solutions – and surfactant molecules in general – are mainly determined by the concentration of the solute, though pH, salinity, pressure and temperature can also have a strong influence, as in the case of DMPG, which displays

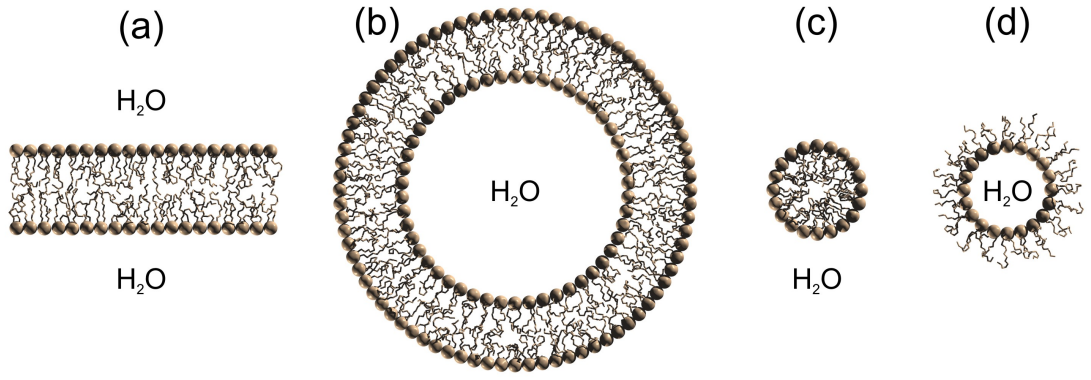

FIG. 1.4: Self-assembly of lipids in water gives different structure, depending on the lipid concentration, the molecular structure, etc. *(a)* Bilayer. *(b)* Unilamellar vesicle. *(c)* Micelle. *(d)* Inverse micelle.

quite complex (and still not fully understood) phase behaviour (Heimburg and Biltonen (1994)). In fact, lipids display a great diversity of structure over a very narrow range of chemical and physical parameters that are close to physiological conditions – more so than any other class of biological molecules (Hazel and Williams (1990)).

When the concentration is increased micelles form. These are groups of lipids arranged in a spherical or cylindrical configuration, so that the polar heads shield the hydrocarbon tails from the aqueous environment. If the concentration is increased even further, the system can undergo a transition to other geometries, such as a state where micelles are ordered in a cubic or hexagonal array or a sponge phase where the intervening spaces are filled with water. Other transitions are also possible, where the internal configurations and lateral order of the lipids change. In the biomembrane literature one normally only distinguishes four difference phases:

- $\mathbf{S_o}$: Crystalline state where the lipids are ordered on a triangular lattice (solid), and with the chains 'all-trans' (ordered) and tilted. This phase is commonly called the solid-ordered phase, or alternatively the gel phase. Due to its low entropy, this phase is favoured at low temperatures.

- $\mathbf{L_o}$: In this phase all the lipid chains are ordered, while the lateral order of the lipids is random (liquid). This phase is commonly called the liquid-ordered phase, and is normally only observed in membranes containing sterols (Nielsen et al. (1999); Mouritsen and Zuckermann (2004)).

- $\mathbf{L_d}$: In this phase all the lipid chains are disordered and the lipids move freely within the bilayer like a two-dimensional liquid. Therefore, this phase is called the liquid-disordered phase, or simply the fluid phase. Due to its high entropy, this phase is favoured at high temperatures.

- $\mathbf{P}_{\beta'}$: This is the so-called 'ripple'-phase, where the system is partially solid and partially fluid, and has a periodic super structure with a length scale of 100–300Å. The occurrence of a ripple-phase is dependent on the lipid head group, chain length, hydration, etc., and it is easily abolished by addition of various biomolecules (Heimburg (2000)).

It has been shown that for very pure ($> 99.94\%$) single component membranes, the transition between the S_o and L_d phase closely approximates an isothermal first-order transition (Albon and Sturtevant (1978)). It should be noted though, that in general the transition is not a phase transition in the strictest, statistical mechanical, sense of the word, but rather at crossover transition. However, in this thesis I will use the term 'phase transition' for both types, as it is commonly seen in the literature.

The transitions between these phases occur at well-defined temperatures. The transition temperature depends on the molecular details of the lipids themselves, such as the chain length, chain saturation (number of carbon-carbon double bonds), head group size and charge, etc. (Nagle (1980)).

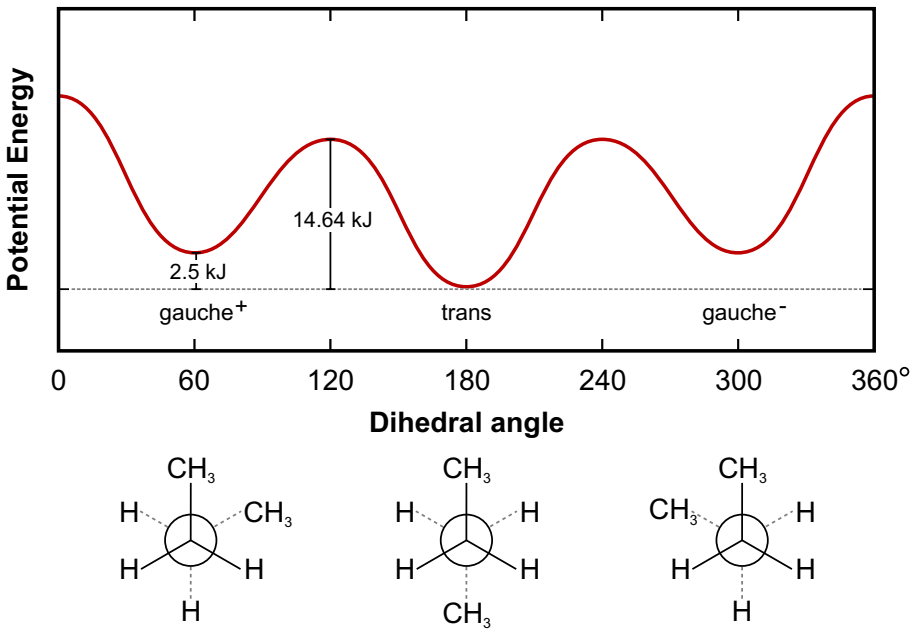

FIG. 1.5: Lipid chains may have various conformations. Different conformations can be generated by rotation around the C–C bonds in the chains ('trans-gauche' isomerisations). The configuration with the lowest energy is the 'all-trans' configuration, which has a characteristic zig-zag pattern as shown in Fig. 1.3. The conformations with 'gauche'-isomers display higher internal energy, but also have a much higher degeneracy. Thus the conformation of the chains will depend strongly on the temperature. Furthermore, the different lipid conformations will occupy different volumes and areas, so the lipid conformations will also depend on bulk and lateral pressure. Figure adapted from Gennis (1989).

Transitions in phospholipids

As described in Sec. 1.2.1 a phospholipid has two hydrocarbon chains. Each of the C–C bonds of the hydrocarbon chains allows for rotations to take place, showing three distinct energy minima at $\pm 120°$ angles as shown in Fig. 1.5, with the lowest one being the trans configuration. Thus, in ground state of the system both chains adopt an all-trans configuration with a minimal entropy (0 in fact). At high temperatures all the trans and the gauche states will be equally probable, resulting in a completely disordered (high entropy) state of the chains which will also tend to disrupt crystalline packing of the lipids.

If we assume that a lipid can only be found in one of two states – all-trans or disordered – the (chain) melting point, T_m, can be defined as the temperature at which the ground state and the excited states are equally likely (or equivalently, the Gibbs free

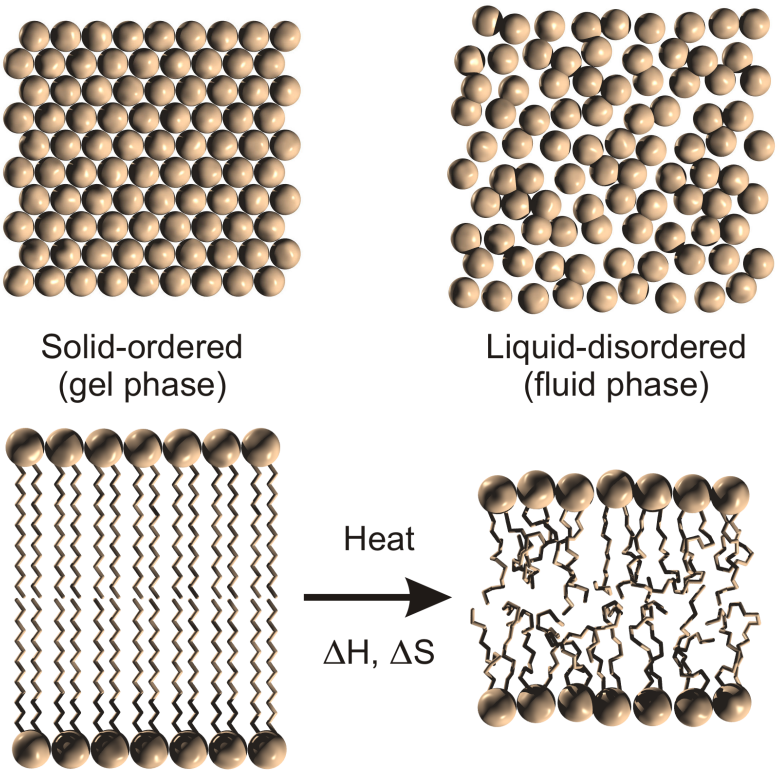

FIG. 1.6: Chain-melting transition of a phospholipid bilayer. When going from low to high temperature there is an increase in the enthalpy, ΔH, and the entropy, ΔS. The change in the chain configurations normally results in a loss of lateral order, causing the membrane area to increase by approximately 25% and the thickness to decrease by approximately −16% (Heimburg (1998)).

energy difference is zero):

$$\frac{P_{disordered}(T_m)}{P_{all-trans}(T_m)} = K(T_m) = e^{-\Delta G/k_B T_m} = 1 \tag{1.1}$$

$$\Rightarrow \quad \Delta G = \Delta H - T_m \Delta S = 0 \Rightarrow T_m = \frac{\Delta H}{\Delta S}, \tag{1.2}$$

where ΔH and ΔS are the enthalpy and entropy of melting, respectively.

In pure lipid membranes, this chain melting occurs at the temperature at which the lateral organisation of the lipids is lost. This is mainly due to the lipid molecules drastically changing shape when the chains get disordered.

Obviously, the entropy and enthalpy of the disordered state depends on the length of the hydrocarbon tails and as a result, so will the transition temperature, T_m. However, in general there are a number of other factors which can strongly influence its value. For instance, cations (divalent ions and lithium in particular) stabilise the solid-ordered

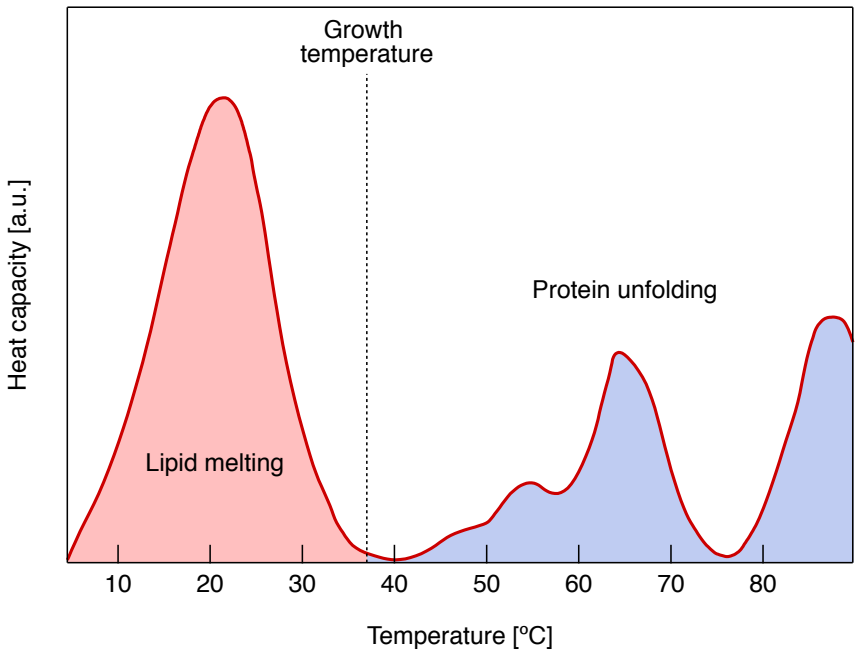

FIG. 1.7: The calorimetric profile of an intact native bacterial membrane (from *E. coli*). The peak at below growth temperature is the melting transition of the lipids, while the peaks at higher temperatures are due to protein unfolding transitions. The figure was adapted from Heimburg and Jackson (2007b).

state, causing a shift of the melting transition to higher temperatures (Sturtevant (1998); Binder and Zschornig (2002); Boeckmann et al. (2003)). The transition temperatures can also be altered by numerous of other factors such as addition of cholesterol, peptides, neurotransmitters or general anaesthetics (e.g. alcohols, chloroform, etc.) (van Osdol et al. (1993); Seeger et al. (2007)), binding of molecules to the surface, membrane hydration (Ulrich et al. (1994); Markova et al. (2000)), high membrane curvature (Gruenewald et al. (1979)), hydrostatic pressure, pH, etc. (Heimburg (2007)). Of particular interest for this thesis is the influence of a transmembrane electric field, where the exact nature of the influence is still not well-understood.

For most natural lipids the melting temperatures are in the biologically relevant temperature regime (−20°C to +60°C) (Tien and Ottova-Leitmannova (2003); Ivanova et al. (2003)), and in general biological membranes have a transition temperature approximately 15°C below the organism's temperature (Heimburg and Jackson (2005)), though the transition is rather broad (≈ 10–15°C).

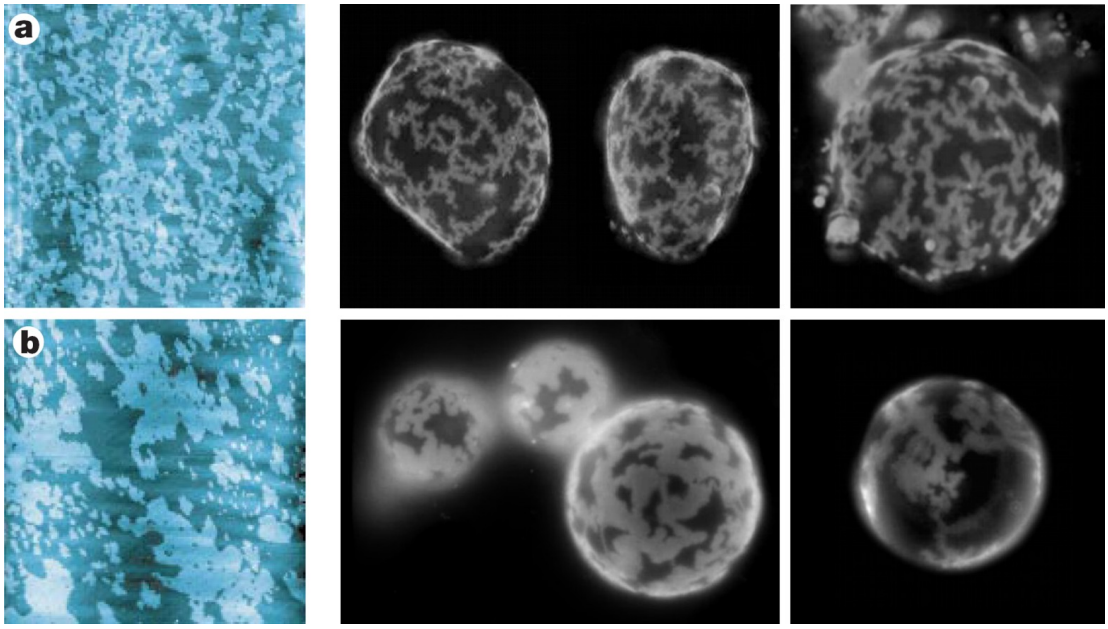

FIG. 1.8: *Left:* Lipid domains in phospholipid monolayers imaged by atomic force microscopy as a height-difference map. *(a)* Image of DMPC ($25 \times 25\mu m^2$) and *(b)* DPPC ($20 \times 20\mu m^2$) monolayers at their respective critical points. Image was taken from Nielsen et al. (2000). *Right:* Lipid domains in giant unilamellar vesicles. *Top:* DMPC/DPPC mixture at $T = 28°C$. *Bottom:* DLPC/Dipentadecanoylphosphocholine mixture at $T = 26°C$. Unpublished data from our group (courtesy of Christian Leirer, NBI, University of Copenhagen).

1.4.2 Membrane heterogeneity and domains

Originally, the lipid bilayer was assumed to form a fairly featureless and homogeneous two-dimensional structure (see Sec. 1.2). However, the existence of large domains near the transition temperature has now been verified numerous times, both experimentally as well as by computer simulation (Nielsen et al. (2000); Bagatolli et al. (2000); Bagatolli and Gratton (2001); Leidy et al. (2001); Bagatolli (2003); Baumgart et al. (2003); Keller et al. (2005); Hac et al. (2005); Marrink et al. (2005); Seeger et al. (2005); Risselada and Marrink (2008); Fidorra et al. (2009a); Seeger et al. (2009, 2010b)).

The temperature range where this occurs strongly depends on the cooperativity of the phase transition. Furthermore, the larger the cooperativity, the more compact the domains are at the melting point, as the system will seek to minimise the length of the energetically unfavourable domain boundaries. Only when the line tension is very high will the system be exclusively in the gel or fluid state. For biological membranes there is no macroscopic phase separation, but rather domains of various size and composition that are stabilised by the interplay between configurational entropy and interfacial free energy.

The appearance of such membrane heterogeneities will have a strong impact on the

biological function, as it can dramatically alter communication pathways and dynamics (Hac et al. (2005)). Moreover, because the free energy of gel and fluid lipids are similar at the domain interfaces, fluctuations in these regions are inevitably large. This makes the local properties of the interfaces significantly different, since many membrane properties are intimately linked to the lipid fluctuations (see Sec. 1.4.4). Consequently, the appearance of packing defects, pores, and geometric fluctuations will be strongly enhanced in these regions, which makes it interesting to understand the dynamics of the domains themselves.

Monte Carlo simulations (see Chapter 3) can provide information about the microscopic configurations of the system in thermodynamic equilibrium, provided that the characteristic length scales are much larger than the atomic level, but still smaller than the system size. For such systems, the statistics of the domain distributions can easily be calculated from these configurations.

1.4.3 Interleaflet coupling

As the name suggests, a lipid bilayer consists of two individual monolayers (or "leaflets") that physically oppose each other. Each monolayer possesses a distinct set of internal degrees of freedom. Even though the internal degrees of freedom in each monolayer can, in principle, behave differently, it is known that there exists some form of coupling between them. In fact, this interleaflet interaction must be strong, since one always observes a perfect mirroring of domains in each monolayer (within the resolution of the experiments), even in asymmetric lipid bilayers (Collins (2008)). This coupling requires that one treats the lipid bilayer as *one* entity of two coupled, two-dimensional monolayers, each of which has in-plane degrees of freedom defined by its state (Hansen et al. (1998)). In particular, this coupling will have a large influence on the cooperativity of the system, as it contributes significantly to the line tension of the phase boundaries (Putzel et al. (2010)).

The interleaflet coupling has also been proposed to explain the existence of the pre-transition, and how this is related to the main transition of the bilayer (Heimburg (2000)). It is, obviously, also one of the major complications when extrapolating information obtained from monolayer experiments (Langmuir-Blodgett) to bilayer systems.

In most theoretical studies of interleaflet couplings it is assumed that it happens primarily through the local bilayer curvatures and a local difference in the two individual in-plane densities or concentration fields characterising the thermodynamic state of the two monolayers. In those studies it is assumed that any *direct* molecular interaction is negligible to first approximation.

However, some argue that even when such interactions are weak, they can significantly influence the thermodynamic behaviour of the lipid bilayer (Georgallas et al. (1984); Zhang et al. (1992); Hansen et al. (1998)). Depending on the details of the model used, it has been estimated that the free energy of mismatch is in the range from 0.01–$0.5 k_b T/\mathrm{nm}^2$ (Georgallas et al. (1984); Collins (2008); Risselada and Marrink (2008); Putzel et al. (2010)). Therefore, the interleaflet mismatch of domains will at most be in the range of a few hundred square nanometers, which is much smaller than what can be

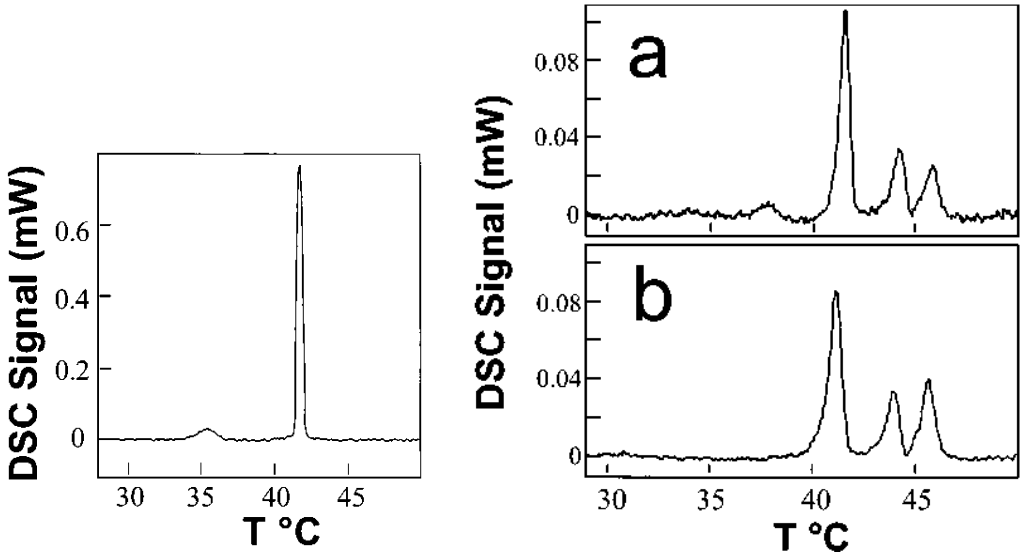

FIG. 1.9: *Left:* Heat capacity profile of multilamellar DPPC vesicles. *Right:* Heat capacity profile of supported DPPC bilayers, with **(a)** for an initial scan and **(b)** for an average of six subsequent scans. The leftmost peak is from residual vesicles in suspension and additional bilayers on top of the supported bilayers. The middle and rightmost peaks are from the distal and proximal leaflets respectively. Figure was taken from Yang and Appleyard (2000).

resolved by optical microscopy.

One limitation of many theoretical studies is that they are based on mean-field models, and thus make a number of simplifying assumptions and neglect e.g. conformational fluctuations (Hansen et al. (1998)). Fortunately, it is possible to directly measure the free energy of mismatch by fairly simple means. In an article by Yang and Appleyard (2000) the phase behaviour of mica-supported bilayers was studied by differential scanning calorimetry. It is well-known that the mica support strongly influences the proximal leaflet, causing it to undergo the melting transition at higher temperatures (Keller et al. (2005); Seeger et al. (2010b, 2009)). This stabilisation of the solid phase is believed to be due to incomplete hydration of the proximal leaflet, as well as steric interactions with the mica. As can be seen from Fig. 1.9, the melting transition peak shifts and splits into two peaks – one from the proximal leaflet and one from the distal leaflet. There are two important things to note about this data, namely that 1) the two peaks have almost identical areas (transition enthalpies), and 2) the peaks are well-separated, indicating that the two leaflets undergo the transition independently of each other.

The transition temperature of the distal leaflet is increased by $\Delta T = 1.1°\text{C}$, or 0.35%, compared to the unperturbed system, which means that the interaction energy of mismatch must be close to 0.35% of the total transition enthalpy. Using the usual transition enthalpy for DPPC of $\Delta H = 36.4\text{kJ/mol}$ (Mabrey and Sturtevant (1976)), this gives us a coupling energy of $\gamma = 127\text{J/mol} \approx 0.096 k_B T_m/\text{nm}^2$. Doing the same

calculation DiC15-PC[4], which was the other lipid system used in the article of Yang and Appleyard (2000), gives us another estimate for the coupling energy. For DiC15-PC the shift is $\Delta T = 1.5°\text{C}$ (i.e. 0.49%), $T_m = 33.9°\text{C}$, and $\Delta H = 25.7\text{kJ/mol}$ (interpolated from the data found in Mabrey and Sturtevant (1976)), which gives us a $\gamma = 124\text{J/mol} \approx 0.097 k_B T_m/\text{nm}^2$. This is in excellent agreement with both the first estimate and the value of $\gamma = 0.15 \pm 0.05 k_B T/\text{nm}^2$ obtained by Risselada and Marrink (2008) in their molecular dynamics study. Note that the only assumptions I have made in these calculations are 1) to assume that the distal leaflet is only influenced via the coupling to the proximal leaflet, and not by direct, long-range interaction with the mica support, and 2) that there is no overlap in the temperature range of the two leaflets' transition regimes. If this latter condition is not completely fulfilled, the real value of γ would be larger, since the amount of mismatched area is overestimated. In Sec. 3.3.3 we will demonstrate the significance of the interleaflet coupling by means of computer simulations.

Lastly, it should be kept in mind that the interleaflet coupling cannot be attributed to a single property such as configurational entropy or van der Waals interactions, but rather seems to arise from a complex interplay between many interactions of varying sign, but of similar magnitude (Putzel et al. (2010)). It is therefore highly non-trivial exactly how the coupling strength will be influenced by e.g. an applied electric field. Sadly, despite some recent insights, the study of interleaflet coupling has received little attention, and still lacks systematic understanding of the coupling mechanisms, coupling strengths, and biological implications (May (2009)).

1.4.4 Fluctuations and susceptibilities

The lipid bilayer fluctuates reversibly in equilibrium, and from these fluctuations a large number of properties of the system can be derived. For sufficiently small fluctuations, $\delta\xi_i$, their magnitudes can be quantified by Taylor expanding the entropy potential:

$$S = S_0 + \sum_i \left(\frac{\partial S}{\partial \xi_i}\right)_0 \delta\xi_i + \frac{1}{2}\sum_i\sum_j \left(\frac{\partial^2 S}{\partial \xi_i \partial \xi_j}\right)_0 \delta\xi_i \delta\xi_j + \ldots \tag{1.3}$$

$$\approx S_0 + \frac{1}{2}\sum_i\sum_j \left(\frac{\partial^2 S}{\partial \xi_i \partial \xi_j}\right)_0 \delta\xi_i \delta\xi_j, \tag{1.4}$$

where $\xi_i = \xi_{i0} + \delta\xi_i$ are the various extensive thermodynamic variable (e.g. volume, area, enthalpy, charge, etc.). The second equality follows from that in equilibrium the entropy is maximal with respect to all variables, i.e. $(\partial S/\partial \xi_i)_0 = 0$.

The strength of the fluctuations is then given by the second moment, i.e.

$$\langle \delta\xi_i \delta\xi_j \rangle = \int \delta\xi_i \delta\xi_j P(\delta\xi_i, \delta\xi_j)\, d\xi_1 d\xi_2 \ldots d\xi_n \tag{1.5}$$

[4] 1,2-dipentadecanoyl-*sn*-glycero-3-phosphocholine

where $\langle \cdot \rangle$ denotes the statistical mean for the probability distribution $P(\delta\xi_i, \delta\xi_j)$. These moments are therefore directly related to the curvature of the entropy potential:

$$\langle \delta\xi_i \delta\xi_j \rangle = -k_B \left(\frac{\partial^2 S}{\partial\xi_i \partial\xi_j} \right)_0^{-1} \tag{1.6}$$

which follows directly from of Eq. (1.4) and that

$$P(\delta\xi_i, \delta\xi_j) = P_0 \exp\left(\frac{S(\delta\xi_i, \delta\xi_j)}{k_B} \right) \tag{1.7}$$

where k_B is the Boltzmann constant. For the full and stringent derivation see e.g. Greene and Callen (1951).

From the first law of thermodynamics we know that

$$TdS = dE + pdV + \Pi dA + fdl + \ldots - \Psi dq + \ldots - \sum_i \mu_i dn_i \tag{1.8}$$

from which it follows directly that

$$T^{-1} = \left. \frac{\partial S}{\partial E} \right|_{V,A,\ldots} \tag{1.9}$$

$$p = T \left. \frac{\partial S}{\partial V} \right|_{E,A,\ldots} \tag{1.10}$$

$$\Pi = T \left. \frac{\partial S}{\partial A} \right|_{E,V,\ldots} \tag{1.11}$$

$$\ldots = \ldots \tag{1.12}$$

The susceptibilities (i.e. the derivative of an extensive variable with respect to an intensive variable) of the system is closely related to the strength of the fluctuations of the extensive variable. This can easily be seen by considering, e.g. the isothermal area compressibility, κ_T^A:

$$\kappa_T^A \equiv -\frac{1}{A}\left(\frac{\partial A}{\partial \Pi} \right)_T = -\frac{1}{A}\left(\frac{\partial \Pi}{\partial A} \right)_T^{-1} = -\frac{1}{A}\left(T\frac{\partial^2 S}{\partial A^2} \right)_T^{-1} = \frac{\langle \delta A^2 \rangle}{A\, k_B T} \tag{1.13}$$

where we used Eq. (1.11) in the second step, and Eq. (1.6) in the final step.

Similarly for the isobaric heat capacity, we find that

$$c_p \equiv \left(\frac{\partial H}{\partial T} \right)_p = -\left(T^2 \frac{\partial (1/T)}{\partial H} \right)_p^{-1} = -\frac{1}{T^2}\left(\frac{\partial^2 S}{\partial H^2} \right)_p^{-1} = \frac{\langle \delta H^2 \rangle}{k_B T^2} \tag{1.14}$$

Thus the heat capacity is proportional to the fluctuations in the enthalpy, the area compressibility is proportional to the area fluctuations, the electrical capacitance is proportional to the fluctuations in charge, and so on.

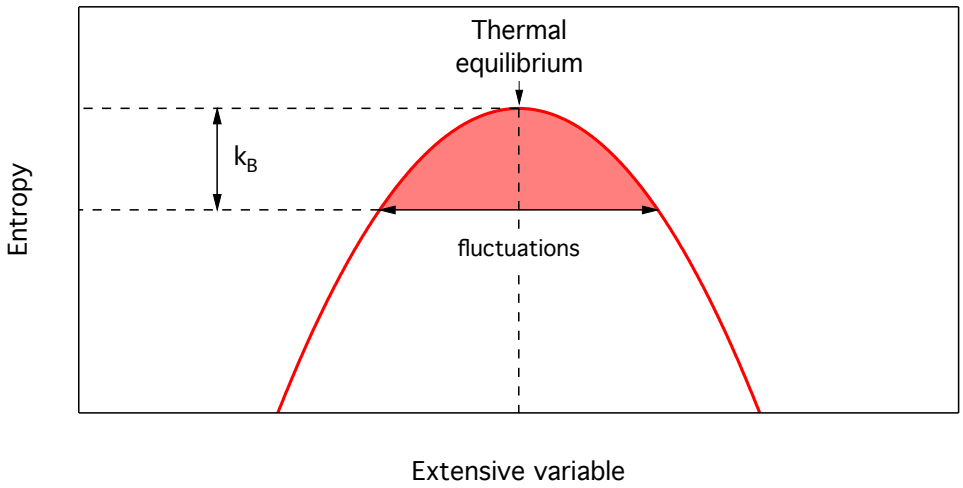

FIG. 1.10: In equilibrium there will be fluctuations around the mean value for all extensive variables, ξ, such as enthalpy, area, charge, etc. The figure was adapted from Heimburg (2010a).

For systems where the changes in some extensive variables are proportional to each other (e.g. $dH \propto dV$), the corresponding susceptibilities will also be linearly related. Such is the case for lipid bilayers, where it has been experimentally found that $\Delta\kappa_T^V \propto \Delta c_p$, and even with the same constant of proportionality for synthetic as well as biological membranes (Heimburg (1998); Ebel et al. (2001)).

In transitions, the difference in free energy between different states becomes zero, meaning that thermal noise will enough to make large changes in state. Consequently, the fluctuations in the extensive variables will become large, and thus also the corresponding susceptibilities will increase.

Since the membrane volume only changes by $\approx 4\%$ during the transition (Heimburg (1998)), the relative thickness fluctuations must be approximately equal to the relative area fluctuations. This means that the membrane thickness fluctuations are large when the isothermal area compressibility is large.

Furthermore, it has been shown that membranes become more pliable during the chain-melting transition. In fact, it has been found that the lateral compressibility and the excess heat capacity are proportional functions near the chain-melting transition, meaning that both the area and the enthalpy fluctuates strongly close to the transition point (Heimburg (1998); Ebel et al. (2001)).

Another important consequence of the fluctuation-dissipation theorem is a fundamental coupling between the magnitude of fluctuations and the relaxation time scale of the lipid membrane. Essentially, when fluctuations are large (high heat capacity, compressibility, etc.), they are also slow, a phenomenon known as "critical slowing down". This has been experimentally verified by several different techniques, and it has been found that close to the main transition there is a direct proportionality between the heat capacity and the relaxation time scale of the system (Tsong (1974); Gruenewald et al.

(1980); Elamrani and Blume (1983); Blume and Hillmann (1986); van Osdol et al. (1989, 1991); Grabitz et al. (2002); Halstenberg et al. (2003); Seeger et al. (2007)).

The presence of these fluctuations means that the hydrophobic barrier of the flexible hydrocarbon chains will inevitably disappear locally given sufficient time. As a pore (hydrophilic or not) is an allowed state of the membrane, one expects that the probability of occurrence will be much higher when the lateral density and thickness fluctuations of the membrane are strongest, such as during the chain-melting transition. Moreover, since to the fluctuation time scale gets longer, one would also expect that the life times of pores would increase in the transition regime. Both of these predictions have been experimentally verified (Blicher et al. (2009); Wunderlich et al. (2009)).

1.5 Musings on the electrical properties of membranes

This section will introduce some of the basic electrical properties of lipid membranes and how the phase state of a lipid bilayer can be influenced by a transmembrane electric field. Sec. A.1 in the Appendix describes a number of methods to measure such couplings (in principle, if not in practice).

1.5.1 Electrostriction

When a voltage is applied across a capacitor it will exert a compressive force on the system due to the charges on each side attracting each other. This effect is known as *electrostriction*. For lipid membranes, this compression can under certain conditions induce gauche conformations in the hydrocarbon chains, in effect pushing the membrane through its melting transition.

The work needed to change the geometry (and therefore the capacitance) of a system at constant voltage, V_m, can be shown to be

$$\Delta W = -\frac{1}{2} V_m^2 \Delta C \tag{1.15}$$

which is simply the capacitive energy of the system minus the electrical work performed by the source keeping the voltage constant (Feynman et al. (1964)).

This effect will, in accordance with our intuition, favour the thinner fluid state which has the larger capacitance. A simple back-of-the-envelope calculation shows that for any biologically relevant membrane potential, i.e. up to a few hundred millivolts, this effect is small, though not insignificant. Assuming an increase in area of about 25%, a decrease in thickness of 16%, and a membrane capacitance of approximately $1\mu F/cm^2$, gives a change of $\approx 7 J/mol$ for $V_m = 100mV$. This should be compared to the melting enthalpy which is usually in the range of 10–40kJ/mol for phospholipids (Mabrey and Sturtevant (1976)). So, at most, this will correspond to a shift in melting temperature of roughly 0.05–0.3°C depending on the lipid type (see Table 1.1). Note that the energy depends on the square of the voltage, so a doubling would give a temperature shift of 0.2–1.2°C, and so on. This is of sufficient magnitude to be detectable, at least in principle.

It should be mentioned here that there have been some attempts in the literature to estimate the influence of electrostriction by means of fairly elaborate mean field models. In the article of Sugar (1979) they found a much stronger influence, claiming that a transmembrane voltage of 140mV could induce a first-order transition in a DPPC bilayer at 20°C, i.e. more than 20°C below the normal transition temperature.

As a final remark, there have been reports of lipid membranes becoming thinner in response to an applied voltage, e.g. by White (2006) and later by Berestovsky et al. (1978). However, the effect found in both papers was very slight, being around $\Delta d/d < -10^{-3}$ at 100mV, though I believe this is due to the peculiar choice of model system used in both articles, namely oxidised cholesterol in decane. Such a system is likely to have a melting transition far below the experimental temperature, and will consequently not show any dramatic response beyond a slight, elastic compression.

1.5.2 Reorientation of head groups

NMR studies have shown that an electric field across a lipid bilayer will strongly affect the orientation of the zwitterionic dipolar head groups (Stulen (1981)). It is also known that the mean orientation of the head groups depends on the phase state of the system. It is therefore worthwhile to estimate to what extent this effect will influence the transition behaviour of the lipid bilayer.

In the presence of an electrostatic field, $\vec{E}$, the head groups will align with the field, giving an additional contribution to the enthalpy change of the transition. This contribution can easily be estimated by a simple back-of-the-envelope calculation based on standard electrostatics (Cotterill (1978)). To first approximation, this contribution will be $\Delta H_{field} = -\vec{m} \cdot \vec{E}$ per head group with a dipole moment of $m = qL$. Assuming that the field is normal to the bilayer surface, we have that

$$\Delta H_{field} = -qLE \cos\theta = -qV_m \frac{L}{d} \cos\theta, \tag{1.16}$$

where θ is the angle between surface normal and the dipole axis, V_m is the transmembrane potential, and d is the thickness of the membrane. Since the angle of the head groups change during the transition, there will be a shift in the melting temperature given by

$$\Delta T_m = \frac{\Delta H_{field}}{\Delta S} = \frac{\Delta H_{field}}{\Delta H} T_m. \tag{1.17}$$

Let us assume a spacing between the phosphate and choline group of $L \approx 5$Å, with $q = 1.602 \times 10^{-19}$ coulomb, and a bilayer thickness like that of DPPC with $d_g = 47.9$Å and $d_f = 39.2$Å for the gel and fluid state respectively. For a change in head group tilt from roughly $\theta_g \approx 69°$ in the gel state to $\theta_f \approx 64°$ in the fluid state (see Sec. 3.3.1), we find that $\Delta H_{field} \approx 1.7 V_m$ kJ/V $\approx 0.7 V_m\ k_B T$/V. The approximate shifts for some common phospholipids at $V_m = 100$mV are shown in Table 1.1.

It is important to note that these calculations are essentially based on a monolayer system. However, as discussed in Sec. 1.4.3 there is a significant coupling between the two leaflets of a bilayer. In the absence of this coupling, the melting point of one leaflet would be raised by the calculated amount, while it would be lowered by the same amount for the other leaflet. In the presence of an interleaflet coupling, the shifts will be partially suppressed as shown in Fig. 3.6 in Sec. 3.3.3. Additionally, a difference in state for the two leaflets will also lead to buckling of the bilayer, causing additional stresses that can

Effect	**Scaling**	**DLPC**	**DMPC**	**DPPC**	**DSPC**
Electrostriction	$\Delta T_m \sim V_m^2$	−0.27°C	−0.09°C	−0.06°C	−0.05°C
Head group alignment	$\Delta T_m \sim V_m$	±6.6°C	±2.3°C	±1.5°C	±1.3°C

TABLE 1.1: Approximate values for the shifts in transition temperature for $V_m = 100$mV shown for various phospholipids using the calorimetric values of Mabrey and Sturtevant (1976). See the text for more details.

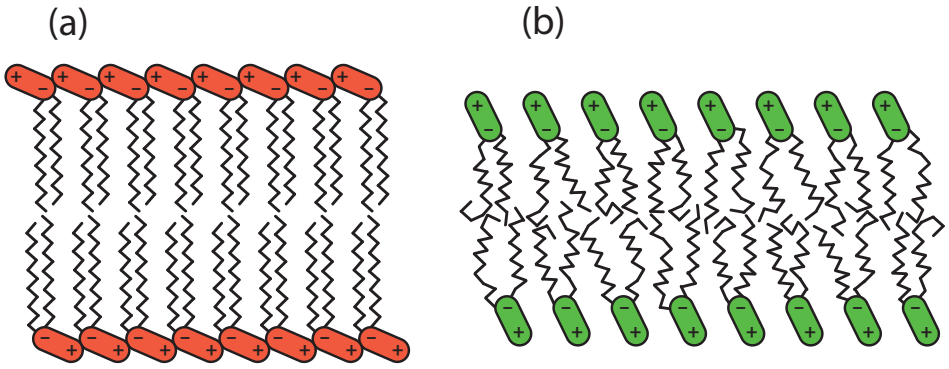

Fig. 1.11: *(a)* Schematic arrangement of lipids in the gel state. *(b)* Arrangement in the fluid state. Note the change in head group orientation.

suppress the shifts in the melting temperatures. Lastly, it is likely that this simple model overestimates the influence, given that the measured value of the dipole moment of the head groups in monolayer experiments is usually an order of magnitude smaller than the simple estimate above. This discrepancy may in part be due to the large dielectric screening of groups embedded in the aqueous phase, but more importantly, it also stems from that one only measures the component of dipole moment that is perpendicular to the surface and not the full dipole moment (Mohwald (1990)).

1.5.3 Other subtle and speculative influences

In addition to the two effects discussed above (electrostriction and reorientation of head groups) one can speculate about other possible influences.

It is known that the interaction with water plays an important role for the phase state of the lipids. Since the water possesses strong dipole moments, these will also realign in the presence of an electric field, so one could imaging that there would be an indirect influence of the field through the water. This effect could manifest for both static fields, where the water structure will be permanently altered, but also for high frequency fields, which might prevent the water from forming any kind of ordered structure.

Another effect of applying a field is that the concentration of salts and protons will change compared to the bulk values. Since the state of the membrane is also influenced by changes in pH and salinity, one could imagine that there would be indirect effects from this (Trauble et al. (1976); Sturtevant (1998); Boeckmann et al. (2003)).

Finally, the field might also have an influence on the van der Waals forces between the lipids' hydrocarbon chains and on the interleaflet coupling, which could lead to changes in the lateral tension of the membrane. Again, the exact extent of such perturbations to the lipid-lipid interactions is unknown and likely to be rather complex.

All of these effects are quite speculative, and it is beyond the scope of this thesis to investigate their significance, but it is worth keeping in mind that there can be influences beyond the first two effects discussed above.

1.6 Permeability and pores

As mentioned in Sec. 1.3 the permeation rate of ions and small molecules through unmodified lipid membranes can increase by several orders of magnitude in the transition regime. The reason for this phenomenon is still not fully understood, though a possible explanation is offered by at least two models, which – for ease of reference – will be called the *line defect model* and the *pore model*. Both of them are based on thermodynamic grounds and they should not be considered to be mutually exclusive.

This section will first introduce these two models for the passive permeability, and then discuss how things will differ in the presence of a transmembrane electric field. Lastly, a framework for analysing the kinetics of spontaneously formed pores will be introduced.

1.6.1 The line defect model

The line defect model was first proposed by Trauble and Haynes (1971) and later Papahadjopoulos et al. (1973) and subsequently followed up on by Cruzeiro-Hansson and Mouritsen (1988). They proposed that the increase in permeability is caused by packing defects that occur at the interfaces between domains and the bulk, which can facilitate the solubility and diffusion of water and other small solutes through the membrane. In short, they proposed that the probability, $P(T)$, of a molecule or ion crossing is closely related to the boundaries between the fluid and gel domains. In this model $P(T)$ can be written as a sum of three terms, namely

$$P(T) = a_i(T)p_i + a_g(T)p_g + a_f(T)p_f, \tag{1.18}$$

where a_i, a_g, and a_f are the fractions of the membrane area occupied by the interfaces, and by the gel and fluid lipids not associated with an interface. The corresponding regional probabilities of permeation are p_i, p_g and p_f respectively. It should be noted that since there is no way of calculating these permeation probabilities from basic principles or other membrane properties, it is necessary to fit these parameters to experimental data.

The line defect model assumes that the interfacial area is associated with a very high relative regional permeability, $p_i \gg p_g, p_f$. The idea behind this is that there should be a high density of defects in the interfacial region which could cause leakiness due to the imperfect molecular packing.

This theory would thus predict that the permeability should increase in the phase transition when domain formation and local fluctuations are strong. It also predicts that membranes with more cooperative transitions will have a lower permeability, since the high line tension will tend to minimise the amount of interfacial area.

1.6.2 The pore model

Another possible mechanism – the pore model – was proposed by a number of people (Linden et al. (1973); Wu and McConnell (1973); Nagle and Scott (1978); Doniach (1978); Kaufmann and Silman (1983a,b); Kaufmann et al. (1989b); Ivanova et al. (2003)). This mechanism assumes that the particles permeate through transient hydrophilic pores that are the result of thermal fluctuations. Thus no dehydration or hydrophobic barrier has to be involved.

We first consider the work needed to create a pore or defect of area ΔA. To first approximation, this is inversely proportional to the lateral area compressibility of the membrane, κ_T^A, i.e.

$$W = \frac{1}{2}\frac{(\Delta A)^2}{A\kappa_T^A}. \tag{1.19}$$

Consequently, if the area compressibility becomes large enough, the energy required to make large defects will become similar to the thermal energy, k_BT. Therefore, one would expect spontaneous defects to become large enough for ions or small molecules to pass through the membrane in the transition regime, where the compressibility is high. As a side effect, one also expects that the membrane will become unstable and prone to rupture when close to the transition.

If we relate the permeability phenomenologically to the area by a Taylor expansion, we find that

$$P(T) = P_0 + P_1\langle\Delta A\rangle + P_2\left\langle\Delta A^2\right\rangle + \ldots \approx P_0 + P_2\left\langle\Delta A^2\right\rangle = P_0 + P_2'\kappa_T^A \tag{1.20}$$

where P_0 is the permeability in the absence of fluctuations, and is assumed to be a monotonously increasing function of the fluid fraction (due to the increase in the average lipid spacing). Note that the linear term drops out since $\langle\Delta A\rangle = 0$ in equilibrium. The second step follows from Eq. (1.13).

Since the heat capacity and area compressibility have been found to be proportional to each other (Ebel et al. (2001); Steppich et al. (2010)), we can also rewrite Eq. (1.20) to read

$$P(T) = P_0 + P_2'\kappa_T^A = P_0 + \alpha\Delta c_p, \tag{1.21}$$

Note that both P_0, P_2' and α may be temperature dependent, though any dependence is assumed to be relatively weak.

Hence, this theory predicts that the permeability be highest in the phase transition. Also, if the cooperativity of the system is reduced – broadening the heat capacity profile – the permeability will decrease at the transition midpoint, while increasing in the wings of the heat capacity profile. Therefore, an important prediction of this model is that one expects higher permeability of membranes with very cooperative transitions, in contrast to the line defect model.

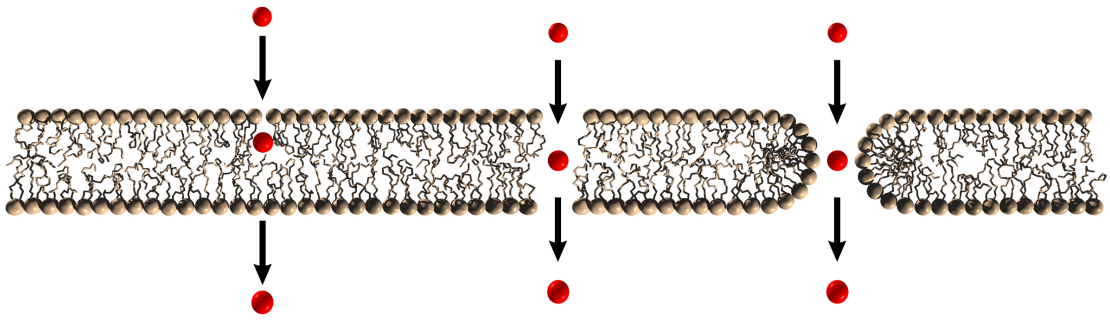

FIG. 1.12: Models for permeation. *Left:* The solubility-diffusion mechanism. Particles enter the hydrophobic core through some small defect and then diffuse across the bilayer. This is an extremely unfavourable mechanism due to the temporary loss of the particle's hydration shell. *Middle:* Hydrophobic pore. *Right:* Hydrophilic pore. Particles traverse the bilayer through transient pores caused by thermal fluctuations.

1.6.3 Correlation with experiments

These two thermodynamic models are, in a sense, very minimalistic models in that they incorporate the fewest possible assumptions about the diffusion mechanism, and neither implies a detailed structural model of the defects.

As mentioned, these two models are not mutually exclusive, but one of the mechanisms will be the dominant one, while the other will simply provide an alternative pathway for permeation. Whatever the specific case may be, these thermodynamic interpretations of ion channel opening and closing due to lipid bilayer fluctuations are free of adjustable parameters, and make several testable predictions.

In the article of Sabra et al. (1996) the influence of the neurotoxin lindane on the melting transition and the passive permeability of DMPC vesicles was investigated. They observed a shift in the melting transition to lower temperatures and a significant decrease in the cooperativity of the system, causing the transition peak to become broader and flatter. An identical change was seen for the passive permeability of the membranes to Co^{2+} ions, indicating that the pore mechanism is the dominant for such ions.

We have also more recently found the same behaviour for permeation of the small fluorophore rhodamine 6G through DPPC:DPPG (95:5 mol:mol) membranes (Blicher et al. (2009)). Here it was also found that the addition of halothane or octanol caused a shift and broadening of the melting transition, with the accompanying change in the permeation rate perfectly mirroring the changes in the heat capacity profile. Again, this speaks strongly in favour of the pore mechanism.

Additionally, using a simple extension of the classical 2-state Ising model that allowed for pore formation, we again found that the mean pore density reflected the changes in the heat capacity and not the amount of interfacial area (Wodzinska et al. (2009)).

Finally, it is worth repeating that neither of these models provide detailed information about the structure of the pore. It has been suggested by Glaser et al. (1988) that if a hydrophobic pore (Fig. 1.12, middle) reaches a size of 0.3–0.5nm it becomes energetically

favourable to reorient the lipids such that a hydrophilic pore (Fig. 1.12, right) is formed. Such hydrophilic pores have been estimated to be stable with a diameter of ∼1nm, which also happens to be the typical size of protein ion channels (Heimburg (2010a)).

Based on the considerations above and our experimental findings (Blicher et al. (2009); Wodzinska et al. (2009)), it seems likely that the macroscopic increase in the permeability in the phase transition regime and the formation of microscopic lipid ion channels that are observed in voltage clamp experiments is, in fact, the same physical process.

1.6.4 Pores in electric fields

A different and more microscopic approach was attempted by Winterhalter and Helfrich (1987) and later by Glaser et al. (1988), where the calculations were based on a continuum model of the membrane and where the effect of voltage was also taken into account.

Based on the considerations found in these articles and in Sec. 1.6.2 we propose that for a hydrophilic pore of radius r the energy of the pore can be approximated by

$$\Delta G(r,U) = \frac{1}{2}\frac{(\pi r^2)^2}{A\kappa_T^A} - \epsilon_W \epsilon_0 r U^2 - \pi r^2 \chi U^2, \tag{1.22}$$

where κ_T^A is the lateral area compressibility of the membrane, A is the area of the membrane, U the transmembrane voltage, and $\chi = (\epsilon_W - \epsilon_L)\epsilon_0/2h$ is a coefficient related to the capacitive energy of the membrane with and without a water filled pore of length h.

In this continuum description, the energy essentially has three contributions[5]:

- The work that has to be performed against the lateral pressure in the membrane.
- A term related the Maxwell stress due to the inhomogeneity of the electric field caused by the conducting pore ($\propto r \cdot U^2$).
- A term related to the change in capacitive energy of the system ($\propto r^2 \cdot U^2$).

From statistical mechanics one would expect that the likelihood of forming a pore is proportional to $\exp(-\Delta G/k_B T)$, and that the conductance of the pore is a simple function of its radius, r. As can be seen from Eq. (1.22), an electric field will reduce the free energy cost of creating a hydrophilic pore. In fact, for sufficiently large voltages ($U \approx 0.5$–1V), the energy barrier for pore growth disappears, meaning that the pore will grow without bounds, causing an irreversible breakdown of the membrane.

It should be noted that Eq. (1.22) is a poor approximation for pores with a radius much smaller than the bilayer thickness. This is unfortunately the regime of the small spontaneous pores that are typically observed in pure lipid membranes. However, based on these simple considerations we expect the free energy of forming a pore to go down as the square of the applied voltage. This in turn implies that the conductivity of the entire membrane is a non-linear function of voltage.

[5]Note that, unlike Winterhalter and Helfrich (1987) and Glaser et al. (1988), we do not consider a line tension around the pore here. This is justified by our experimental findings in Blicher et al. (2009).

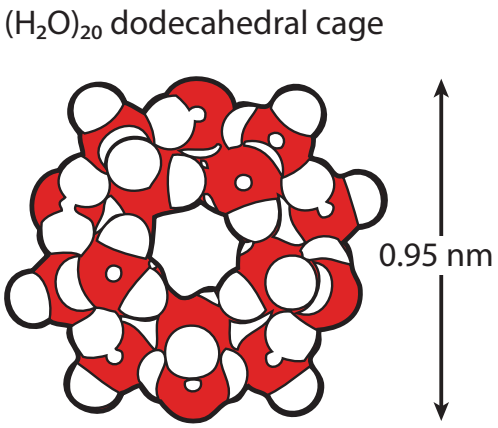

FIG. 1.13: A view down the z-axis of a dodecahedral water cage.

1.6.5 Water in narrow channels

The lipid barrier presents a barrier to small ions primarily due to the electrostatic self-energy of the ion. This energy may be lowered significantly by surrounding the ion with molecules that posses either induced or permanent electric dipole moments. This gives rise the so-called 'solvation shell' or (in the case of water) 'hydration shell' – a layer of ordered molecules with their dipoles pointing towards the ion. When moving the ion from an aqueous environment to a non-polar environment (such as the interior of a lipid membrane), the change in this self-energy is in the range of hundreds of k_BT, making it virtually impossible for it to happen spontaneously.

Therefore, for the ion to cross a lipid membrane it is necessary to provide an environment for the ion that results in a similar self-energy as that of a fully hydrated ion. One possibility is to line the inside of a channel with molecules with electric dipole moments. Model calculations show that during transit, small monovalent ions need to be continuously in contact with approximately four or five molecules with the dipole moment of water (Edmonds (1981)). One way to achieve this is to have a static ring- or cage-like structure.

For lipid pores this structure can either arise from the lipid head groups themselves, but it has also been suggested there is, in fact, a layer of ordered water lining the insides of the pore (Edmonds (1981). One particularly stable water structure is the dodecahedron composed of pentagon rings (see Fig. 1.13). One possibility would be to form a channel by stacking such dodecahedrons along a common z-axis, parallel to the membrane normal.

The details of such a model have been theoretically explored to some degree by Edmonds (1979, 1980, 1981, 1998), and it explains a number of characteristics of ion channeling. In particular, it predicts the possibility of switching between two polarised states, that can be brought about by a transmembrane electric field and that would be selective for unhydrated ion size and valence (Edmonds (1980)).

In this model the step-wise nature of the conductance events is explained by the

requirement that a pore is only conducting when the full array of water structures is aligned and intact (this gives rapid switching), and the fixed conductance arises from the well-defined structure, which only allows for single-file ion flow.

There are a couple of experiments that support this hypothesis, where people have observed quantised conductance events in systems without proteins or lipid membranes. One example is the experiment by Sachs and Qin (1993), where they found that the gigaohm seals made between patch pipettes and hydrophobic substrates (Sylgard and Vaseline) show quantised gating events that are cation selective and "indistinguishable from the gating of biological ion channels".

Another striking example was reported in the same year by Lev et al. (1993), where quantised gating events were observed for ions flowing through purely synthetic filters made of polyethylene terephthalate that had been etched to produce narrow pores of about 1nm in radius. Again, they also observed cation selectivity and even "inhibition" by divalent cations and protons.

Given the remarkable similarity between these findings and the data presented in this thesis, it is natural to speculate that many of the gating characteristics of the lipid pores can be explained on the basis of ordered water.

1.6.6 Pore formation kinetics

It has previously been found that the open-time histogram of lipid ion channels under certain conditions show a power law – or "fractal" – behaviour with an exponent of approximately -3/2. This, in turn, implies a open-close transition rate, $k(t)$, that is a function of the time that the channel has been open, and that it decreases as $k(t) \propto t^{-1}$ (Gallaher et al. (2010)).

It has been proposed that the fractal behaviour of the lipid ion channels is due to "pore freezing" (Gallaher et al. (2010)). The idea is that the pores are primarily formed close to domain boundaries where fluctuations are high. They are therefore also likely to be subsequently completely surrounded by rigid gel state lipids. Due to the crystalline structure of the gel phase, this will make it difficult for the pore to reseal, since it will require some deformation of pore neighbourhood. In effect, this will stabilize the pore, since the only way for it to reseal is to wait for the local neighbourhood to melt. Since the characteristic timescale of domain fluctuations gets longer in the transition regime, this model also naturally explains why and how the mean pore opening times depend on the phase state of the membrane.

Gallaher et al. (2010) proposed a kinetic scheme for this mechanism

$$\text{no pore} \xleftarrow{\alpha} S_1 \underset{k_{21}}{\overset{k_{12}}{\rightleftharpoons}} S_2 \underset{k_{32}}{\overset{k_{23}}{\rightleftharpoons}} \dots \rightleftharpoons S_N \tag{1.23}$$

It is assumed that the transitions between the states are Markovian, and that state 1 to N all have the same pore size and conductance, with the only difference being that the pore is trapped in an increasingly larger gel state region.

It was shown by Millhauser et al. (1988) that if all rates in Eq. (1.23) are identical and $N \to \infty$, such a kinetic scheme can be analytically solved and will lead to a time

dependent transition rate, $k_{eff} = k(t)$, from the (set of) open states back to the closed (no pore) state.

For any α and with all $k_{ij} = \omega$, one finds that the tail ($t \gg \omega^{-1}$) of the probability density function of open times will be given by

$$f(t) \approx \frac{\sqrt{\omega}}{2\sqrt{\pi}\alpha \cdot t^{\frac{3}{2}}}, \tag{1.24}$$

where α and ω can depend on the temperature, voltage, and phase state of the system. The corresponding effective kinetic rate will in this limit be

$$k(t) \approx \frac{1}{2t}, \tag{1.25}$$

and for shorter times and $\alpha \ll \omega$, they found that $f(t) \propto t^{-1/2}$ and $k(t) \propto t^{-1/2}$.

If every pore appearing in the data traces is due to the spontaneous creation of a new pore, we would have a constant rate of formation, $k_o(t)$, and an exponential distribution of closed times. However, this is clearly not case as we will see in the next section, indicating that a poreless membrane has a memory of how long ago the most recent pore closed. To explain this puzzling closed time distribution Gallaher et al. (2010) proposed that a significant fraction of the observed openings are in fact "re-openings". That is, an otherwise stable pore will show some "flickering" (to use the terminology of the protein ion channel field) if some of the lipids lining the walls of hydrophilic pores temporarily undergo conformational changes, whereby they get un-stuck and clog ("inactivate") the channel. In the ordered water picture the fluctuating lipid would simply disrupt the water ordering, and thereby make the channel non-conducting.

If the pore formation is mediated by a local defect (an embedded protein, a chip in the glass pipette, etc.), then there is another possible explanation. If we assume that pores will exclusively form in the highly fluctuating regions (i.e. close to domain boundaries; see Sec. 1.6.2), then a scheme like that in Eq. (1.23) can again be applied, leading to similar kinetics for both the opening and the closing of the pores.

1.7 Materials and methods

This section describes the sample preparation protocols as well as the experimental methods and considerations. The results are shown and discussed in Sec. 1.8 and Sec. 1.9.

1.7.1 Lipid samples

The saturated phospholipids 1,2-Dilauroyl-*sn*-Glycero-3-Phosphocholine (DLPC) and 1,2-Dimyristoyl-*sn*-Glycero-3-Phosphocholine (DMPC) were purchased from Avanti Polar Lipids (Birmingham/AL, USA) and used without further purification.

For all of the experiments a 10:1 (mol:mol) mixture of DMPC:DLPC was used. This mixture was chosen because it shows a fairly cooperative phase transition just below room temperature. Equally important is that the transition is not too narrow, which would make it prohibitively difficult to make measurements within the main phase transition. Lastly, the pre-transition also occurs at positive temperatures, making it in principle possible to make measurements on a system that is fully in the solid-ordered state (see Fig. 1.18).

The sample was prepared from 10mM stock solutions, where the each lipid type had been dissolved separately in an organic solvent (dichloromethane:methanol 2:1), after which the two components were mixed in the desired ratio. This mixture was then dried by gentle heating while being exposed to an air stream. The remaining organic solvent was then removed by placing the sample in a high vacuum desiccator for a couple of hours.

The resulting lipid film was then resuspended by adding a highly volatile solvent (hexane:ethanol 4:1 by volume), for a final concentration of 1–2mM. The exact concentration is not critical for the success of the experiments, and is additionally difficult to keep constant, due to the extremely volatile nature of hexane. Some of the ethanol is likely to be still be present in the electrolyte solution, but since it both has a low partition coefficient in lipids, and the bath volume is much larger than the membrane volume, the membrane is assumed to be completely free of ethanol.

The NaCl electrolyte solutions used for both calorimetry as well the patch clamp experiments were buffered with 2mM HEPES (Sigma-Aldrich, Germany) and 1mM disodium EDTA (Fluka, Switzerland), and with the pH adjusted to 7.4 with NaOH. The specific conductivity of the solution was measured to be 1.412S/m at 21°C. Lastly, in order to get rid of dust particles and other possible contaminants, the buffer was always pressed through a sterile 0.2µm filter (Minisart® #16532, Sartorius Stedim Biotech, France) immediately before use.

All chemicals used were of the highest purity grade available and any water used was purified (resistivity $> 18\text{M}\Omega \cdot \text{cm}$) on a desktop EASYpure RF water purification system from Barnstead/Thermolyne (Dubuque/IA, USA).

1.7.2 Bilayer formation

> *He [Finkelstein] noted, "... that some manipulation of variables is required before everything is working properly. Then, one can make stable membranes quickly and reliably week after week until, as happens to everyone I know who works with this system, one day a stable membrane cannot be formed. After a few agonizing days of changing and permuting the lipid, the septa, the brush, the distilled water source, and your socks, everything works properly again. Most likely, the conditions are the same as before." I have been asked many times if it is truly necessary to change your socks. The answer is yes.*
>
> – Ehrlich (1992) relaying a piece of advice from Finkelstein

In this section I will briefly describe three methods for creating planar lipid bilayers (sometimes also called "black lipid membranes") for electrical characterisation studies. These methods are well suited for such studies since the two volumes separated by the bilayer are both easily accessible, allowing for simple placement of large electrodes.

The Montal-Mueller method

The most common method to form planar lipid bilayers is the method of Montal and Mueller (1972), where a bilayer is formed over a small aperture (usually 50–250µm in diameter) in a thin hydrophobic film such as Teflon.

This hydrophobic film separates two Teflon compartments and is pre-painted by a non-volatile organic solvent such as hexadecane to reduce the mechanical tension at the edges of the aperture. The two compartments are then partially filled with an electrolyte solution, such that the surfaces are initially below the hole in the film. A few microlitres of concentrated lipid solution (≈25mg/mL) is spread on the water surface in each compartment, forming two dense monolayers. After waiting for 10–15 minutes to allow for the evaporation of the solvent, the water level of the compartments is lowered and raised several times until a bilayer is formed. Finally, an Ag/AgCl electrode is immersed into each compartment and measurements can begin.

This method allows for measuring on systems with different electrolyte solutions on each side of the bilayer, and even allows for the creation of asymmetric bilayers by spreading different lipid solutions in each compartment. However, it is also an inherently problematic method, in that it requires the use of non-volatile organic solvents. Since it is not know exactly how much of the solvent is dissolved in the membrane, the composition of the membrane is always somewhat unclear even when the composition of the lipids is exactly known. This makes the method unsuited for thermodynamic studies.

Another, less profound, problem with the Montal-Mueller method is that it uses a non-disposable setup (Teflon chambers and film), which requires extensive cleaning before use. This combined with a very low success rate for forming stable bilayers, makes the method extremely tedious to work with.

The droplet method

Fortunately, another method exists, the droplet method, whereby the planar lipid bilayer membranes is formed on the tip of a patch-clamp glass pipette that has been filled with electrolyte solution (Hanke et al. (1984)).

Lipids are dissolved in a volatile organic solvent (in our experiments hexane and ethanol), and are then brought into contact with the outer surface of the glass pipette. When the solution flows down the pipette a membrane spontaneously forms at the tip of the pipette as schematically shown in Fig. 1.14.

The solvent was allowed to evaporate for at least 30 seconds before the pipette was lowered 4–5mm below the bath surface. Submerging the pipette was done to minimise the risk of membrane rupture due to water evaporation or mechanical disturbances from surface vibrations, and additionally to keep the temperature more stable.

The main advantage of this method is that the resulting membrane is practically solvent free, since highly volatile solvents can be used (Heimburg (2010a)). Furthermore, the resulting bilayers are significantly more mechanically and electrically stable (Hanke et al. (1984)). Lastly, thanks to the disposable nature of the glass pipettes, one can also ensure a clean system with minimal effort, and with a setup time of a few minutes rather than half an hour or more, as is the case with the Montal-Mueller method.

The tip-dipping method

There also exists a variation of the droplet method known as "tip-dipping", whereby a bilayer is formed by slowly dipping the pipette tip into a lipid monolayer a couple of times (Hanke et al. (1984); Coronado and Latorre (1983)). In our experience, this method has a lower success rate than the droplet method, though it is still more forgiving than the Montal-Mueller method. It also seems to produce bilayers that are less mechanically stable than the ones formed by the droplet method. Its main advantage lies in that the membrane is guaranteed to be completely solvent free, since the lipid monolayer can be formed without impurities (Hanke et al. (1984)). This method also allows for the interesting option of creating asymmetrical bilayers by spreading two monolayers of different composition, and then moving the pipette between the two monolayers.

One or multiple bilayers?

A common way to verify that only a single lipid bilayer has been formed across the aperture / pipette tip, is to measure the capacitance of the membrane and compare it to the normal value of 0.5–1$\mu F/cm^2$. However, since the area of the membrane is much smaller in the pipette methods (usually two orders of magnitude or more), the resulting membrane capacitance is also very small. Additionally, the capacitance of the thin pipette walls themselves is also non-negligible, making it impossible to determine whether the membrane capacitance is corresponds to one or multiple bilayers.

Similarly, it is not possible to optically observe the membrane thinning out and becoming black. So in the end, the criterium for a single bilayer became that the current started to fluctuate strongly around 300mV or less.

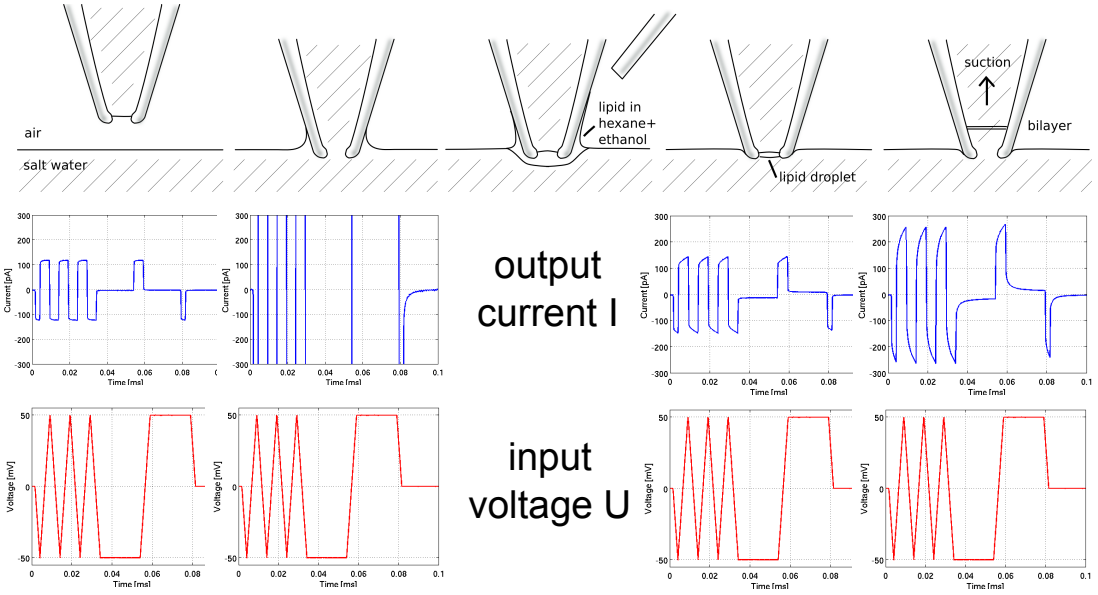

FIG. 1.14: Procedure for creating a bilayer on the tip of a glass pipette. *From left to right:* the pipette is dipped a few microns into the bath solution, causing a short circuit; a droplet of hexane/ethanol/lipid solution is spread on the surface, sealing the pipette; the solvent evaporates, leaving a lipid monolayer on the bath surface and a lipid droplet sealing the pipette; eventually, the lipid droplet forms a bilayer spanning the tip of the pipette; if necessary, one can apply gentle suction so that the lipid droplet thins out into a bilayer. The figure was kindly provided by Katrine Rude Laub.

1.7.3 Pipette preparation

Pipettes were pulled from 1.5mm / 0.84 mm (outer diameter / inner diameter) borosilicate glass capillaries (#1B150F-3, World Precision Instruments, USA) with a vertical PC-10 puller from Narishige Group, Japan. A two-step pulling procedure was used, where the first pull was 8mm and the heater was set to 80% of the instrument's maximum output. For the second pull the heating coil was lowered 4mm and the heater setting was reduced to 45%. This produced fairly short and thick pipettes with an hourglass-like taper (see Fig. 1.15).

It is desirable for the pipettes to be broad and thick-walled until the very end in order to lower both the access resistance and the pipette capacitance. This reduces the noise as well as the characteristic charging time of the pipette itself.

For some experiments the pipette was subsequently fire polished using a Narishige MF-900 Microforge. This created pipettes that had a pipette opening in the range from 5–15µm in diameter. As a general rule, larger openings made it more difficult to create a stable membrane, with 20µm being the practical upper limit.

In most experiments it was chosen to use the pipette as-is without any fire polishing. These pipettes had openings of less than a 1µm, but the exact dimensions could not be

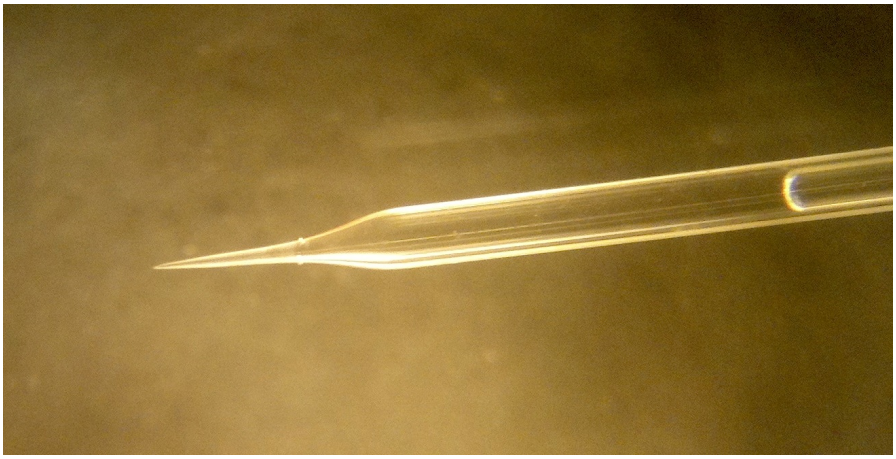

Fig. 1.15: Photograph of a typical "mini" pipette that has been filled with electrolyte solution.

determined due to the limits of optical resolution. The reason for using these unpolished pipettes (usually referred to as "mini" pipettes) was that we wanted to minimise the variation between experiments, which was next to impossible when performing fire polishing manually.

The pipettes were back-filled and special attention was paid to avoiding air bubbles getting trapped in the tip. The pipettes were only filled with 4–5mm of electrolyte solution, as overfilling can cause solution to spill over into the pipette holder, which will introduce additional background noise.

The electrodes were made of high-purity, chlorinated silver wires, which were frequently re-chlorinated to avoid baseline drift and additional noise (Penner (1995)).

Lastly, pipettes were always freshly prepared immediately before use.

1.7.4 Patch clamp amplifier setup

Fig. 1.16 shows the main setup, which consisted of a glass beaker with an electrolyte solution placed in a brass block ("jacket") that could be thermostatted by water circulation (Haake DC30-K10, Biolab). The temperature was measured with a thermocouple (NiCr-Ni, type K) and an in-house constructed amplifier, which gave an analog output that could be interfaced with the 12-bit analog/digital converter (DigiData 1200B, Axon Instruments Inc.) which also digitised the signal from the Axopatch 200B patch clamp amplifier (Axon Instruments Inc., Union City/CA, USA).

The pipette and electrodes were mounted on a cooled capacitor feedback integrating headstage amplifier (Headstage CV 203BU, Axon Instruments Inc.). The headstage itself was mounted on a micro-manipulator (model SM1, Luigs and Neumann, Germany), allowing for careful and precise control of the pipette position relative to the bath surface. Lastly, the headstage and micro-manipulators were wrapped in a finely meshed metal cloth that acted as a Faraday cage.

Data traces were recorded with Clampex 9.2 software (Axon Instruments) using the *Whole Cell* (headstage gain, $\beta = 1$), voltage clamp mode. The sampling frequency was either 10kHz or 20kHz, and the signal was filtered by the patch clamp amplifier's analog 4-pole lowpass Bessel filter with the cut-off (-3dB) frequency set to 2kHz. The attenuation of the signal above the cut-off frequency was 80dB/decade.

The output gain, α, was always adjusted before the measurement such that the signal output was not clipped and amplification would remained linear. For most experiments this meant an output gain of $\times 10$, allowing for measurements in the range of ± 1.0nA. Further increasing the output gain did not result in a significant improvement of the signal to noise ratio.

All data was analysed in IGOR Pro 6.21 (WaveMetrics, USA), using routines developed by myself.

A note on noise

A practical experience learned from working with the patch clamp setup is that it is of utmost importance to obsessively connect *everything* to the ground (earth), including the Faraday cage, reference electrode, amplifiers, brass heating jacket, waterbaths, thermocouple, computer, etc.. This is absolutely necessary to minimise line-frequency pickup or "hum". This hum will not only show up at the line frequency (50Hz in Denmark), but also at integer multiples of it (harmonics).

Reduction of the occurrence of spurious current spikes, hum, and the general noise level also improved by keeping the power sources for the waterbaths, computer and amplifiers separate. For this reason, our setup uses two isolation transformers which provide galvanic isolation and suppress electrical noise.

Temperature control

Controlling and measuring the temperature precisely turned out to be notoriously difficult. The first issue was that the bath was heated from the bottom, creating a temperature gradient in the system. This required that one measured the temperature as close as possible to the tip of the pipette, but that, in turn, resulted in increased noise and a risk of accidentally breaking the tip of the pipette with the thermocouple.

Secondly, the thermocouple used for measuring the temperature used an in-house constructed amplifier, that turned out to exhibit a slight drift of both the zero-point as well as in gain. Numerous re-calibrations were performed throughout the project, but in the end the temperature readings were never fully reliable, resulting in a temperature precision of 0.5°C at best.

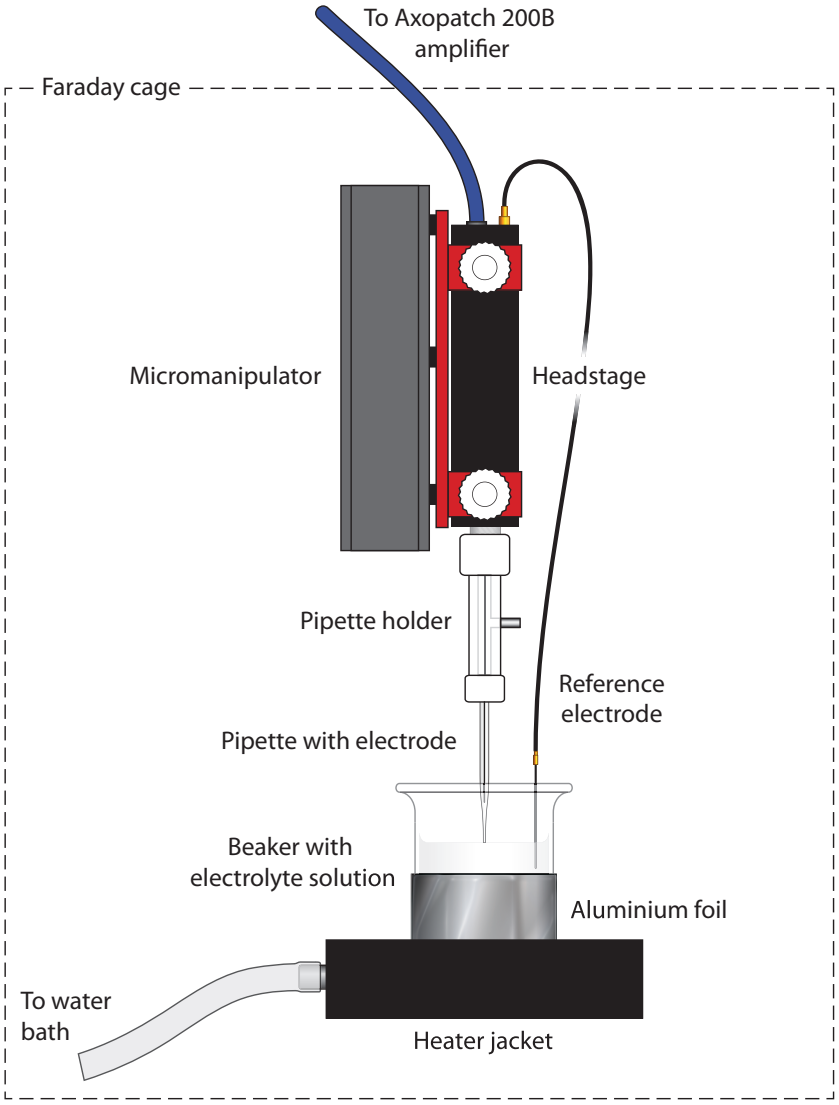

Fig. 1.16: Schematic drawing of the setup used for the patch clamp experiments.

1.7.5 Differential Scanning Calorimetry

Differential Scanning Calorimetry (DSC) is a powerful thermoanalytical technique by which one measure a number of characteristic properties of a sample, such as fusion, melting, crystallisation, as well as certain chemical reactions. This method has also been used to study of melting processes in artificial or biological membrane systems for than three decades now (see e.g. Hinz and Sturtevant (1972)).

In short, one measures the difference in the amount of heat required to increase the temperature of a sample and a reference as a function of temperature. Depending

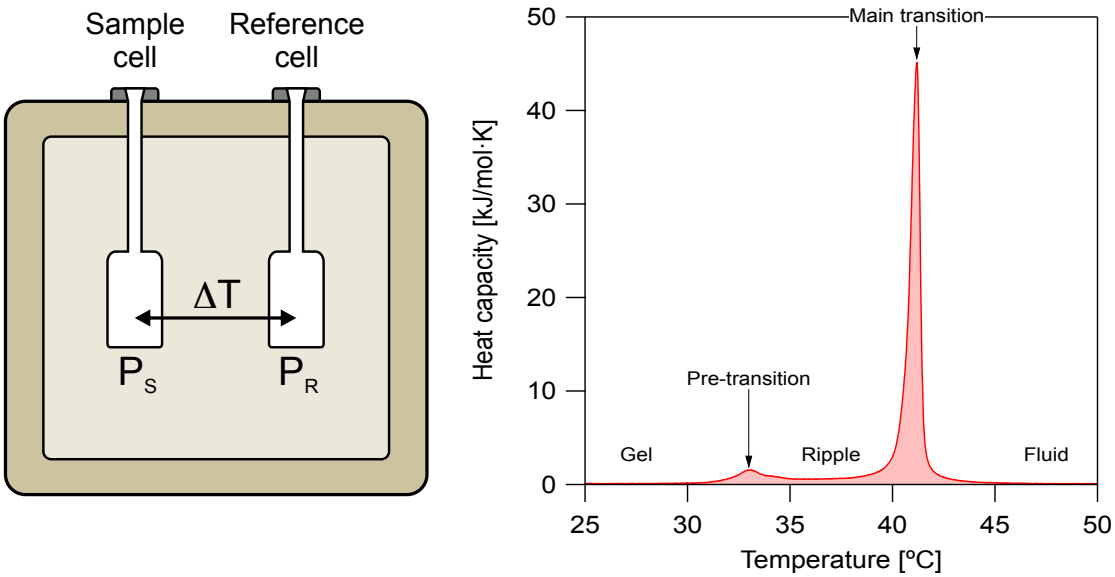

FIG. 1.17: *Left:* Schematic drawing of a Differential Scanning Calorimeter. A sample and a reference cell are isolated from the outer environment by an adiabatic shield. The temperature difference between the two cells, ΔT, is kept zero. The difference between the heat flows to each of the cells, ΔP, is proportional to the excess heat capacity. *Right:* Measured heat capacity profile of unilamellar DPPC vesicles.

on the nature of the process (exothermic or endothermic), more or less heat must flow to the sample. For instance, as a solid-ordered lipid membrane melts (an endothermic phase transition) it will require more heat flowing to the sample in order to increase its temperature at the same rate as the reference.

The basic principle of a DSC instrument is shown in Fig. 1.17. The DSC consists of two cells that are enclosed by an adiabatic shield to prevent uncontrolled heat leakage. One cell is filled with sample (e.g. a lipid/buffer solution) and the other with a reference solution (usually a buffer). The temperature of the cells is then increased linearly as a function of time while keeping the temperature difference between the two cells at zero. If an exothermic or endothermic process takes place within the sample, there will be a significant deviation in the difference between the two heat flows ($\Delta P = P_{sample} - P_{reference} \neq 0$), and a peak will show up in the DSC curve.

By integrating the excess power, ΔP, with respect to time, the excess heat flow to the sample is consequently

$$\Delta Q = \int_{t}^{t+\Delta t} \Delta P(t')dt' \simeq \Delta P \cdot \Delta t \tag{1.26}$$

The heat capacity is given by the energy needed, ΔQ, to heat the system ΔT at constant

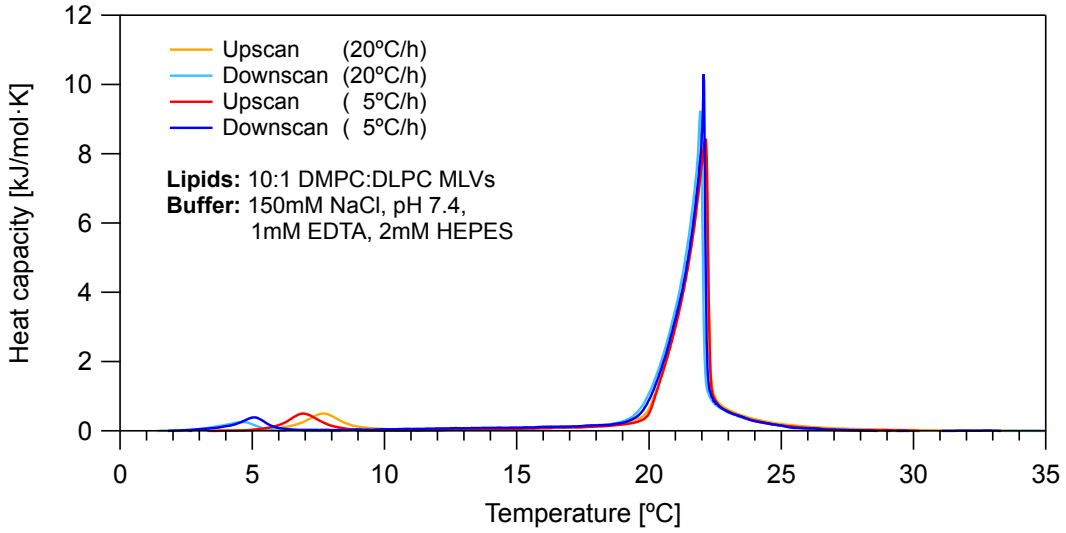

Fig. 1.18: The excess heat capacity profile for multi-lamellar lipid vesicles determined by DSC. The peak at ≈6°C is the pre-transition, while the peak at 20–22°C is the chain-melting (or 'main') transition. Note that the main transition is fairly insensitive to the scanning speed and direction, while the pre-transition clearly exhibits hysteresis.

pressure, i.e.

$$\Delta c_p = \left(\frac{\Delta Q}{\Delta T}\right)_p = \frac{\Delta P}{\Delta T/\Delta t} \tag{1.27}$$

where $\Delta T/\Delta t$ is known as the scan rate.

So by simply monitoring the power difference of the two cells one has a direct measure of the excess heat capacity of the sample substance, from which one can easily determine the transition enthalpy and entropy:

$$\Delta H = \int_{low}^{high} \Delta c_p dT \quad \text{and} \quad \Delta S = \int_{low}^{high} \frac{\Delta c_p}{T} dT = \frac{\Delta H}{T_m} \tag{1.28}$$

The heat capacity profiles in this thesis were all recorded using a VP-DSC, produced by MicroCal (Northhampton/MA, USA). In all the experiments the pressure in the calorimeter was approximately 50psi = 3.4atm (above atmospheric pressure), and the scan rate was either 5°C/hour or 20°C/hour. When setting the scan rate there is always a trade-off between limiting hysteresis effects[6] by reducing the scan rate, and getting a proper signal-to-noise ratio, which requires a high scan rate so that the heat release / uptake per second will be large. All scans were performed using the *High Gain Feedback Mode*, which gives the fastest possible instrument response which is necessary when studying very sharp thermal transitions.

[6]The slow relaxation times of lipid systems and the slow instrument response can result in a shift and smearing of the measured heat capacity profiles.

1.8 Patch clamp results

This section will present the data obtained from the patch clamp experiments. In order to keep the amount of data presented to a manageable number, additional plots of the data can be found in Sec. A.4 in the Appendix.

1.8.1 Voltage gating of lipid pores

Fig. 1.19 shows a beautiful example of spontaneous quantised events (pores) in a protein-free membrane on the tip of a patch clamp pipette. This trace was obtained at $T = 30°\text{C}$, i.e. approximately 8°C above the melting transition of the membrane (cf. Fig. 1.18). The transmembrane voltage used was only $U = +50\text{mV}$, i.e. in the physiological range that is often investigated in patch clamp experiments on protein ion channels.

Fig. 1.20 shows current traces for various voltages. Clearly, the event amplitudes, life time, and likelihood of occurrence strongly increases with the applied voltage. In other words, under certain conditions – and not just limited to the main melting transition regime – one can observe voltage-gated ion channels, even in the absence of proteins.

As for the amplitudes, Fig. 1.20 shows the current-voltage relationship of these spontaneous pores. Clearly, the pores are completely ohmic (linear I-U) in this voltage regime. Within the experimental accuracy, this seems to be the a consistent finding across all of the experiments reported in this thesis, which were performed at moderate voltages (normally below 100mV).

In order to better quantify this behaviour, we calculated the current histograms for the traces as shown in Fig. 1.21. Again, one clearly observes an increased likelihood of finding a conducting pore with increasing voltage. The free energy difference of between and open and a closed pore can then be calculated from the current histograms

$$\Delta G = -RT \ln \left(\frac{P(open)}{P(closed)} \right), \tag{1.29}$$

where $P(open)$ and $P(closed)$ are the probabilities of being open and closed respectively.

As discussed in Sec. 1.6.4 one expects an approximately quadratic dependence on the membrane potential for a constant pore size. The outcome of this has been plotted in Fig. 1.21.

Another phenomenon that was observed in several, independent experiments, was that there would be voltage gating thresholds at several different voltages. Because of the strong dependence on voltage, the lower threshold pore would be completely stable at higher voltages, in effect resulting in an increased baseline level. Data from such an experiment can be seen in Fig. 1.22.

The results of these experiments showing voltage gating have been summarised in Table 1.2. Plots from some of these other experiments can be found in the Appendix.

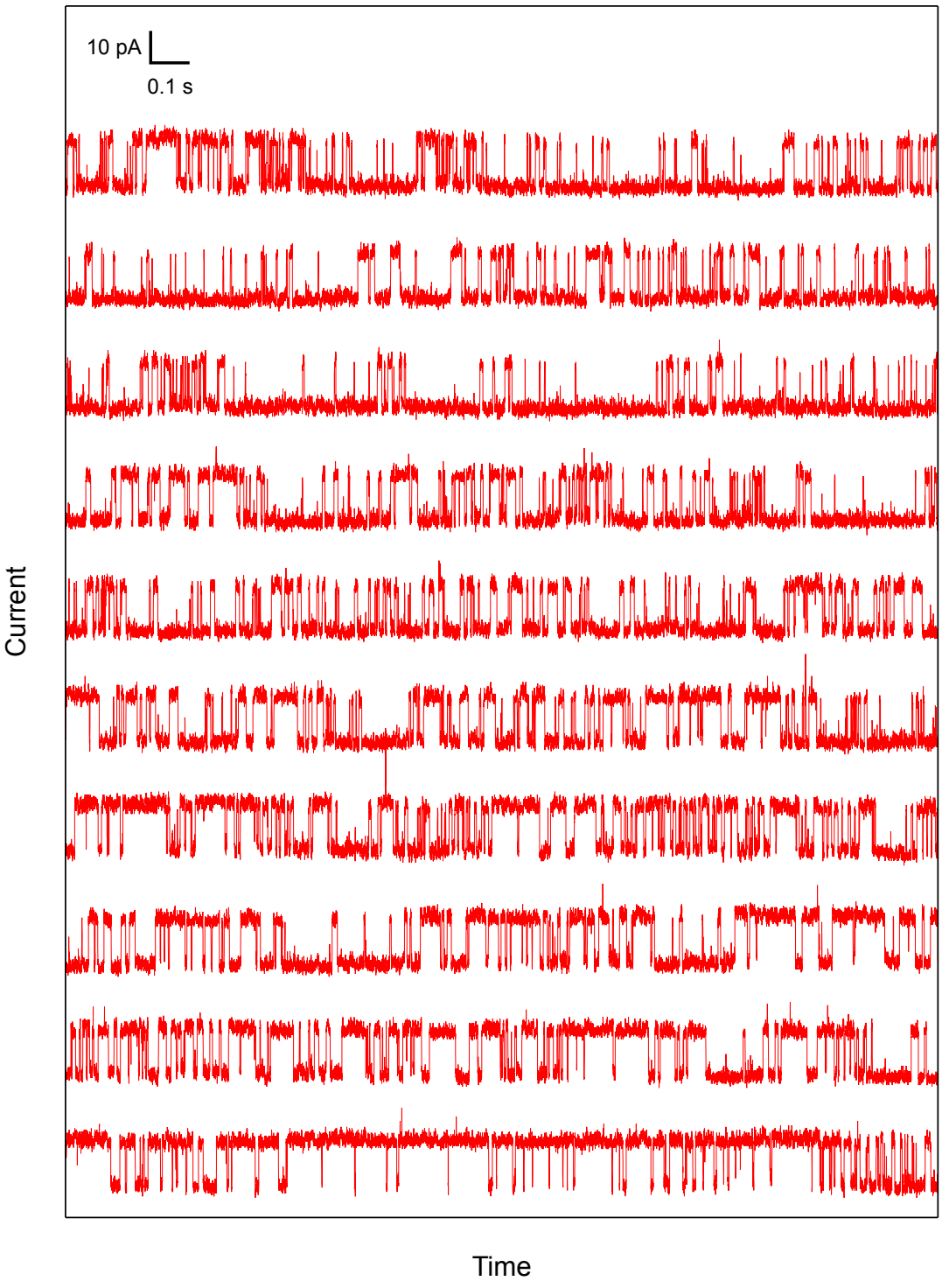

Fig. 1.19: Example of approximately 20 consecutive seconds of data showing well-defined quantised events. Membrane was 10:1 DMPC:DLPC at $T = 30°\mathrm{C}$ and $U = +50\mathrm{mV}$.

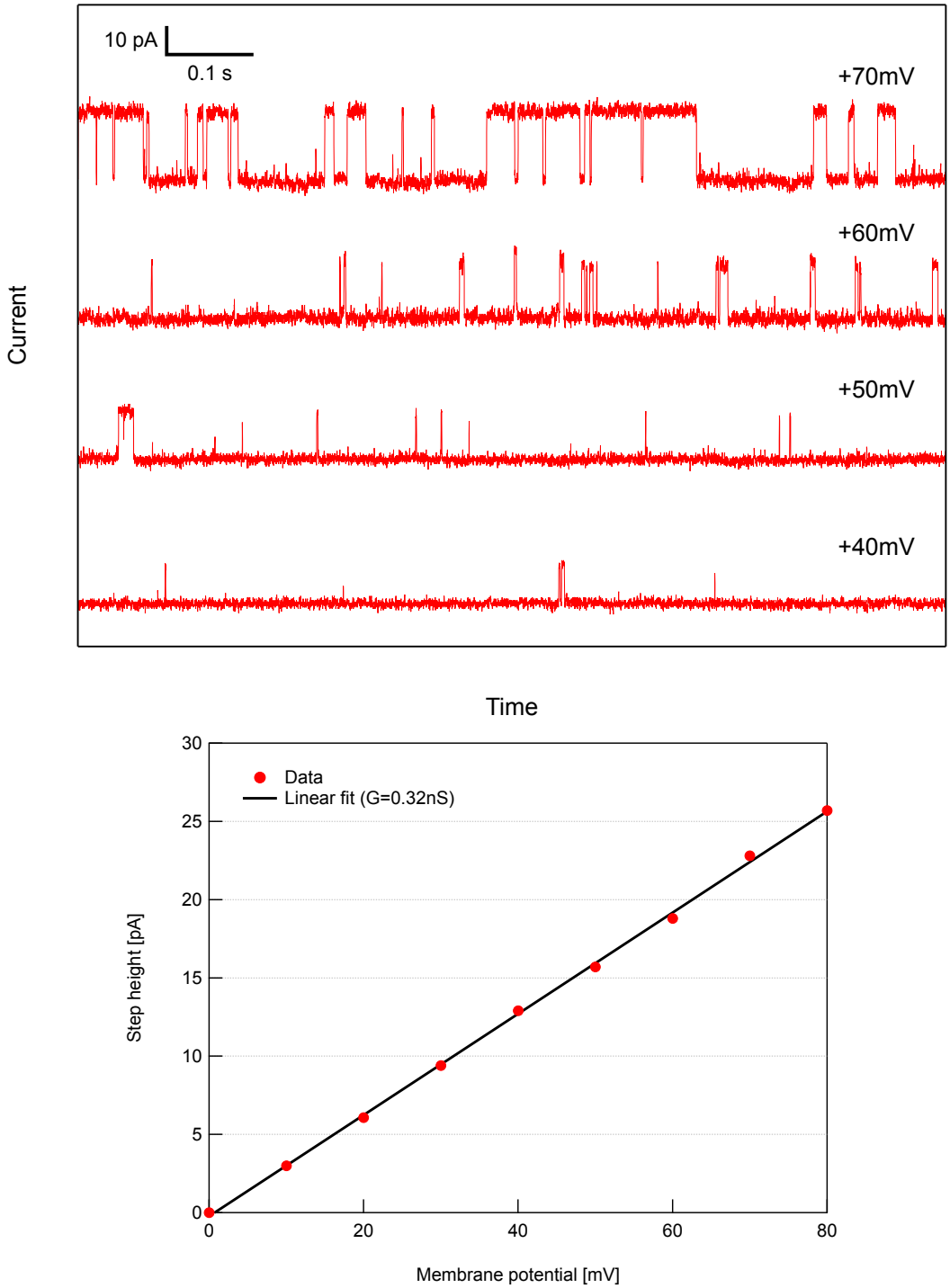

FIG. 1.20: Quantised events shown for various voltages. Note how the event likelihood and time scale increases with voltage. *Bottom:* Corresponding current-voltage relationship for the quantised events shown. Within the experimental error, the relationship is completely linear in this voltage range with a conductance of $G = 0.32$nS. Membrane was 10:1 DMPC:DLPC at $T = 30°$C.

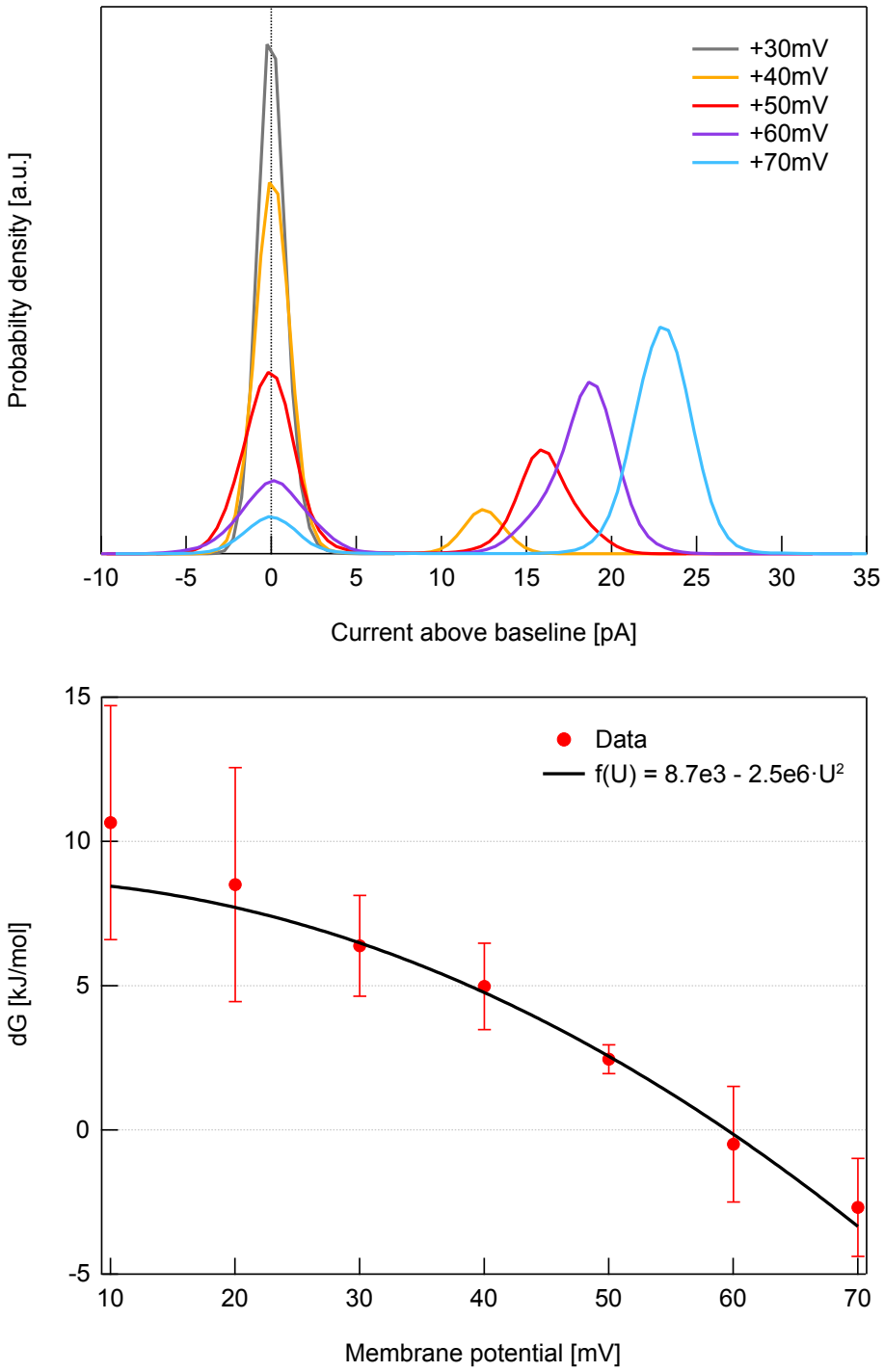

Fig. 1.21: *Top:* Histograms calculated from the membrane shown in Fig. 1.20. *Bottom:* Free energy difference, $\Delta G = -RT \ln(P_{open}/P_{closed})$, calculated from the histograms above (dots), and a quadratic fit to the data (solid line). Membrane was 10:1 DMPC:DLPC at $T = 30°C$.

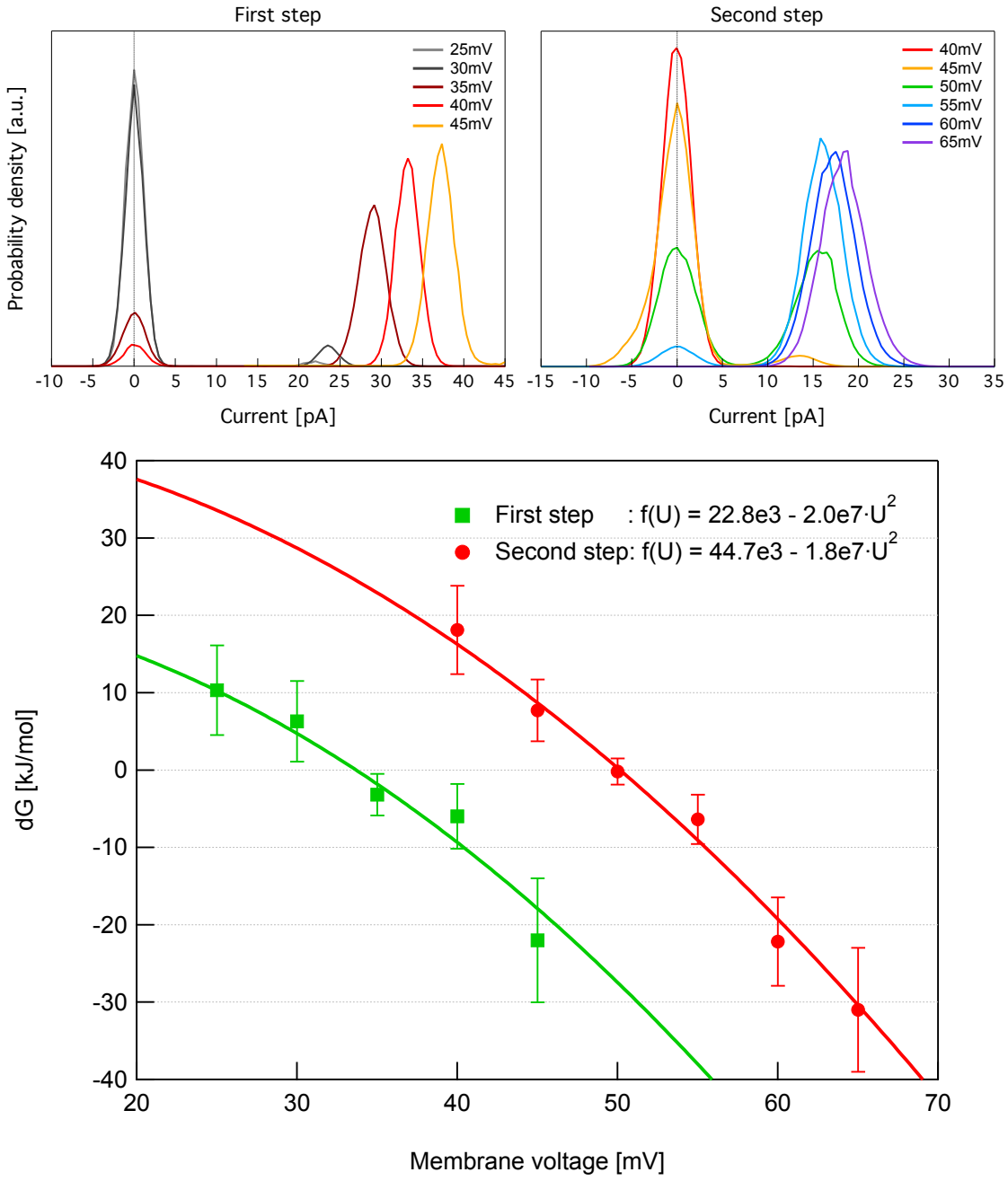

FIG. 1.22: *Top:* Current histograms for the events appearing around 30mV (*left:* G = 0.82nS) and around 50mV (*right:* G = 0.29nS). *Bottom:* Corresponding free energy differences for the data shown above. Membrane was 10:1 DMPC:DLPC at $T = 29°C$.

Temp. [°C]	Conductance [nS]	Threshold [mV]	k_0 [kJ/mol]	k_2 [MJ/V$^2\cdot$mol]
21	0.6	79	26.1 ± 3.1	4.2 ± 0.6
29	1.47	69	15.1 ± 2.7	3.2 ± 0.5
29	1.7	116	23.2 ± 5.2	1.7 ± 0.4
29	0.82	94	35.7 ± 5.2	4.0 ± 0.6
29	1.6	99	22.5 ± 3.7	2.3 ± 0.4
29*	0.82	34	22.8 ± 7.1	20 ± 6
29**	0.29	50	44.7 ± 7.0	18 ± 3
29*	0.4	30	16.3 ± 4.5	18 ± 4
29**	0.4	50	33.2 ± 6.8	13 ± 3
30	0.32	60	8.7 ± 1.3	2.5 ± 0.5
30	1.1	117	14.7 ± 4.6	1.1 ± 0.4

TABLE 1.2: Voltage gating data. k_0 and k_2 are the fit coefficients to the free energy as a function of voltage, $\Delta G = \Delta G(U)$. The fitted function was $f(U) = k_0 - k_2 U^2$, where U is the membrane potential. The threshold is where $\Delta G(U_t) = 0$, i.e. the pores are open 50% of the time. (*) and (**) are two different pores in the same data trace, but with different properties (conductance, threshold, etc.).

Determination of pore size

If we assume that pore is a water filled channel that is approximately a uniform cylinder of radius r and length ℓ, the pore size can be estimated as (Cruickshank et al. (1997)):

$$r = \frac{\rho G}{2\pi}\left(\frac{\pi}{2} + \sqrt{\frac{\pi^2}{4} + \frac{4\pi\ell}{\rho G}}\right) \tag{1.30}$$

where ρ is the specific resistivity of the solution, G is the conductance of the channel.

Since we do not know the exact properties of the water inside the channel, we use the values measured for the bulk, giving us $\rho = 0.876\Omega\cdot\mathrm{m}$ for the 150mM NaCl buffer solution. The real value will be higher, since the water in pore will be more ordered ("crystalline"). It could also be argued that the resistivity should only be based on the conducted cation (sodium), making the resistivity approximately twice as large.

One can also estimate the radius from the curvature of the free energy (Eq. (1.29)) with respect to the voltage

$$r = \frac{1}{2\pi\chi}\Big(-\epsilon_W\epsilon_0 + \sqrt{\epsilon_W^2\epsilon_0^2 + 4\pi\chi k_2}\Big), \tag{1.31}$$

which follows trivially from Eq. (1.22). Here k_2 is the coefficient obtained by fitting $f(U) = k_0 - k_2U^2$ to the $\Delta G(U)$ data.

The results of these two methods have been summarised in Table 1.3. As expected, the two methods do not yield the same results, with the conductance based model underestimating the pore size, whereas the free energy curvature model overestimates it.

Temp. [°C]	Radius from conductance [Å]	Radius from free energy [Å]
21	8.6 ± 0.5	39 ± 4
29	15 ± 0.9	33 ± 4
29	16 ± 1	22 ± 4
29	10 ± 0.6	38 ± 4
29	15 ± 1	27 ± 3
29*	10 ± 0.6	99 ± 16
29**	5.7 ± 0.3	93 ± 8
29*	6.8 ± 0.4	93 ± 12
29**	6.8 ± 0.4	77 ± 9
30	6.0 ± 0.3	28 ± 4
30	12 ± 1	16 ± 4

TABLE 1.3: Estimates of pore radii estimated from the conductance (Eq. (1.30)) and from the free energy curvature (Eq. (1.31)). Here it was assumed that the channel length is equal to the membrane thickness ($\approx$ 4nm). The order of the data is the same as in Table 1.2.

However, given that the two approaches are based on completely different assumptions, the estimated values agree fairly well in most cases, the notable exception being the experiments marked with asterisks. Currently, we have no good explanation for this disparity.

1.8.2 Fractal kinetics of lipid pores

Changes in the conductance histograms can arise from several factors, e.g. longer times between events, changes in the duration of the events, and so on. Therefore, they give a limited picture of the system – essentially, they will (at best) only show differences in equilibrium properties (free energy differences between open and closed channels), and nothing about the kinetics of the system.

Sec. A.3 in the Appendix describes how one can determine the opening and closing kinetics of the spontaneous pores. Usually in the literature, one plots this open and closed time distributions in a linear-linear plot, and then fits one or more exponential functions to estimate the characteristic time scales of the channel. However, as can be seen from the probability density functions (PDFs) and the corresponding effective kinetic rates (Fig. 1.23), the PDFs do not follow a simple exponential distribution, but rather something closer to a stretched exponential or even a power law distribution.

In Sec. 1.6.6 it was predicted that close to the critical point, the distribution of the durations of the quantised events should exhibit a power law distribution with an exponent of -1/2 for short time scales and -3/2 for long time scales. It was also predicted that the corresponding effective kinetic rates should change as $k_{eff} \propto t^{-1/2}$ and $k_{eff} \propto t^{-1}$. These predictions seem consistent with the data as demonstrated in Fig. 1.23, which was estimate from a membrane at $T = 30°\mathrm{C}$.

Another observation that can be made from Fig. 1.23 is that within the experimental

accuracy, the open times a strongly dependent on the voltage, whereas the time between events ("closed times") is fairly insensitive to changes in the voltage. In other words, the main reason for the increased likelihood of finding a conducting pore with increased voltage is not because they form more frequently, but rather because they persist for a longer time once they do appear. Whether this is a general characteristic of this phenomenon is not clear at the present time.

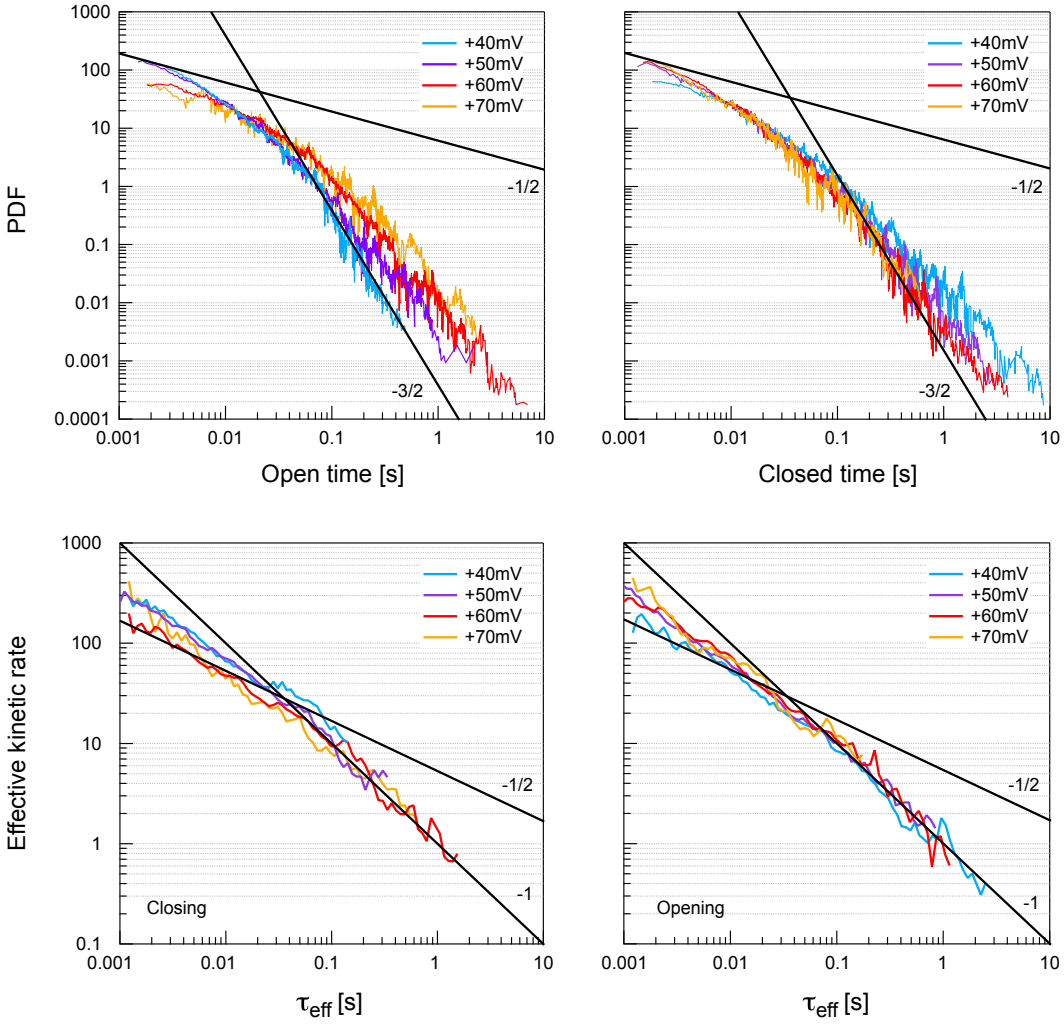

Fig. 1.23: *Top:* Probability density function (PDF) for the membrane shown in Fig. 1.20. *Top, left:* Open time PDF. Notice how the likelihood of long open times increase with voltage. *Top, right:* Closed time PDF. Apart from the lowest voltage (+40mV), the waiting time between events seems to be independent of voltage. *Bottom:* Corresponding effective kinetic rates. *Bottom, left:* Closing rate as a function of event life time. *Bottom, right:* Opening rate as a function of waiting time. The black lines show the theoretical limiting slopes for short and long time scales, as predicted in Sec. 1.6.6. Membrane was 10:1 DMPC:DLPC at $T = 30°\mathrm{C}$.

1.8.3 Additional findings

This section will present some of the other phenomena that we observed while working with the pure lipid membranes.

Membrane rectification

When the membrane conductance varies with voltage, the current-voltage relationship becomes non-linear, and the ionic currents are said to be rectified (Johnston and Wu (1997)). An example of membrane rectification can be seen in Fig. 1.24, showing that the overall membrane conductance increases with voltage. Another striking example can be seen in Fig. 1.25 which shows a clear asymmetry between positive and negative applied voltage.

Comparison with biological preparations

This short section will show some of the striking similarities between recordings from synthetic bilayers and biological preparations. The protein channel experiments were made by Katja Witschas, Ph.D. student at the University Hospital Aachen. The measurements were done on different types of human transient receptor potential (TRP) channels. This family of channels is believed to play a critical role in sensory physiology, and they are known to display a greater diversity in activation mechanisms and selectivities than any other group of ion channels. Reported modulators of activity includes mechanical stretching, voltage, heat, cold, pH, Ca^{2+}, and ethanol (Venkatachalam and Montell (2007)). Numerous other examples can be found in the literature.

All of the measurements on the TRP channels were performed at room temperature (22–23°C) using an Axopatch 200B patch clamp amplifier. All data was recorded with a sample rate of 20kHz and lowpass filtered at 2kHz. Thus, the experimental setup was essentially identical to the one used for the lipid channel data presented above.

Fig. 1.26 shows an example of the activity of a sarcoplasmic reticulum channel (ryanodine receptor) that has been reconstituted into synthetic planar lipid bilayers. This channel has been found to be activated by lipid domain formation, exhibiting a pronounced maximum in activity at the transition temperature of the lipid bilayer (Cannon et al. (2003)). Typical values for the conductance of ryanodine receptor-channels lie in the 0.2–0.9nS range, i.e. similar to the conductances reported here (see Table 1.2). Compared to e.g. Fig. 1.19 there are no obvious differences to the eye in neither amplitude or typical time scales.

In addition to the classical step-like events, one also finds a rich variety of other phenomena that are normally associated with protein ion channel activity. Fig. 1.27 to Fig. 1.30 demonstrate that these events are not unique to the proteins, and can occasionally also be observed in pure lipid membrane experiments.

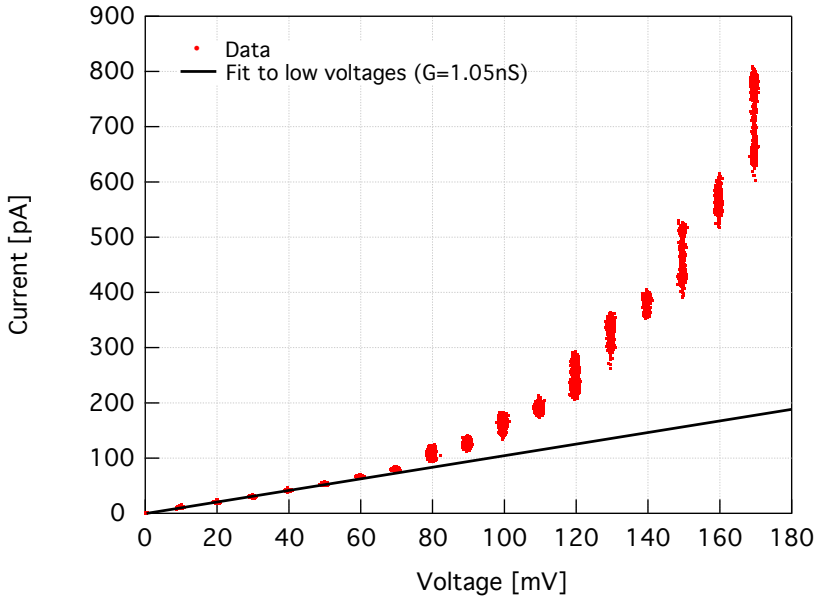

Fig. 1.24: Current-voltage relationship for the overall conductance of a membrane at $T = 30°C$. A commonly observed behaviour is a non-linear relationship, i.e. the membrane conductance is a function of the voltage. The membrane was 10:1 DMPC:DLPC.

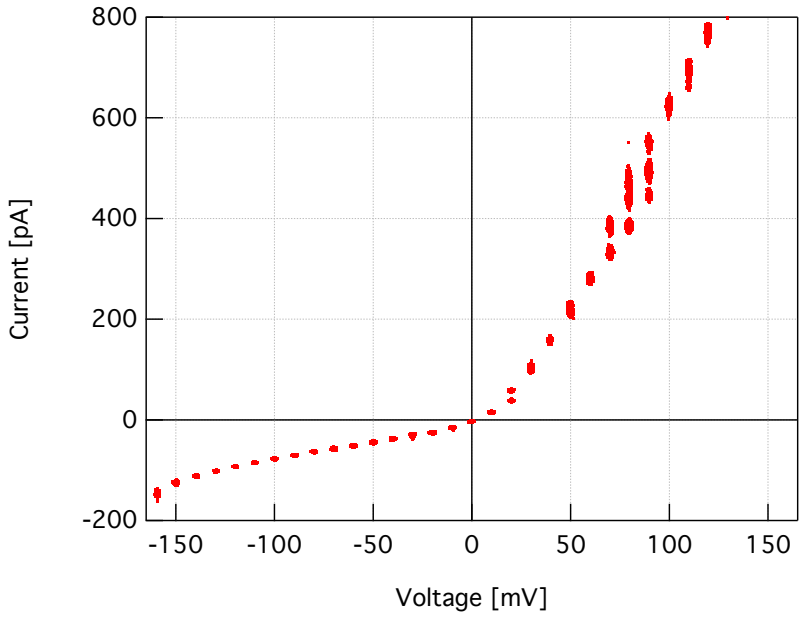

Fig. 1.25: Current-voltage relationship for another membrane. For this membrane there was a pronounced asymmetry between positive and negative voltages ("rectification"). At $U = 20$mV and $U = 50$mV the curve jumps due to pores. Membrane was 10:1 DMPC:DLPC at $T = 30°C$.

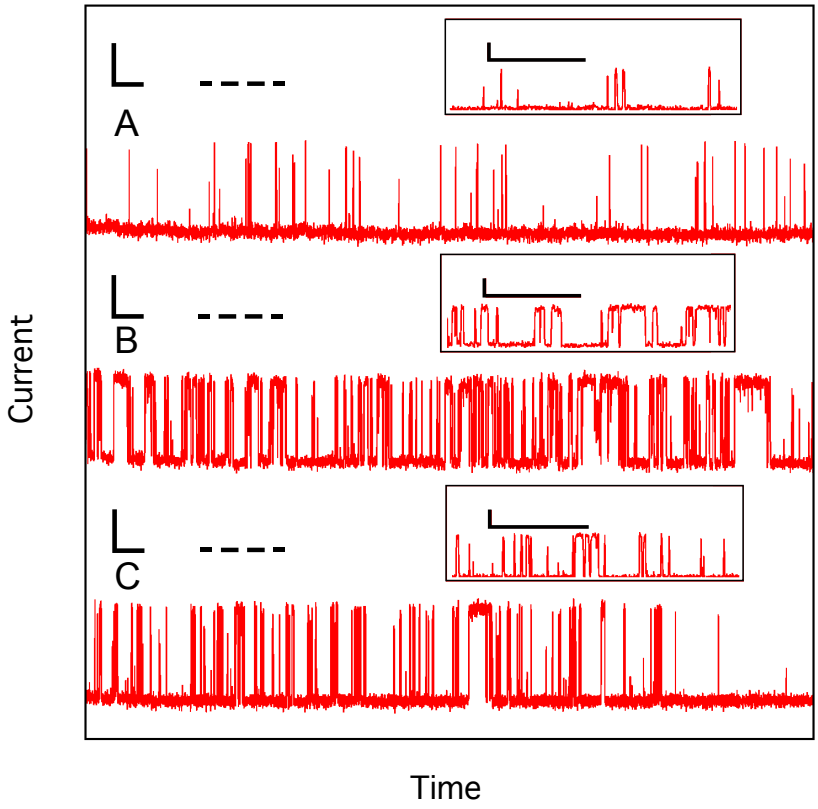

FIG. 1.26: Gating activity for a single RyR/Ca^{2+} channel reconstituted into POPE:POPC bilayers with different mole fractions, 41:59 (A), 81:19 (B), and 90:10 (C). The (B) membrane has its melting transition maximum at the experimental temperature, and clearly shows the most activity. The scale bars for current and time are 10pA and 50ms, respectively. The insets show magnified views of the regions highlighted by the dashed lines. The experiments were done at $T = 22.4°C$ and $U = +40mV$. The figure was adapted from Cannon et al. (2003).

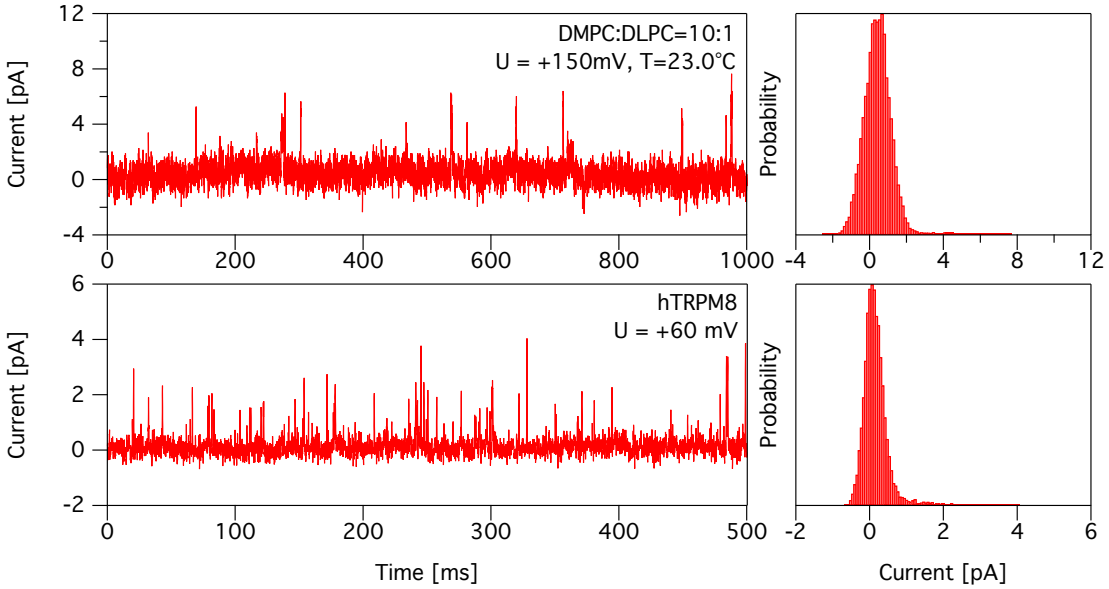

Fig. 1.27: Comparison of data from synthetic bilayers and from biological preparations. *Top:* Spikes seen in a bilayer made of a DMPC:DLPC=10:1 mixture in 150mM KCl. $U = +150$mV and $T = 23°$C. Data courtesy of Katrine Rude Laub. *Bottom:* Spikes seen from hTRPM8 in HEK293 cells in on-cell configuration at $U = +60$mV. Data courtesy of Katja Witschas.

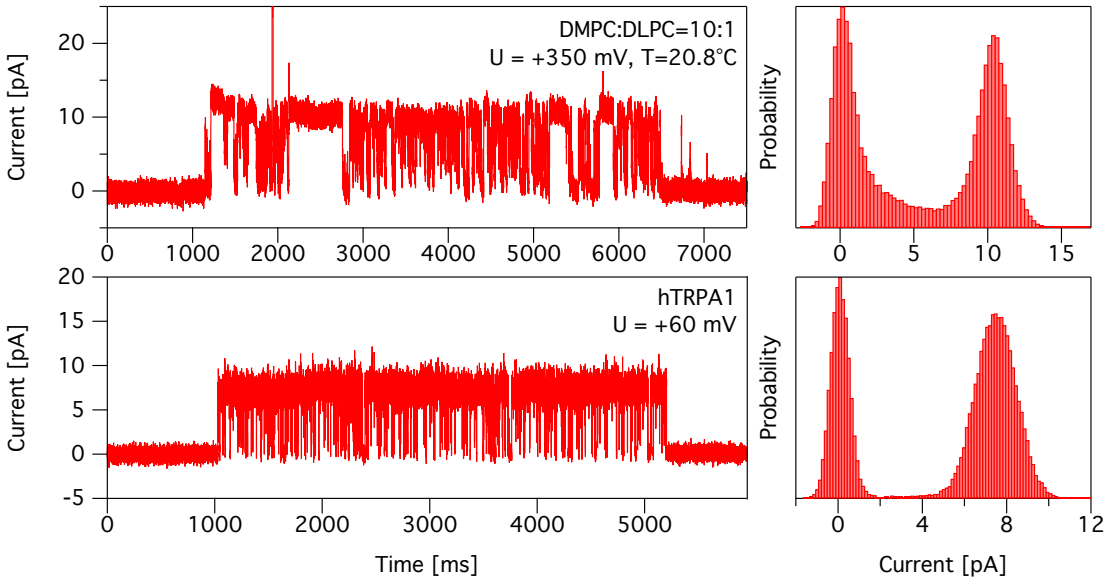

Fig. 1.28: Comparison of flickering channels. *Top:* Flickering seen in a bilayer made of a DMPC:DLPC=10:1 mixture in 150mM KCl. $U = +350$mV and $T = 20.8°$C. Data courtesy of Katrine Rude Laub. *Bottom:* Flickering made by hTRPA1 in HEK293 cells in on-cell configuration at $U = +60$mV. Data courtesy of Katja Witschas.

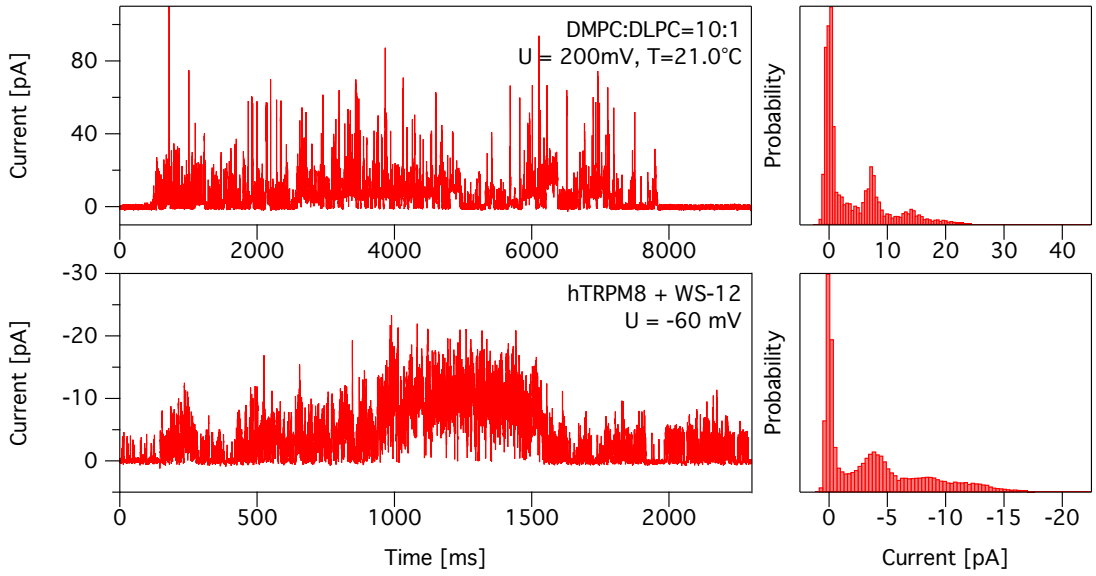

FIG. 1.29: Comparison of burst events in synthetic bilayers and in biological preparations. *Top:* Spontaneous burst activity seen in a bilayer made of a DMPC:DLPC=10:1 mixture in 150mM KCl. $U = +200$mV and $T = 21°$C. Data courtesy of Katrine Rude Laub. *Bottom:* Burst activity seen in hTRPM8 in HEK293 cells after addition of a synthetic cooling agent (WS-12) at $U = -60$mV. Data courtesy of Katja Witschas.

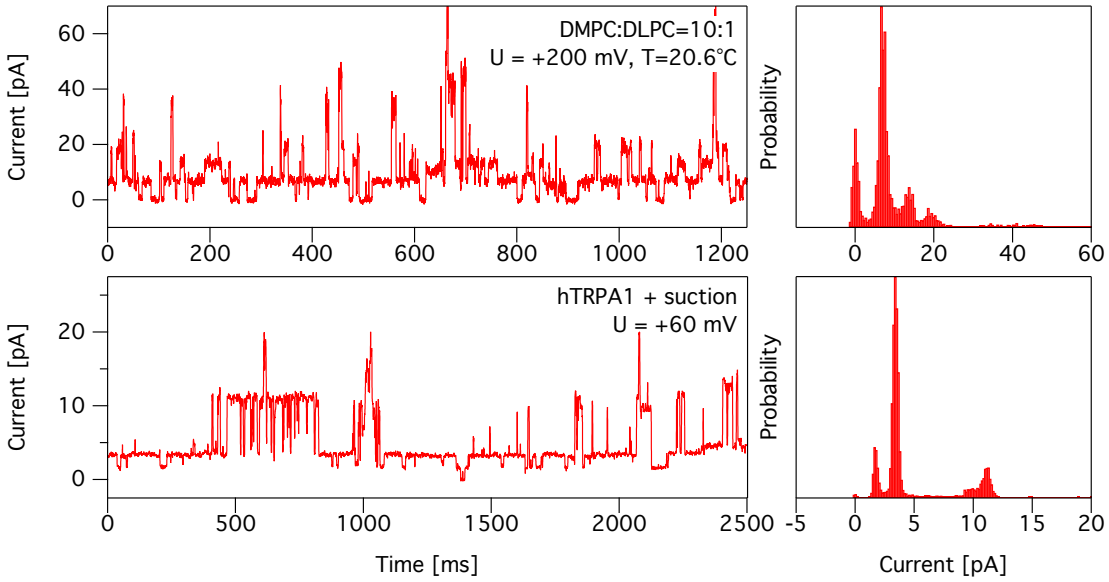

FIG. 1.30: Comparison of quantised channel events in synthetic bilayers and in biological preparations. *Top:* Quantised events in a bilayer made of a DMPC:DLPC=10:1 mixture in 150mM KCl. $U = +200$mV and $T = 20.6°$C. Data courtesy of Katrine Rude Laub. *Bottom:* Subconductance states seen in hTRPA1 in HEK293 cells after suction is applied. Made in the inside-out configuration at $U = +60$mV. Data courtesy of Katja Witschas.

1.9 Discussion

First of all, it is important to emphasise that the data presented above is *not* representative of the average experiment. The overall success rate was, at best, 10%, with the remaining 90% of the experiments only resulting in immediate membrane rupture, clogged pipettes, strongly drifting or even oscillating baselines, or simply completely uneventful traces.

The pipette method suffers from two problems. Firstly, it is not known exactly how the membrane is attached to the glass walls of the pipette, nor how the glass influences the state of the membrane. From AFM experiments it is known that glass will strongly influence the phase state of the lipid bilayer, pushing the melting transition to higher temperatures. This means that there will be a boundary layer of gel state lipids, such that even at 5–10°C above the (unperturbed) transition temperature, one will still see strong fluctuations in state close to the pipette walls, with the corresponding increased likelihood of pore formation. Also, there is no guarantee that the membrane is strongly anchored to the pipette, so it might slide in response to changes in the lateral tension of the membrane or slight pressure differences in the pipette, making it impossible to determine the area of the membrane precisely.

Secondly, and more crucially, it was not possible to reliably detect the phase transition, since the variation in membrane behaviour between different experiments was larger than the differences induced by varying external parameters like temperature or voltage. It is quite likely that this is related to the first issue of interactions with the pipette walls.[7]

Additionally, it seems likely that most of the quantised events observed in our experiments were not appearing stochastically in the bulk of the membrane, but were rather mediate by some local perturbation that makes pore formation easier in its neighbourhood. This can be deduced from the fact that in most experiments only *one* pore was open at any given instance of time, even when the open-to-closed ratio was significantly above 1. These local perturbations can either be small defects at the rim of the patch clamp pipette, or they can arise from impurities in the lipid membranes. This fits well with the idea that proteins can function as local and controlled perturbations of the lipid matrix, thereby indirectly giving rise to increased permeability of the membrane.

However, independently of these experimental difficulties, the data that has been presented in this thesis clearly shows that under certain conditions a wealth of phenomena – quantised conduction, flickering, burst activity, etc. – can be observed in pure lipid membranes, even when far away from the melting transition of the membranes. In fact, it seems that the whole spectrum of protein ion channel characteristics can be observed under certain circumstances.[8]

[7] On a side remark, it seems that experiments done on suspensions of lipid vesicles (Papahadjopoulos et al. (1973); Georgallas et al. (1987); Corvera et al. (1992); Sabra et al. (1996); Blicher et al. (2009)) give more consistent results and clearly demonstrate a strong influence of the phase transition. In addition to having the benefit of being based on the average behaviour of large ensembles, they also do not suffer from interactions with boundaries.

[8] Note that the experimental setup we used is similar (identical even) to those used by protein ion

A key issue of the spontaneous events observed in our experiments is reproducibility, especially when close to the melting transition of the membrane. Unfortunately, it is also hard to tell how carefully data is selected in the protein ion channel literature and what the overall success rate for such experiments is. Admittedly, it does seem that those groups manage to produce more consistent and reproducible data than what we observe for pure lipid membranes. Some of this is likely due to decades of experience and carefully designed protocols, but a large part of it might very well be due to the nature of the system under investigation. One could imagine that when working on complex lipid bilayers (either trinary mixtures of cholesterol and various lipids, or even native membranes), one is usually in a regime that is "far away" from any membrane transition. However, local perturbations by the pipette walls or the presence of proteins could, in principle, lead to a more confined and controllable level of fluctuations, giving rise to a more consistent behaviour for such systems. Indeed, working with pure and highly cooperative phospholipid bilayers does mean that the system will fluctuate more strongly when pushed into the transition regime, with the accompanying gamut of different phenomena.

Lastly, it is worth pointing out that most of these phenomena were observed for all the lipid mixtures we tried, including mixtures of charged and zwitterionic lipids as well as mixtures of saturated and unsaturated phosphocholines.

1.9.1 Voltage-gated lipid pores

> *The main types of stimuli that are known to cause [protein] ion channels to open are a change in the voltage across the membrane (voltage-gated channels), a mechanical stress (mechanically gated channels), or the binding of a ligand (ligand-gated channels).*
>
> – Alberts et al. (2008)

The finding of extremely voltage sensitive quantised conductance events in the absence of proteins is interesting for a number of reasons. Firstly, independently of whether it can be attributed to pure lipid fluctuations, defect mediated pore formation, or even the properties of ordered water in narrow channels, the mere fact that one observes such events proves that the phenomenon of voltage gating is a much more general one than previously thought. Clearly, voltage gating does not require complicated protein structures with finely tuned gating particles that move in response to the electric field.

The most likely explanation for the voltage gating observed in our experiments is that it is related to the difference in the capacitive energy (including the edge energy) of the system with and without a pore. This difference arises from replacing a non-conducting patch of membrane of low dielectric constant by a water-filled pore. This is supported by the fair agreement between the expected order of magnitude for the free energy dependence on the membrane potential (about -1 $\mathrm{MJ}/(\mathrm{mol}\cdot\mathrm{V}^2)$), and the experimentally determined values.

channel researchers, so any experimental "artefacts" we observed will also be an issue in those studies.

One obvious question remains regarding the spontaneous pores – there does not seem to be a particular reason for why the conductance (and therefore size) of the spontaneous pores is so stable in a given experiment. While there was variation from experiment to experiment (see Table 1.3), the conductance was extremely well-defined, with no detectable voltage-dependence in the investigated voltage range. This suggests that the pore size is perhaps not purely determined by the properties of the lipids themselves, but might depend strongly on the geometry of a local defect.

1.9.2 Pore kinetics

The theoretical framework for analysing the pore kinetics (Sec. 1.6.6) was originally developed by Millhauser et al. (1988) to explain the non-Markovian behaviour (e.g. burst activity and desensitisation) of certain protein ion channels. As demonstrated here, it is not limited to such systems, and can equally well explain the kinetics of lipid pores. Consequently, observing complex or "fractal" kinetics in a given experiment cannot be taken as a proof of the presence of a protein ion channel.

As previously mentioned, the open times for the voltage-gated pores were found to be strongly dependent on the voltage, whereas the time between pore openings was fairly insensitive to changes in the voltage. A possible explanation for this could be that the pore opening rate (which determines the waiting time between events) is mainly determined by an energy barrier that is located at small radii, e.g. by a barrier associated with the conversion from a small hydrophobic pore into a larger hydrophilic pore. If we consider the expression that was proposed for the free energy of a hydrophilic pore (Eq. (1.22)), we note that the voltage dependent terms also depend on the radius. Thus, if the energy barrier is located at very small radii ($r \ll r_{pore}$), then its height will only be weakly influenced by changes in the applied voltage. By contrast, the height of the energy barrier as seen from the "open state", would increase with the square of the voltage. This would account for the strong voltage dependence of the open times. Whether this holds in general remains to be seen.

1.10 Conclusions and outlook

So far it has been found that the quantised events observed even in the absence of proteins show the following properties:

Conductance: Conductance is of a similar magnitude as those of protein ion channels, and can even show "subconductance" states (this thesis).

Ion selective: The conductance of the channels is sensitive to the specific ion being conducted (Woodbury (1989); Antonov et al. (2005)).

Complex kinetics: Fluctuation life times are similar to that of protein ion channels, but can be anything from sub-experimental resolution to several seconds long. Lipid pores events can show both stable activity, burst activity, flickering, and even exhibit power law kinetics under certain conditions (this thesis).

Voltage gated: Under certain conditions, the spontaneous pores can exhibit a strong dependence on the transmembrane potential (this thesis).

Ligand-sensitive: The magnitude and life time of the spontaneous events can be modified and even "blocked" by the presence of e.g. anaesthetics (Blicher et al. (2009)).

Mechano-sensitive: The likelihood of pore formation is very sensitive to the lateral tension of the membrane (Kaufmann et al. (1989a)).

Rectification: Often the membrane conductance varies with voltage, and under certain conditions even shows a pronounced asymmetry with regards to the the sign of the membrane potential (this thesis).

So, from these studies we can conclude that the finding of quantised currents in itself does not prove the activity of a channel protein since protein-free membranes show very similar or even identical phenomena. Neither does complex kinetics or voltage-gating in themselves prove the action of a channel protein, since this behaviour is not limited to proteins. Similarly, the effect of drugs on the conduction events does not prove that the drug is binding to a protein, because membrane soluble drugs (e.g. general anaesthetics) have been shown to strongly influence spontaneous conductance events through their effect on the thermodynamics of the membrane. In conclusion, an analysis of channel proteins that is exclusively based on conduction events and their alteration by voltage, drugs, or some other variable must be considered logically incomplete. While the pores in lipid membranes have unambiguously been shown to exist in the absence of channel proteins, the conduction of ions through proteins cannot be measured in the absence of lipid membranes. Since the events are so similar to those found in the protein ion channel recordings, there is clearly a need for an unambiguous criterion for how to distinguish the events originating from the proteins from those of the lipid membranes. To the best of our knowledge, no such criterion exists.

1.10.1 Outlook

Verifying the predicted influence of an electric field on the phase state of the membrane still remains to be done. Sec. A.1 in the Appendix outlines a number of possible methods for measuring an influence. Nevertheless, designing a reliable experimental setup and protocol still remains a major challenge.

A different, and possibly better, approach would be to perform calorimetric studies of unilamellar vesicles that have a permanent membrane potential. This can be accomplished by creating vesicles that incapsulate charged macromolecules that are so large that they cannot penetrate the membrane (probably at least a couple of kilodaltons in molecular weight). This will give rise to a permanent Nernst potential, provided that there are other mobile ions in the solution to which the membrane is permeable (see Sec. A.2 in the Appendix for an outline). Thus, one can directly obtain the thermodynamic data with a minimum of interpretation. The main complications arise from finding an appropriate charged macromolecule that generates a sufficiently large Nernst potential without requiring buffers, and that also does not interact directly with the membranes. Caution should also be taken so as to avoid osmotic stresses on the vesicles, though this can be taken care of by the addition of some large and neutral molecules (e.g. dextran). Obviously, a number of control experiments will be required to rule out direct interaction between the molecules and the membranes, but the overall idea is simple and would allow for a direct comparison with the predictions of Sec. 1.5.1 and Sec. 1.5.2.

Currently, in our group we are trying to create giant unilamellar vesicles which one can insert an electrode into, thus allowing us to directly control the membrane potential. Ideally, this will allow us by fluorescence microscopy to directly observe a change in domain formation and structure. The main issue with this approach is that one still needs to relate the microscopy images to the precise phase state of the membranes, which is notoriously hard to do in a reliable manner.

Mobile phones and membrane permeability

2

2.1 Introduction

Ever since mobile phones became a ubiquitous part of modern life, there has been concerns about the potentially harmful effects of radio-frequency electromagnetic fields (RF EMFs) on the human body. With the growing number of other wireless devices at the office and in our homes, and the construction of more powerful cell phone towers to meet the communication demands, these concerns seem more pertinent than ever.

Exposure to low-frequency electric and magnetic fields normally results in negligible energy absorption. However, exposure to electromagnetic fields at frequencies above approximately 100kHz can lead to a significant absorption of energy and a resulting increase in body temperature (Ahlbom et al. (1998)).

For this reason, the International Commission of Non-Ionizing Radiation Protection has created guidelines for the maximally allowed exposure levels. However, these limits were set so as to avoid thermal effects – mainly excessive localised tissue heating or whole-body heat stress – of the EMF radiation, but do not take any long-term, non-thermal effects into account (Ahlbom et al. (1998)).

A large number of studies in the field have focused on the question of whether RF EMFs can promote cancer growth or result in adverse pregnancy outcomes, and the results have so far not been conclusive (Salford et al. (2003)). In general, it seems that the biological effects of amplitude-modulated EMF vary considerably with the exposure parameters and the types of cells and tissues involved, and that any such effects are small and difficult to detect.

However, some groups have found evidence for neuronal damage in the cortex, hippocampus, and basal ganglia in the brains of exposed rats (Salford et al. (2003)). Furthermore, it was also found that weak pulsed microwaves can give rise to a significant leakage of albumin through the blood-brain barrier[1], even at non-thermal exposure levels (Salford et al. (2010)).

Since no specific molecular pathway has been found for this leakage, it is of interest to investigate whether it is related to an increased passive permeability of the lipid membranes.

2.1.1 Motivation

My involvement with this side-project was when my supervisor and Dr. Salford[2] met at a conference and discussed the possibility of measuring permeability changes in model membranes when exposed to strong EMF radiation. The outcome of this meeting was that Dr. Salford's group would provide a GSM signal transmitter, which I should incorporate into our setup in order to investigate whether the increased leakage of albumin can be directly linked to an enhanced rate of pore formation induced by the EMF.

[1] The blood-brain barrier is a functional concept that was introduced to explain why many substances from the bloodstream will readily enter other tissues but not the brain.

[2] Professor at the Department of Neurosurgery, Lund University, Sweden.

2.2 Experimental setup

The radio-frequency radiation emitted from mobile phones was initially of the CW (continuous wave) type, but was later on largely replaced by the GSM (Groupe Spécial Mobile) mobile phones with pulsed fields at frequency levels of 900MHz (GSM-900) or 1,800MHz (GSM-1800) with a pulse modulation of 217Hz. The power emitted by a mobile phone can be in the range of 1–2W. Currently, most Wi-Fi devices work in the 2.4Hz or 5.8GHz band with the maximum power output restricted to 1.0W if they use omni-directional antennas.

In our setup, a computer controlled GSM-1800 mobile phone with an external antenna was used to produce an electromagnetic field with the standard pulse modulation of 217Hz.In all experiments the antenna was placed 4cm away from the membrane, and angled such that the membrane was receiving maximal exposure (i.e. the antenna's normal vector was pointing directly at the membrane as shown in Fig. 2.1). All exposures were done at non-thermal exposure levels. Unless otherwise noted, all protocols and materials were exactly as described in Sec. 1.7.

The average power output, P_{EMF}, from the GSM mobile phone could be adjusted between 1–2000mW. However, it was generally necessary to limit the power to $P \lesssim$ 100mW to avoid overloading the patch clamp amplifier. It should also be noted that P_{EMF} is the *average* output, but since the EMF is pulse modulated the peak power will be significantly higher. Modern phones are designed to reduce the output power to the minimum required for reliable communication once a call is in progress. Under optimal conditions this can be as low as 20mW, so the power levels used in our experiments were still in the relevant range.

2.2.1 Protocol

To test for an influence of the EMF, we created a lipid bilayer as in Sec. 1.7 and adjusted the voltage such that the system was close to a "voltage gating" threshold, i.e. where a small change in the membrane's properties from the EMF would be most likely to change the pore opening probability. Throughout the experiment both voltage and temperature were kept constant.

To check for reproducibility, we proceeded as follows:

I. Measure the currents for ∼5 minutes with the EMF turned *off*.

II. Turn *on* the EMF and measure for another 5 minutes or so.

III. Turn *off* the EMF again and measure for 5 minutes.

IV. Finally, turn *on* the EMF again and measure for 5 minutes.

The reasoning behind this protocol was that it allowed us to compare the data from segment (I) vs. (III) and segment (II) vs. (IV) so that we could get an idea about any slow drift in membrane behaviour. Only then was it possible to gauge how strongly the EMF influenced the membrane.

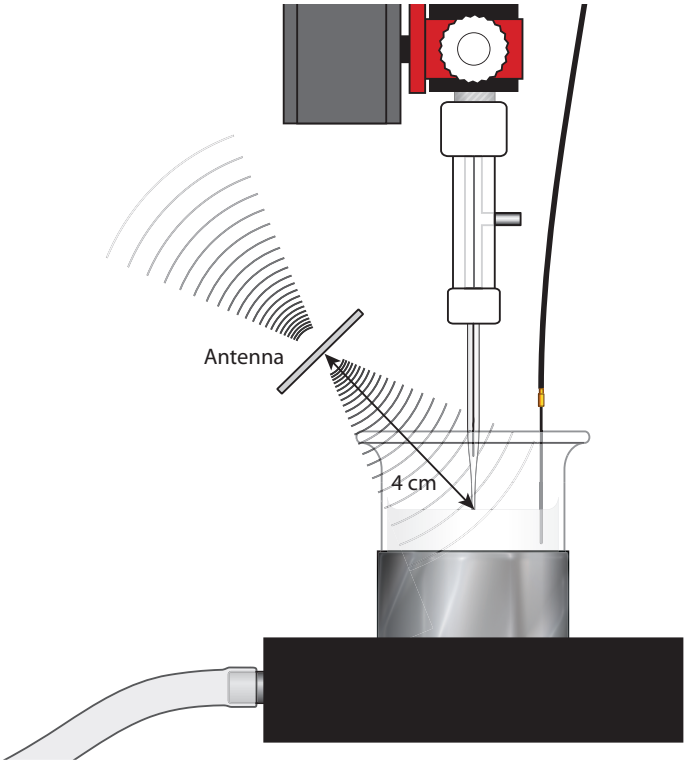

FIG. 2.1: Schematic drawing of the modified setup showing the position of the external mobile phone antenna. See Fig. 1.16 for a larger view of the setup.

2.3 Results

A typical data trace is shown in Fig. 2.2. As can clearly be seen, when the EMF was turned on, large amplitude noise appeared that partially obscured the actual signal. This noise was also present, though of lower amplitude, even with an open circuit, indicating that it was not related to a real (ohmic) current between the electrodes (data not shown).

Fig. 2.3 shows the current histograms from the same trace. While there is a slight drift in pore open probability, there does not seem to be any significant influence of the EMF within the experimental reproducibility.

Unfortunately, due to the high noise, it was not possible to reliably extract the event time distributions and associated kinetic rates, so instead power density spectra were calculated (Fig. 2.3, bottom), since these can – in principle – be used to tell whether the kinetics are changed significantly. The spectra shown in Fig. 2.3 do show a reproducibly influence, having a slight change in slope and a pronounced shoulder above ∼100Hz. However, subsequent experiments failed to show this (see e.g. Fig. 2.4), so it is not possible to draw any real conclusions. In particular, it is not clear whether the change is simply a noise signature of the GSM signal, or due to a actual changes in membrane behaviour.

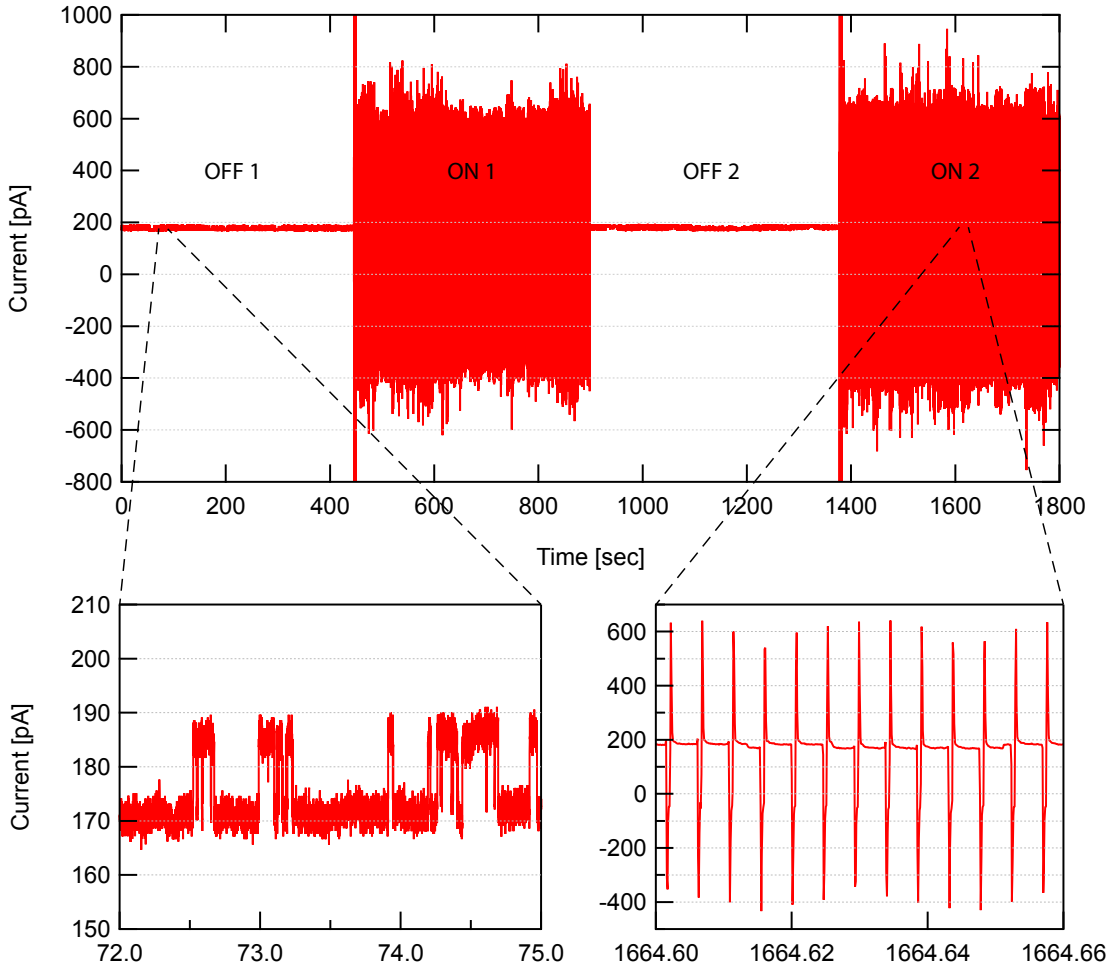

Fig. 2.2: Raw data from the experiment with $P_{EMF} = 30$mW. *Top:* measured current showing how the pulse modulated EMF adds large amplitude noise. *Bottom:* Magnified view of the data trace showing clear quantised events (*left*), and periodic spikes arising from the EMF's pulse frequency of 217Hz (*right*). The holding potential was +50mV and the temperature was 29°C.

Lastly, if the P_{EMF} was set to more than 200mW, the membrane was often destabilised, i.e. showing a dramatic change in baseline level or even complete membrane rupture. It is quite likely that this was caused by the patch clamp electrodes themselves picking up the EMF, which can give rise to a transient potential difference of several volts (personal communication with the Niels Bohr Institute's electrical engineers). This is more than sufficient for outright electroporation of the membrane.

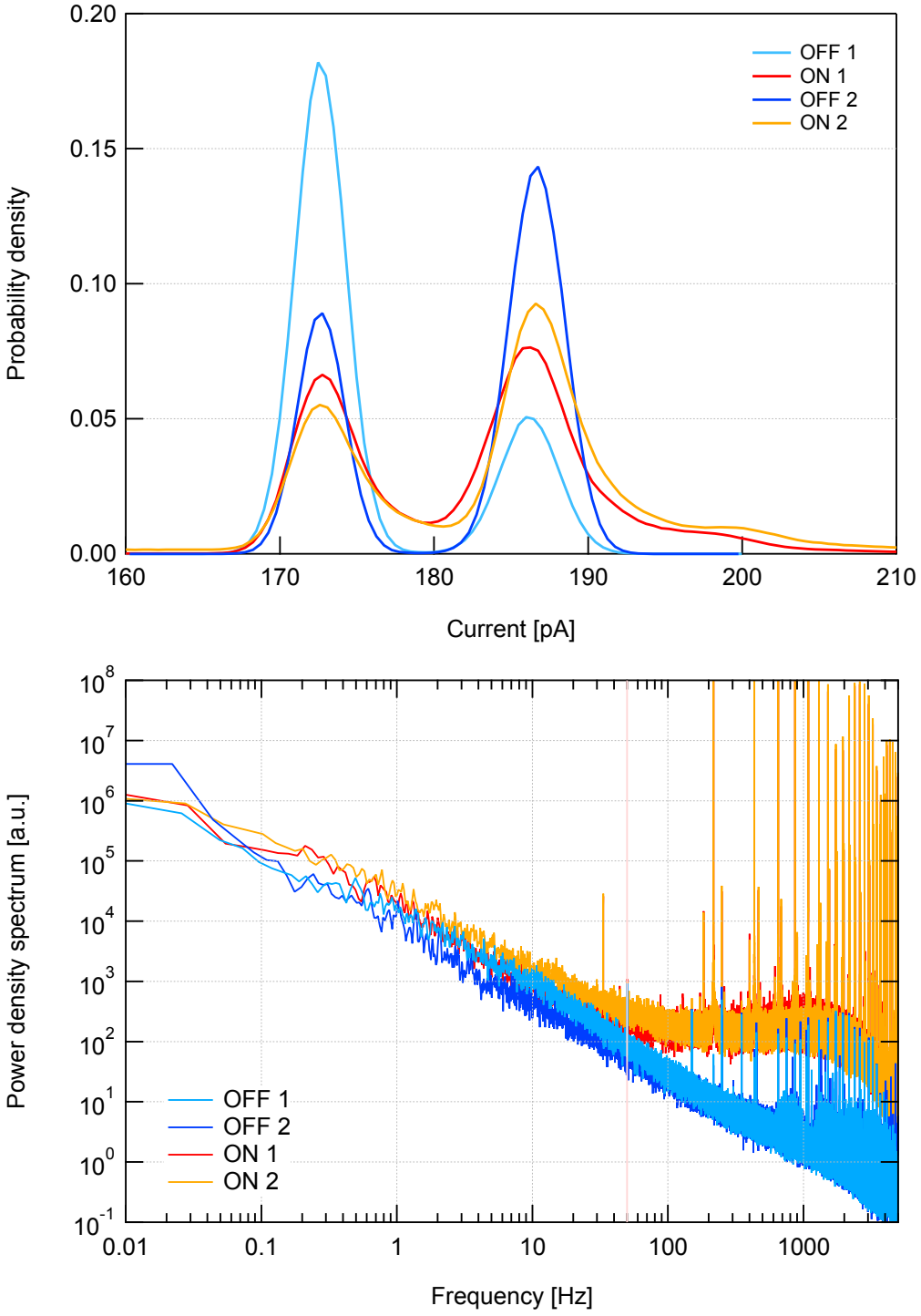

FIG. 2.3: Analysis of the trace in Fig. 2.2. *Top:* Current histograms showing two clear conductances levels (pore open or closed). *Bottom:* Power density spectrum of the current trace showing a pronounced increase in high-frequency noise in addition to the sharp peaks from the pulse frequency of 217Hz and its harmonics.

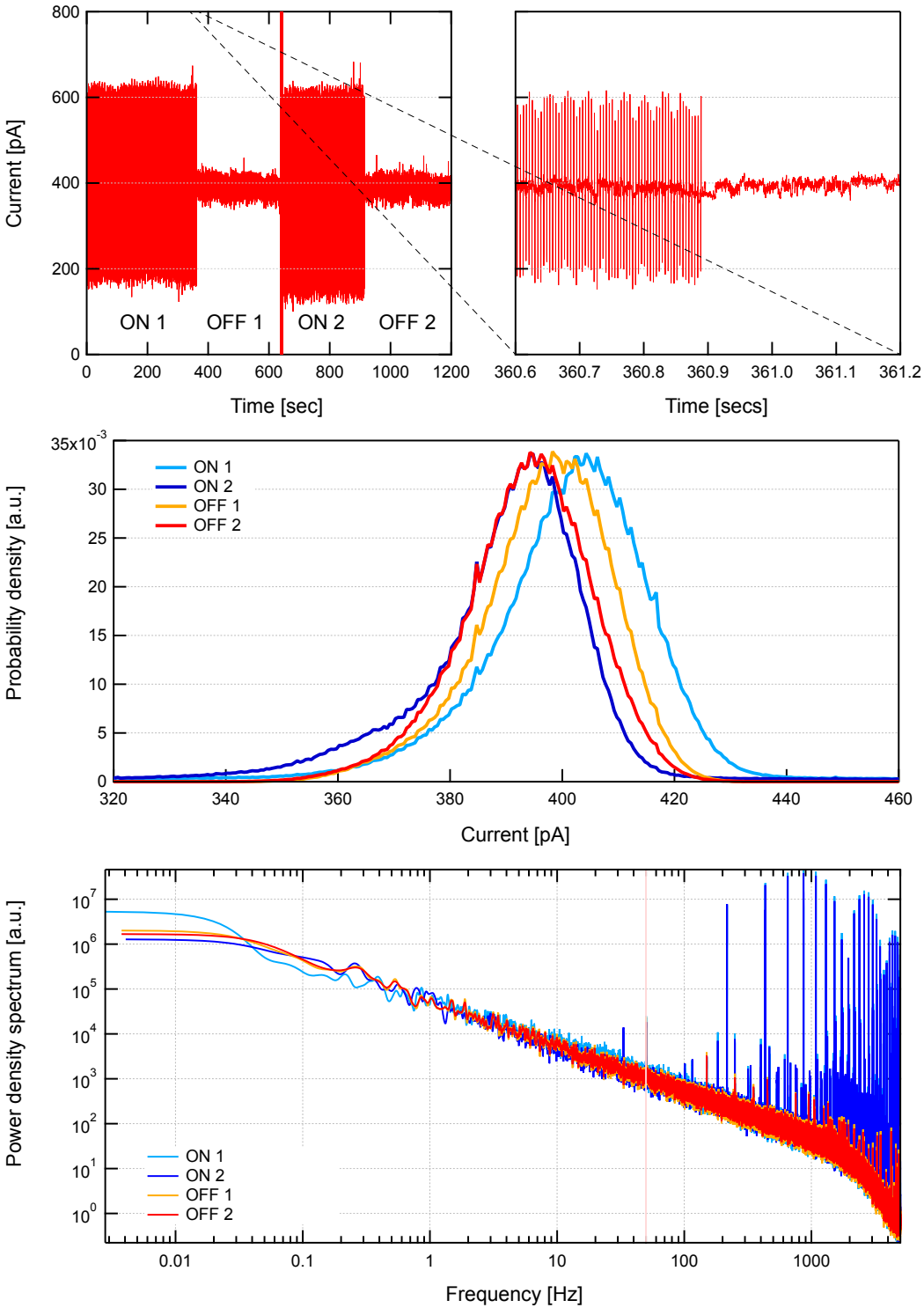

Fig. 2.4: Another measurement on a different membrane, using a holding potential of +80mV, the temperature set to 29°C, and P_{EMF} = 30mW. *Top:* Raw data again clearly showing the additional noise caused by the EMF. *Middle:* Current histograms showing only a slight change with time. This is most likely to be due to a slight baseline drift, and not due to an influence of the EMF. *Bottom:* Power density spectrum of the current trace showing no influence of the EMF, apart from the 217Hz noise (plus harmonics).

2.4 Discussion

Ultimately, we decided not to pursue these experiments any further for a couple of reasons.

First and foremost, there is an inherent problem with using a patch clamp setup for such measurements, since the electrodes themselves act as antennas and therefore pick up the EMF directly. This results in an additional, uncontrollable potential difference between the electrodes, making it impossible to attribute any changes in the measured signal to changes in membrane properties, since the membrane potential will be unknown and possibly unstable (depending on the construction of the amplifier and headstage). It is conceivable that with sufficient screening and correct positioning and angling of the electrodes and antenna it would be possible to reduce this problem to a manageable level. Unfortunately, such method development was beyond the scope of this thesis.

Secondly, it seemed that when the issue above did not drown out the real signal, there was no significant and reproducible influence on the membrane behaviour (mean conductance or pore formation likelihood). So it seems that the influence of the mobile phone EMF at normal levels must be small, e.g. on the level of a change in the transmembrane potential by less than 5mV.

While I find the fundamental question intriguing and worth serious investigation, I can only conclude that other methods are better suited for such studies. One option could be to use an ensemble method where one studies the passive leakage of ions or small molecules out of a large population of lipid vesicles (see e.g. Blicher et al. (2009)). These methods have the great advantage that they will not suffer from uncontrollable EMF pickup by the experimental equipment. They also use setups that would usually allow for easy incorporation of the GSM antenna.

Monte Carlo simulations of lipid membranes

3

3.1 Introduction

It could be argued that modern physics research can be divided into three areas, namely theoretical, experimental, and computational. The use of computers to mimic physical systems as accurately as possible provides a useful and unique tool to bridge the gap between theory and experiment, as they can provide well-behaved experimental systems.

The range of applicability and accuracy of computer models is only limited by the computational processing power available – a limitation which gets less severe every year, thanks to the continual development of more advanced computer technology.

This chapter will describe two simple models of lipid membranes that we have studied by means of numerical simulations.

3.1.1 The Monte Carlo method

The Monte Carlo method is a particularly powerful and versatile approach which was introduced by Metropolis et al. (1953) at the dawn of the computer age. Monte Carlo simulations encompass a very broad variety of algorithms and variations, from what is generically known as statistical sampling to the more recent Quantum Monte Carlo. It is a universal algorithm that can be applied to a large range of systems, but it is especially useful when studying systems with a large number of coupled degrees of freedom (liquids, disordered materials, polymers, or even economics). In fact, its relative efficiency (when compared to other numerical methods) increases with the dimension of the problem. Monte Carlo simulations – like genetic algorithms and artificial neural networks – are stochastic in that they rely heavily on the use of random or pseudo-random number generators to mimic the fluctuations characteristic of finite temperatures.

In short, a Monte Carlo simulation can be thought of as a random walk through state space of the model under study, exploring the Boltzmann distribution of states in an effective manner. If properly set up, the Monte Carlo simulation will bring the system to its equilibrium state (or rather equilibrium distribution of states), which makes it possible to evaluate thermodynamic averages for the equilibrium state.

3.1.2 Motivation

The appeal of the Monte Carlo method is that it is straightforward to implement and analyse, making it ideally suited as a first attempt at understanding the cooperative behaviour of a system. For this reason we have used it to get a rough idea about the qualitative behaviour of a lipid bilayer, especially in the vicinity of the main melting transition. In this thesis the interleaflet coupling (Sec. 1.4.3) and head group tilt (Sec. 1.5.2) have been investigated. In the past we have used it to describe membrane permeability (see Wodzinska et al. (2009) in the Appendix).

3.2 Theory

This section will introduce the key concepts behind the various Monte Carlo simulations presented in this thesis.

3.2.1 Importance sampling

A common aim in statistical mechanics is to determine the average value of some thermodynamic observable, such as the enthalpy, area, or magnetisation, which is a weighted sum over all possible states (following the Boltzmann distribution):

$$\langle X \rangle = \frac{\sum_i X_i W_i}{\sum_j W_j} = \frac{\sum_i X_i e^{-H_i/RT}}{\sum_j e^{-H_j/RT}} \tag{3.1}$$

For a two-state Ising model on a lattice with N sites, this sum will be over 2^N configurations. So even for a relatively small system this number will be so large that a direct evaluation will be impossible. For instance, if $N = 100$ one would have to sum over $2^{100} \approx 10^{30}$ configurations, which would not be possible to complete within one's lifetime[1].

So for anything but the most conservative system sizes, getting an exact answer by direct evaluation is simply impossible. However, there are two important considerations that make Monte Carlo simulations useful by ensuring that a good estimate can be calculated with high accuracy.

1. Despite the fact that Eq. (3.1), in principle, is a sum over a very large number of configurations, in many cases the Boltzmann weights, W_i, will be finite only in a small region of state space. That is, even if the number of configurations outside this region is very large, if their weights are exponentially small, the answer will depend almost exclusively on a tiny fraction of the entire parameter space.

2. In particular, very often $\langle X \rangle$ will not depend on the details of most sub-states. So, if we have a representative set of states, S_i, we can get a very accurate estimate for $\langle X \rangle$. For example for the Ising model, the magnetisation $\langle M \rangle$ of a system of N spins can only have $N + 1$ different values. Therefore, a representative set for this system will only be of order N.

So in other words, if one can find a representative set of configurations to sum over, and picking from these at random, it is possible to get a good estimate for $\langle X \rangle$. Even better, if one can select configurations such that the ones with larger weights are more likely to be chosen, then one can obtain an equally accurate answer by summing over even fewer terms. Lastly, thanks to the fluctuation-dissipation theorem, it is also straight forward to determine various susceptibilities of the system, since these are related in a simple manner to the first and second moment of the related variables (Sec. 1.4.4).

[1] A modern supercomputer can perform around 10^{15} floating point operations per second, which means that it would take tens of millions of years to finish!

3.2.2 Implementing the Monte Carlo method

Having a statistical mechanical model is only half the work – one also has to obtain actual information from it. As very few models are tractable to analytical approaches or direct evaluation, one needs another way to handle this, as described in Sec. 3.2.1.

The Monte Carlo algorithm generates a series of random configurations – or Markov chain[2] – which will then be accepted or rejected in the sum according to some probability, which are functions of the weight ratios. It is here crucial that the random generation of configurations is ergodic, i.e. given sufficient time, all possible configurations must eventually be generated.

In general terms, the Markov chain is generated in the following way:

1. One starts from the actual system configuration, S_1. Then one of several possible trial moves are performed, resulting in a new configuration, S_2.

2. Calculate the difference in the free energy of the two configurations, $\Delta G = G(S_2) - G(S_1)$, and calculate a Boltzmann factor, i.e. $K(T) = e^{-\Delta G/RT}$, where R is the gas constant and T the temperature.

3. Generate a random number, z, with $z \in [0:1]$, and compare it to the acceptance probability, $P_{acc} \equiv \frac{K(T)}{1+K(T)}$.

4. If $z < P_{acc}$ then the new configuration, S_2, is accepted. If $z > P_{acc}$ then the new configuration is discarded, and the system reverts to the old configuration, S_1.

At the heart of the sampling algorithm is the step where a given sub-state is either included or rejected. The purpose of the rejection sampling algorithm is basically to generate a sequence of samples from a probability distribution that is difficult to directly sample from, such that

$$\frac{\sum_i X_i N_i}{\sum_j N_j} \rightarrow \frac{\sum_i X_i W_i}{\sum_j W_j}, \tag{3.2}$$

where N_i is the number of times the state S_i was summed, and W_i are the Boltzmann weights as in Eq. (3.1).

This rejection procedure is the well-established Glauber algorithm (Glauber (1963)). Alternatively, one can use the algorithm of Metropolis et al. (1953), where one sets the probability to $P_{acc} = K(T)$ or $P_{acc} = 1$ if $K(T) > 1$. As both algorithms obey detailed balance, they will lead to the same result[3]. Regardless of the specific choice, the system will converge to a steady state where each state is sampled in accordance with Boltzmann statistics, i.e. $P_i \propto \exp(-G_i/RT)$.

Once we have defined the Monte Carlo steps and a procedure, we can also define a Monte Carlo cycle. A Monte Carlo cycle is defined as one iteration (on average) of each type of Monte Carlo step per lattice site.

[2] A Markov chain is a series of states of a system which are conditionally independent of the past states (the path of the process).

[3] To be more precise, they will only lead to the same result after sufficiently long runtime as the equilibration times may differ.

3.3 Models

This section will describe two models for lipid membranes. The first one seeks to estimate the mean orientation of the lipid head groups. The second model investigates the consequences of interleaflet coupling. This is then followed by a simulation of the asymmetric influence of an electric field on a lipid bilayer of symmetric composition, using the results obtained from the first model.

3.3.1 Modeling head group tilt

Since the late 1970'ies it has been known that the electrical dipole of the lipid head group is oriented mostly in the plane of the bilayer. However, getting an exact orientation is difficult because of the high flexibility of lipid head groups. Moreover, how much the orientation changes with the phase state is not exactly known either.

In order to be able to make a rough estimate of the head group tilt, I made a simple Monte Carlo simulation based on the model of Mbamala et al. (2006).

In this model, the membrane is mimicked by a single, two-dimensional triangular lattice, where each lattice site contains a zwitterionic lipid. It is furthermore assumed that the negative charge of the zwitterion is fixed at $z = 0$, and that each pair of negative and positive charges are separated by a constant bond length, $L_{\pm}$. The positive end of the zwitterion is free to explore the immediate environment with the upper half-sphere of radius, $L_{\pm}$, via the tilt angle, $\theta \in [0, \pi/2]$, and the azimuthal angle, $\varphi \in [0, 2\pi]$ (Fig. 3.1).

It assumed that the charges are in an aqueous environment of dielectric constant, $\epsilon_w \approx 80$, and with a Bjerrum length of $\ell_B = 7.15$Å. The aqueous environment also contains a binary salt that gives a screening length of $\ell_D = 10$Å.

With these assumptions, we model the interaction between the charges at location $\vec{r}_i$ and $\vec{r}_j$ with a screened Coulomb potential

$$\frac{u_{ij}(r_{ij})}{k_B T} = \ell_B Q_i Q_j \frac{\exp(-r_{ij}/\ell_D)}{r_{ij}}, \tag{3.3}$$

where $r_{ij} = |\vec{r}_i - \vec{r}_j|$ and $Q_i = \pm 1$ is the charge of the ions in units of the elementary charge, e. The energy of a given configuration is then calculated as the sum over all charge pairs, i.e. $G = \sum_{i,j} u_{ij}$.

In the article of Mbamala et al. (2006) they also tried to include the effect of induced image charges from the low dielectric constant membrane interior, but found that it did not qualitatively change their results. Furthermore, the very concept of image charges is not very well defined for systems on the molecular scale, with discrete, point-like charges interacting. Consequently, they were not included.

The model was evaluated by means of the standard algorithm discussed in Sec. 3.2.2 with two kinds of Monte Carlo steps. The first step was to choose a random site and change the azimuthal angle, φ, to a new and random value between $[0, 2\pi]$. The second step was to change the tilt, θ, of the dipole to a random value between $[0, \pi/2]$. For infinite screening, we know that the positive charges must distribute evenly between

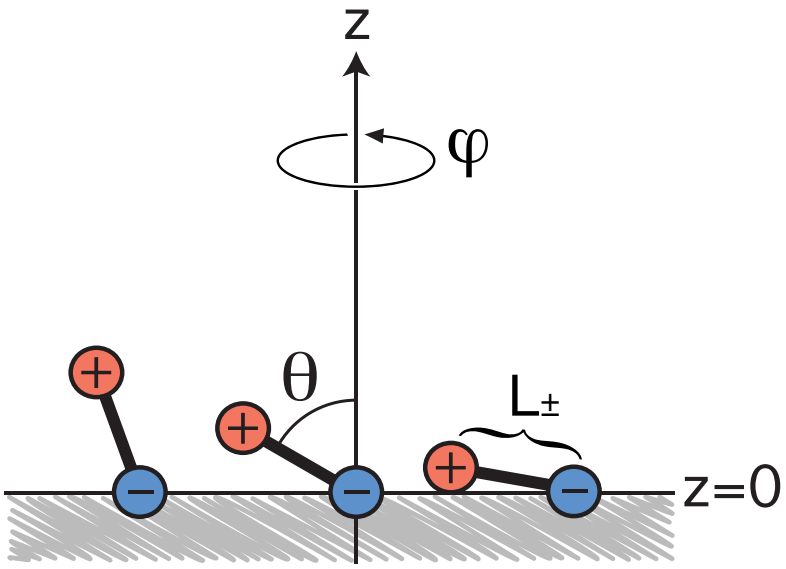

FIG. 3.1: Illustration of the head group tilt model showing the definitions of the variables.

$0 < z < L$. This means that the the random tilt angle can be generated by setting $\theta_{new} = \arccos(Z)$, where Z is randomly drawn from a uniform distribution between 0 and 1. This gives a $\langle\theta\rangle = 57.29°$ for $\ell_D \to 0$.

The system was first equilibrated for 2000 Monte Carlo cycles and then sampled θ_i, to calculate the average tilt for the zwitterions for the next 2000 cycles.

By using this model to evaluate the average tilt of the head groups as a function of lipid spacing (Fig. 3.2), we found that $\langle\theta\rangle_{gel} = 68.7°$ and $\langle\theta\rangle_{fluid} = 64.1°$, i.e. that in the denser phase the head groups are more parallel with the bilayer surface. This is perhaps not very surprising, given that as distances increase, the head group orientation will be more and more random, going asymptotically towards $\langle\theta\rangle_{random} = 57.29°$.

This simple model also shows that in the realistic range of lipid spacing, the force between head groups is *repulsive*, which is in nice agreement with the findings of Jacobs et al. (1975). Also the magnitude of the electrostatic energy per head group agree fairly well, being about $2.9k_BT$ in the gel state, as compared to the $6.6k_BT$ estimated in the article. Note that the exact value from my simulation is strongly dependent on the screening lengths, as each ion interacts with a larger and larger neighbourhood.

The mean tilt is not very sensitive to the ionic screening (Debye length), varying by a few degrees at most (data not shown). This is because the nearest neighbour interaction is dominating, making the longer ranged interactions fairly unimportant. Lastly, it must be emphasized that the exact numbers should not be taken too seriously, but merely serve to give a rough idea of how things qualitatively behave, allowing us to make estimate the influence of an electric field on the state of the membrane as discussed in Sec. 1.5.2. The aim of the following model is to the qualitatively describe this influence.

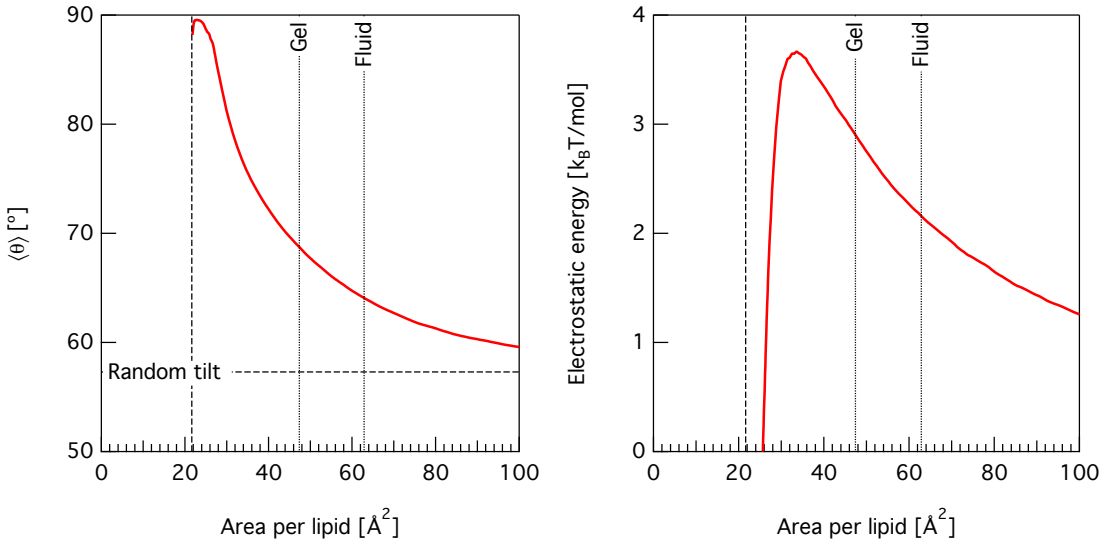

FIG. 3.2: *Left:* Average head group tilt as a function of lipid area. $\langle\theta\rangle$ denotes the mean tilt (in degrees) of the head groups with respect to the membrane surface normal. *Right:* Mean electrostatic energy per head group as a function of lipid area. As can be seen, the head group interactions are repulsive. The divergence at small area stems happens when the lattice spacing exactly matches the dipole length, $L_{\pm}$. The parameters were as follows: $\ell_D = 10$Å, $\ell_B = 7.15$Å, and $L_{\pm} = 5$Å. System consisted of 32×32 zwitterions on a triangular lattice.

3.3.2 Simple model for lipid melting

Our model is based on the famous spin$\frac{1}{2}$ Ising model. This model was first proposed by Wilhelm Lenz in 1920 to study the phase transition of ferromagnets at the Curie temperature (Brush (1967)). It was later fully worked out by his pupil Ernst Ising for the one dimensional case (Ising (1925)), while the two-dimensional case (in the absence of a field) was worked out by Lars Onsager 19 years later (Onsager (1944)).

At its most basic, the Ising Hamiltonian is given by

$$\mathcal{H} = -\frac{\epsilon}{2}\sum_{\langle i,j\rangle}\sigma_i\sigma_j - h\sum_i \sigma_i, \tag{3.4}$$

where $\sigma_i = \pm 1$ are the two spin states allowed on each lattice site, ϵ is the nearest neighbour interaction parameter (also known as the coupling constant), and h is the magnetic field. Here $\langle i,j\rangle$ denotes that the sum is only over nearest neighbours. The first term in Eq. (3.4) is responsible for the cooperative behaviour and the possibility of a phase transition.

This simple model is of great importance and has wide applicability, as any two-state system can be mapped onto it with only slight modifications. Examples include lattice gasses, CuZn mixing, and lipid membrane melting.

The two-state Ising model for the melting of lipid membranes was first proposed by

Doniach (1978), and the fundamental assumptions are essentially the following: each lipid molecule can only be in one of two states, namely

- A gel state with low enthalpy H_g and low entropy S_g
- A fluid state with high enthalpy H_f and high entropy S_f

Though more complex lattice models such as the 10-state Pink model have been used in the literature (Pink et al. (1980); Georgallas and Pink (1982); Mouritsen et al. (1983)), the added complexity of these models does not significantly alter the overall physical behaviour of the two-state model (Mouritsen et al. (1983)). The reason for this is that the melting transition is a cooperative phenomenon with a length scale much larger than a single lipid, making the modelling of molecular details superfluous. In addition, the two-state model has the advantage that it contains very few parameters, all of which can be determined by calorimetric experiments (Ivanova and Heimburg (2001)).

The interactions between molecules are normally governed by van der Waals and electrostatic forces as well as interchain steric repulsion. However, in the our simplest model each lipid will only interact with its nearest neighbours on the lattice, implicitly assuming that the lipids' interactions with next-nearest neighbours and the other membrane leaflet are negligible.

Lastly, all of the lipids are assumed to be hexagonally packed[4], which means that each lipid has $z = 6$ adjacent lipid neighbours (z is the so-called coordination number). The assumption of a hexagonal packing does not strictly hold in the fluid phase, and will consequently also influence the shape of the domains. Also, this will neglect the contributions to the entropy from the spatial disordering, but since the melting transition is dominated by the chain melting entropy, the effect of this will be minor (Doniach (1978)).

With these approximations, the model only contains three parameters, namely the enthalpy of melting, $\Delta H = H_f - H_g$, the entropy of melting, $\Delta S = S_f - S_g$, and an unlike nearest neighbour interaction, ω_{fg}[5]. So, for a given configuration, the total Gibbs free energy will be

$$G = G_g + N_f(\Delta H - T\Delta S) + N_{fg}\omega_{fg}, \tag{3.5}$$

where G_g is the free energy of the pure gel state membrane and can be set to zero, N_f is the number of lipids in the fluid state, and N_{fg} is the number of contacts between fluid and gel lipids.

In this model ω_{fg} is a cooperativity parameter, similar to the coupling constant, ϵ, in the spin$\frac{1}{2}$ Ising model, and it determines the sharpness of the transition. Thus, all three of these parameters can be uniquely determined from calorimetric measurements, meaning that there are no free parameters with arbitrary values (Ivanova and Heimburg (2001)).

[4] This is realised by placing the lipids on a triangular lattice with periodic boundaries, resulting in a topology akin to that of a torus.

[5] $\omega_{fg} \equiv \epsilon_{fg} - (\epsilon_{gg} - \epsilon_{ff})/2$, where ϵ_{ij} is the interaction energy between lipids in state i and j.

This model is essentially a two-state Ising model on a triangular lattice with a temperature dependent field. So if we set $\sigma_i = -1$ for lipids in the gel state and $\sigma_i = +1$ for those in the fluid state, the "field" would be $h = (T\Delta S - \Delta H)/2$. Note that at the transition point $h = 0$, and one can therefore apply some of the analytical results from two-dimensional spin$\frac{1}{2}$ Ising model results. For instance, for a triangular lattice the critical interaction strength is given by (Wannier (1945))

$$\omega = RT_m \frac{\ln 3}{2} = 1434.8 \text{ J/mol}, \tag{3.6}$$

for $T_m = 314.15$K, the melting point of DPPC.

Since pure, single-component lipid systems are known to be close to their critical point (Albon and Sturtevant (1978)), one would expect the right value for ω_{fg} to be close to this value. Indeed, the best agreement with calorimetric data is obtained if we set $\omega_{fg} = 1326$J/mol for a simulation of unilamellar DPPC membrane ($\Delta H = 36.4$kJ/mol and $\Delta S = 115.87\text{J}/(\text{K}\cdot\text{mol})$).

Obviously, this model is not correct on molecular scales since it only contains two states of the lipid – which is, of course, a gross approximation. Furthermore, interactions with the other monolayer as well as fluctuations in the third dimension are also ignored. However, the two-dimensional Ising model has its strength in the description of macroscopic fluctuations (Mouritsen et al. (1983)), irrespective of molecular details, and is quite successful despite its apparent simplicity. For instance, with a few simple additions we have managed to described the intimate coupling of the membrane permeability to the melting transition. For the full details of this model I refer to Blicher (2007) or Wodzinska et al. (2009).

3.3.3 Simple model for bilayers

The two-state model described above is as simple as it gets, and has been studied in great detail by a number of people in a variety of contexts (Doniach (1978); Georgallas and Pink (1982); Mouritsen et al. (1983); Georgallas et al. (1984); Mouritsen and Zuckermann (1985); Heimburg and Biltonen (1996); Sugar et al. (1999); Heimburg (2000); Ivanova and Heimburg (2001); Ivanova et al. (2003); Hac et al. (2005); Fidorra et al. (2009b)).

Fortunately, it is easy to expand upon, so in this section we will introduce a minimalistic model for a bilayer with two interacting leaflets. This allows us to estimate how a membrane would behave under the influence of an asymmetric perturbation such as an electric field.

To take the interleaflet coupling into account, we introduce a weak coupling between the monolayers, using the value estimated in Sec. 1.4.3 of 127J/mol. In this model, the coupling is expressed in the simplest possible manner, namely each lipid is only interacting with one lipid in the opposing leaflet in addition to its six neighbours within its own leaflet. In this case, it is straightforward to show that the Hamiltonian takes the following form:

$$G = G_g + N_f(\Delta H - T\Delta S) + N_{fg,nn}\omega_{fg} + N_{fg,tb}\omega_{fg,tb} \tag{3.7}$$

where N_f again is the number of lipids in the fluid state, ΔH and ΔS the enthalpy and entropy of melting, $N_{fg,nn}$ and $\omega_{fg,nn}$ the number and energy cost of nearest neighbour interactions within the leaflets, and $N_{fg,tb}$ and $\omega_{fg,tb}$ are similarly the interactions between top and bottom leaflet.[6]

As discussed in Sec. 1.4.3, having a positive coupling between the two leaflets gives rise to a higher line tension and cooperativity, which is also evident in Fig. 3.3. In effect, even a relatively weak interleaflet coupling will push the system to its critical point, as has also been found in early Monte Carlo studies of interleaflet coupling (Georgallas et al. (1984); Zhang et al. (1992)). To adjust for this additional contribution such that the simulated heat capacity matches the calorimetric one, it was necessary to reduce the nearest neighbour interaction to $\omega_{fg,nn} = 1250\text{J/mol}$. The end result is something that is very similar, though not identical, to the simpler model of Sec. 3.3.2. Also, it was found that even for a relatively weak positive coupling, the domains stay in close registry, as expected and in perfect agreement with experiments (Fig. 3.5).

Lastly, it was found that a *negative* coupling between the leaflets will cause the heat capacity profile to split up, as each leaflet tries to undergo its transition before or after the opposing leaflet (see Fig. 3.4 and Fig. 3.5).

Asymmetric perturbations

When an asymmetric perturbation is applied to the bilayer, the enthalpies take the form

$$\Delta H_{top} = \Delta H + \delta H \tag{3.8}$$

$$\Delta H_{bottom} = \Delta H - \delta H \tag{3.9}$$

where $\delta H = qV_m \frac{L}{d}(\cos\theta_f - \cos\theta_g)$ is the perturbation to the enthalpy due to an electric field. Here qL is the dipole moment of the lipid head group, V_m the membrane potential, d the bilayer thickness, and θ_i the tilt of the head group in state i (see Sec. 1.5.2). It is also assumed that it does not significantly change the entropy of either state.

As can be seen in Fig. 3.6 a sufficiently strong electric field will first cause a simple broadening of the heat capacity profile, and finally result in a splitting of the melting peak into a peak for each leaflet. This, of course, is under the assumption that the interleaflet interaction energy is not significantly influenced by the electric field and that the main influence on a given lipid leaflet is an energetic favouring of either the fluid or the gel state. Also, electrostriction has not been taken into account, since this will have a trivial influence on the heat capacity profile.

[6] In Sec. 1.4.3 this was called γ, but has been renamed here for the sake of a clearer notation.

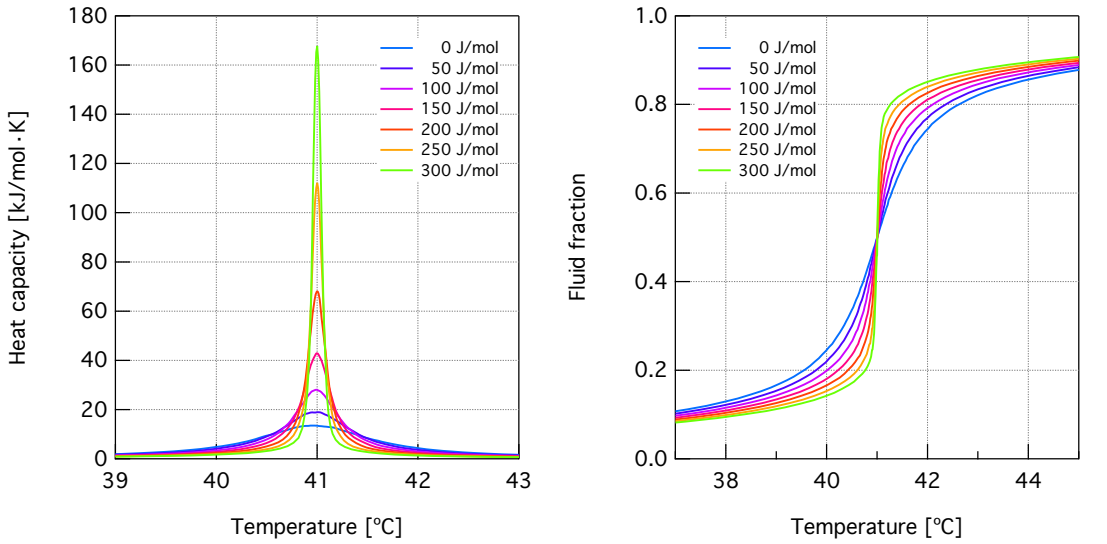

FIG. 3.3: Simulated heat capacity and fluid fraction for a DPPC bilayer, shown as a function of interleaflet coupling strength. As can be seen, the transition regime becomes increasingly confined with increasing coupling strength. System size was 32×32 lipids in each leaflet, and $\omega_{fg,nn} = 1250\text{J/mol}$, $\Delta H = 36.4\text{kJ/mol}$, and $T_m = 41°\text{C}$.

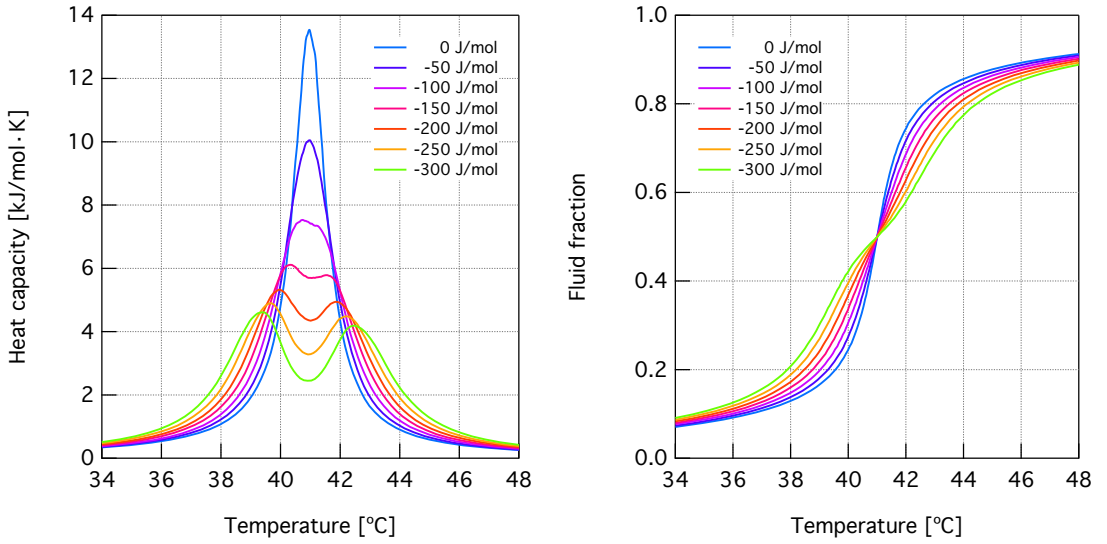

FIG. 3.4: Simulated heat capacity and fluid fraction for a DPPC bilayer with various negative mismatch energies, $\omega_{fg,tb}$. At larger values the two leaflets' melting temperatures shift. Apart from $\omega_{fg,tb}$, all parameters were as in Fig. 3.3.

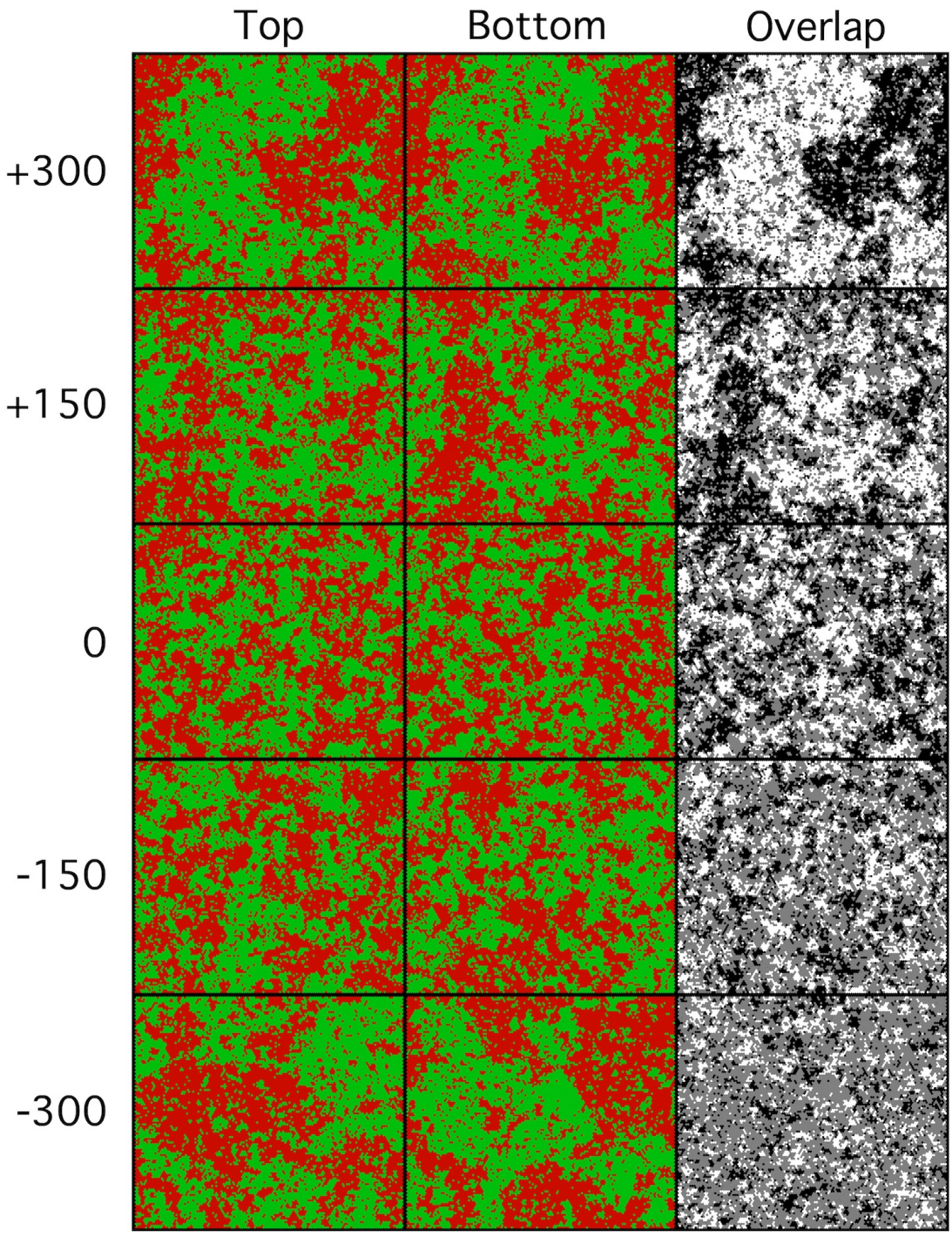

FIG. 3.5: Snapshots from a DPPC bilayer simulation shown at the transition temperature, $T = T_m$, and with varying mismatch energies, $\omega_{fg,tb}$. Gel state lipids are shown as red, fluid state as green, and the overlap as white for fluid/fluid, grey for fluid/gel, and black for gel/gel. System size was 128×128 lipids in each leaflet, and apart from $\omega_{fg,tb}$, all parameters were as in Fig. 3.3.

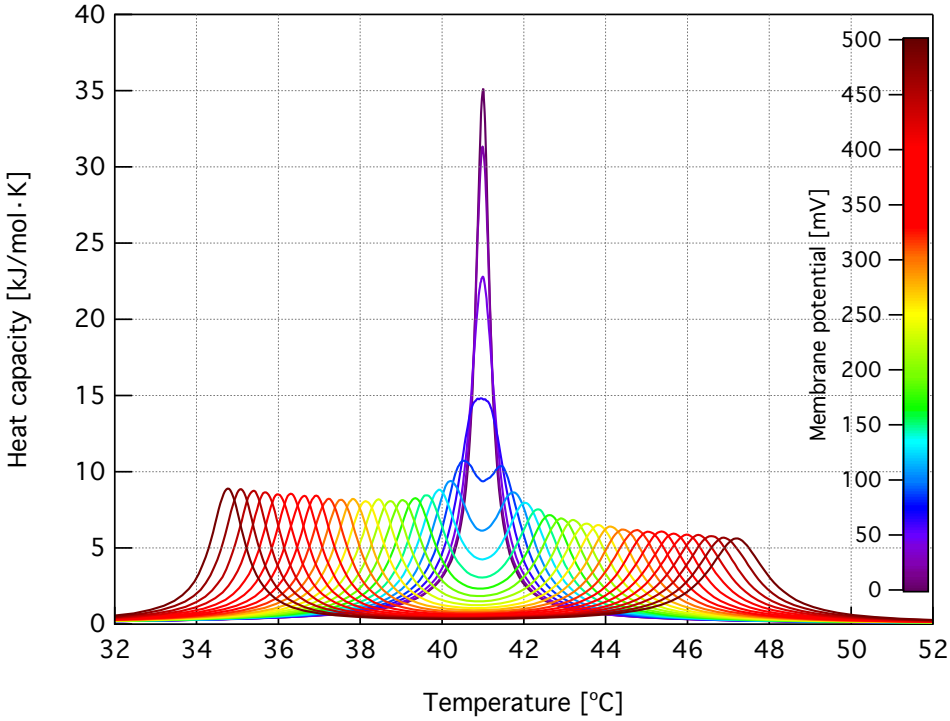

Fig. 3.6: Simulated heat capacity for an DPPC bilayer under the influence of a strong electric field. This causes one leaflet to shift its melting point to higher temperatures, and the other one to lower temperatures due to the asymmetric influence. Notice that the two peaks are, in fact, not completely identical, but the left one is narrower and with higher amplitude, due to one leaflet getting closer to its critical point. System size was 32×32 lipids in each leaflet and parameters were as described in the text.

3.4 Discussion

The models presented in this chapter showed the usefulness of Monte Carlo simulations for getting an approximate feeling for how the head group tilt depends on the lipid state or area. This in turn allowed us to estimate how strongly a bilayer will react to a transmembrane electric potential under the assumption of a strong coupling between head group orientation and the phase state of the lipid. It was found that the head groups get more parallel with the membrane surface in the dense gel phase. Even though the change in average tilt is slight ($\langle\theta\rangle_{gel} = 68.7°$ versus $\langle\theta\rangle_{fluid} = 64.1°$), this is enough to see a significant change in melting behaviour even at moderate voltages.

Both of the models used here clearly rely on a number of strong assumptions, and most likely overestimate the influence of the field. However, as is evident from Table 1.1 on p. 24 the field is expected to have a stronger influence on the state of short-chained phosphocholines due to their lower melting enthalpies. So even if the parameters used in these models exaggerate the effects, one might still be able to observe them experimentally for the short-chained DLPC or ditridecanoylphosphocholine, while still keeping the membrane potential low enough to avoid electroporation and full membrane rupture.

Nerve pulses in crayfish motor neurons

4

4.1 Introduction

Already in 1791 Luigi Galvani discovered that the muscles of dead frogs' legs twitched when stimulated by static electricity. This is considered to be one of the very first biophysical experiments, and even to this day the study of how the nervous impulse propagates continues to be a field of intense research.

4.1.1 The Hodgkin-Huxley model

In the seminal article by Hodgkin and Huxley (1952) a mathematical model was proposed for describing how the nervous impulse, or action potential, is initiated and propagates in giant squid axons. It was originally only intended as the simplest possible empirical description, but it has since then gained widespread acceptance, culminating in Hodgkin and Huxley receiving the 1963 Nobel Prize in Physiology or Medicine for their work.

The Hodgkin-Huxley model is based on the assumption that within the nerve cell there is a high potassium concentration, while outside of the cell one finds a high sodium concentration. These concentration differences give rise to a voltage difference between inside and outside that is related to the Nernst potentials. Furthermore, it is assumed that the plasma membranes of the neurons contain voltage-gated ion channel proteins that are specifically conducting either sodium or potassium ions. If there is a change in membrane potential, the conductance of these channel proteins increases, resulting in a flow of ions through the membrane. This will further depolarise the membrane, leading to more channels opening in the immediate environment, and so on. This process leads to a cascade effect, and it is this moving region of charged membrane that is considered to be the nerve signal.

The Hodgkin-Huxley model explains a wide range of data from e.g. the squid axon, like the shape of the action potential, its sharp threshold, refractory period, accommodation and sub-threshold oscillations. However, as Hodgkin and Huxley themselves wrote in their original article (Hodgkin and Huxley (1952)):

> *The agreement must not be taken as evidence that our equations are anything more than an empirical description of the time-course of the changes in permeability to sodium and potassium. An equally satisfactory description of the voltage clamp data could no doubt have been achieved with equations of very different form, which would probably have been equally successful in predicting the electrical behaviour of the membrane. [...] the success of the equations is no evidence in favour of the mechanism of permeability change that we tentatively had in mind when formulating them.*

That is, the model only addresses the voltage-related aspects of the nervous impulse, and does not provide any explanation for the complex voltage- and time-dependence of the channel proteins. This causes difficulties when trying to apply the Hodgkin-Huxley model (or an extension of it) to any new system, because all of the parameters have to be re-evaluated, and in most cases many of the parameters are not directly measurable (Ulinski et al. (1999)).

Of equal concern is the fact that data obtained from single-channel recordings has had very little success in correctly reproducing the expected macroscopic current behaviour. The usual explanation is that the kinetics of the channels are believed to be significantly altered when subjected to the single-channel recording environment (Ulinski et al. (1999)). To make matters worse, because the model has so many free parameters and imposes few constrains on their values, the literature seems to be fraught with contradictions and errors as pointed out by Ulinski et al. (1999):

> *In the process of analyzing the modeling reports, it became clear that a significant obstacle was the difficulty of reproduction, independent of any issues associated with specific interpretations of the electrophysiological data – essentially every model analyzed within this review (including the author's previous work!) presented various degrees of internal inconsistencies at the parameter or equation level.*

In short, the Hodgkin-Huxley model does not make testable predictions, because it is essentially an *a posteriori* description of the measurements (Heimburg (2010b)).

An important observation regarding the Hodgkin-Huxley model is that it solely describes the electrical phenomena based on ion currents flowing along their concentration gradients, and it is therefore inherently of a dissipative nature. One would intuitively expect that there should be a net production of heat. As it turns out, within the accuracy of the measurement the heat release is fully reabsorbed, indicating that the action potential is actually an adiabatic and reversible process (Abbott et al. (1958); Howarth et al. (1968, 1975); Howarth (1975); Ritchie and Keynes (1985)). The implications of this will be discussed in the next section.

Lastly, it is worth noting that there is a number of additional unresolved questions about action potential propagation. For instance, it was shown by Tasaki et al. (1966) that action potentials can propagate even in the complete absence on monovalent ions in the external medium. Nor does it explain the geometrical changes of the nerves that has been observed in experiments (Iwasa and Tasaki (1980); Iwasa et al. (1980); Tasaki and Iwasa (1980, 1981); Tasaki (1999a,b)).

4.1.2 The thermodynamic approach

As explained above, there are several unresolved issues within the Hodgkin-Huxley model, foremost among them the reversible heat signal. This observation prompted Heimburg and Jackson (2005) to propose an alternative explanation for the mechanism behind the action potential. A highly successful approach in physics is to search for explanations on length scales that are characteristic of the phenomenon one is trying to describe – for instance, it is pointless to describe macroscopic phenomena like the propagation of sound or the flow of a liquid on an atomic level, since the molecular details are simply not important for the fundamental physics of these phenomena.

The action potential lasts for a few milliseconds and propagates with 1–100m/s, meaning that the pulse must be several milli- to centimetres long. It is therefore natural to look for a description on this length scale, and not on the microscopic level, as is

the case for the Hodgkin-Huxley model, which relies on channel proteins that are a few nanometers in size, i.e. more than six orders magnitude smaller than the pulse width.

The model of Heimburg and Jackson (2005) – commonly known as *the soliton model* – is a simple macroscopic model that relies exclusively on classical thermodynamics and hydrodynamics and on the macroscopic properties of the lipid membranes. In short, it proposes that the nervous impulse is a special kind of density wave – a solitary wave – that can occur when two effects are balancing each other. These effects are a *non-linearity* of the speed of sound as a function of amplitude, and *dispersion* which is the frequency dependence of the sound velocity. Exactly these requirements are fulfilled by lipid membranes close to the melting transition.

A key feature of the model is that it relies on reversible mechanisms, and does therefore not give rise to dissipative phenomena. In particular, the reversible heat release can be explained by the heat of melting of the lipids. One of the strong points of this model is that it unifies many observations that has been made regarding nerves, in particular the phenomenon of anaesthesia whose mechanism has remained unexplained for more than a century.

For historical reasons the nervous impulse has primarily been thought of as an electrical phenomenon, and not a mechanical or thermodynamic one. This is primarily because of the ease with which the electrical aspects can be measured in contrast to the mechanical and thermodynamic ones, which remain technically challenging. As such, any model for the nervous impulse should also address the existence of the obvious electrical component. This is introduced into the soliton model by the observation that nerve membranes carry electrical charge. Essentially, the membranes can be considered to be charged capacitors, and – as in the Hodgkin-Huxley picture – the nervous impulse consists of a nerve segment of charged capacitor that travels along the axon. However, in contrast to the Hodgkin-Huxley model, the measured currents are mainly capacitive in origin. In essence, the nervous impulse can be considered to be a piezo-electrical pulse, and – since it is based on reversible physics – does not consume energy. Furthermore, it provides a framework for addressing the influence of any thermodynamic variable, and is not just limited to the electrical aspects. It explains the reversible heat release, the changes in nerve length and thickness (Iwasa and Tasaki (1980); Tasaki and Iwasa (1980)), and can even account for many aspects of anaesthesia (Heimburg and Jackson (2007a)).

Lastly, one of the most important aspects of the soliton model is that it has predictive power, because the influence of many variables on the thermodynamic and mechanical properties of lipid membranes is already known. For instance, as an example, there has been reports about so-called "thermoreceptors", which are thought to be sensitive to cold and warmth, though little is known about how these receptors produce electrical activity upon changes in temperature (Reid and Flonta (2001)). In the context of a thermodynamic model, such phenomena would be a direct consequence of the couplings between the system's variables.

4.1.3 Motivation

Since the soliton model was proposed in 2005, very little experimental work has been undertaken to test its validity. This is in part because our research group simply did not have the facilities or expertise to carry out the neurophysiological experiments ourselves.

My involvement in this project started when our research group purchased an Atomic Force Microscope (AFM). The aim was to measure the mechanical aspects of the action potential with a modern instrument, since the handful of previous studies had all been performed with more primitive, home-built instruments more than three decades ago (Iwasa et al. (1980); Tasaki and Iwasa (1980); Iwasa and Tasaki (1980)).

It quickly became apparent that it was necessary to devise a method to correlate the AFM signal with the electrophysiological signal, since the signal to noise ratio (SNR) of the AFM signal was less than 1. Note that this is orders of magnitude worse than the electrophysiological one, which is also the primary historical reason why the action potential is primarily considered an electrical pulse.

My initial task in this project was to create a user-friendly set of analysis tools for processing the raw data. This program would then be used for analysing the electrophysiological data we measured in crayfish nerves, and then compare the outcome with the predictions of the soliton model.

4.2 Theory

This section will outline the theory behind the soliton model. Discussing this model in full detail is beyond the scope of this thesis, so for a clear and accessible introduction I recommend Heimburg (2010b) or the original article (Heimburg and Jackson (2005)).

4.2.1 The soliton model

The soliton model of Heimburg and Jackson (2005) is based on the simple wave equation for sound propagation in one dimension. It considers the nerve axon as a (infinitely) long and narrow (1D) cylinder with lateral density excitations moving along its axis, x (Fig. 4.1). In the absence of dispersion, sound propagation is governed by the well-known equation

$$\frac{\partial^2}{\partial t^2}\Delta\rho^A = \frac{\partial}{\partial x}\left[c^2\frac{\partial}{\partial x}\Delta\rho^A\right], \tag{4.1}$$

where $\Delta\rho^A = \rho^A - \rho_0^A$ is the lateral density of the nerve membrane and is a function of x and t, and c is the velocity of sound.

A key property of lipid membranes is that the isentropic area compressibility, κ_S^A, depends sensitively on the phase state (and therefore also the density) of the membrane, displaying non-linear properties close to the melting transition. Together with dispersion, this gives rise to the possibility of localised pulses that propagate without attenuation and without changes in shape. Such pulses are known as solitons[1]. Since nerve membranes carry charges, these solitons are of an electromechanical nature, which accounts for the observed voltage changes during an action potential.

Next we use that the sound velocity is a function of density, $c^{-2} = \kappa_S^A(\rho^A)\cdot\rho^A$, and introduce a simple dispersive term, $-h\partial^4\Delta\rho^A/\partial x^4$ with the dispersion constant, $h > 0$. The dispersion is necessary for the existence of solitons, but the exact functional form is not very critical for the final outcome (Heimburg and Jackson (2005)).

Transforming the equation to a moving coordinate system where $z = x - vt$, results in the final equation

$$v^2\frac{\partial^2}{\partial z^2}\Delta\rho^A = \frac{\partial}{\partial z}\left[\frac{1}{\kappa_S^A\cdot\rho^A}\left[\frac{\partial}{\partial z}\Delta\rho^A\right]\right] - h\frac{\partial^4}{\partial z^4}\Delta\rho^A. \tag{4.2}$$

This equation can be solved analytically if one assumes that the solution is exponentially localised, and with a Taylor expansion of the sound velocity as a function of $\Delta\rho^A$, i.e. $c^2 \approx c_0^2 + p\Delta\rho^A + q(\Delta\rho^A)^2$. Here $p < 0$ and $q > 0$ are Taylor expansion coefficients which can be experimentally determined.[2]

[1] More precisely, they are *solitary waves*, and not solitons in the strictest sense as the pulses interact during a collision. This interaction comes about due to having an upper limit to the amplitude of $\Delta\rho^A$ given by the difference in the area density of the fluid and the gel state of the membrane.

[2] For unilamellar DPPC at $T = 45°\mathrm{C}$ one finds that $\rho_0^A = 4.035\cdot10^{-3}\mathrm{g/m^2}$, $c_0 = 176.6\mathrm{m/s}$, $p = -16.6c_0^2/\rho_0^A$, and $q = 79.5c_0^2/(\rho_0^A)^2$. This gives a limiting velocity of $v_{limit} = 0.650c_0 \approx 115\mathrm{m/s}$.

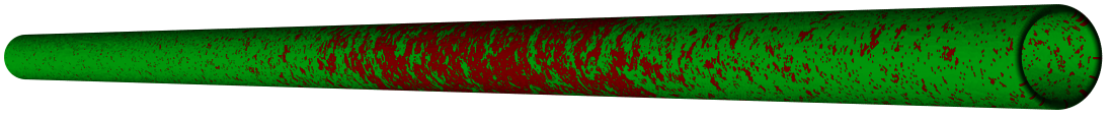

Fig. 4.1: Illustration of a soliton in a lipid cylinder. Red represents lipids in the high density (gel) state and green represents the lower density (fluid) state. The length of the soliton is not shown to scale, normally being two or three orders of magnitude longer than the thickness of the nerve.

By integrating Eq. (4.2) thrice one finds that

$$h\Big(\frac{\partial}{\partial z}\Delta\rho^A\Big)^2 = C\Delta\rho^A + (c_0^2 - v^2)(\Delta\rho^A)^2 + \frac{p}{3}(\Delta\rho^A)^3 + \frac{q}{6}(\Delta\rho^A)^4, \tag{4.3}$$

where C is an integration constant that depends on the experimental boundary conditions.[3] Fig. 4.2 shows a typical solution of Eq. (4.3) together with real nerve data by Iwasa and Tasaki (1980) and Ritchie and Keynes (1985).

It was shown by Lautrup et al. (2005) that the solutions are stable with respect to small perturbations, and can be produced by an arbitrary localised, but non-solitonic, excitation. These two points are very important, since nerve membranes are not perfectly homogeneous along the axon, i.e. they can vary both in thickness and specific composition of lipids and proteins, so that the elastic constants may therefore vary locally. Thus, stable solitons are viable even in a realistic physiological environment, and can be created by any perturbation that is of sufficient magnitude.

Predictions and limitations of the model

One immediate consequence of the soliton model is that pulses will have a limiting amplitude and velocity, with larger amplitude pulses having a slower propagation speed. The speed, amplitude and width of the solitons will uniquely depend on the energy of the excitation (Heimburg and Jackson (2005)).

In its present form the nature of the equations is such that the pulse will invariably be symmetric and strictly positive. To account for the often observed hyperpolarisation of action potentials and their asymmetric profiles, additional assumptions would be necessary.

Due to the direct coupling between area density and phase state of the lipids, a soliton will push the membranes partially through the melting transition. As a consequence, one expects it to display a number of secondary effects like an increase in nerve thickness by about 1nm, voltage changes and capacitive currents from the changes in geometry and charge density, an increased membrane permeability and the appearance of quantised conduction events (see Sec. 1.3), and – most importantly – a reversible heat change in phase with the action potential.

[3] For instance, for a single, exponentially localised, pulse in an infinitely long nerve, $C = 0$.

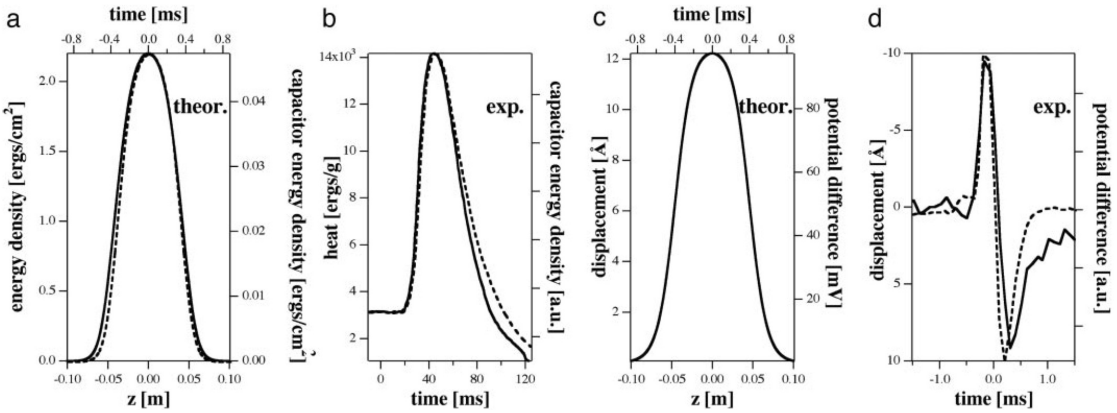

FIG. 4.2: Properties of solitons ($C = 0$) and action potentials. *(a)* Calculated total energy and capacitive energy densities stored in the soliton in a slightly asymmetrically charged membrane. *(b)* Experimental heat changes during the action potential of garfish olfactory nerve and the capacitive energy density. *(c)* Calculated thickness changes and voltage changes of a soliton. *(d)* Experimentally determined thickness and potential changes of a giant squid axon. Figure was taken from Heimburg and Jackson (2005).

It is worth stressing that the model described above was developed to describe myelinated axons. In fact, it could be argued that there is no real basis for assuming that the soliton model will be applicable for non-myelinated axons, where the pulse velocity is about 100 times slower. Naïvely, this would mean that if the pulse only depends on the elastic properties of the membranes, then the compressibility ($\kappa_S^A \propto c^{-2}$) would have to be 10^4 higher. This clearly not being the case, it is likely that very different mechanisms are involved for the non-myelinated nerves. For instance, without a myelination sheet it is possible that there will be out-of-plane components of the mechanical dislocations, which will make the pulse significantly slower.

Another limitation is that the model does not address the properties of single macromolecules (e.g. ion channel proteins or neurotoxins) in detail, but only through how a given protein or drug is influencing the thermodynamic properties of the system as a whole.

Periodic solutions and refractory periods in the soliton theory

Depending on the experimental boundary conditions one can get other solutions. Of particular interest is the situation where the total length of the nerve is fixed. Because of mass conservation, the mean density of the nerve must be constant, i.e. $\langle \Delta\rho^A \rangle = 0$. This means that positive peaks must be surrounded by regions of negative density change. It was shown in Vargas et al. (2011) that this condition leads to periodic solutions with a minimum distance (or "refractory period") between pulses, and also an undershoot (or "hyperpolarisation"). Fig. 4.3 shows a few examples of various solutions for a fixed velocity of $v = 0.8c_0$.

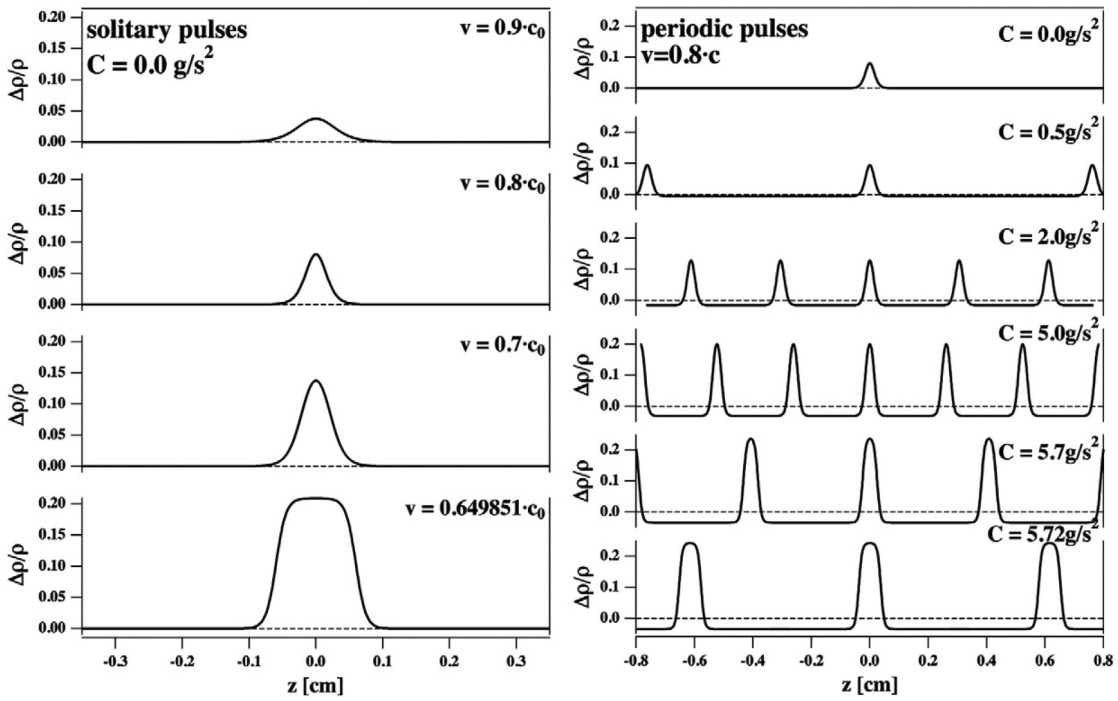

Fig. 4.3: Solutions for Eq. (4.2) for a DPPC membrane, shown for different values of the velocity and different boundary conditions. The minimum pulse distance is about 8 pulse widths. No stable solutions exist for $C > 5.72\mathrm{g/s^2}$ and for $C < 0\mathrm{g/s^2}$. The figure was taken from Vargas et al. (2011).

Moreover, for each pair of pulse amplitude and pulse distance, there will be exactly one propagation velocity. This implies that the velocity of pulse trains will depend on the amplitude and frequency of the stimulation process. Additionally, changes in a thermodynamic variable (e.g. temperature, pressure or even the presence of anaesthetics) should have a predictable influence on the propagation velocity and the spatial distance between the pulses in a pulse train.

Naturally, one should keep in mind that a real neuron has a finite length and will therefore only be able to fit a limited number of pulses at any given time, leading to pulse trains "multiplets" (doublets, triplets) rather than truly periodic solutions. It is important to note that the theory does not actually allow for stable doublet solutions, but merely considers doublets and triplets as an approximation to the periodic solutions in nerves that are only slightly larger than 2–3 pulse intervals. Also, real nerves are not necessarily completely fixated, and there will be additional effects from the boundaries of the axon, such that the final result may differ somewhat from the idealised situation described here.

4.3 Materials and methods

These experiments were carried out by Rolf Justesen Pedersen and Katrine Rude Laub who were master's students in our group at the time of this project. I will therefore only briefly introduce the experimental setup and procedure and refer to Pedersen (2010) for the full details. The Appendix contains a discussion of some of the considerations that went into creating the analysis tools to analyse the action potential measurements. Since a detailed understanding of those tools is not necessary to understand this section, it has been provided there for the interested reader and for future users.

4.3.1 Biological system

For our experiments on real nerves, specimens of the Australian red claw crayfish (*Cherax quadricarinatus*) were used. The animals were raised at a temperature of $T = 27°\text{C}$. Fig. 4.4 shows a schematic drawing of the animal seen from below, with a cross-section through the abdomen, approximately at the site of measurement. In all experiments we measured on the so-called 'nerve 3', which can be seen in the colour-stained view of one segment of the tail in Fig. 4.5.

The nerve 3 is a convenient system to measure on for a number of reasons. Firstly, the nerve contains a bundle of six axons, each from a different neuron. This is a suitably low number to allow for separation of signals from each individual neuron, while at the same time allowing for simultaneous measurement of neurons of varying thickness. Secondly, nerve 3 is a pure motor nerve, which means that all signals in it run exclusively from the central nerve cord out to the muscle at the outer end of the nerve. No signals go the other way. This is convenient when measuring the time delay between two electrodes on the nerve of a signal, in order to find determine its propagation speed. Lastly, the nerves spontaneously fire on their own, without the need for stimulation, for periods of sometimes up to 48 hours, even though the abdomen part of the crayfish had been severed from the rest of the animal.

4.3.2 Suction electrode setup

The spontaneously occurring action potentials from nerve 3 was recorded by use of differential electrodes. This method consists of two electrodes that are used to simultaneously measure the extracellular potential at two different positions of the nerve, usually separated by a few millimeters. In differential recordings the potential difference between two electrodes are measured by subtracting the potential measured by a reference electrode far away from the nerve, from the potential measured by the electrode close to the nerve.[4]

The specimen place in a thermostatted tray (ThermoMetric 5510 Thermostat water bath, Thermometric AB, Sweden) and was covered with a buffered saline solution, that

[4] Another commonly used method is to measure action potentials with differential recording is to place one electrode at one point of the nerve and its corresponding reference at another point further down the same nerve, in the direction in which the signal travels.

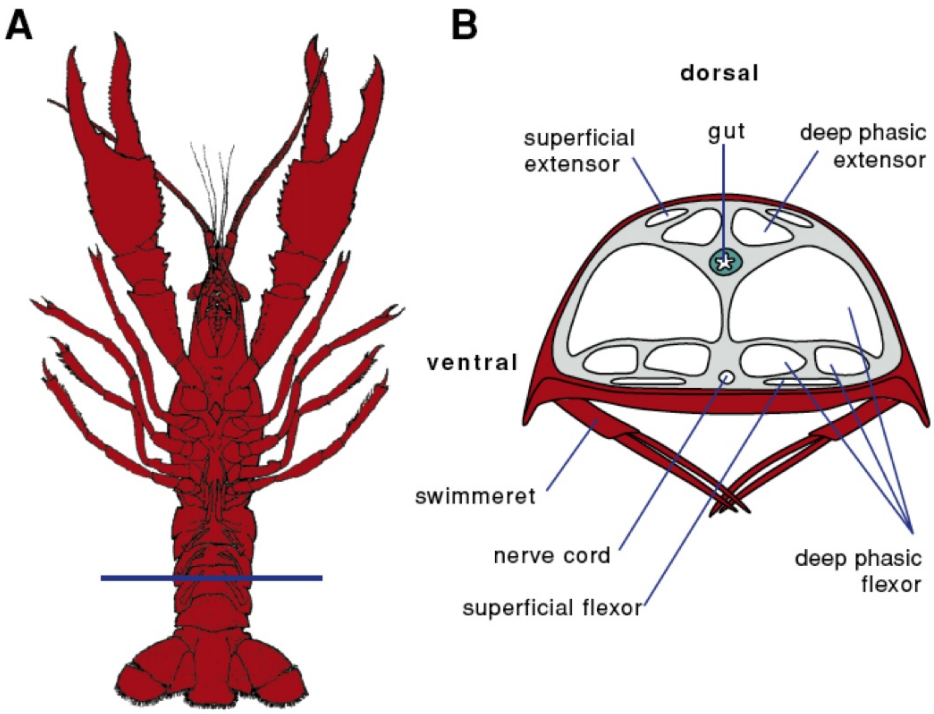

Fig. 4.4: Schematic drawing of a red claw crayfish. *A:* The animal as seen from below. *B:* Cross section from the blue line in *(A)*. The nerve used to measure on extends from the central nerve cord in the middle out to the superficial flexor muscle, which it innervates. The figure was taken from Pedersen (2010).

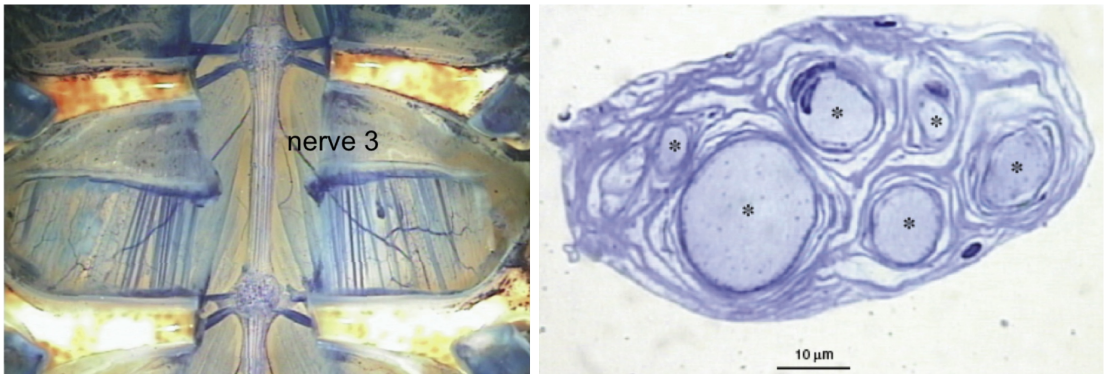

Fig. 4.5: *Left:* Colour-stained segment of a crayfish tail showing the nerve used for measurements, nerve 3, as the thin line running through the "n". *Right:* Cross section image of a nerve 3, showing the six axons of different diameters, each marked with an asterisk. The rest consists of glial cells and other facilitating cells. The figures were taken from Pedersen (2010).

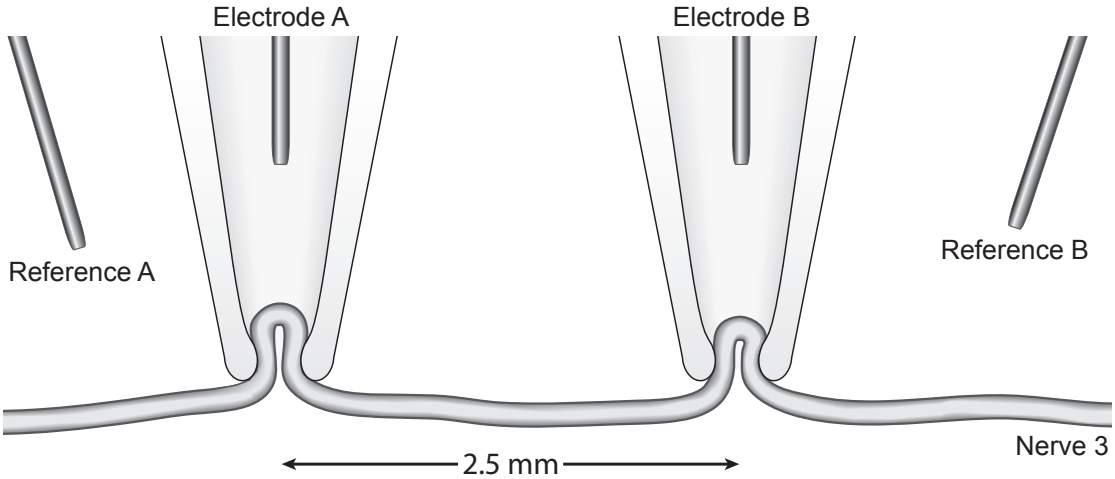

FIG. 4.6: Schematic drawing of the suction electrode setup. Everything was immersed in crayfish saline solution and thermostatted. The positions of the reference electrodes are not to scale.

was made to emulate the natural concentrations of salt ions in the extracellular fluid around the nerves.

More specifically, the crayfish saline was 5.4mM KCl, 205mM NaCl, 10mM $CaCl_2$, 2.6mM $MgCl_2$, 2.3mM $NaHCO_3$, and 1.8mM glucose. All chemicals used were of the highest purity grade available and any water used was purified (resistivity $> 18\text{M}\Omega \cdot \text{cm}$) on a desktop EASYpure RF water purification system from Barnstead/Thermolyne (Dubuque/IA, USA).

The electrodes were attached to the nerve by means of suction clamping. The suction clamping electrode consists of a chlorinated silver wire inside a borosilicate glass capillary (#1B150F-3, World Precision Instruments, USA) filled with saline solution. The capillary's tip opening was fire polished and made to be on the same scale as the diameter of the nerve, which is on the order of $\approx$40–80µm.

In total the setup used five electrodes: two for measuring the voltage at two different locations of the nerve, two for use as their references, and finally one electrode used for connecting the saline solution to earth. The two main electrodes were mounted on microelectrode holders that were, in turn, mounted on mechanical NMN-25 micromanipulators from Narishige, Japan. The reference electrodes were always placed several centimeters away from the nerve.

The signals were amplified and digitized by a PowerLab 26T amplifier (ADInstruments, Australia), connected to an ordinary desktop iMac (model 7,1 with 4GB of RAM; Apple Inc., California) running Scope 4.1.1 (ADInstruments). The sampling frequency was set to 100kHz, and the data was filtered digitally (high-pass at 51Hz; low-pass at 10kHz) prior to analysis.

4.4 Results

This section will present a selection of findings from our measurements of the spontaneous action potentials in a nerve 3, first focussing on multiplet (singlets, doublets, triplets) signals, and then on the temperature dependence of the various properties of the action potentials.

4.4.1 Action potential multiplets

The data presented in this section is from one-point measurements of the spontaneous action potentials in a nerve 3. All data shown was obtained from the same animal, though all of the findings were qualitatively reproduced in other, independent experiments.

Fig. 4.7 shows a representative segment of data, showing four different neurons firing, one with triplets, two of them as doublets, and the lowest amplitude one only having singlets. Fig. 4.8 shows how the action potentials from the different neurons can be neatly classified, purely based on the amplitude of the positive and negative peak. While the nerve 3 contains six axons, it was rare that all six different classes could be observed in a given experiment. This might be related to slight tissue damage during dissection, or simply that the signals were too weak to be reliably detected above the baseline noise. The number of active neurons also seemed to vary with temperature and clamping. Also, two comments regarding the occurrence of multiplets: firstly, this was not completely stable, with significant variation between different experiments and with temperature (seemingly more frequently occurring at low temperatures). Secondly, a given neuron under constant conditions did not produce multiplets each time it fired, though it seemed that it did so at least 90% of the time in our experiments.

Once classified, a number of statistics can be calculated and compared for the individual classes (neurons). Fig. 4.9 and Fig. 4.10 shows histograms of the time between action potentials from the same class at $T = 14°\mathrm{C}$. All of the observed classes has a spontaneous firing rate of about 0.7–2Hz at this temperature. However, there is also a distinct peak around 10–15ms which stems from the doublet (classA1 and classA2) or even triplet pulses (classA3). This interpulse interval clearly has a well defined value, and was never observed to be shorter than approximately 10ms in any experiment.

At first glance the pulses of a doublet or triplet seem to be completely identical. However, as can be seen from Fig. 4.10 and Fig. 4.11, there is a consistent difference between the first and the subsequent pulses in a multiplet. The second action potential is either physically broader or slower than the first one. Also, the amplitude goes down by about 2–3%, though this seems to lessen with increasing interpulse interval (data not shown). This indicates that there is an interaction between the pulses, either due to them being in neuron at the same time, or from the system not having fully relaxed yet.

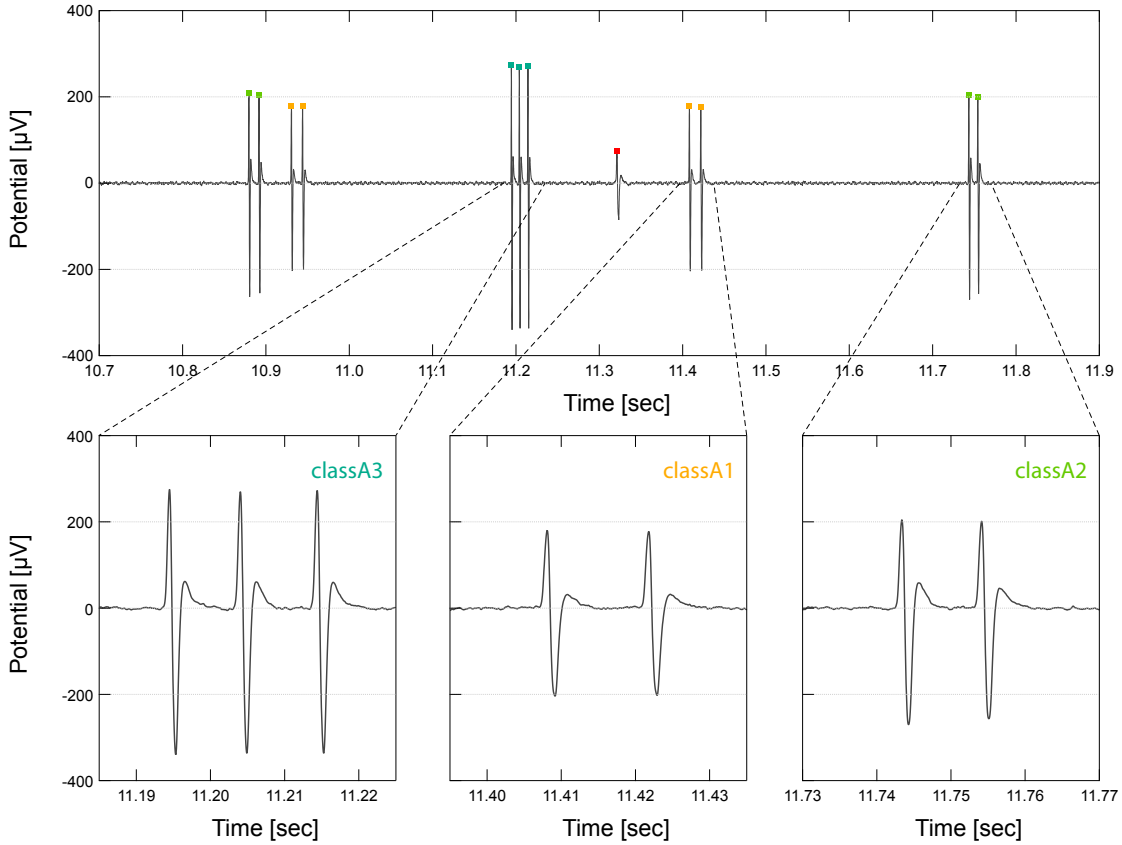

FIG. 4.7: Example of multiplets in a nerve 3 recording at $T = 14°C$. The coloured markers show action potentials belonging to the same neurons ("class").

4.4.2 Temperature dependence of the action potential

This section will present a selection of findings from two-point measurements of the spontaneous action potentials in a nerve 3 at various temperatures. All the data shown was obtained from the same animal, though all of the findings were qualitatively reproduced in other, independent experiments.

From a two-point measurement one can use the delay between the signal in the two channels to determine the propagation speed of the action potentials. This is shown in Fig. 4.12, where one channel (A) has been used to align the signal of the other channel (B). As can be seen, the action potentials are not identical in width or amplitude in the two channels. Since there does seem to be a variation in the shape of the signals between experiments, it was not clear whether this arose from a genuine change in the shape of the action potential, or was purely due to differences in the suction clamping (amount of nerve sucked into the pipette, tightness of the clamping seal, etc.).

A very consistent observation that we made, was that the voltage amplitude of an action potential is strongly correlated with its propagation speed, with faster pulses

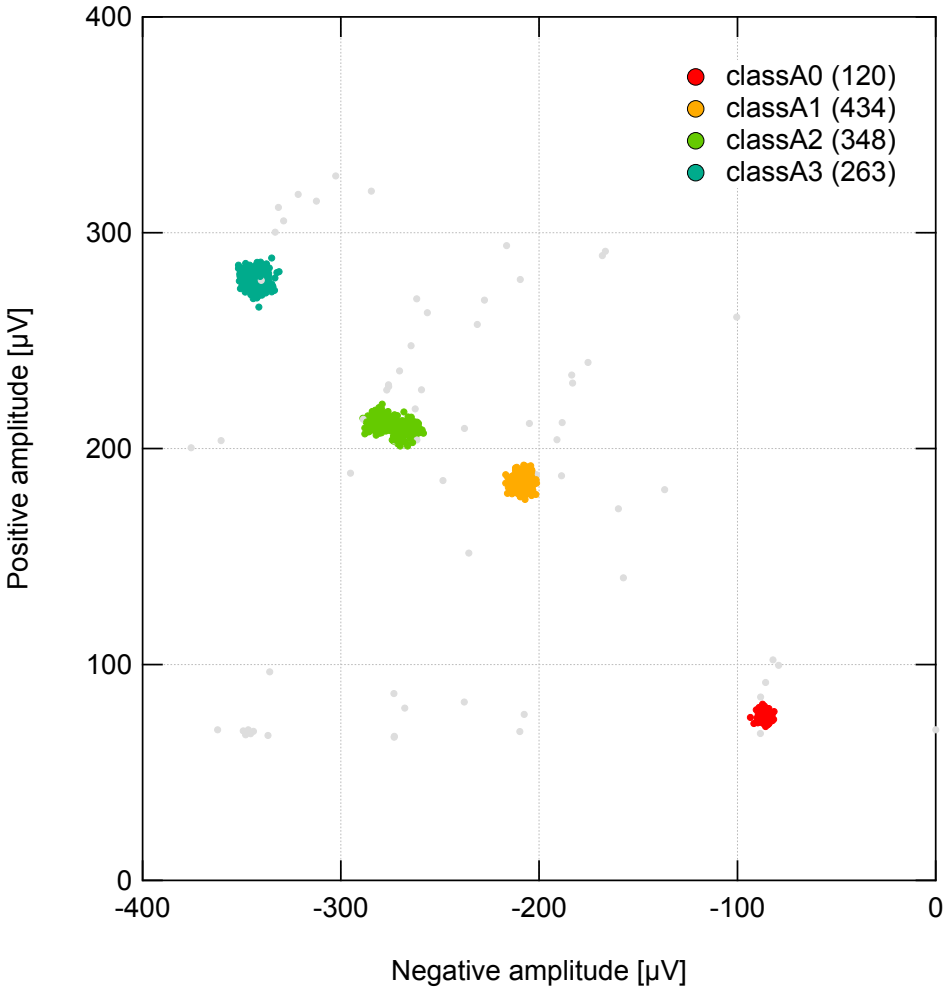

Fig. 4.8: Scatter plot of the action potential amplitudes from the recording shown in Fig. 4.7. In this data set there was a neat grouping of the different pulses, here coloured and labelled *classA0–classA3*. The grey points stem from random noise and overlapping action potentials from different neurons. The numbers in the parentheses indicate the number of action potentials in that class.

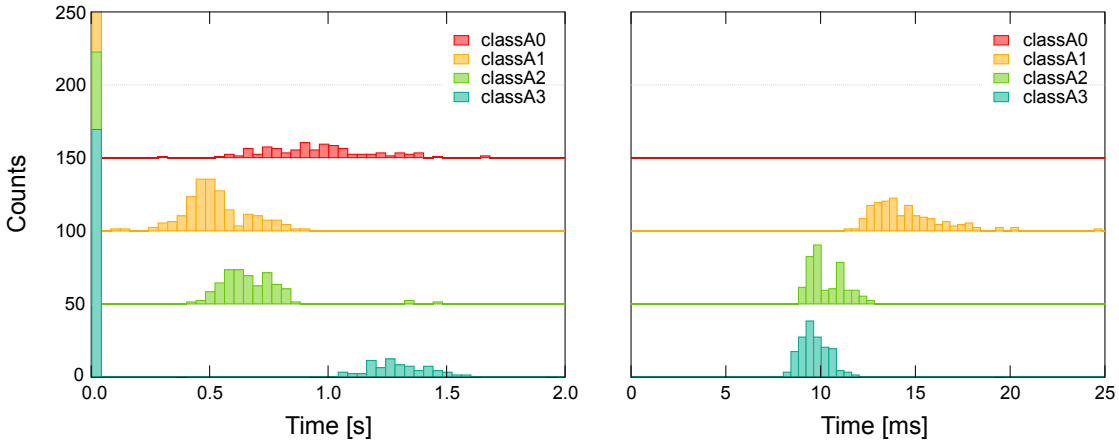

FIG. 4.9: Histograms showing the delay times between the pulses of Fig. 4.8. For some classes the histograms are bimodal, with the long time peak the characteristic firing frequency of the neuron (*left*), and the short time peak being the interpulse interval (*right*).

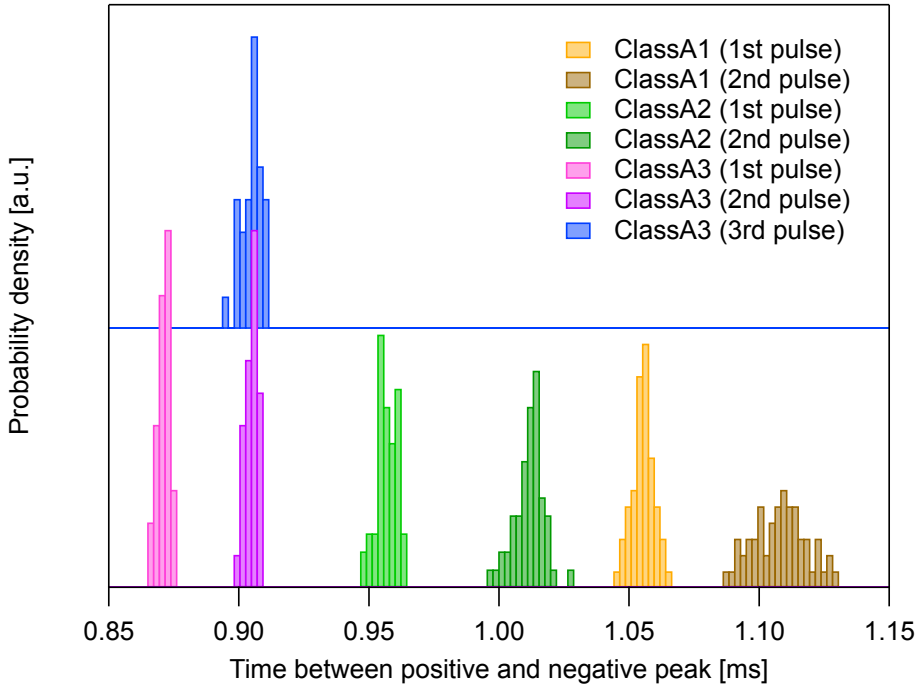

FIG. 4.10: Differences between the first and following pulses in a multiplet. Time between the maximum and minimum of an action potential. Note how the second (and third) pulse always has a larger delay between the two extrema. The experimental temperature was $T = 14°\mathrm{C}$.

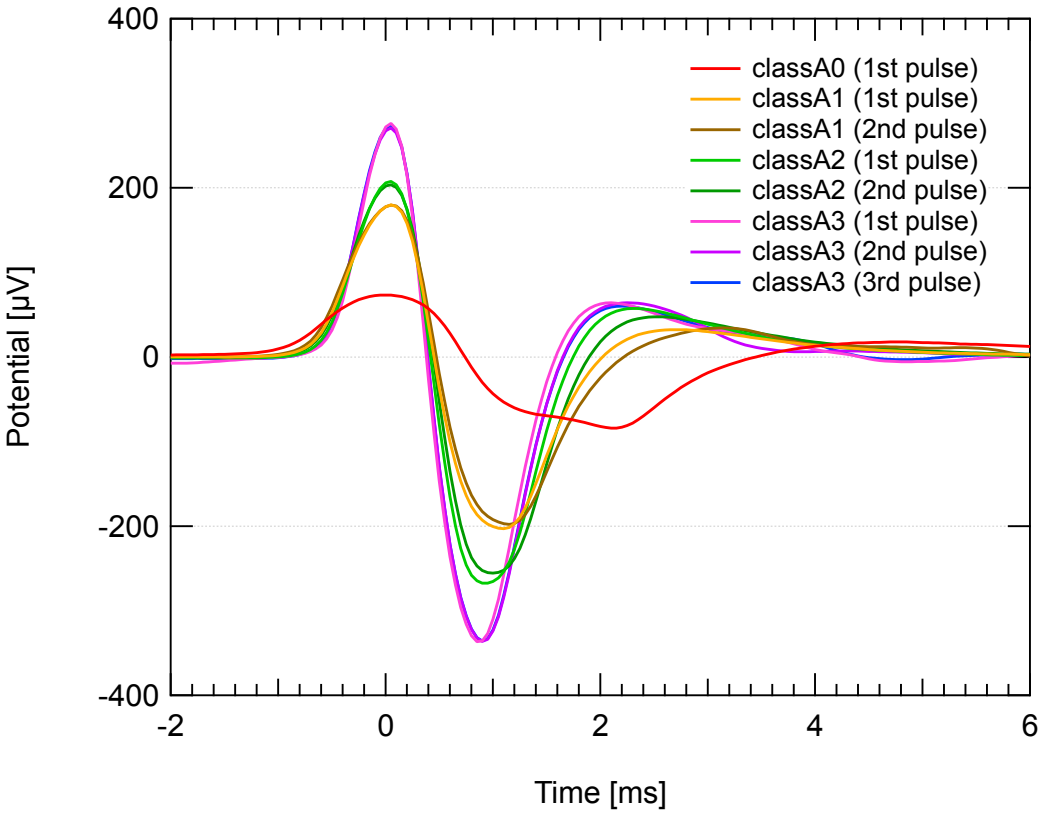

Fig. 4.11: Average shape of the various pulses of the multiplets. While similar, there is a consistent change between the first and the following pulses, with the first pulse being of larger amplitude and narrower than the rest. The experimental temperature was $T = 14°C$.

having a higher amplitude. In fact, there seems to be an (almost) linear proportionality between the two as shown in Fig. 4.15 (*top*).

Since we can determine the speed of each action potential, it is also a simple matter to determine the physical width of the signals. Fig. 4.13 shows that, within the experimental accuracy, all of the pulses are identical in width (also see Fig. 4.15). In fact, it seems that the pulse widths are also independent of temperature, and only change in apparent width due to changes in the propagation speed (Fig. 4.17).

Finally, Fig. 4.14 show the interpulse distance, i.e. the distance between the two action potentials of a doublet. For one of the neurons (classA1) this distance was also independent of temperature, i.e. the ratio of the interpulse separation to the pulse width is a constant (12.5mm, which is roughly 10 times the pulse width, depending on the exact definition). For the fastest class of action potentials in this experiment (classA2), the interpulse distance was about 35mm at low temperatures, but then switched to $\approx$ 14mm around 11–12°C in an abrupt, rather than smooth way.

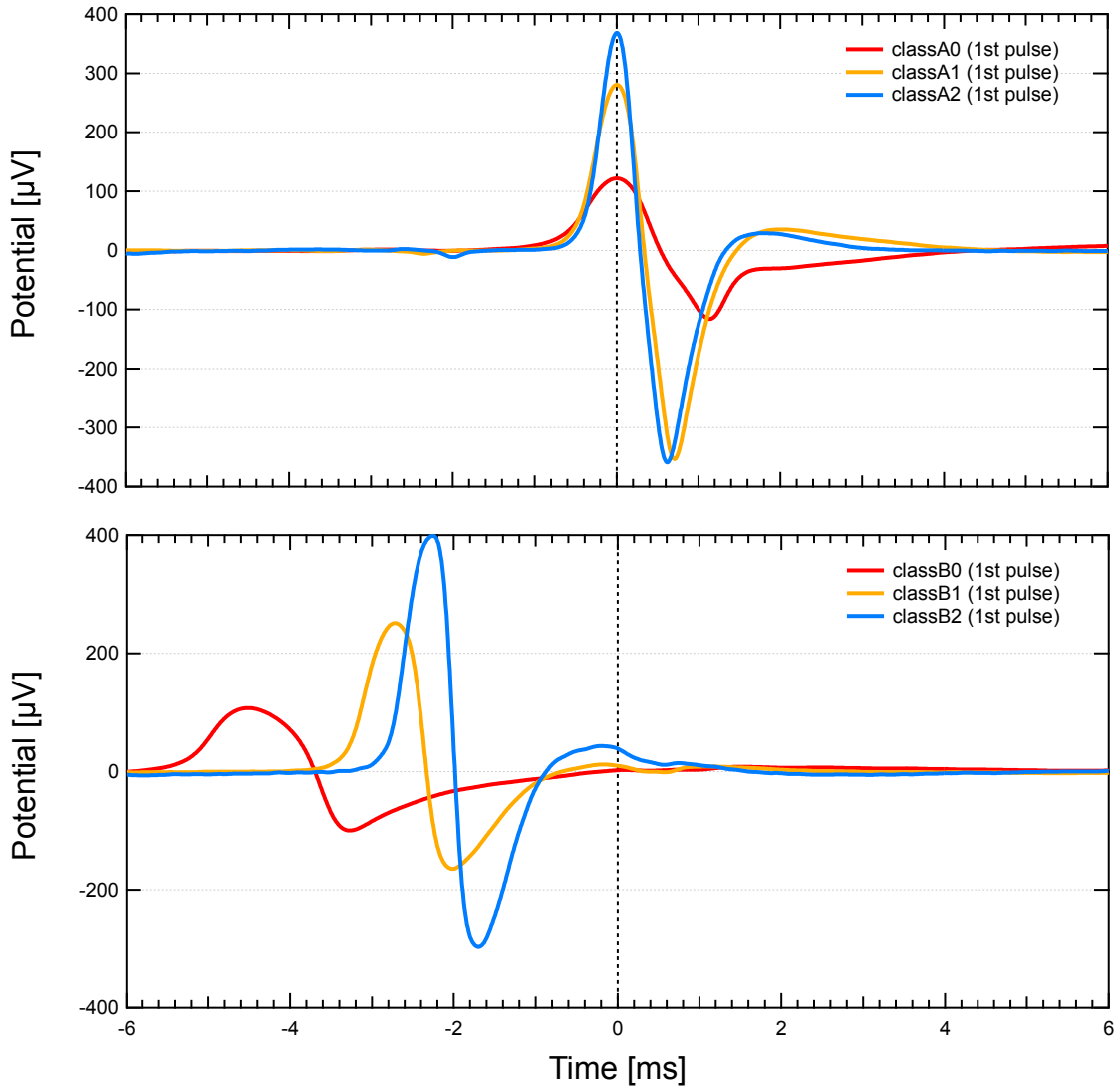

FIG. 4.12: Average signals as seen in the primary channel (A) and the secondary channel (B), showing the different time delays, which reflects the different propagation speeds. The pulse shape also changes width between the two channels. The experimental temperature was $T = 7°\mathrm{C}$.

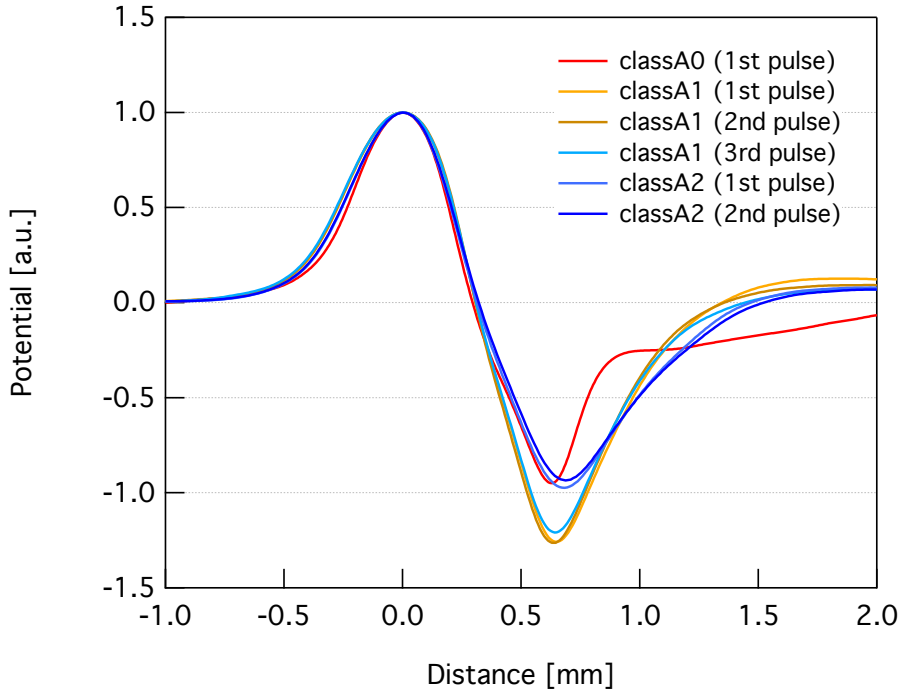

Fig. 4.13: Average signals as seen in the primary channel (A), converted into physical width based on their measured speeds, and then rescaled to have the same amplitude. Within the experimental accuracy, these pulses are identical in width. The experimental temperature was $T = 7°\mathrm{C}$.

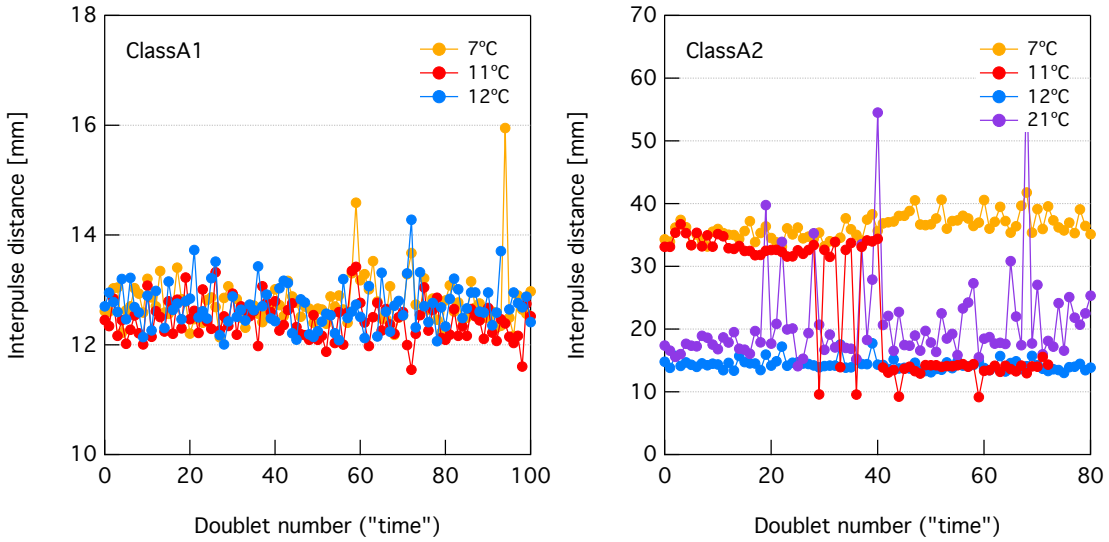

Fig. 4.14: Distance between pulses at various temperatures. *Left:* Within the experimental uncertainty, the interpulse distance is independent of temperature for ClassA1. *Left:* At low temperatures the interpulse distance is constant, and large (≈35mm), but while slowly heating (midway through the trace at $T = 11°\mathrm{C}$), the distance became bistable, and finally settles at a new, constant value of ≈ 14mm.

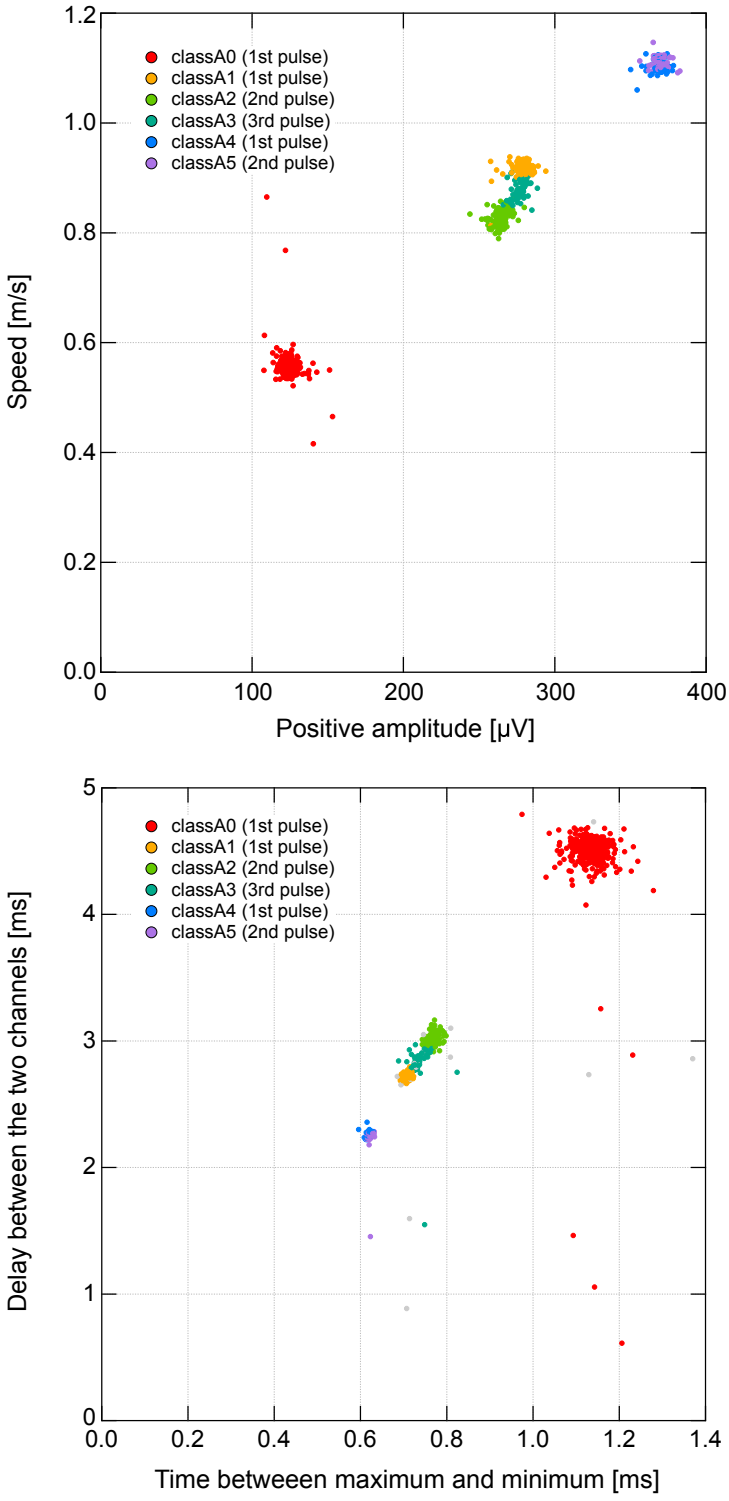

FIG. 4.15: *Top:* Scatter plot of the pulse speed vs amplitude, showing an almost linear relation between the two. *Bottom:* Scatter plot of the delay between the two channels vs pulse width also showing a linear relationship. This indicates that pulse widths (in mm) are the same for all pulses, independent of the "class" (neuron). The experimental temperature was $T = 7°\mathrm{C}$.

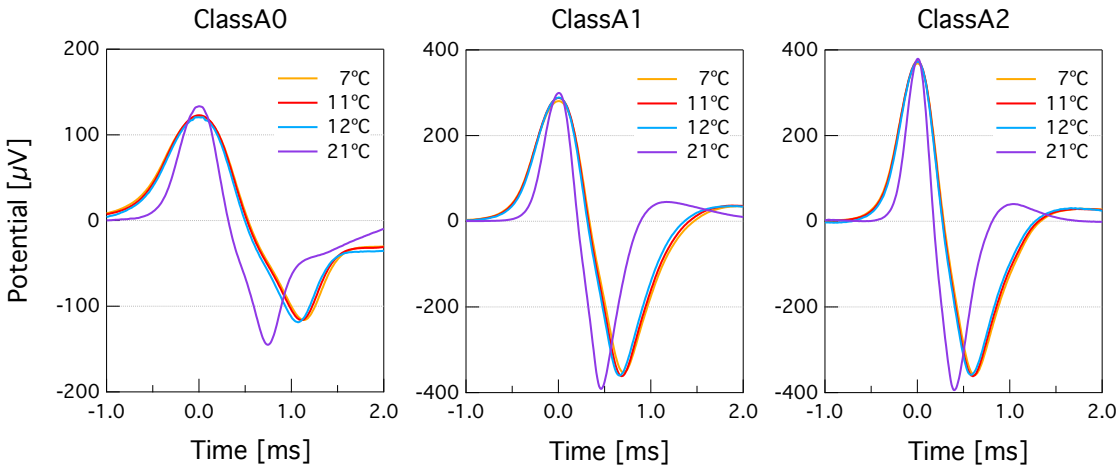

Fig. 4.16: Average shape of the action potentials plotted at various temperatures. The change in width *exactly* reflects the changes in speed (Fig. 4.17 and Fig. 4.15). Note that the voltage scale of ClassA0 is different from the other two.

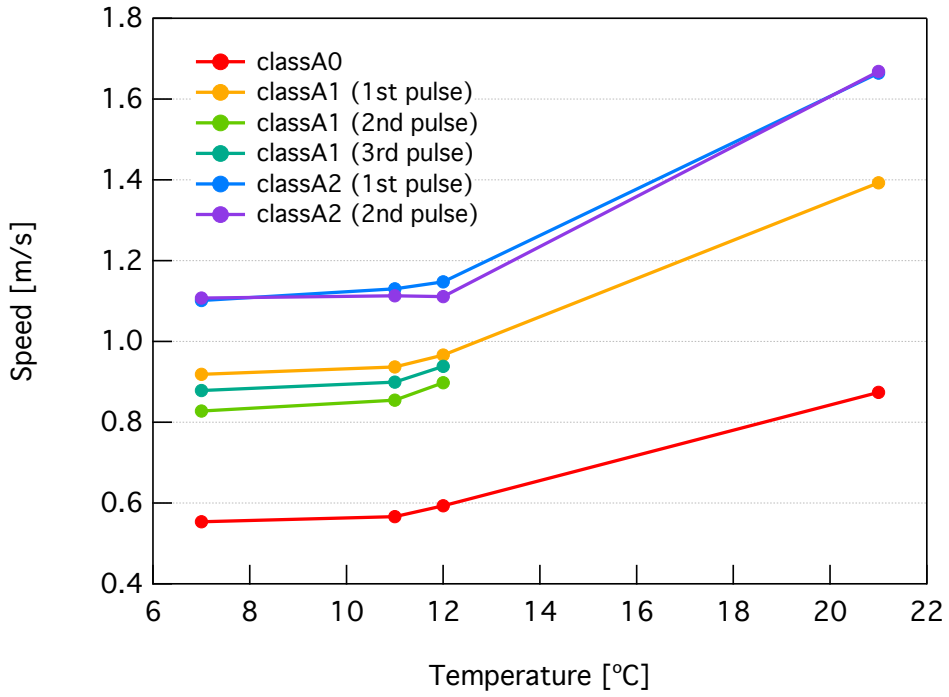

Fig. 4.17: Temperature dependence of the propagation speed shown for the different pulse classes. The speed measurement assumed that the distance between the two suction pipettes was $d = 2.5 \pm 0.5$mm.

4.5 Discussion and conclusions

This section will discuss the results of the previous section in the context of the soliton model, and then provides suggestions regarding possible future research.

4.5.1 Temperature dependence in the soliton model

One of the strong points of the soliton model is that it makes specific predictions about the couplings between various thermodynamic variables and how they influence the nerve pulse propagation. The Hodgkin-Huxley model, in contrast, provides no real framework to answer such questions (Heimburg (2010b)).

However, as discussed earlier the soliton model in its current form has severe limitations when it comes to interpreting data from non-myelinated axons. Also, there is still a lack of an unambiguous relationship between the mechanical excitation and the resulting voltage pulse, in particular in regard to how this depends on the axon's geometry and lipid composition.

It was found that the spontaneous action potentials are all of identical physical width, independent of the temperature and which neuron is firing. Within the framework of the soliton model this indicates that all pulses are created with the same total energy. The soliton model predicts that all pulses should then propagate with the same velocity, given that the dispersion constant, h, and the lipid composition are the same for all axons. However, the experimental finding was that the propagation speeds differ by more than a factor two between the slowest and the fastest action potentials in the crayfish motor neurons.

As previously mentioned, it also was consistently found that the voltage amplitude of an action potential was strongly correlated with its propagation speed. Fig. 4.15 shows that there seems to be an almost linear proportionality between the two, with the faster pulses have a higher amplitude. Given that the measured voltage can, in principle, be strongly dependent on the nature of the clamping, as well as how well-isolated the given neuron is, it is not given that there should be such a coupling. However, if we assume that the measured amplitude of the voltage signal is directly related to the amplitude of the density pulse in an identical manner for all axons, this finding seems to contradict the soliton model, which clearly predicts that higher amplitude solitons have a lower propagation speed.

A third finding was that the propagation speeds go down with temperature. Since nerve membranes are found in a state above their transition point, lowering the temperature would move the system closer to the melting transition. This, in turn, implies that the compressibility of the membranes increases, and consequently the speed of sound will decrease. It therefore seems that this finding is completely consistent with the soliton model.

In the end many of these findings cannot be satisfactorily explained without a clearer understanding of the exact coupling between the mechanical and electrical aspects of the action potential. In conclusion, the relevance of the soliton model to non-myelinated axons is not fully supported by our data.

4.5.2 Multiplets and the soliton model

It was found that the distance between the pulses in a doublet is about 10 times the width of the individual pulses, depending on temperature and a somewhat arbitrary criterion for defining width. An almost identical result was recently obtained by Vargas et al. (2011) for the action potentials in the femoral nerve of the locust (*Locusta migratoria*). The closest distance of the theoretical periodic pulses is very similar, giving a distance-to-width ratio of about 8 (see Fig. 4.3). It was suggested by Vargas et al. (2011) that the doublets correspond to the closest possible pulses in the soliton theory. The length of the nerves we used in our experiments were roughly 1cm. Compared to the interpulse separation of about 12–14mm (possibly shorter, depending on the exact distance between the electrodes), it seems only borderline possible to "fit in" two pulses at the same time.

A hint as to that the two pulses in fact do occupy the axon at the same time can be found in Fig. 4.10 and Fig. 4.11. Here it was found that there is a statistically significant difference between the first and the second pulses in a doublet, indicating an interaction between the pulses. Whether this interaction is due to the pulses simultaneously occupying the axon, or whether it is related to the mechanism that creates the pulses is not clear.

4.5.3 Outlook

The original aim of this project was to create a suitable analysis tools suite for comparing mechanical (AFM) measurements to a simultaneous electrophysiological recording. Since this task has been completed, what is clearly lacking is the actual AFM data.

Mechanical changes have (with difficulty) been measured in the past, but even with current technology it is not a simple task. One aspect of our current setup that can be significantly improved is vibration isolation. The reduction of noise from external mechanical vibrations would hopefully improve the signal-to-noise ratio to above 1, making the experiments significantly easier.[5]

If it is possible to accurately measure the geometry (thickness, length) changes of the nerves, it would allow for the determination of the relation between the shape of the voltage pulse and the density pulse. This knowledge would be a vital step towards verifying the predictions and couplings of the soliton model, since the some of the measurements presented in this thesis are difficult to fit into that framework. Note that this by no means disproves the soliton model, but merely makes clear that there are details that have yet been satisfactorily addressed, especially for the non-myelinated axons.

Another thing that remains to be investigated, is the effect of changing other thermodynamic variables (adding general anaesthetics, in particular) on the properties of the action potentials. If a given change could be compensated for by e.g. increasing or decreasing the temperature, then this would be strong support of the soliton model.

[5] In fact, our group did order a dynamic vibration isolation table (TableStable 150, HWL Scientific Instruments GmbH, Germany) for this exact purpose, but the instrument for unknown reasons never arrived.

Summary

In this thesis four related studies were presented:

- An experimental study of spontaneous pore formation in pure lipid membranes. It was shown that ion currents through lipid pores in membranes can under various conditions exhibit a wide spectrum of behaviours, like quantised conductance steps, voltage-gating, flickering, burst activity, rectification, and sub-conductance states. It was also found that the spontaneous lipid pores can have fairly complex kinetics, showing power law-like distribution of the form t^{-a} with the exponent $1/2 \leq a \leq 3/2$.
- An experimental study of the influence of electromagnetic radiation from mobile phones on the permeability of membranes. While it was concluded that the experimental setup was unsuited for such studies, it was found that the influence must be small – or even negligible – at normal exposure levels.
- A theoretical study of the influence of a transmembrane electric field on the state of the membrane by means of Monte Carlo simulations. Under the assumption of a strong coupling between the tilt of the head group and the phase state of the lipid, it was found that a transmembrane potential of a few hundred millivolts can cause the two membrane leaflets to melt independently of each other.
- A careful analysis of the spontaneous action potentials in unmyelinated axons at various temperatures. This was used to study the limits of the soliton model of nerve pulse propagation. It was found that the physical width of the action potentials is independent of temperature and which neuron is firing. Furthermore, it was found that the voltage amplitude and the speed of the action potentials were strongly correlated, but in an opposite manner of what we expect from the soliton model. It was also found that the speed of propagation was significantly reduced with decreasing temperature, which is consistent with the theory.

The study of the various electrical aspects of pure lipid membranes has received remarkably little attention from the biomembrane community. It is my hope that this work will provide a significant contribution to the understanding of the couplings between the membrane potential and the properties and dynamics of the lipid membrane itself.

Bibliography

B. Abbott, A. Hill, and J. Howarth. The positive and negative heat production associated with a nerve impulse. *P Roy Soc Lond B Bio*, 148(931):149–187, 1958.

A. Ahlbom, U. Bergqvist, J. Bernhardt, and J. Cesarini. Guidelines for limiting exposure to time-varying electric, magnetic, and electromagnetic fields (up to 300 ghz). international commission on non-ionizing radiation protection. *Health Phys*, 74(4): 494–522, 1998.

B. Alberts, D. Bray, J. Lewis, M. Raff, K. Roberts, and J. D. Watson. *Molecular Biology of the Cell*, chapter 11: Membrane Transport of Small Molecules and the Electrical Properties of Membranes. Garland Publishing, 5th edition, 2008.

N. Albon and J. Sturtevant. Nature of gel to liquid-crystal transition of synthetic phosphatidylcholines. *P Natl Acad Sci Usa*, 75(5):2258–2260, 1978.

V. Antonov, V. Petrov, A. Molnar, D. Predvoditelev, and A. Ivanov. Appearance of single-ion channels in unmodified lipid bilayer-membranes at the phase-transition temperature. *Nature*, 283(5747):585–586, 1980.

V. Antonov, E. Shevchenko, E. Kozhomkulov, A. Molnar, and E. Y. Smirnova. Capacitive and ionic currents in blm from phosphatidic-acid in ca2+-induced phase-transition. *Biochem Bioph Res Co*, 133(3):1098–1103, 1985.

V. Antonov, E. Y. Smirnova, and E. Shevchenko. Electric-field increases the phase-transition temperature in the bilayer-membrane of phosphatidic-acid. *Chem Phys Lipids*, 52(3-4):251–257, 1990.

V. Antonov, A. Anosov, V. Norik, and E. Y. Smirnova. Soft perforation of planar bilayer lipid membranes of dipalmitoylphosphatidylcholine at the temperature of the phase transition from the liquid crystalline to the gel state. *Eur Biophys J*, 34(2):155–162, 2005.

L. Bagatolli. Direct observation of lipid domains in free standing bilayers: from simple to complex lipid mixtures. *Chemistry and Physics of Lipids*, 122(1-2):137–145, 2003.

L. Bagatolli and E. Gratton. Direct observation of lipid domains in free-standing bilayers using two-photon excitation fluorescence microscopy. *J Fluoresc*, 11(3):141–160, 2001.

L. Bagatolli, T. Parasassi, and E. Gratton. Giant phospholipid vesicles: comparison among the whole lipid sample characteristics using different preparation methods - a two photon fluorescence microscopy study. *Chemistry and Physics of Lipids*, 105(2): 135–147, 2000.

T. Baumgart, S. Hess, and W. Webb. Imaging coexisting fluid domains in biomembrane models coupling curvature and line tension. *Nature*, 425(6960):821–824, 2003.

A. Benedetti, A. Birarelli, E. Brunelli, G. Curatola, G. Ferretti, U. Delprete, A. Jezequel, and F. Orlandi. Modification of lipid-composition of erythrocyte-membranes in chronic-alcoholism. *Pharmacol Res*, 19(10):651–663, 1987.

G. Berestovsky, M. Gyulkhandanyan, V. Ivkov, and V. Razhin. Voltage-induced reflectivity relaxation of bilayer lipid-membranes - on changes of bilayer thickness. *J Membrane Biol*, 43(2-3):107–126, 1978.

H. Binder and O. Zschornig. The effect of metal cations on the phase behavior and hydration characteristics of phospholipid membranes. *Chem Phys Lipids*, 115(1-2): 39–61, 2002.

A. Blicher. Permeability studies of lipid vesicles by fluorescence correlation spectroscopy and monte carlo simulations. Master's thesis, University of Copenhagen, 2007.

A. Blicher, K. Wodzinska, M. Fidorra, M. Winterhalter, and T. Heimburg. The temperature dependence of lipid membrane permeability, its quantized nature, and the influence of anesthetics. *Biophys J*, 96(11):4581–4591, 2009.

A. Blume and M. Hillmann. Dimyristoylphosphatidic acid cholesterol bilayers - thermodynamic properties and kinetics of the phase-transition as studied by the pressure jump relaxation technique. *Eur Biophys J Biophy*, 13(6):343–353, 1986.

R. A. Boeckmann, A. Hac, T. Heimburg, and H. Grubmueller. Effect of sodium chloride on a lipid bilayer. *Biophysical Journal*, 85(3):1647–1655, 2003.

G. Boheim, W. Hanke, and H. Eibl. Lipid phase-transition in planar bilayer-membrane and its effect on carrier-mediated and pore-mediated ion-transport. *P Natl Acad Sci Usa*, 77(6):3403–3407, 1980.

S. Brush. History of lenz-ising model. *Rev Mod Phys*, 39(4):883–893, 1967.

J. Burt, H. Morgan, and R. Pethig. The detection and analysis of multiple-membrane-channel events by convolution. *Phys Med Biol*, 39(10):1527–1535, 1994.

B. Cannon, M. Hermansson, S. Gyorke, P. Somerharju, J. Virtanen, and K. Cheng. Regulation of calcium channel activity by lipid domain formation in planar lipid bilayers. *Biophysical Journal*, 85(2):933–942, 2003.

R. Cantor. Lateral pressures in cell membranes: a mechanism for modulation of protein function. *J. Phys. Chem. B*, 101(10):1723–1725, 1997a.

R. Cantor. The lateral pressure profile in membranes: A physical mechanism of general anesthesia. *Biochemistry-Us*, 36(9):2339–2344, 1997b.

M. D. Collins. Interleaflet coupling mechanisms in bilayers of lipids and cholesterol. *Biophysical Journal*, 94(5):L32–L34, 2008.

R. Coronado and R. Latorre. Phospholipid-bilayers made from monolayers on patch-clamp pipettes. *Biophysical Journal*, 43(2):231–236, 1983.

E. Corvera, O. G. Mouritsen, M. Singer, and M. Zuckermann. The permeability and the effect of acyl-chain length for phospholipid-bilayers containing cholesterol - theory and experiment. *Biochim Biophys Acta*, 1107(2):261–270, 1992.

R. Cotterill. Field effects on lipid-membrane melting. *Phys Scripta*, 18(3):191–192, 1978.

C. Cruickshank, R. Minchin, A. LeDain, and B. Martinac. Estimation of the pore size of the large-conductance mechanosensitive ion channel of escherichia coli. *Biophysical Journal*, 73(4):1925–1931, 1997.

L. Cruzeiro-Hansson and O. G. Mouritsen. Passive ion permeability of lipid-membranes modeled via lipid-domain interfacial area. *Biochim Biophys Acta*, 944(1):63–72, 1988.

J. Danielli and H. Davson. A contribution to the theory of permeability of thin films. *J Cell Compar Physl*, 5(4):495–508, 1935.

S. Doniach. Thermodynamic fluctuations in phospholipid bilayers. *J Chem Phys*, 68 (11):4912–4916, 1978.

D. Doyle, J. Cabral, R. Pfuetzner, A. Kuo, J. Gulbis, S. Cohen, B. Chait, and R. MacKinnon. The structure of the potassium channel: Molecular basis of k+ conduction and selectivity. *Science*, 280(5360):69–77, 1998.

H. Ebel, P. Grabitz, and T. Heimburg. Enthalpy and volume changes in lipid membranes. i. the proportionality of heat and volume changes in the lipid melting transition and its implication for the elastic constants. *J Phys Chem B*, 105(30):7353–7360, 2001.

D. T. Edmonds. Reversible electrostatic channel for ion-transport. *Chem Phys Lett*, 65 (3):429–433, 1979.

D. T. Edmonds. Membrane ion channels and ionic hydration energies. *Proceedings of the Royal Society B: Biological Sciences*, 211(1182):51–62, 1980.

D. T. Edmonds. A physicists view of membrane ion channels. *Trends Biochem Sci*, 6 (4):92–94, 1981.

D. T. Edmonds. The behaviour of ions in narrow water-filled pores. *Bioscience Rep*, 18 (6):313–327, 1998.

B. Ehrlich. Planar lipid bilayers on patch pipettes - bilayer formation and ion channel incorporation. *Meth Enzymol*, 207:463–470, 1992.

M. Eisenberg and S. McLaughlin. Lipid bilayers as models of biological-membranes. *Bioscience*, 26(7):435–443, 1976.

K. Elamrani and A. Blume. Phase-transition kinetics of phosphatidic-acid bilayers - a pressure-jump relaxation study. *Biochemistry-Us*, 22(14):3305–3311, 1983.

R. Feynman, R. B. Leighton, and M. Sands. *The Feynman Lectures On Physics: Volume 2: Mainly Electromagnetism And Matter*, chapter 8: Electrostatic Energy, pages 1–12. Pearson Addison Wesley, 1st edition, 1964.

M. Fidorra, T. Heimburg, and L. Bagatolli. Direct visualization of the lateral structure of porcine brain cerebrosides/popc mixtures in presence and absence of cholesterol. *Biophys J*, 97(1):142–154, 2009a.

M. Fidorra, T. Heimburg, and H. Seeger. Melting of individual lipid components in binary lipid mixtures studied by ftir spectroscopy, dsc and monte carlo simulations. *Bba-Biomembranes*, 1788(3):600–607, 2009b.

C. Fox. Structure of cell-membranes. *Sci Am*, 226(2):30–38, 1972.

J. Gallaher, K. Wodzinska, T. Heimburg, and M. Bier. Ion-channel-like behavior in lipid bilayer membranes at the melting transition. *Phys Rev E*, 81(6):061925, 2010.

R. B. Gennis. *Biomembranes - Molecular Structure and Function*. Springer, 1989.

A. Georgallas and D. Pink. Phase-transitions in monolayers of saturated lipids - exact results and monte-carlo simulations. *J Colloid Interf Sci*, 89(1):107–116, 1982.

A. Georgallas, D. Hunter, T. Lookman, M. Zuckermann, and D. Pink. Interactions between 2 sheets of a bilayer-membrane and its internal lateral pressure. *Eur Biophys J Biophy*, 11(2):79–86, 1984.

A. Georgallas, J. MacArthur, X. Ma, C. Nguyen, G. Palmer, M. Singer, and M. Tse. The diffusion of small ions through phospholipid-bilayers. *J Chem Phys*, 86(12):7218–7226, 1987.

R. Glaser, S. Leikin, L. Chernomordik, V. Pastushenko, and A. Sokirko. Reversible electrical breakdown of lipid bilayers - formation and evolution of pores. *Biochim Biophys Acta*, 940(2):275–287, 1988.

R. Glauber. Time-dependent statistics of the ising model. *Journal of Mathematical Physics (New York)(US)*, 4(2):294–307, 1963.

E. Gorter and F. Grendel. On bimolecular layers of lipoids on the chromocytes of the blood. *J Exp Med*, 41(4):439–443, 1925.

P. Grabitz, V. P. Ivanova, and T. Heimburg. Relaxation kinetics of lipid membranes and its relation to the heat capacity. *Biophysical Journal*, 82(1 Pt 1):299–309, 2002.

R. Greene and H. Callen. On the formalism of thermodynamic fluctuation theory. *Physical Review*, 83(6):1231–1235, 1951.

B. Gruenewald, S. Stankowski, and A. Blume. Curvature influence on the cooperativity and the phase-transition enthalpy of lecithin vesicles. *Febs Lett*, 102(2):227–229, 1979.

B. Gruenewald, A. Blume, and F. Watanabe. Kinetic investigations on the phase-transition of phospholipid-bilayers. *Biochim Biophys Acta*, 597(1):41–52, 1980.

A. Hac, H. Seeger, M. Fidorra, and T. Heimburg. Diffusion in two-component lipid membranes—a fluorescence correlation spectroscopy and monte carlo simulation study. *Biophysical Journal*, 88(1):317–333, 2005.

S. Halstenberg, W. Schrader, P. Das, J. Bhattacharjee, and U. Kaatze. Critical fluctuations in the domain structure of lipid membranes. *J Chem Phys*, 118(12):5683–5691, 2003.

W. Hanke, C. Methfessel, U. Wilmsen, and G. Boheim. Ion channel reconstitution into lipid bilayer-membranes on glass patch pipettes. *Bioelectroch Bioener*, 12(3-4): 329–339, 1984.

P. Hansen, L. Miao, and J. Ipsen. Fluid lipid bilayers: Intermonolayer coupling and its thermodynamic manifestations. *Phys Rev E*, 58(2):2311–2324, 1998.

S. Hansen. Estimation of the relaxation spectrum from dynamic experiments using bayesian analysis and a new regularization constraint. *Rheol Acta*, 47(2):169–178, 2008.

J. Hazel and E. Williams. The role of alterations in membrane lipid-composition in enabling physiological adaptation of organisms to their physical-environment. *Prog Lipid Res*, 29(3):167–227, 1990.

T. Heimburg. Mechanical aspects of membrane thermodynamics. estimation of the mechanical properties of lipid membranes close to the chain melting transition from calorimetry. *Bba-Biomembranes*, 1415(1):147–162, 1998.

T. Heimburg. A model for the lipid pretransition: Coupling of ripple formation with the chain-melting transition. *Biophysical Journal*, 78(3):1154–1165, 2000.

T. Heimburg. Lipid ion channels. *Biophys Chem*, 150(1-3):2–22, 2010a.

T. Heimburg. The physics of nerves. *arXiv*, physics.bio-ph, 2010b.

T. Heimburg. *Thermal biophysics of membranes.* Wiley-VCH, Berlin, 1st edition, 2007.

T. Heimburg and R. Biltonen. Thermotropic behavior of dimyristoylphosphatidylglycerol and its interaction with cytochrome-c. *Biochemistry-Us*, 33(32):9477–9488, 1994.

T. Heimburg and R. Biltonen. A monte carlo simulation study of protein-induced heat capacity changes and lipid-induced protein clustering. *Biophysical Journal*, 70(1): 84–96, 1996.

T. Heimburg and A. Jackson. On soliton propagation in biomembranes and nerves. *P Natl Acad Sci Usa*, 102(28):9790–9795, 2005.

T. Heimburg and A. Jackson. The thermodynamics of general anesthesia. *Biophys J*, 92 (9):3159–3165, 2007a.

T. Heimburg and A. Jackson. On the action potential as a propagating density pulse and the role of anesthetics. *Biophysical Reviews and Letters*, 2(1):57–78, 2007b.

D. Hilgemann. Getting ready for the decade of the lipids. *Annu Rev Physiol*, 65:697–700, 2003.

B. Hille. *Ion Channels of Excitable Membranes.* Sinauer Associates, 3rd edition, 2001.

H. Hinz and J. Sturtevant. Calorimetric studies of dilute aqueous suspensions of bilayers formed from synthetic l-alpha-lecithins. *Journal of Biological Chemistry*, 247(19): 6071–6075, 1972.

A. Hodgkin and A. Huxley. A quantitative description of membrane current and its application to conduction and excitation in nerve. *J Physiol-London*, 117(4):500–544, 1952.

J. Howarth. Heat production in non-myelinated nerves. *Philos T Roy Soc B*, 270(908): 425–429, 1975.

J. Howarth, R. Keynes, and J. Ritchie. Origin of initial heat associated with a single impulse in mammalian non-myelinated nerve fibres. *J Physiol-London*, 194(3):745–793, 1968.

J. Howarth, R. Keynes, J. Ritchie, and A. Muralt. Heat production associated with passage of a single impulse in pike olfactory nerve-fibers. *J Physiol-London*, 249(2): 349–368, 1975.

E. Ising. Report on the theory of ferromagnetism. *Z Phys*, 31:253–258, 1925.

V. P. Ivanova and T. Heimburg. Histogram method to obtain heat capacities in lipid monolayers, curved bilayers, and membranes containing peptides. *Physical review E, Statistical, nonlinear, and soft matter physics*, 63(4 Pt 1):041914, 2001.

V. P. Ivanova, I. Makarov, T. Schaffer, and T. Heimburg. Analyzing heat capacity profiles of peptide-containing membranes: Cluster formation of gramicidin a. *Biophysical Journal*, 84(4):2427–2439, 2003.

K. Iwasa and I. Tasaki. Mechanical changes in squid giant-axons associated with production of action-potentials. *Biochem Bioph Res Co*, 95(3):1328–1331, 1980.

K. Iwasa, I. Tasaki, and R. Gibbons. Swelling of nerve fibers associated with action potentials. *ScienceNew Series*, 210(4467):338–339, 1980.

R. Jacobs, B. Hudson, and H. Andersen. Theory of chain melting phase-transition of aqueous phospholipid dispersions. *P Natl Acad Sci Usa*, 72(10):3993–3997, 1975.

K. Jacobson, E. Sheets, and R. Simson. Revisiting the fluid mosaic model of membranes. *Science*, 268(5216):1441–1442, 1995.

M. Jansen and A. Blume. A comparative-study of diffusive and osmotic water permeation across bilayers composed of phospholipids with different head groups and fatty acyl chains. *Biophysical Journal*, 68(3):997–1008, 1995.

P. V. Jensen and P. Prentø. *Cellebiologi: Teori og Metoder*. Cellebiologisk-Anatomisk Laboratorium, Zoologisk Institut, Københavns Universitet, 1994.

D. Johnston and S. M.-S. Wu. *Foundations of Cellular Neurophysiology*, chapter 5: Nonlinear Properties of Excitable Membranes. MIT Press, 1997.

K. Kaufmann and I. Silman. Proton-induced ion channels through lipid bilayer-membranes. *Naturwissenschaften*, 70(3):147–149, 1983a.

K. Kaufmann and I. Silman. The induction by protons of ion channels through lipid bilayer-membranes. *Biophys Chem*, 18(2):89–99, 1983b.

K. Kaufmann, W. Hanke, and A. Corcia. Ion channel fluctuations in pure lipid bilayer membranes: Control by voltage. *Book*, 3:40, 1989a.

K. Kaufmann, W. Hanke, and A. Corcia. *Ion Channel Fluctuations in Pure Lipid Bilayer Membranes: Control by voltage*, volume 3. Unpublished, 1989b. URL http://www.membranes.nbi.dk/Kaufmann/pdf/1989_Kaufmann_book3_ed.pdf.

D. Keller, N. Larsen, I. Moller, and O. G. Mouritsen. Decoupled phase transitions and grain-boundary melting in supported phospholipid bilayers. *Phys Rev Lett*, 94(2): 025701, 2005.

B. Lautrup, A. Jackson, and T. Heimburg. The stability of solitons in biomembranes and nerves. *arXiv*, physics.bio-ph, 2005. 7 pages, 5 figures.

A. Lee. Ion channels - a paddle in oil. *Nature*, 444(7120):697–697, 2006.

G. Leidy, W. Wolkers, K. Jorgensen, O. G. Mouritsen, and J. Crowe. Lateral organization and domain formation in a two-component lipid membrane system. *Biophysical Journal*, 80(4):1819–1828, 2001.

A. Lev, Y. Korchev, T. Rostovtseva, C. Bashford, D. T. Edmonds, and C. Pasternak. Rapid switching of ion current in narrow pores - implications for biological ion channels. *P Roy Soc Lond B Bio*, 252(1335):187–192, 1993.

L. Liebovitch, D. Scheurle, M. Rusek, and M. Zochowski. Fractal methods to analyze ion channel kinetics. *Methods*, 24(4):359–375, 2001.

C. Linden, K. Wright, H. McConnell, and C. Fox. Lateral phase separations in membrane lipids and mechanism of sugar transport in escherichia-coli. *P Natl Acad Sci Usa*, 70 (8):2271–2275, 1973.

J. Logue, A. D. Vries, E. Fodor, and A. Cossins. Lipid compositional correlates of temperature-adaptive interspecific differences in membrane physical structure. *J Exp Biol*, 203(14):2105–2115, 2000.

S. Mabrey and J. Sturtevant. Investigation of phase-transitions of lipids and lipid mixtures by high sensitivity differential scanning calorimetry. *P Natl Acad Sci Usa*, 73 (11):3862–3866, 1976.

A. MacDonald. Application of the theory of homeoviscous adaptation to excitable-membranes - pre-synaptic processes. *Biochem J*, 256(2):313–327, 1988.

N. Markova, E. Sparr, L. Wadso, and H. Wennerstrom. A calorimetric study of phospholipid hydration. simultaneous monitoring of enthalpy and free energy. *J Phys Chem B*, 104(33):8053–8060, 2000.

A. Marr and J. Ingraham. Effect of temperature on composition of fatty acids in escherichia coli. *J Bacteriol*, 84(6):1260–1267, 1962.

S. J. Marrink, H. J. Risselada, and A. Mark. Simulation of gel phase formation and melting in lipid bilayers using a coarse grained model. *Chemistry and Physics of Lipids*, 135(2):223–244, 2005.

S. May. Trans-monolayer coupling of fluid domains in lipid bilayers. *Soft Matter*, 5(17): 3148–3156, 2009.

E. Mbamala, A. Fahr, and S. May. Electrostatic model for mixed cationic-zwitterionic lipid bilayers. *Langmuir*, 22(11):5129–5136, 2006.

N. Metropolis, A. Rosenbluth, M. Rosenbluth, A. Teller, and E. Teller. Equation of state calculations by fast computing machines. *J Chem Phys*, 21(6):1087–1092, 1953.

G. Millhauser, E. Salpeter, and R. Oswald. Diffusion-models of ion channel gating and the origin of power law distributions from single-channel recording. *Biophys J*, 53(2): 1503–1507, 1988.

H. Mohwald. Phospholipid and phospholipid-protein monolayers at the air/water interface. *Annu Rev Phys Chem*, 41:441–476, 1990.

M. Montal and P. Mueller. Formation of bimolecular membranes from lipid monolayers and a study of their electrical properties. *P Natl Acad Sci Usa*, 69(12):3561–3566, 1972.

O. G. Mouritsen and M. Bloom. Mattress model of lipid-protein interactions in membranes. *Biophysical Journal*, 46(2):141–153, 1984.

O. G. Mouritsen and M. Zuckermann. Softening of lipid bilayers. *Eur Biophys J Biophy*, 12(2):75–86, 1985.

O. G. Mouritsen and M. Zuckermann. What's so special about cholesterol? *Lipids*, 39 (11):1101–1113, 2004.

O. G. Mouritsen, A. Boothroyd, R. Harris, N. Jan, T. Lookman, L. MacDonald, D. Pink, and M. Zuckermann. Computer-simulation of the main gel fluid phase-transition of lipid bilayers. *J Chem Phys*, 79(4):2027–2041, 1983.

J. Nagle. Theory of the main lipid bilayer phase-transition. *Annu Rev Phys Chem*, 31: 157–195, 1980.

J. Nagle and H. Scott. Lateral compressibility of lipid monolayers and bilayers theory of membrane-permeability. *Biochim Biophys Acta*, 513(2):236–243, 1978.

E. Neher and B. Sakmann. Single-channel currents recorded from membrane of denervated frog muscle-fibers. *Nature*, 260(5554):799–802, 1976.

L. Nielsen, T. Bjornholm, and O. G. Mouritsen. Critical phenomena - fluctuations caught in the act. *Nature*, 404(6776):352–352, 2000.

M. Nielsen, L. Miao, J. Ipsen, M. Zuckermann, and O. G. Mouritsen. Off-lattice model for the phase behavior of lipid-cholesterol bilayers. *Physical review E, Statistical physics, plasmas, fluids, and related interdisciplinary topics*, 59(5 Pt B):5790–803, 1999.

L. Onsager. Crystal statistics i a two-dimensional model with an order-disorder transition. *Physical Review*, 65(3/4):117–149, 1944.

E. Overton. On the general osmotic properties of the cell, their probable origin, and their significance for physiology. *Vierteljahrschrift der Naturforschende Gesselschaft (Zurich)*, 44:88–135, 1899.

D. Papahadjopoulos, K. Jacobson, S. Nir, and T. Isac. Phase-transitions in phospholipid vesicles - fluorescence polarization and permeability measurements concerning effect of temperature and cholesterol. *Biochim Biophys Acta*, 311(3):330–348, 1973.

M. Parmahamsa, K. Reddy, and N. Varadacharyulu. Changes in composition and properties of erythrocyte membrane in chronic alcoholics. *Alcohol Alcoholism*, 39(2):110–112, 2004.

S. Paula, A. Volkov, and D. Deamer. Permeation of halide anions through phospholipid bilayers occurs by the solubility-diffusion mechanism. *Biophys J*, 74(1):319–327, 1998.

R. J. Pedersen. Electrophysiological measurements of spontaneous action potentials in crayfish nerve in relation to the soliton model. *Master's thesis*, pages 1–59, 2010.

R. Penner. *Single-channel recording*, chapter 1: Practical guide to patch clamping, pages 3–30. Springer, 2nd edition, 1995.

A. Petrov. Electricity and mechanics of biomembrane systems: flexoelectricity in living membranes. *Anal Chim Acta*, 568(1-2):70–83, 2006.

D. Pink, T. Green, and D. Chapman. Raman-scattering in bilayers of saturated phosphatidylcholines - experiment and theory. *Biochemistry-Us*, 19(2):349–356, 1980.

G. G. Putzel, M. Uline, and I. Szleifer. Interleaflet coupling and domain registry in phase-separated lipid bilayers. *phys.washington.edu*, 2010.

R. Q. Quiroga, Z. Nadasdy, and Y. Ben-Shaul. Unsupervised spike detection and sorting with wavelets and superparamagnetic clustering. *Neural computation*, 16(8):1661–87, 2004.

G. Reid and M. Flonta. Physiology - cold current in thermoreceptive neurons. *Nature*, 413(6855):480–480, 2001.

H. J. Risselada and S. J. Marrink. The molecular face of lipid rafts in model membranes. *P Natl Acad Sci Usa*, 105(45):17367–17372, 2008.

J. Ritchie and R. Keynes. The production and absorption of heat associated with electrical-activity in nerve and electric organ. *Q Rev Biophys*, 18(4):451–476, 1985.

J. Robertson. New observations on the ultrastructure of the membranes of frog peripheral nerve fibers. *J Biophys Biochem Cy*, 3(6):1043–1048, 1957.

M. Sabra, K. Jorgensen, and O. G. Mouritsen. Lindane suppresses the lipid-bilayer permeability in the main transition region. *Bba-Biomembranes*, 1282(1):85–92, 1996.

F. Sachs and F. Qin. Gated, ion-selective channels observed with patch pipettes in the absence of membranes - novel properties of a gigaseal. *Biophysical Journal*, 65(3): 1101–1107, 1993.

L. Salford, A. Brun, J. Eberhardt, L. Malmgren, and B. Persson. Nerve cell damage in mammalian brain after exposure to microwaves from gsm mobile phones. *Environ Health Persp*, 111(7):881–883, 2003.

L. Salford, H. Nittby, A. Brun, J. Eberhardt, L. Malmgren, and B. Persson. Effects of microwave radiation upon the mammalian blood-brain barrier. *Non-thermal effects and mechanisms of interaction between electromagnetic fields and living matter*, pages 1–28, 2010.

D. Schmidt, Q.-X. Jiang, and R. MacKinnon. Phospholipids and the origin of cationic gating charges in voltage sensors. *Nature*, 444(7120):775–779, 2006.

W. Schrader, H. Ebel, P. Grabitz, E. Hanke, T. Heimburg, M. Hoeckel, M. Kahle, F. Wente, and U. Kaatze. Compressibility of lipid mixtures studied by calorimetry and ultrasonic velocity measurements. *J Phys Chem B*, 106(25):6581–6586, 2002.

H. Seeger, M. Fidorra, and T. Heimburg. Domain size and fluctuations at domain interfaces in lipid mixtures. *Macromol. Symp.*, 219(1):85–96, 2005.

H. Seeger, M. Gudmundsson, and T. Heimburg. How anesthetics, neurotransmitters, and antibiotics influence the relaxation processes in lipid membranes. *J Phys Chem B*, 111(49):13858–13866, 2007.

H. Seeger, G. Marino, A. Alessandrini, and P. Facci. Effect of physical parameters on the main phase transition of supported lipid bilayers. *Biophys J*, 97(4):1067–1076, 2009.

H. Seeger, L. Aldrovandi, A. Alessandrini, and P. Facci. Changes in single k+ channel behavior induced by a lipid phase transition. *Biophys J*, 99(11):3675–3683, 2010a.

H. Seeger, A. D. Cerbo, A. Alessandrini, and P. Facci. Supported lipid bilayers on mica and silicon oxide: Comparison of the main phase transition behavior. *J Phys Chem B*, 114(27):8926–8933, 2010b.

K. Simons and E. Ikonen. Functional rafts in cell membranes. *Nature*, 387(6633):569–572, 1997.

M. Sinensky. Homeoviscous adaptation - homeostatic process that regulates viscosity of membrane lipids in escherichia-coli. *P Natl Acad Sci Usa*, 71(2):522–525, 1974.

S. Singer and G. Nicolson. Fluid mosaic model of structure of cell-membranes. *Science*, 175(4023):720–731, 1972.

D. Steppich, J. Griesbauer, T. Frommelt, W. Appelt, A. Wixforth, and M. Schneider. Thermomechanic-electrical coupling in phospholipid monolayers near the critical point. *Phys Rev E*, 81(6):061123, 2010.

G. Stulen. Electric-field effects on lipid-membrane structure. *Biochim Biophys Acta*, 640 (3):621–627, 1981.

J. Sturtevant. The effect of sodium chloride and calcium chloride on the main phase transition of dimyristoylphosphatidylcholine. *Chemistry and Physics of Lipids*, 95(2): 163–168, 1998.

I. Sugar. Theory of the electric field-induced phase-transition of phospholipid-bilayers. *Biochim Biophys Acta*, 556(1):72–85, 1979.

I. Sugar, T. Thompson, and R. Biltonen. Monte carlo simulation of two-component bilayers: Dmpc/dspc mixtures. *Biophysical Journal*, 76(4):2099–2110, 1999.

I. Tasaki. Rapid structural changes in nerve fibers and cells associated with their excitation processes. *Jpn J Physiol*, 49(2):125–138, 1999a.

I. Tasaki. Evidence for phase transition in nerve fibers, cells and synapses. *Ferroelectrics*, 220(3-4):305–316, 1999b.

I. Tasaki and K. Iwasa. Shortening of nerve-fibers associated with propagated nerve impulse. *Biochem Bioph Res Co*, 94(2):716–720, 1980.

I. Tasaki and K. Iwasa. Temperature-changes associated with nerve excitation - detection by using polyvinylidene fluoride film. *Biochem Bioph Res Co*, 101(1):172–176, 1981.

I. Tasaki, F. Watanabe, and I. Singer. Excitability of squid giant axons in absence of univalent cations in external medium. *P Natl Acad Sci Usa*, 56(4):1116–1122, 1966.

H. T. Tien and A. Ottova-Leitmannova. *Planar lipid bilayers (BLMs) and their applications*, chapter 8, pages 269–293. Elsevier Science, 1st edition, 2003.

H. Trauble and D. Haynes. Volume change in lipid bilayer lamellae at crystalline-liquid crystalline phase-transition. *Chemistry and Physics of Lipids*, 7(4):324–335, 1971.

H. Trauble, M. Teubner, P. Woolley, and H. Eibl. Electrostatic interactions at charged lipid-membranes .1. effects of ph and univalent cations on membrane structure. *Biophys Chem*, 4(4):319–342, 1976.

T. Tsong. Kinetics of crystalline-liquid crystalline phase-transition of dimyristoyl l-alpha-lecithin bilayers. *P Natl Acad Sci Usa*, 71(7):2684–2688, 1974.

K. Turnheim, J. Gruber, C. Wachter, and V. Ruiz-Gutierrez. Membrane phospholipid composition affects function of potassium channels from rabbit colon epithelium. *Am J Physiol-Cell Ph*, 277(1):C83–C90, 1999.

P. S. Ulinski, E. G. Jones, and A. Peters. *Cerebral Cortex: Models of Cortical Circuits*, chapter 2: Interpretations of Data and Mechanisms for Hippocampal Pyramidal Cell Models (Author: Lyle J. Borg-Graham), pages 19–138. Springer, 1st edition, 1999.

A. Ulrich, M. Sami, and A. Watts. Hydration of dopc bilayers by differential scanning calorimetry. *Bba-Biomembranes*, 1191(1):225–230, 1994.

W. van Osdol, R. Biltonen, and M. Johnson. Measuring the kinetics of membrane phase-transitions. *J Biochem Bioph Meth*, 20(1):1–46, 1989.

W. van Osdol, M. Johnson, Q. Ye, and R. Biltonen. Relaxation dynamics of the gel to liquid-crystalline transition of phosphatidylcholine bilayers - effects of chainlength and vesicle size. *Biophysical Journal*, 59(4):775–785, 1991.

W. van Osdol, Q. Ye, M. Johnson, and R. Biltonen. The effects of the anesthetic dibucaine on the kinetics of the gel-liquid crystalline transition of dppc multilamellar vesicles. *Biophysical Journal*, 64(2):A70–A70, 1993.

E. V. Vargas, A. Ludu, R. Hustert, P. Gumrich, A. Jackson, and T. Heimburg. Periodic solutions and refractory periods in the soliton theory for nerves and the locust femoral nerve. *Biophys Chem*, (153):159–167, 2011.

K. Venkatachalam and C. Montell. Trp channels. *Annu. Rev. Biochem.*, 76(1):387–417, 2007.

G. Wannier. The statistical problem in cooperative phenomena. *Rev Mod Phys*, 17(1): 50–60, 1945.

S. H. White. A study of lipid bilayer membrane stability using precise measurements of specific capacitance. *Biophysical Journal*, 10(12):1127–1148, 2006.

M. Winterhalter and W. Helfrich. Effect of voltage on pores in membranes. *Phys Rev A*, 36(12):5874–5876, 1987.

K. Wodzinska, A. Blicher, and T. Heimburg. The thermodynamics of lipid ion channel formation in the absence and presence of anesthetics. blm experiments and simulations. *Soft Matter*, 5(17):3319–3330, 2009.

D. Woodbury. Pure lipid vesicles can induce channel-like conductances in planar bilayers. *J Membrane Biol*, 109(2):145–150, 1989.

S. Wu and H. McConnell. Lateral phase separations and perpendicular transport in membranes. *Biochem Bioph Res Co*, 55(2):484–491, 1973.

B. Wunderlich, C. Leirer, A.-L. Idzko, h Keyser, A. Wixforth, V. M. Myles, T. Heimburg, and M. Schneider. Phase-state dependent current fluctuations in pure lipid membranes. *Biophysical Journal*, 96(11):4592–4597, 2009.

M. Yafuso, S. Kennedy, and A. Freeman. Spontaneous conductance changes, multilevel conductance states and negative differential resistance in oxidized cholesterol black lipid-membranes. *J Membrane Biol*, 17(3-4):201–212, 1974.

J. Yang and J. Appleyard. The main phase transition of mica-supported phosphatidylcholine membranes. *J Phys Chem B*, 104(34):8097–8100, 2000.

K. Yoshikawa, T. Fujimoto, T. Shimooka, H. Terada, N. Kumazawa, and T. Ishii. Electrical oscillation and fluctuation in phospholipid-membranes - phospholipids can form a channel without protein. *Biophys Chem*, 29(3):293–299, 1988.

Z. Zhang, M. Zuckermann, and O. G. Mouritsen. Effect of intermonolayer coupling on the phase-behavior of lipid bilayers. *Phys Rev A*, 46(10):6707–6713, 1992.

Additional material

A

A.1 Detecting the state of the membrane

Describing the influence of a transmembrane electric field is both a highly non-trivial theoretical problem, but also experimentally quite challenging.

One approach is to use the fluctuations in current through a membrane as a fingerprint for the state of the system. The idea is that there will a clear dependence of the both the mean current and the fluctuations on the phase state of the membrane. Also, the timescales of the fluctuations might provide another hint about the state of the membrane, as everything is close coupled to each other as discussed in Sec. 1.4.4.

This section will go through a number of methods to, in principle, detect the influence of the field.

A.1.1 Fluctuations and noise

If we measure the current (flux of ions) through the membrane, we see that the variance of the current changes with voltage.

This can have many causes:

- Number fluctuations, i.e. the natural (Poisson distributed) variation in the number of ions passing through in any given time interval. For instance, for a 10pA current measured for 0.1ms (sampling rate of 10kHz), this corresponds to a flux of about 6250 ± 80 ions, or about 1.3% variation. This is more than an order of magnitude lower than the intrinsic (thermal) noise level of the patch-clamp amplifier.

- Johnson-Nyquist noise, i.e. spontaneous fluctuations in the membrane potential. For an RC-circuit the Johnson-Nyquist noise takes a particularly simple form that is independent of the resistance. This can easily be derived from the fluctuation-dissipation theorem (Sec. 1.4.4):

$$C = \frac{dq}{d\Psi} = \frac{\langle \Delta q^2 \rangle}{k_B T} \quad \Rightarrow \quad \Delta\Psi_{\mathrm{JN}} = \frac{\sqrt{\langle \Delta q^2 \rangle}}{C} = \sqrt{\frac{k_B T}{C}}. \tag{A.1}$$

  For a system with a capacitance of $C = 10\mathrm{pF}$ we find that $\Delta\Psi_{\mathrm{JN}} \approx 30\mu\mathrm{V}$, which is an insignificant contribution to the baseline noise and can therefore be disregarded.

- The flexoelectric effect, i.e. the curvature-induced surface polarisation of the membrane, which has the phenomenological form:

$$\Delta\Psi_{\mathrm{flex}} = \frac{f}{\epsilon_0}(c_1 + c_2), \tag{A.2}$$

  where f is the area flexoelectric coefficient (for non-charged lipids $f \approx 1 \times 10^{-20}\mathrm{C}$), and c_1 and c_2 are the two principle radii of the membrane curvature. Under most circumstances, this effect is rather small, i.e. on the order of 1mV or less (for a radius of curvature of 1µm, and probably even less for the spontaneous curvatures; see Petrov (2006)). Again this is lower than the intrinsic noise of the amplifiers.

- Current fluctuations can also arise from actual fluctuations in the conductance of the membrane. Such conductance changes can stem from both fluctuations in geometry or from defect density of the membrane. For constant membrane potential, V_m, we have

$$\sigma^2 = \langle \Delta I^2 \rangle = \langle (\Delta G \cdot V_m)^2 \rangle + \sigma_{bg}^2 \tag{A.3}$$

  where G is the membrane conductance in ohms [Ω], and σ_{bg}^2 is the (constant) background noise stemming from thermal noise in the electronics and various external sources (the water bath, the power supplies, the lamps in the room, and so on).

  From this we see that the current variance should increase as the square of the applied voltage. However, the data shows that this is decidedly not so, meaning that the conductance fluctuations are also influenced the electrical field.

- Lastly, the fluctuations might not even be due to ohmic currents, but rather to capacitive currents that, again, can arise from e.g. Johnson-Nyquist noise and fluctuations in membrane geometry.

A.1.2 Conductance changes

As discussed in Sec. 1.3 the permeability and mean conductivity of the membrane depends on the state of the membrane and on the properties of the particle (ion, molecule, proton) that is passing through the membrane.

A simple, borderline naïve, approach would be to determine the conductance of the membrane as a function of temperature (and hence the phase state of the membrane), and then, at a given temperature, observe how membrane conductance changes with the applied voltage. Alternatively, one could keep a fixed voltage, and then perform a temperature scan, using the change in conductance as an indicator for the phase state of the membrane.

In practice this did not work reliably with our setup, because the membrane seal was prone to changing slightly during the experiment, making it difficult to attribute conductance changes to changes in membrane state. Furthermore, the pipette offset was also prone to drifting, complicating things additionally. Admittedly, it might be possible to work around these problems by means of good statistics, but in the end I chose to focus on other experiments.

While there has been very few experiments on the coupling of an electric field to the phase state of a lipid membrane, one attempt was that of Antonov et al. (1990) which was in fact based on similar considerations as made here. They found that the negatively charged phospholipid (DPPA) was strongly influenced, increasing the melting point by about 8–12°C at 150mV. For the zwitterionic lipid DPPC, the effect was similar, though weaker, showing only an increase of about 2–3°C at 150mV. However, it should be pointed out that Fig. 1–3 and Table 1 in the article all contradict each other, so I am not fully convinced of the reliability of their findings.

A.1.3 Conductance fluctuations

If membrane leak conductance is primarily due to unresolved conductance events , and if such events mostly occur at the fluctuating domain interfaces, then one would expect to see both an increase in membrane leak conductance close to the phase transition (basically the basis of first approach based on conductance changes). Another interesting consequence is that the membrane conductance itself would also have a greatly increased variance close to the phase transition, since the length of the domain interfaces fluctuate strongly (Seeger et al. (2005)).

The main issue with this method is that current fluctuations need not be related to fluctuations in the membrane conductance (though, of course, the reverse will be true), since the measured current is a combination of both ohmic and capacitive currents. This will not necessarily interfere with detecting the phase transition by means of measuring the current, since the capacitance (and hence the capacitive currents) are also expected to fluctuate in the phase transition, due to geometric fluctuations (and possibly even from fluctuations in membrane permittivity) due to the large changes in the membrane's elastic constants (Ebel et al. (2001); Schrader et al. (2002)).

A.1.4 Capacitance changes

The capacitance is one of the simplest properties of the membrane, being a measure of the system's ability to hold an electrical charge.

$$C = \frac{q}{V_m} \tag{A.4}$$

where C is the capacitance measured in farads [F], q is the charge on the capacitor in coulombs [C], and V_m is the transmembrane voltage in volts [V].

The capacitance is closely related to the geometry of the system and the dielectric properties of the insulator separating the charges. For the simplest case of a parallel-plate capacitor, the capacitance is approximatively given by

$$C = \epsilon_r \epsilon_0 \frac{A}{d} \tag{A.5}$$

where ϵ_r is the dielectric constant of the insulator ($\approx$ 2.1–2.4 for hydrocarbons), ϵ_0 is the vacuum permittivity ($\approx 8.854 \times 10^{-12}$ F m^{-1}), A is the area of the membrane, and d is the membrane thickness.

Since membrane expands and thins out in the fluid phase, a significant increase in the membrane capacitance will also occur (Boheim et al. (1980)). This increase will be slightly suppressed by the fact that the dielectric constant of hydrocarbons decrease with temperature (typically around -0.05% per degree celsius) and with density (the lipid density decreases by a few percent when changing state). Thus, in principle it should be possible to uniquely correlate changes in membrane capacitance with its phase state.

Since an exact determination of the membrane area is usually not possible, and since there are always additional contributions to the capacitance from the experimental

setup (wires, electrodes, pipette walls, etc.), in practice one would be limited to look at changes in capacitance, rather than measure its absolute value. So in line with the ideas presented above, one could first measure the capacitance as a function of temperature and voltage, using the abrupt change as an indicator for the phase transition. Also, one would have to correct for electrostriction effects, since this is known to mechanically compress the membrane, resulting in capacitance changes even when far away from the main phase transition.

As a side note, it has been reported that monolayers show a linear relationship between the electric capacitance, compressibility, and heat capacity close to the phase transition regime (Steppich et al. (2010)). If this relationship also holds for lipid bilayers, it should make it significantly easier to detect a transition induced by an applied electric field.

Accurately measuring the capacitance of a membrane with an area in the square micron range is not a trivial ask, as the capacitance will be of the order 1pF or less. A common way to measure the capacitance with a patch clamp amplifier is to apply an oscillating voltage, $U(t)$, since this will give rise to capacitive currents

$$I = \frac{dq}{dt} = C\frac{dV_m}{dt} + V_m\frac{dC}{dt} \tag{A.6}$$

So for system with a constant capacitance, a triangular voltage input ($dV_m/dt = \pm\text{const.}$) will result in a square output, with the amplitude being a direct measure of the capacitance.

However, in practice this does not provide particularly good resolution, especially if the membrane conductance is high or the charging time of the capacitor is long, or significant low-pass filtering is necessary. One alternative method is to perform a voltage jump instead. The change in voltage will result in a transient current spike with an area (total charge moved) that is simply given by $\Delta q = C\Delta V_m$. There will be an additional contribution from the finite conductance of the membrane, giving an offset of the baseline, and finally there will be a finite settling time of the membrane voltage as shown in Fig. A.1.

Naturally, there are also commercially available instruments for making high precision capacitance measurements. Our group was kindly allowed to borrow a capacitance bridge from Andeen-Hagerling Inc. (AH-2700A Ultra-precision Capacitance Bridge) costing about 250,000DKK. Under optimal conditions, this instrument has a resolution of about 1aF, which is about four orders of magnitude smaller than the capacitance of a $1\mu m^2$ lipid bilayer. As it turned out, the instrument was only able to achieve such spectacular resolution by applying fairly large voltages (in the range of 15V). When limiting the voltages to be in the millivolt range, the resolution deteriorated by more than three orders of magnitude, making it comparable to what can be achieved with a modern patch clamp amplifier. Since the general user friendliness of the AH-2700A was markedly worse than the Axopatch 200B amplifier we use, and it additionally required some modifications to the setup, it was deemed unsuited for our purposes and – in my opinion – biomembrane experiments in general.

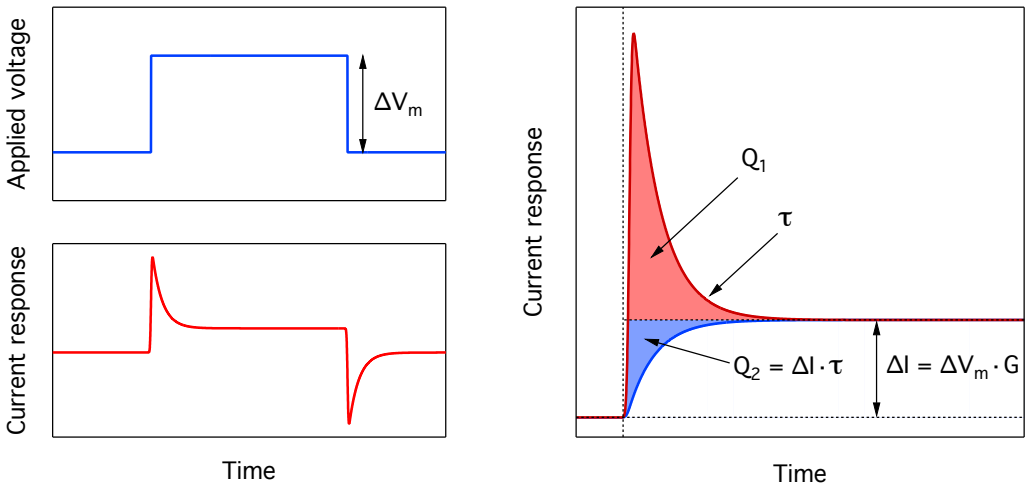

FIG. A.1: Determination of membrane capacitance from a voltage jump. *Left:* Applied voltage and the resulting current. *Right:* Enlargement of the first transient spike, showing the various contributions to the signal. Q_1 is the charge in under the transient above the steady-state response. $Q_2 = \tau \Delta I$ is a correction factor from the finite settling time of the membrane voltage, where τ is the time constant of the instrument and is related to the access resistance, system capacitance, and low-pass filtering frequency. Finally we get that $C_m = (Q_1 + Q_2)/\Delta V_m$.

A.1.5 Relaxation measurements

At fourth way to detect the influence of an applied electric field on the phase state of the membrane, also could look at the relaxation behaviour of a membrane in response to a jump in voltage, since it is well-documented that the relaxation timescale of lipid membranes is closely related to its phase state (Sec. 1.4.4). The main requirement here is that one looks at a property that has a sufficiently strong dependence on the membrane phase state. An obvious example would be the conductance or capacitance.

The main issue here is that jumps in voltage also results in capacitive currents which can be completely unrelated to the membrane, e.g. charging of the pipette walls or even just the capacitance of the electrodes. Some of these things can be taken into account for by having a sufficiently low access resistance and low system capacitance, i.e. $R_{access} \cdot C_{system} \ll \tau_{relax}$.

In particular, it might be possible to determine a relaxation timescale spectrum from the autocorrelation function of the current trace. One option is to estimate the relaxation spectrum by using Bayesian analysis (see e.g. Hansen (2008)). This does, however, involve a number of assumptions, and might not produce reliable results.

Note that, in principle, the two fluctuation measures are independent – i.e. the timescales can change without the magnitude of the fluctuations change, and vice versa.

A.2 Vesicles with a permanent membrane potential

Let us consider two volumes separated by a semi-permeable membrane. Let b denote the outside (bulk) volume and v the inside of the vesicles. Let us for simplicity's sake also assume that the pH is neutral or high, such that the H_3O^+ ions will not contribute to the charge balance. Lastly, we assume that the membrane is permeable to Na^+, Cl^-, and OH^- and that the vesicles contain macro molecules, M^{+z}, to which the membrane is impermeable.

Charge neutrality gives us that:

$$\sum_i z_i[C_i] = 0, \tag{A.7}$$

where z_i is the charge of species i (i is Na^+, Cl^-, OH^-, and M^{+z}).

More explicitly, this gives us the one equation for each volume:

$$[Na^+]_b - [Cl^-]_b - [OH^-]_b = 0 \tag{A.8}$$
$$z[M^{+z}] + [Na^+]_v - [Cl^-]_v - [OH^-]_v = 0 \tag{A.9}$$

For all the ions in electro-chemical equilibrium we know from the Nernst equation that

$$\frac{[Na^+]_b}{[Na^+]_v} = \frac{[Cl^-]_v}{[Cl^-]_b} = \frac{[OH^-]_v}{[OH^-]_b} \tag{A.10}$$

From the conservation of mass we get

$$[Na^+]_b V_b + [Na^+]_v V_v = [Na^+] V_{tot} \tag{A.11}$$
$$[Cl^-]_b V_b + [Cl^-]_v V_v = [Cl^-] V_{tot} \tag{A.12}$$

where $[Na^+]$ and $[Cl^-]$ (no index) are the initial (controllable) concentrations of the salts, V_b and V_v are the respective volumes, and V_{tot} is the total volume.

If we assume that the combined volume of the vesicles is much smaller than the bulk volume[1], i.e. $V_v \ll V_b$, then we have that

$$V_{tot} \approx V_b \quad \Rightarrow \quad [Na^+]_b \approx [Cl^-]_b \approx [Na^+] = [Cl^-]. \tag{A.13}$$

This gives us

$$[Na^+][Cl^-] \approx [Na^+]_b[Cl^-]_b \tag{A.14}$$
$$= [Na^+]_v[Cl^-]_v \tag{A.15}$$
$$= [Na^+]_v([Na^+]_v + z[M^{+z}] - [OH^-]_v) \tag{A.16}$$

Using the chemical equilibrium equation (Eq. (A.10)) for OH^- gives us:

$$[OH^-]_v = [OH^-]_b \frac{[Na^+]_b}{[Na^+]_v} \approx [OH^-]_b \frac{[Na^+]}{[Na^+]_v} \tag{A.17}$$

[1] For a 1mM lipid solution of 100nm diameter vesicles, this ratio is roughly 200:1, i.e. it is a very good approximation.

Plugging this into Eq. (A.16) gives a simple quadratic equation:

$$[\mathrm{Na}^+][\mathrm{Cl}^-] \approx [\mathrm{Na}^+]_v^2 + z[M^{+z}][\mathrm{Na}^+]_v - [\mathrm{OH}^-]_b[\mathrm{Na}^+] \tag{A.18}$$

$$\Rightarrow \quad [\mathrm{Na}^+]_v \approx \frac{1}{2}\Big(- z[M^{+z}] + \sqrt{z^2[M^{+z}]^2 + 4[\mathrm{Na}^+]([\mathrm{Cl}^-] + [\mathrm{OH}^-]_b)}\Big) \tag{A.19}$$

This results in a Nernst potential given by the well-known expression:

$$V_m = \frac{RT}{z_{Na}F} \ln\left(\frac{[\mathrm{Na}^+]_b}{[\mathrm{Na}^+]_v}\right) \approx \frac{RT}{z_{Na}F} \ln\left(\frac{[\mathrm{Na}^+]}{[\mathrm{Na}^+]_v}\right) \tag{A.20}$$

where R is the gas constant, F the Faraday constant, and T is the temperature. The result of this has been plotted below for a macromolecule with $z = +8$, shown as a function of the bulk salt concentration. Note that in practice, one should probably avoid using buffers, since they will also contribute with a mobile ions which can reduce the Nernst potential.

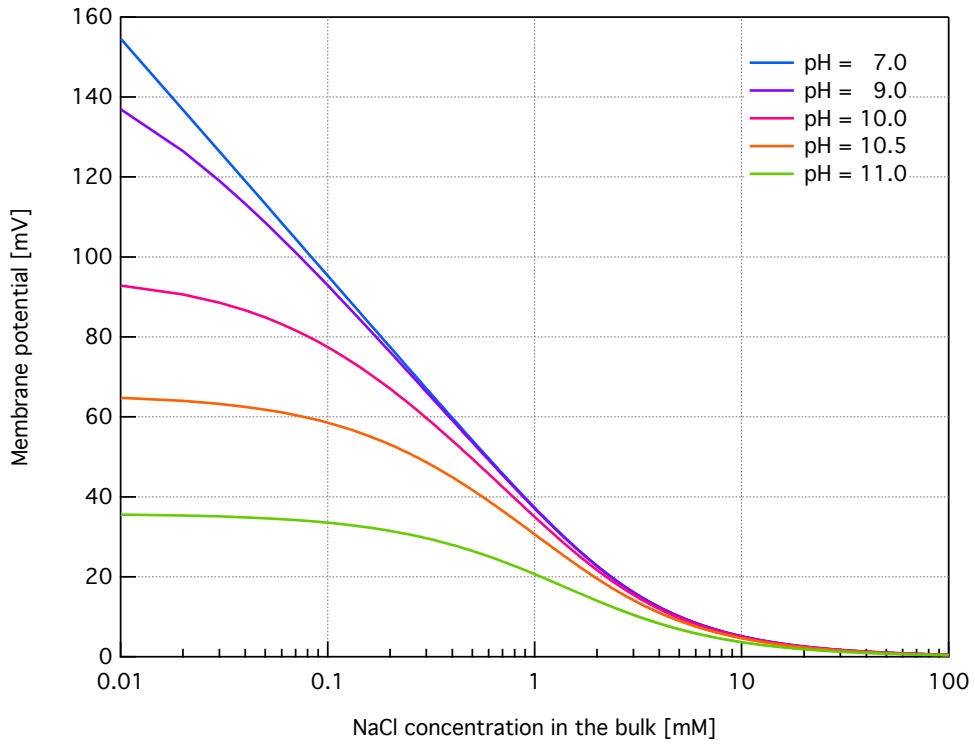

FIG. A.2: Plot of the calculated Nernst potential at 0.5mM of a macromolecule with $z = +8$, $T = 300$K, as a function of salt concentration and at various pH values for the bulk volume. For the sake of simplicity, it was assumed that the charge of the macromolecule is independent of the pH, which is not true in general.

A.3 Determination of pore kinetics

Determination of pore kinetics involve two stages. The first step is to robustly detect when there is a pore opening and for how long it lasts. Second step is to calculate the multi-scale probability density functions (PDF) and effective transition rates for the opening and closing events.

A.3.1 Detection of events

There are several ways to go about detecting when an event happens. The simplest and therefore most common method is to simply set a threshold value, and then define that an event (opening or closing) occurs whenever the signal crosses this threshold level. This method works well if the data has a good signal-to-noise ratio, but will fail miserably when this ratio approaches 1. This method is also very sensitive to baseline drift, which will require additional corrections and filtering of the data.

An alternative approach is to use convolution (Burt et al. (1994)), which has the great advantage that it is insensitive to slow changes in the baseline level and to high frequency noise. By convoluting the signal with an appropriate function, one can transform "step" data into a series of positive (opening) and negative (closing) spikes. Once this is done, the next stage is to detect peaks, which is normally done by the simpler threshold method. By varying the width of the convolution function one can adjust the method's sensitivity to noise and slow changes. Once the positive and negative peaks have been detected, the final stage involves pairing up peaks that correspond to the opening and closing of the same pore. And herein lies the main problem with this method, in that it is very prone to producing errors in this last stage[2], since failing to detect a single event will cause all of the following pairings of peaks to be miscomputed. It is especially prone to this when two events happen in rapid succession, since this will lead to peaks of (roughly) twice the amplitude, which introduces the need to decide whether a given peak corresponds to one or two events. This quickly gets extremely difficult to handle automatically and robustly, and for this reason I did not rely on this method for my analysis.

Finally, I devised an algorithm that shares similarities with the threshold method, but is significantly more robust to noise.

1. Estimate the standard deviation, σ of the baseline noise, and an event amplitude, A.

2. Starting from $t = 0$ and going to the right, search for first data point, t_n that is more than 4σ away from the current reference level.

3. Increase or decrease the current reference level accordingly by $\pm A$.

4. Search to the *left* for the first data point, t_n that deviates from the new reference level by more than 4σ.

[2] I tried and failed. Data not shown.

5. The location of the event is now defined as a weighted average of t_n and t_o.

6. Starting from $t = t_n$ search to the right for the next data point that deviates from the new reference level by more than 4σ.

7. Repeat step 2–5 until all events has been detected.

This method relies on the fact that less than 0.01% of the data points will be more than four standard deviations away from the mean level. This means that once a larger deviation is seen, it can normally be attributed to stemming from a pore opening/closing, though for long event times there is a small chance that spurious spikes will cause misdetections. However, such misdetections will lead to an abnormally short lived opening or closing (below the filtering level), and can therefore be filtered out afterwards.

A remark on step 4–5: without these the algorithm tends to overshoot, i.e. fail to immediately detect an event if the noise level is high. This tweak corrects for this by searching backwards, and then using these two limits to determine exactly where the jump happened.

In the end, this method gives a very robust means to detect events, even when the signal-to-noise ratio is low. It should be mentioned, though, that it is still sensitive to having a fairly stable baseline level.

Once all of the opening and closing events have been detected, one final task remains, namely that of determining the duration of the events. Unfortunately, there is an inherent difficulty in interpreting channel event data (both for protein channels and spontaneous pores), in that two simultaneous events of the same amplitude cannot be unambiguously decomposed. This dilemma is illustrated in Fig. A.3.

Unless otherwise noted, in this thesis I used the *first to open, last to close* interpretation, since this is less prone to creating artefacts if there is a jump in the general baseline level or the true level is not known.

A.3.2 Multi-scale Probability Density Function

Once a list of the opening and closing times has been constructed, one of the most common things to examine is the distribution of these event times. When constructing a histogram the choice of bin width will always constitute a compromise between good resolution and low noise. For a small bin width, the number of events in each bin may become very small, and for longer event times, the statistical variations from bin to bin will obscure any general trend. For larger bin widths, one loses information in the region of the shorter time scales.

One trick to overcome these limitations is to use a multi-scale method of Liebovitch et al. (2001), where data for different bin width, Δt_i, are joined into one probability density function, $P(t)$. In order to fit the histograms with different bin widths together, it is more necessary to normalise each histogram by the factor $N_{tot}\Delta t_i$ (essentially calculating probability density functions). This can then be performed with increasing bin width, with a convenient choice being a geometric progression, i.e. $\Delta t_i = \alpha \Delta t_{i-1}$ with

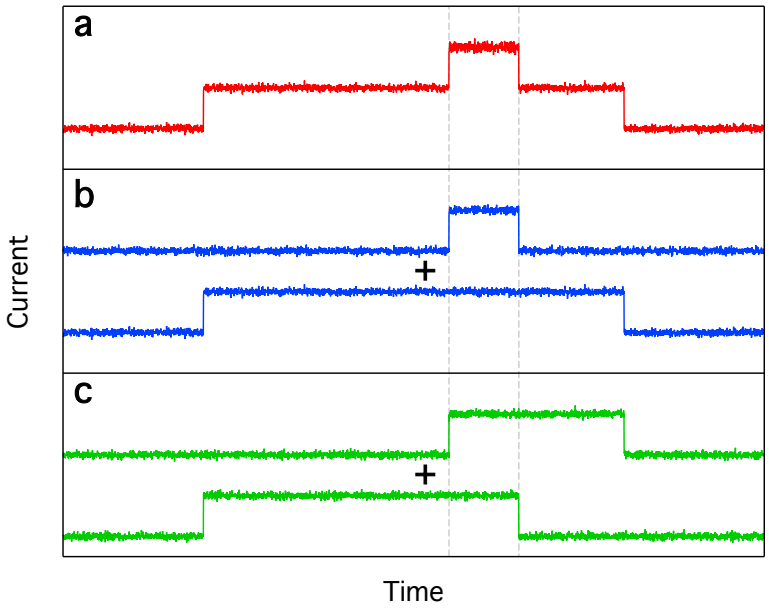

Fig. A.3: The two possible ways to interpret a double event (a). There is no way to objectively tell whether a double event stems from one long and one short event (b) or from two events of medium duration (c). Interpretation (b) was termed *first to open, last to close* and (c) was termed *first to open, first to close*.

$1 < \alpha \leq 2$. Lastly, for each of these histograms it is necessary to excluded the first bin, since it will contain all of the times unresolved at time Δt_i.

The transition rate, $k(t)$, out of a particular state can be calculated by

$$k(t) = -\frac{d}{dt} \ln P(t) \tag{A.21}$$

or, alternatively, by fitting a single exponential to the 2^{nd}, 3^{rd}, and 4^{th} bins. This fitting of an exponential gives a measure of the effective transition rate on the timescale of Δt_i, and is in principle equivalent to the definition in Eq. (A.21). In practice, the two approaches give slightly different values due to noise and numerical errors.

Summing up, the multi-scale method allows us to accurately determine the probability density function over time scales differing by orders of magnitude and to determine how the effective transition rates depends on the effective time scale at which it is measured. For the full details on how to implement the multi-scale method I refer to Liebovitch et al. (2001).

A.4 Patch clamp data

This section presents some additional data from the patch clamp experiments.

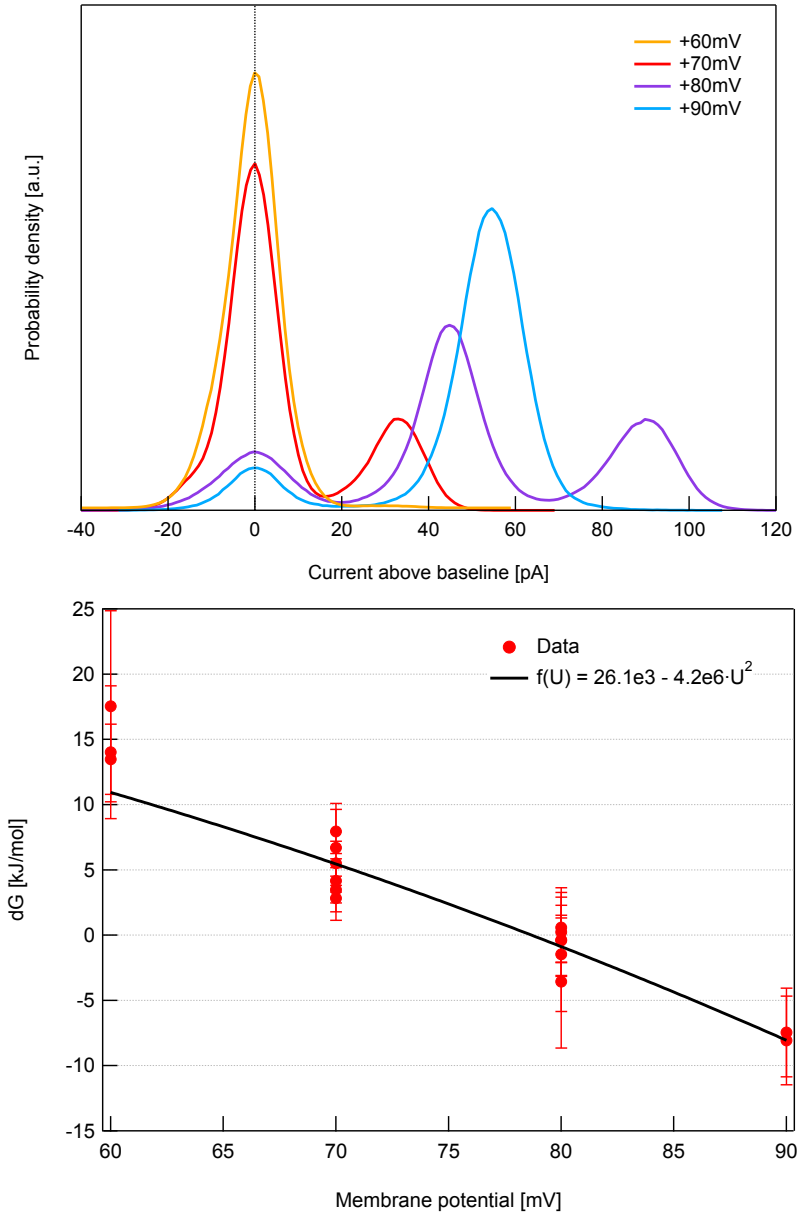

FIG. A.4: *Top:* Current histograms for a 10:1 DMPC:DLPC membrane at $T = 21°C$. *Bottom:* Corresponding free energy differences calculated from the histograms.

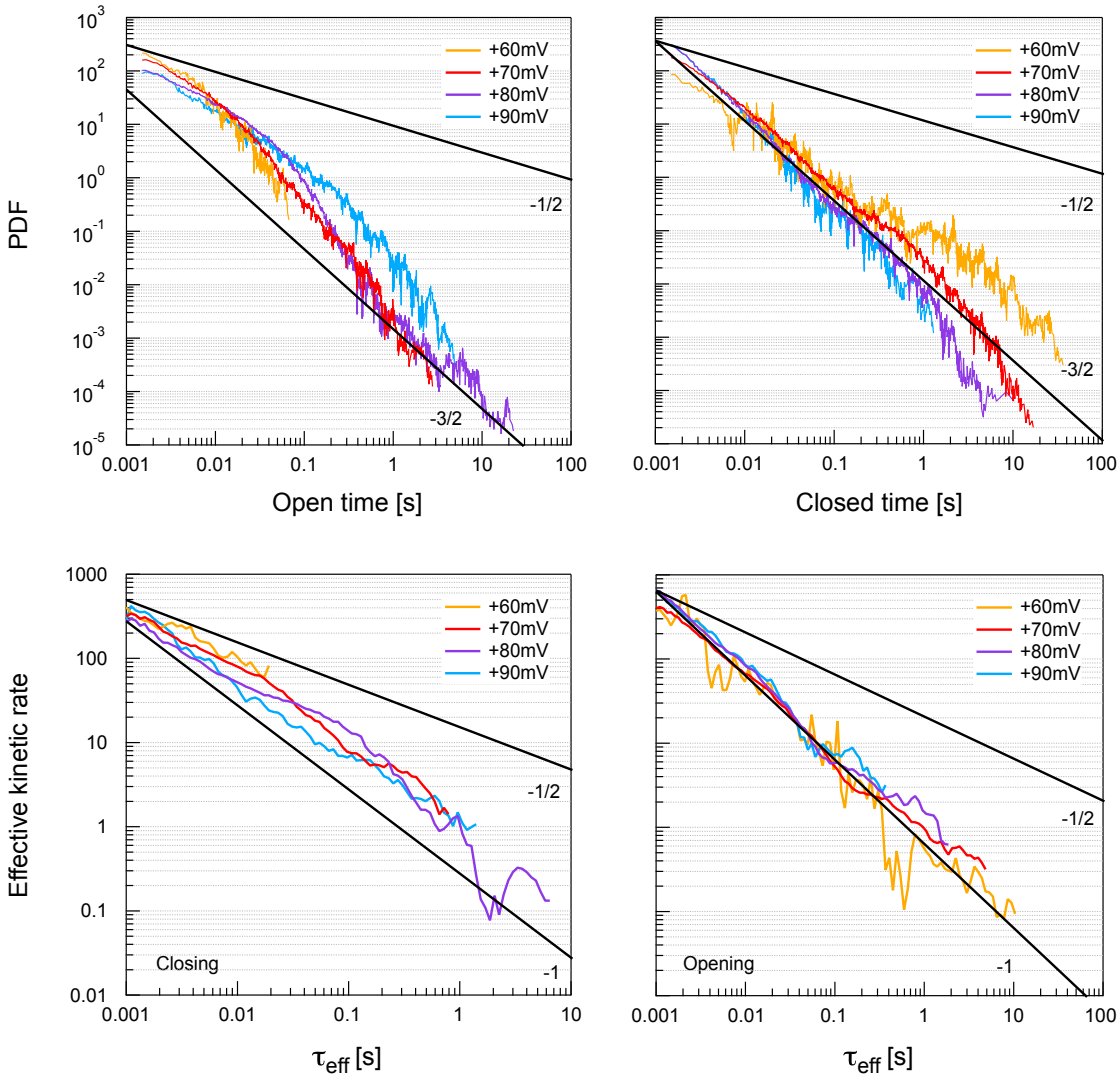

Fig. A.5: *Top:* Probability density functions for the event life times and waiting times. The solid, black lines are not fits, but shows the limiting exponents predicted in Sec. 1.6.6 for short and long time scales. For the open time distributions this is not particularly well supported by the data. However, for the closed (waiting) times the data agrees nicely over almost four decades. *Bottom:* Corresponding effective kinetic rates. Membrane was 10:1 DMPC:DLPC at $T = 21°C$.

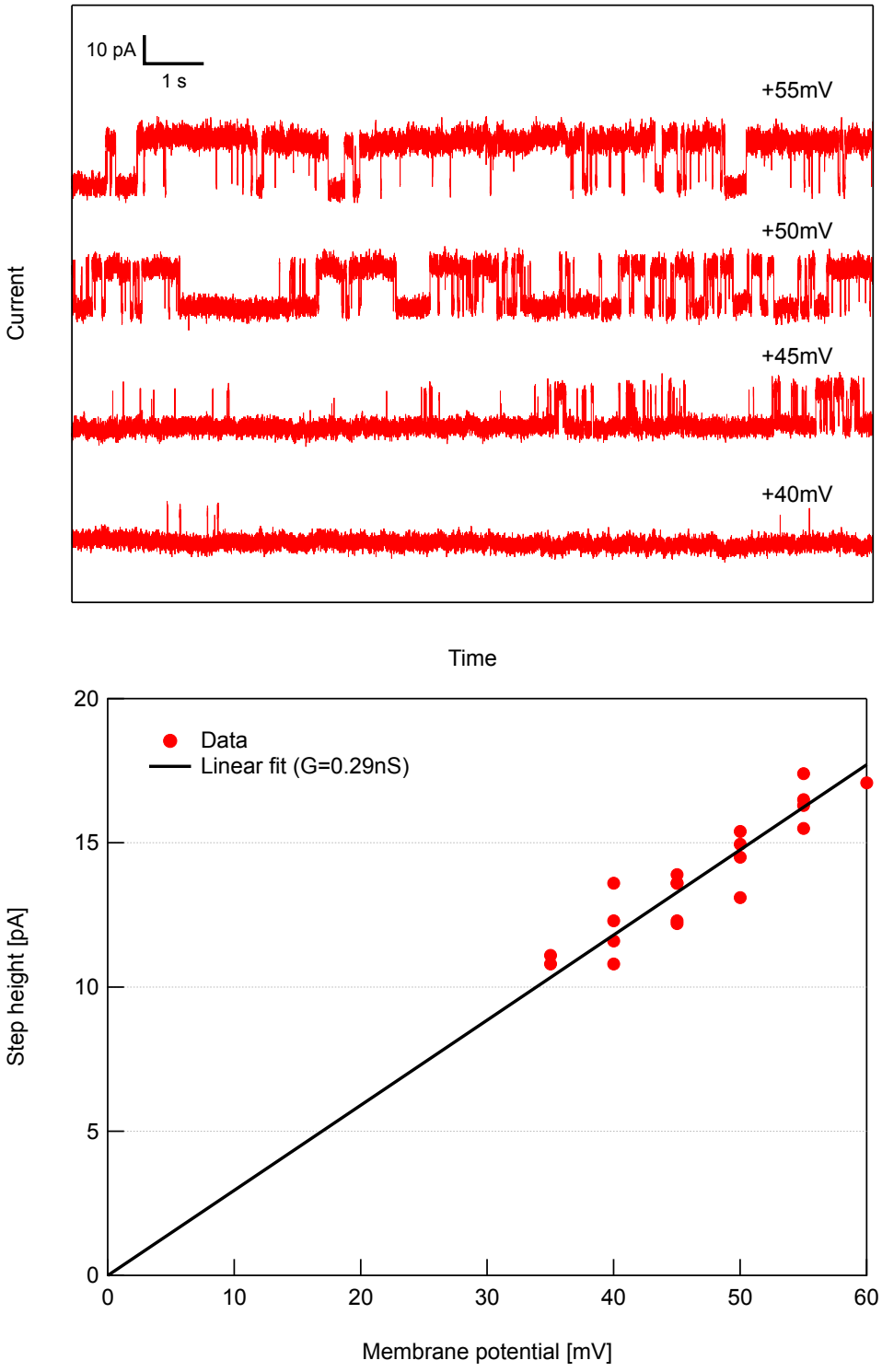

FIG. A.6: *Top:* Current trace showing clear "voltage gating", i.e. a pronounced increase in event likelihood and life time with voltage. *Bottom:* Current-voltage relationship for the data set above. Membrane was 10:1 DMPC:DLPC at $T = 29°C$.

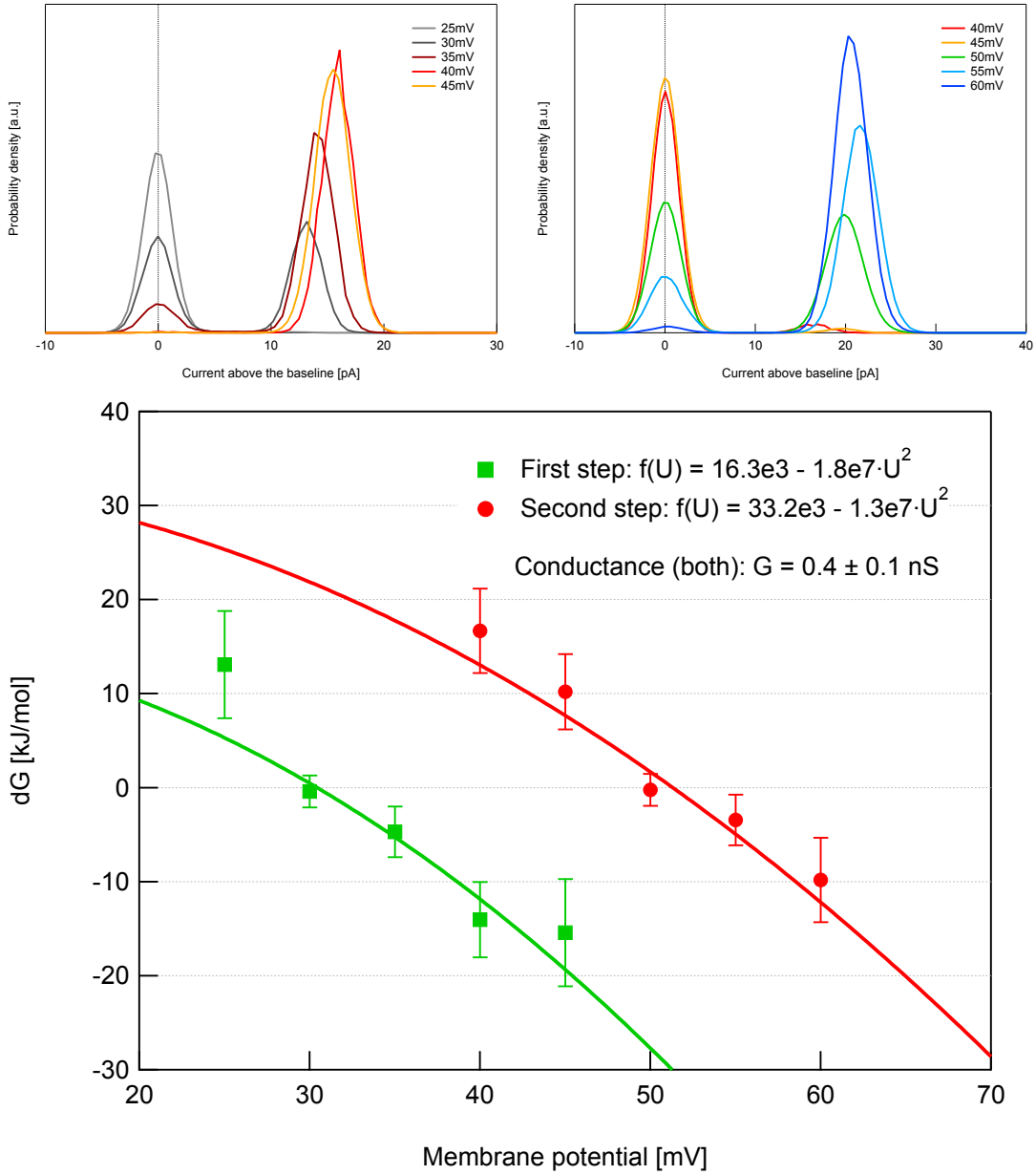

Fig. A.7: *Top:* Current histograms for the events appearing around 30mV (*left*) and around 50mV (*right*). *Bottom:* Corresponding free energy differences for the data shown above. Membrane was 10:1 DMPC:DLPC at $T = 29°C$.

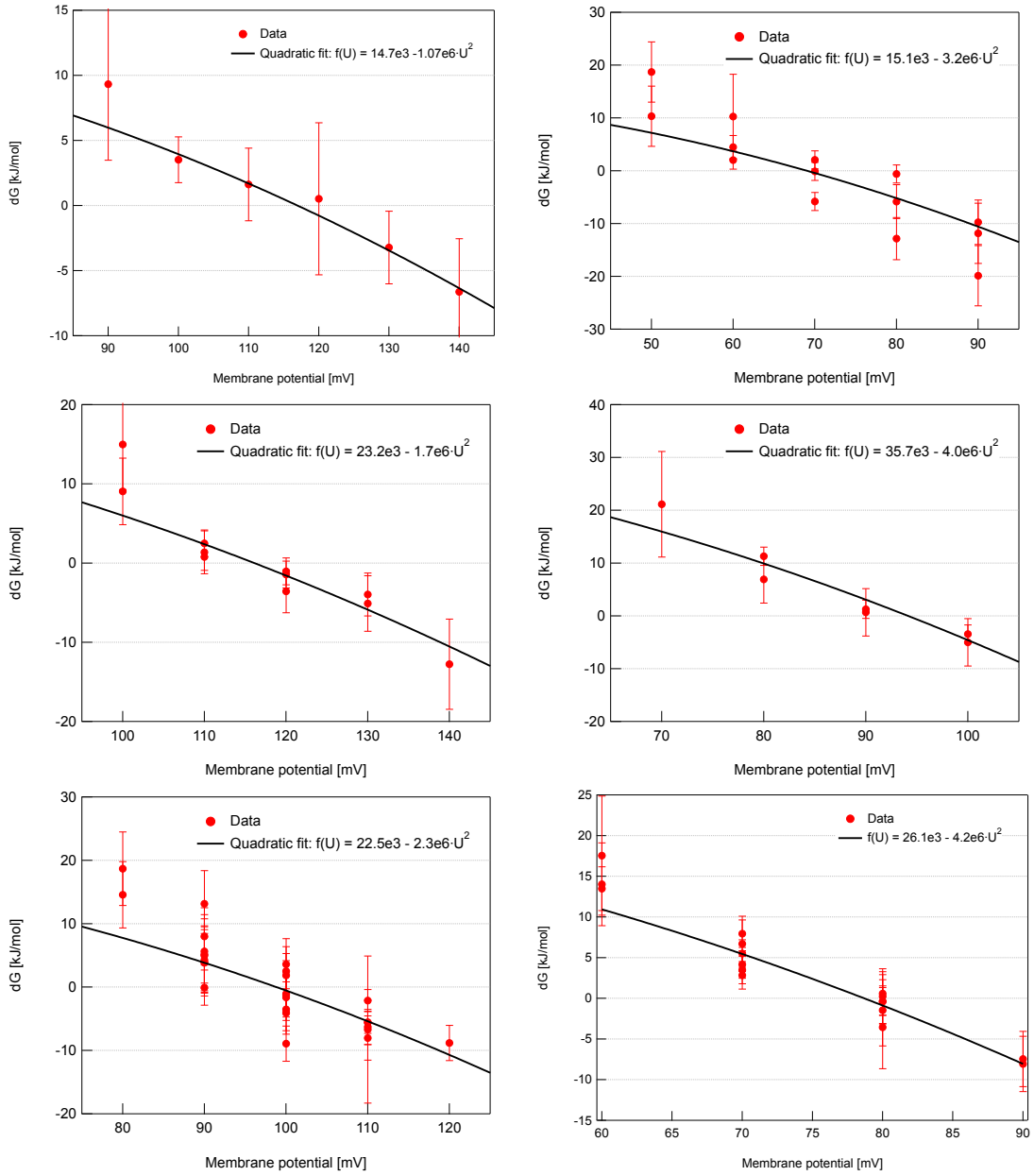

FIG. A.8: *Right top to left bottom:* $T = 30°C$; $T = 29°C$; $T = 29°C$; $T = 29°C$; $T = 29°C$; $T = 21°C$. Membrane was 10:1 DMPC:DLPC. The results of these fits are listed in Table (1.2).

A.5 Monte Carlo simulations

This section will show a few plots of some of the additional control simulations I performed in the context of the work presented in Sec. 3.3.3. They are included here for the convenience of any person who might wish to continue my Monte Carlo simulation work.

A.5.1 Bifurcation and finite size effects

To test for how large a system I needed to simulate, I performed a series of simulation at increasing system size. Fig. A.9 shows how the amplitude of the heat capacity gets attenuated for small systems, indicating that the fluctuations are constrained by the finite size of the system.

Also out of simple curiosity, a bifurcation diagram of the system was made. As can be seen from Fig. A.10 a supercritical pitchfork bifurcation occurs at $T = T_m$ and $\omega_{fg} = 1434.77\text{J/mol}$ (if there were no finite-size effects). Though the figure only shows the stable solutions, there is, for instance, also a solution for $T = T_m$ with a constant fluid fraction of 0.5. However, this solution is unstable for $\omega_{fg} > 1434.77\text{J/mol}$ and will practically never occur due to the constant thermal disturbances of the system.

A.5.2 Cooperativity and domains

The average size of the domains is shown in Fig. (A.11). A domain is defined as a cluster of lipids (two or more) in the fluid state when below the melting temperature, and gel state lipids when above. The domain size is simply the number of lipids in the cluster. Fig. A.12 shows that the domain sizes follows a power law distribution at the transition temperature, as expected for a system near its critical point.

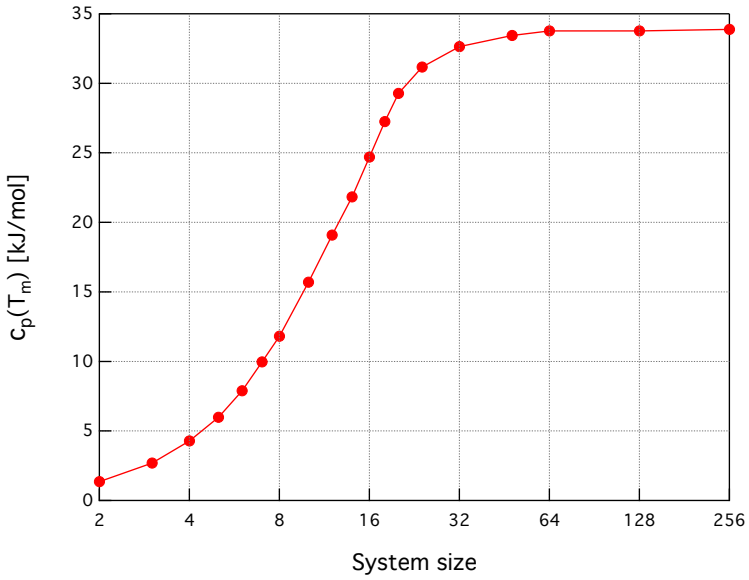

FIG. A.9: Finite size effects. Maximum heat capacity as a function of system size (here shown as the number of lipids per side of a square membrane). The parameters used for this simulation was $\Delta H = 36.4$kJ/mol, $T_m = 41°$C, and $\omega_{fg} = 1326$J/mol. For these parameters a system of approximately 64×64 lipids is sufficient.

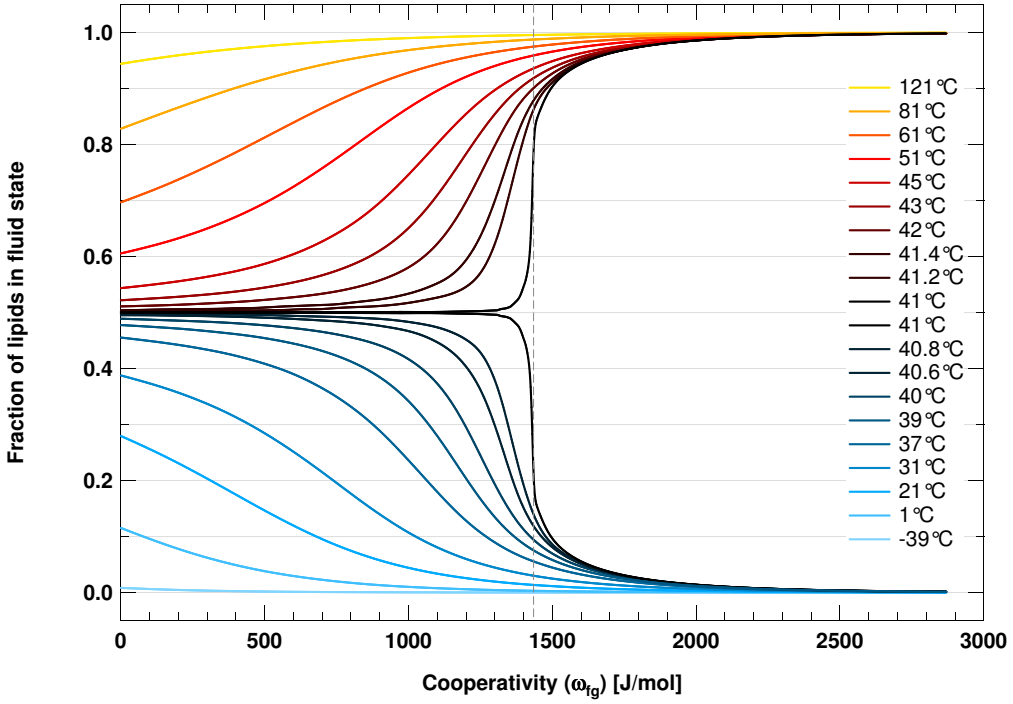

FIG. A.10: Bifurcation diagram for a 50×50 system (DPPC, single leaflet). The dashed lined is the theoretical critical value from Eq. (3.6). The finite-size effects are evident near the critical point at $T = 41^{\circ}$C and $\omega_{fg} = 1434.77$ J/mol.

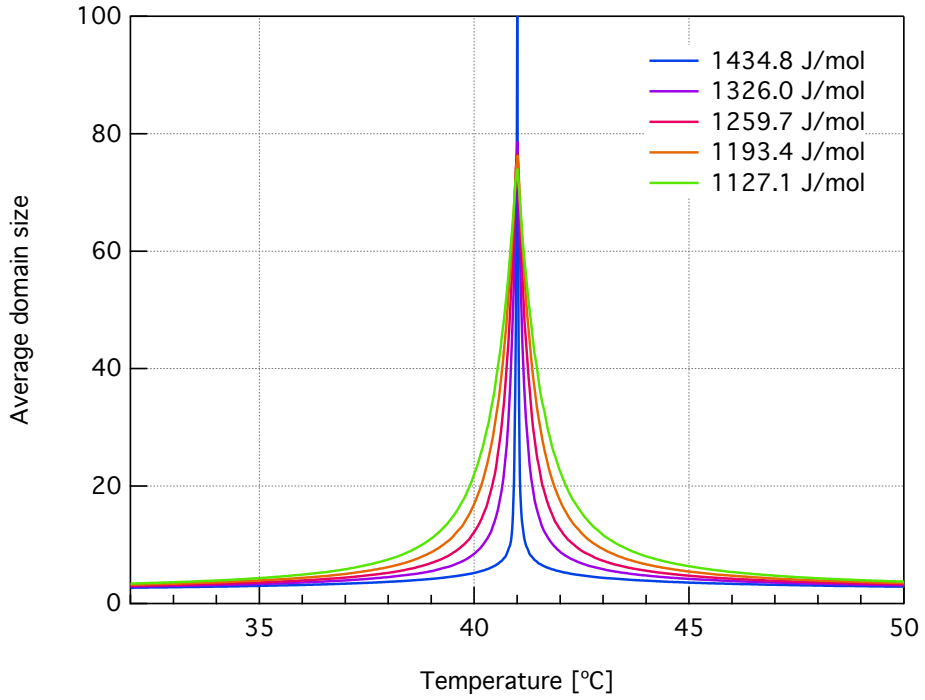

Fig. A.11: Average domain sizes in a simulated one-component system (DPPC) with varying cooperativity, ω_{fg}. The standard choice is $\omega_{fg} = 1326$kJ/mol. The critical value from Eq. (3.6) corresponds to $\omega_{fg} = 1434.8$J/mol.

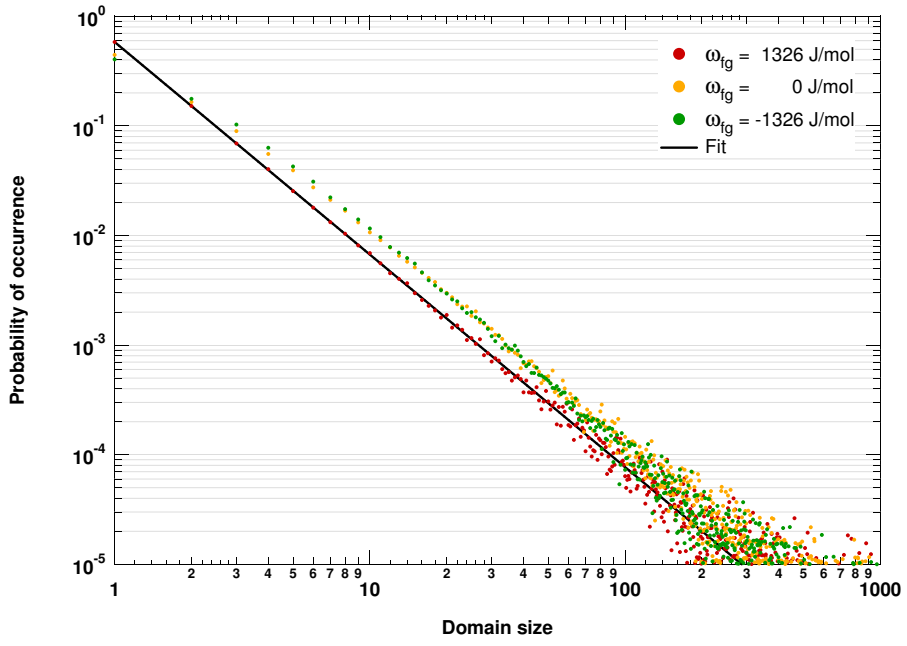

Fig. A.12: The domain size distribution for different values of ω_{fg} at $T = T_m$ in a simulation. Note that the slope is independent of ω_{fg}.). The offset is due to the slight differences for very small domains ($l^\alpha < 3$). The fitted function shown is $f(l) = 0.58 \cdot l^{-1.94}$.

A.6 Nerve pulse data analysis suite

The initial idea behind the program was to compare the electrical signal of the nerve pulse with the mechanical signal. The main issue facing us with the atomic force microscope (AFM) measurements of the mechanical signal was that the baseline noise of the instrument (using appropriately soft cantilevers) was roughy twice as large as the expected signal. To overcome this issue, the idea was to collect data from two channels: one from the high signal-to-noise ratio (SNR) electrophysiological signal and one from the AFM. By using the high SNR signal to detect the action potentials one would able to identify the relevant parts of the complementary AFM signal. These AFM data segments would then be overlaid and averaged to yield an acceptable SNR for the mechanical measurements.

One could, in principle, also use a simpler measure to detect whether there is a detectable mechanical aspect of the action potential. The easiest way would be to simply calculate the cross-correlation of the electrical and mechanical recordings. This has the advantage that it allows for a clear-cut way to detect whether there is a connection or not. It does not, however, allow us to determine e.g. the magnitude of the mechanical response, since it will be an average over all of the six different neurons, which has different signal amplitudes. Most likely, when performing the AFM experiment, one will only be able to detect changes in a single neuron due to the small size of the AFM cantilever tip and the nature of the setup. Furthermore, the cross-correlation does not give us any detailed information about the exact shape of the mechanical response – only whether there is one or not. For these reasons, I chose to focus on the idea that was outlined above, which – in principle – would allow us to get detailed information out about the mechanical aspects for each neuron.

A second feature of the program was that it should be able to read in two electrophysiological signals for the purpose of determining the speed of the action potential and how this depends on the various thermodynamic variables (e.g. temperature, anaesthetic concentration, pH, salinity, etc.). Being able to measure the speed of individual action potentials was also key to be able to determine both how the physical pulse width (in millimetres) varied between neurons and with the thermodynamic variables as well as to determine the interpulse separation of doublets.

Lastly, it was also desirable to be able to quickly and easily calculate statistics (e.g. histograms) of the spontaneous action potentials, e.g. the firing rates, pulse width, pulse speed, etc.

A.6.1 Efficient workflow

As time went on, more and more features were requested by the experimentalists and, in particular, the need for a fast and memory efficient program increased as a typical experiments would produce data files containing around 10^8 data points each. To efficiently process and analyse this large files on an ordinary desktop compute required numerous tricks and optimisations.

Two things were central to keep the memory bloat to a minimum and the analysis

process tolerable: firstly, the program allowed for an initial pulse detection, which would then be used to discard all of the data of baseline noise *between* potential events. This simple trick usually made it possible to reduce the data files by a factor 10 or more, without loosing any vital information about the action potentials. Secondly, a simple point-and-click interface significantly sped up the overall workflow.

A.6.2 Automatic pulse detection and classification

Detection and sorting of pulses is not a new problem or even unique to neuroscience. There is a broad range of different approaches, from the simple (and therefore common) threshold methods to elaborate methods that use wavelet transforms to automatically pick out distinctive features.

For our purposes, the simple threshold method was perfectly adequate to detect the action potentials. The only issue with this approach is how to determine an appropriate threshold value. An initial estimate was automatically calculated for each data channel as (Quiroga et al. (2004))

$$\text{threshold} = 4 \cdot \text{median}\left(\frac{|x|}{0.6745}\right), \tag{A.22}$$

where x is the signal that may have been bandpass filtered in advance.

By using an estimate based on the median instead of e.g. the mean, the contribution from the spikes is significantly diminished (under the reasonable assumption that spikes amount to a small fraction of all the data trace).

This method gave a fairly good initial guess, though it was prone to setting the threshold so low, that the secondary positive peak of the action potentials got detected. This would normally result in "shadow peaks", that appeared as real action potentials, if one did not do a visual inspection of the results. However, once aware of this tendency, it was easy to adjust the threshold accordingly.

Once a pulse can be reliably characterised by having various measures for its shape (e.g. amplitude, width, area, etc.) the next step is to sort them accordingly. Doing so manually can be a very time-consuming task, and – depending on the quality of the data – also be error-prone if differences are of a similar level as the noise. One of the more interesting ways to automatically classify pulses is a clustering algorithm, (e.g. superparamagnetic clustering or k-means clustering), which can be combined with e.g. the wavelet transform method (Quiroga et al. (2004)). However, for our purpose where the biological system only showed a maximum of six classes of action potentials, implementing a fully automatised sorting algorithm turned out to be overkill, and often *less* reliable than the manual sorting (data not shown). Accordingly, the program was made such that classification was done by using the mouse to mark an area on a scatter plot of e.g. the positive pulse amplitude vs. the negative amplitude. By being able to switch between various scatter plots (amplitude, width, integral, speed, etc.) it was always possible to quickly and easily distinguish the different classes (see e.g. Fig. 4.8 and Fig. 4.15).

A.6.3 Speed measure

At its most basic, measuring the speed of propagation is merely a matter of making a two-point measurement. The speed will then be given by the distance between suction pipettes, divided by the time delay between the signal shows up in each data channel.

However, there is an inherent dilemma with measuring the speed accurately, namely that the shape of the action potentials often differs between the two channels. This might be caused by differences in clamping, or it might be dispersion effect. Whatever the cause, the problem remains that it one needs to measure a time difference between two points. But which? The first peak? The point where the sign changes (what if there is only a positive phase)? The "centre of mass" of the first peak? The onset of the action potential (terribly ill defined, especially when there is significant noise)?

We never came up with a definite answer, so in the end we chose to use the peak-to-peak distance, since this led to the smallest scatter in the measured values.

The reason for the pulse broadening can come about in (at least) three ways:

1. Difference in clamping will result in a difference in the length of the nerve segment that we observe. This is only an issue if the pulse width short compared to the segment that has been sucked into the pipette.

2. Deceleration, i.e. the pulse slows down resulting in a longer (broader) observed pulse. This might be due to changes in the neuron geometry or possibly from interactions with the surrounding tissues.

3. Dispersion, i.e. that the pulse actually changes shape ("dies out") as it propagates, again possibly due to changes in the neuron itself or due to interactions with the surrounding tissues.

Unfortunately, with a two-electrode setup there is no way to distinguish between issue 2 and 3. While issue 1 can be examined, we unfortunately never found the time to investigate it in a systematic manner.

Publications

B

The Temperature Dependence of Lipid Membrane Permeability, its Quantized Nature, and the Influence of Anesthetics

Andreas Blicher,[†] Katarzyna Wodzinska,[†] Matthias Fidorra,[†‡] Mathias Winterhalter,[§] and Thomas Heimburg[†*]
[†]Niels Bohr Institute, University of Copenhagen, Copenhagen, Denmark; [‡]MEMPHYS, University of Southern Denmark, Odense, Denmark; and [§]Jacobs University, Bremen, Germany

ABSTRACT We investigate the permeability of lipid membranes for fluorescence dyes and ions. We find that permeability reaches a maximum close to the chain melting transition of the membranes. Close to transitions, fluctuations in area and compressibility are high, leading to an increased likelihood of spontaneous lipid pore formation. Fluorescence correlation spectroscopy reveals the permeability for rhodamine dyes across 100-nm vesicles. Using fluorescence correlation spectroscopy, we find that the permeability of vesicle membranes for fluorescence dyes is within error proportional to the excess heat capacity. To estimate defect size we measure the conductance of solvent-free planar lipid bilayer. Microscopically, we show that permeation events appear as quantized current events very similar to those reported for channel proteins. Further, we demonstrate that anesthetics lead to a change in membrane permeability that can be predicted from their effect on heat capacity profiles. Depending on temperature, the permeability can be enhanced or reduced. We demonstrate that anesthetics decrease channel conductance and ultimately lead to blocking of the lipid pores in experiments performed at or above the chain melting transition. Our data suggest that the macroscopic increase in permeability close to transitions and microscopic lipid ion channel formation are the same physical process.

INTRODUCTION

Lipid membranes are regarded as insulators that are practically impermeable to ions and larger charged molecules. This is crucial for the Hodgkin-Huxley model for the action potential (1), but also for the interpretation of many microscopic permeation events associated with proteins. Near the melting transition, however, membranes become permeable to water (2), ions (3,4), and even to large molecules. This may be of some relevance since many biological membranes are in fact found close to such a regime (5,6). It has been known since the early 1970s that the permeability of lipid membranes approaches a maximum in the chain-melting regime of lipids in the absence of proteins (7), and this is also likely to be so for biological membranes in the transition regime. The reason for this enhanced permeability is the enhanced area fluctuations that lead to a maximum in the lateral compressibility (8,9). Nagle and Scott (8) proposed that the changes in lateral compressibility lead to a facilitation of pore formation since the increased compressibility lowers the work necessary to create a membrane defect. In the melting transition, one also finds domain formation. Papahadjopoulos et al. (7) suggested in their seminal article that permeation events take place at domain boundaries. This view has also been adopted by Cruzeiro-Hansson and Mouritsen (10) and Corvera et al. (11). At domain boundaries, fluctuations in lipid state are maximal, and this suggests that domain interfaces are especially leaky. However, this view is not identical to that of Nagle and Scott (8) since the overall length of domain interfaces is not identical to large fluctuations. Unfortunately, the overall quality of permeation data for membranes so far has been low. This is partially due to difficulties in maintaining constant temperature during optical experiments. Melting transitions of single lipid LUV display half-widths of -1°. For a quality permeability experiment on such a system, an accuracy of at least 0.1 K is required.

Although the measurements mentioned above refer to ensembles, i.e., dispersions of vesicles, one can also monitor permeability for ions on microscopic scales. This is done either by using black lipid membrane (BLM) spanning a small hole in a Teflon film with a diameter of 50–100 μm (Montal-Müller technique (12)) or in patch-clamp measurements where one uses membrane patches of ~1 μm^2. Surprisingly, measurements of the conductance of pure synthetic lipid membranes can display quantized steps very similar to those reported for ion channel proteins. Although there is, to our knowledge, no convincing explanation of why such currents should be quantized, there are several publications documenting such channellike behavior. The first article on this is from Yafuso et al. (13) on oxidized cholesterol films, which appeared two years before the famous article by Neher and Sakmann (14) on quantized currents through the acetylcholine receptor (quantized currents through protein-containing BLMs were actually already shown significantly earlier by (15)). Antonov et al. (3) were the first to show that these lipid membrane conduction events are strongly enhanced in the phase transition regime. Using pure synthetic lipids, they could switch permeation on and off merely by shifting the temperature by a few degrees. This basically rules out the possibility that one is observing proteins or peptide impurities. Kaufmann and Silman (16,17) and Kaufmann et al. (18) showed that the occurrence of such lipid ion channels depends not only on temperature but also on other intensive variables

Submitted July 30, 2008, and accepted for publication January 13, 2009.

*Correspondence: theimbu@nbi.dk

A. Blicher and K. Wodzinska contributed equally to this work.

Editor: Joshua Zimmerberg.

© 2009 by the Biophysical Society

0006-3495/09/06/4581/11 $2.00

doi: 10.1016/j.bpj.2009.01.062

such as lateral tension and pH (i.e., the chemical potential of protons). Along the same lines, Antonov et al. (19) as well as Gögelein and Koepsell (20) showed that channellike events are influenced by calcium concentration (i.e., the chemical potential of calcium). Furthermore, they depend on voltage (21). All of these changes are also known to influence transition temperatures in lipid membranes. Several other publications describe quantized ion currents in pure lipid membranes in the absence of proteins (4,22–24). Despite the putative relevance of such findings that are well documented and which show the coupling to thermodynamical variables convincingly, this phenomenon is not well known to a broad community.

It is well established that anesthetics change the melting behavior of membranes. In particular, they lead to a lowering of the transition temperature (25–27). Thus, it seems obvious to study the effect of anesthetics on permeability. It is an interesting historical note that Charles Ernest Overton, who first demonstrated the general action of anesthetics and its relationship to membrane solubility (Meyer-Overton rule (28)) was also the first to studied the permeability of membranes to anesthetics (60).

In this publication, we compare ensemble permeation experiments on lipid vesicles with ion conductance measurements in planar lipid membranes. We use the fluorescence correlation spectroscopy (FCS) technique to measure the ensemble permeation rate for fluorescent dyes. In particular, we study the influence of temperature and the presence of anesthetics on permeability. Then, we determine the permeability for ions in a BLM setup. Here, we vary temperature, voltage, and anesthetic concentration. The goal is to demonstrate the thermodynamic couplings that lead to changes in permeability. In particular, we show that anesthetics influence the permeability in a manner closely related to their influence on the melting of lipid membranes that can be explained by freezing-point depression.

MATERIALS AND METHODS

Chemicals

Decane and 1-octanol were purchased from Fluka Chemie (Deisenhofen, Germany); *n*-hexadecane, chloroform, and methanol were obtained from Merck (Hohenbrunn, Germany); *n*-pentane was provided by BDH (Poole, UK); and potassium chloride from J.T. Baker (Deventer, Holland). 1,2-dipalmitoyl-*sn*-glycero-3-phosphocholine (DPPC), 1,2-dipalmitoyl-*sn*-glycero-3-phosphoglycerol (DPPG), and 1,2-dioleoyl-*sn*-glycero-3- phosphocholine (DOPC) were purchased from Avanti Polar Lipids (Birmingham, AL) and used without further purification. Rhodamine 6G and tetramethylrhodamine dextrane were purchased from Invitrogen/Molecular Probes (Carlsbad, CA). For all experiments, MilliQ water (18.1 MΩ; Millipore, Billerica, MA) was used.

Fluorescence correlation spectroscopy

Sample preparation

We prepared unilamellar lipid vesicles (LUV) from DPPC/DPPG = 95:5 mol/mol with an Avestin extruder (Avestin Europe, Mannheim, Germany) using a filter with a pore size of 100-nm diameter. Extrusion was performed in the presence of high concentrations of Rhodamine 6G fluorescence markers (50 μM). Subsequently, remaining free dye was removed on a G50 Sephadex column at temperatures below the melting temperature of the lipids where the membranes are nearly impermeable. We used vesicles made of a DPPC/DPPG = 95:5 mixture. DPPG is negatively charged and was added to prevent the aggregation of vesicles. All experiments were performed in a 200-mM NaCl buffer. At this salt concentration, vesicles do not aggregate but R6G (positively charged) does, nevertheless, not associate with the membranes.

Fluorescence correlation spectrometer

Our inverted microscope setup has been described in detail in Hac et al. (29). We used a linearly polarized continuous wave 532 nm Nd:Yag laser (Laser 2000, Wessling, Germany) with a power of 5 mW. Further, we used a 1.20 NA 60 × water immersion objective (UPLAPO; Olympus, Melville, NY) and a confocal setup with pinhole sizes of 30 μm. The fluorescence signal was detected by a SPCM-AQR-13 avalanche photo diode (Laser Components, Olching, Germany). Timescales were calibrated with a Rhodamine 6G solution at 296 K with a known diffusion coefficient of $D = 3 \times 10^{-6}$ cm^2/s at 22°C. The signal from the APD was analyzed using a FLEX5000/fast correlator card by Correlator.com (Bridgewater, NJ). To adjust temperatures in the FCS experiment, both sample and microscope objective were temperature-controlled using a HAAKE DC30 K20 (Thermo Fisher Scientific, Waltham, MA) waterbath. Additionally, the entire setup was heated by a ventilating radiator so that ambient temperature was close to the experimental temperature at the objective.

Calorimetry

Differential scanning calorimetry experiments were performed on a VP-DSC Calorimeter (MicroCal, Northampton, MA) with a scan rate of 5°C/h. The calorimetric experiment related to the FCS experiment (see Figs. 2 and 3) was performed on the same sample as the one used in the FCS experiments. For the DCS experiments related to the BLM experiments (see Figs. 4 and 5), the lipid samples were prepared by predissolving in chloroform and drying the solvent under vacuum overnight. The dried lipid mixtures were dispersed in MilliQ water to a final concentration of 20 mM. The buffer used was the same as for the BLM experiments. Before filling the calorimeter, the solutions were degassed for 10 min.

Black lipid membranes

Planar bilayers were formed over a round aperture in a Teflon film of 25-μm thickness, dividing two compartments of a Teflon chamber embedded in a brass block that could be heated by a circulating water bath. The aperture of $\approx$80 μm radius was punctured by a steel needle (experiments in Figs. 5 and 6) or by an electric spark (see Fig. 4). Lipid mixtures were prepared from chloroform-methanol solutions. The samples were dried under a weak flow of nitrogen gas/air and placed under vacuum overnight to remove the residual solvent. The aperture in the Teflon film was prepainted with 5% hexadecane in pentane. The BLMs were painted with DOPC/DPPC 2:1 lipid solutions in decane/chloroform/methanol 7:2:1 and formed following the method described by Montal and Müller (12). The two compartments of the Teflon block were filled with unbuffered 150-mM KCl (pH 6.5). Lipid solution (25 mg/mL) was spread on the buffer surface in each compartment (~3 μL on each side). Ag/AgCl electrodes were placed into both compartments of the chamber. After 15–30 min to allow for the evaporation of the solvent, the water level of the compartments was lowered and raised several times until a bilayer was formed over the hole. The formation of BLMs was controlled visually and by capacitance measurements (with triangular 100-mV voltage input pulse). The specific capacitance of the membranes was found to be 0.9–1.2 μF/cm^2. These values are close to literature values (0.85 μF/cm^2 for DPPC (30), 0.61 μF/cm^2 for a DOPC/1,2-dioleoyl-*sn*-glycero-3-phosphatidylethanolamine (DOPE) = 50:50 mixture (31), and 0.93 μF/cm^2 for a pure DOPC membrane as deduced from monolayer measurements (32)). Our values have been obtained by dividing the total capacitance (~80 pF) by the area of the hole as determined under the microscope. Our value for the

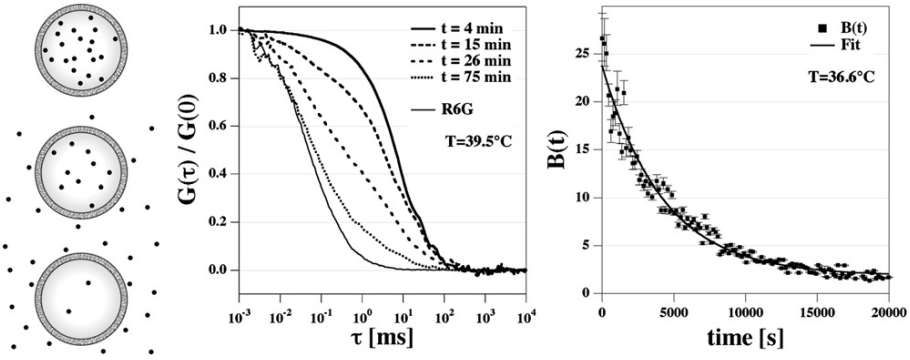

FIGURE 1 Principle of the measurement of permeation of the fluorescence dye R6G in the FCS experiment. (*Left*) Schematic drawing. Dye molecules trapped in vesicles smaller then microscopic focus size diffuse with the characteristic time constant of the vesicles. With time, molecules permeate through the vesicle membranes and diffuse with the characteristic time constant of free molecules. (*Center*) The correlation profiles of this situation show two correlation steps corresponding to free molecules and vesicles. The relative step size changes as a function of time such that the number of free molecules increases and the number trapped in vesicles decreases. Five experiments are shown that were performed after the times indicated. (*Right*) The mean number of dye molecules per vesicle (calculated from the mean brightness, see text) decreases exponentially with time. Data shown have been recorded on DPPC/DPPG (95:5 mol/mol) LUV in 200 mM NaCl at temperatures of 39.5°C (*center panel*) and 36.6°C (*right panel*) below the chain melting transition maximum (see Fig. 2). At 36.6°C, the time constant of permeation is 4200 s. Each data point corresponds to an FCS experiment as shown in the center panel.

capacitance serves only as a quality control for bilayer. To measure accurately the capacitance of a planar lipid bilayer, one must carefully vary the parameters during the measurement (for example, the area by bulging). The most critical unknown is the status of the bilayer at the edge. The rim depends on the experimental method, e.g., prepainting, applied volume and solvent, or solvent for the lipid. This rim may cover more than half of the surface of the actual hole. Bulging may push the membrane out of the hole, allowing much larger surfaces (even twice) compared with the hole in the septa. A second contribution is caused by the solvent applied for the prepainting or to solubilize the lipid. Although, in our approach, we used solvent free membranes, there is definitely some solvent associated with the lipid. Revisiting published data revealed values differing by a factor of three. A careful study was done by Dilger and Benz (33). They used solvent containing membranes and varied the solvent systematically. Using hexadecane to solubilize the lipid revealed very thin membranes with a specific capacitance of 0.585 μF/cm^2. In our case, the membranes are slightly thinner. Further, the capacitance of a membrane should be higher in the lipid-melting transition region, since it is proportional to charge density fluctuations. Those fluctuations should be high in the melting regime, as both area and thickness have maximum fluctuation (9).

For the experiments with octanol, 15% v/v octanol in methanol solution was prepared and added symmetrically on both sides of the Teflon chamber.

Conductance measurements were performed on an Axopatch 200B amplifier in voltage-clamp mode connected to a DigiData 1200 digitizer (both Molecular Devices, Sunnyvale, CA). Current traces were filtered with 1 kHz low-pass Bessel filter and recorded with Clampex 9.2 software (Axon Instruments, Foster City, CA) on the hard drive of the computer using an AD converter with a time resolution of 0.1 ms. The data was further analyzed with Clampfit 9.2 and low-pass filtered with Bessel (eight-pole) filter at a cutoff frequency of 300 Hz. Temperature was controlled by a HAAKE DC30 K20 (Thermo Fisher Scientific) waterbath and a thermocouple (WSE, Thermocoax, Alpharetta, GA).The BLM experiments in Fig. 4 were performed in the laboratory of M. Winterhalter in Bremen, and the experiments shown in Figs. 5 and 6 were performed using a very similar setup in the laboratory of T. Heimburg in Copenhagen.

The FCS correlation function of vesicles with variable content of fluorescence dyes

The correlation function of a freely diffusing dye in a microscope focus of Gaussian cross section is given by

$$G(\tau) = \frac{1}{\langle N\rangle}\left[1+\frac{\tau}{\tau_D}\right]^{-1}\left[1+\left(\frac{r_0}{z_0}\right)^2\frac{\tau}{\tau_D}\right]^{-\frac{1}{2}}. \quad (1)$$

If one has several markers of similar brightness, the correlation functions add, and the number of diffusing particles can be deduced from the relative amplitude of the steps in the correlation function. The situation becomes more complicated if different objects with different brightnesses are present or if there is a distribution of brightnesses since the brightness enters the correlation as a square,

$$G(\tau) = \frac{1}{\left(\sum_j B_j\langle N_j\rangle\right)^2}\sum_i B_i^2\langle N_i\rangle\left[1+\frac{\tau}{\tau_{D_i}}\right]^{-1} \times\left[1+\left(\frac{r_0}{z_0}\right)^2\frac{\tau}{\tau_{D_i}}\right]^{-\frac{1}{2}}, \quad (2)$$

where the brightness of particle species i is given by $B_i = \kappa_i\varepsilon_i Q_i$ (34). Here, κ_i is the efficiency of the fluorescence detector, ε_i is the molar extinction

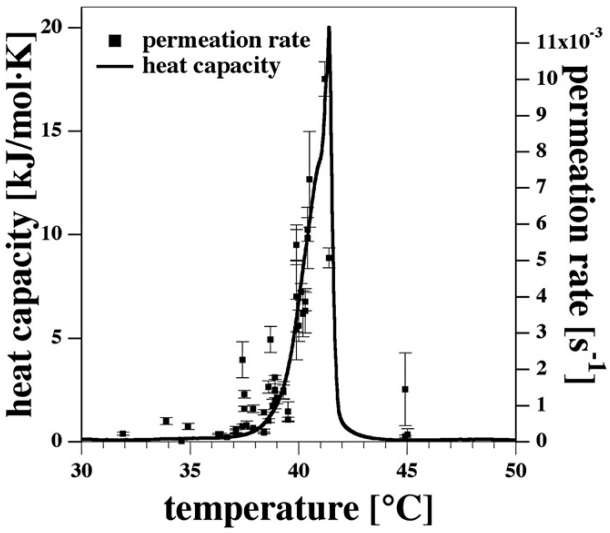

FIGURE 2 Permeation rate of R6G through DPPC/DPPG (95:5) LUV (200 mM NaCl) as a function of temperature compared with the heat capacity profile of the identical sample. The permeation rate is closely related to the heat capacity as predicted by Eq. 12.

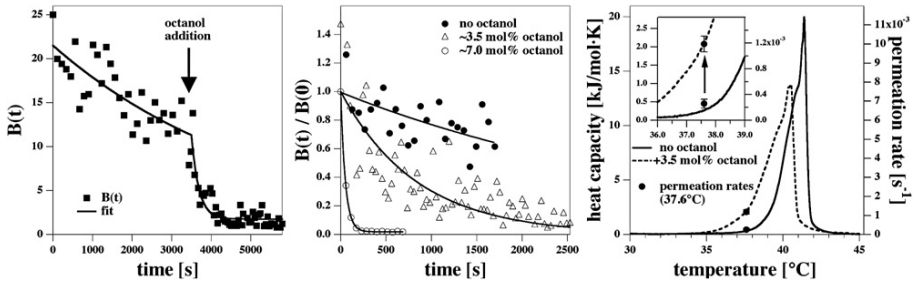

FIGURE 3 Effect of the anesthetic octanol on the permeation rate. (*Left*) Permeation of R6G through DPPC/DPPG (95:5) LUV at 37.1°C after the sudden addition of 1-octanol at the time indicated by the arrow. Permeation increases dramatically. (*Center*) Permeation in the absence and the presence of 3.5 mol % and 7 mol % octanol in the membrane at 37.6°C. (*Right*) Heat capacity profiles of the lipid LUV in the absence of octanol (see Fig. 2) and in the presence of 7 mol % octanol. In the presence of octanol, the melting events occur at lower temperature. The solid circles indicate the permeation rates at 37.6°C in the absence of octanol and in the presence of 7 mol % octanol. The increase in permeability caused by octanol correlates nicely with the increase in heat capacity at 37.6°C.

coefficient of the fluorophore at the wavelength of excitation, and Q_i is the quantum yield of the fluorophore. For fluorophores of equal brightness, the B_i values cancel. In the presence of a single dye species, one obtains Eq. 1.

Permeation through vesicles studied by FCS

In this work, we wish to monitor the permeation of fluorescence markers from the inside of a 100-nm vesicle to the outside. These vesicles are smaller than the microscope focus. Even though all markers have the same brightness in this particular experiment, a vesicle that contains n dye molecules is n times brighter than a single dye molecule (neglecting quenching effects). In particular, vesicles do not all contain precisely the same number of fluorophores. The dye entrapped in vesicles, and that free in solution, is rhodamine 6G. Thus, the difference in brightness between freely diffusing single dye molecules and the vesicles is directly proportional to the number of dye molecules trapped within the vesicle. Therefore, in the following only the number of dye molecules per vesicles will appear. From statistics, one expects a Poisson distribution of the dye content of the vesicles,

$$p(B_i) \approx \frac{\exp(-\tilde{B})\tilde{B}^i}{i!}, \tag{3}$$

where $\tilde{B}$ is the mean number of dyes per vesicle. If one inserts this distribution into Eq. 2, one obtains

$$G(\tau) = \frac{\langle N_{R6G}\rangle}{\left(\langle N_{R6G}\rangle + \tilde{B}\langle N_V\rangle\right)^2}\left[1+\frac{\tau}{\tau_{R6G}}\right]^{-1} \times \left[1+\left(\frac{r_0}{z_0}\right)^2\frac{\tau}{\tau_{R6G}}\right]^{-\frac{1}{2}} + \frac{\tilde{B}^2\langle N_v\rangle\left(1+\tilde{B}^{-1}\right)}{\left(\langle N_{R6G}\rangle + \tilde{B}\langle N_V\rangle\right)^2} \times \left[1+\frac{\tau}{\tau_V}\right]^{-1}\left[1+\left(\frac{r_0}{z_0}\right)^2\frac{\tau}{\tau_V}\right]^{-\frac{1}{2}}. \tag{4}$$

The detailed derivation can be found in the MSc thesis of A. Blicher (35). This equation contains five unknown parameters that must be determined from experiment. The correlation function yields the two diffusion correlation times τ_{R6G} and τ_V of rhodamine 6G and the vesicles, respectively. The mean number of free dye molecules in the focus, $\langle N_{R6G}\rangle$, the mean number of vesicles in the focus, $\langle N_V\rangle$, and the mean number of dye molecules per vesicle, $\tilde{B}$, can be obtained from the absolute fluorescence intensity of the uncorrelated data, and the magnitude of the two steps in the correlation function (Fig. 1). In a time-dependent experiment, the mean number of dye molecules per vesicle will decrease. The change of $\tilde{B}$ with time is proportional to the permeation rate through the vesicular membrane. The permeation rate is likely to be closely related to the pore formation rate, assuming fast diffusion inside the vesicle and through the pore. However, the vesicles contain a small fraction of negatively charged lipids, whereas the dye itself carries a positive charge. Therefore, there may be a finite influence from dye adsorption to the vesicle walls. We tried to minimize this by adding salt into the buffer.

THEORY

The connection among compressibility, heat capacity, and permeability

The permeability of the membrane is maximal in the transition regime. This phenomenon is related to the well-known phenomenon of the opalescence of fluids close to critical transitions. In this regime, fluctuations in density may approach the length scale of visible light. Einstein (36) calculated the work required to generate density fluctuations on the length scale of light. In particular, he determined the work necessary to change the density of box of size L^3 by moving volume into another box of equal dimensions. Close to transitions, this is considerably easier because the volume

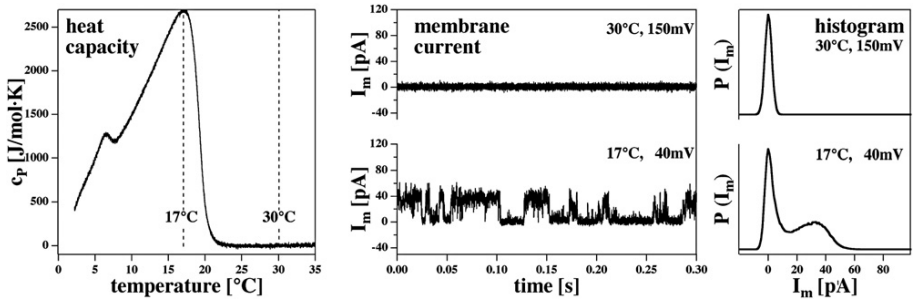

FIGURE 4 Spontaneous quantized currents through BLMs made of a DOPC/DPPC = 3:1 mixture (150 mM KCl) as a function of temperature. (*Left*) Heat capacity traces with a heat capacity maximum around 17°C. At 30°C, the sample above the melting regime in its fluid phase. (*Center*) Current traces at 17°C (40 mV) and 30°C (150 mV). One only finds current steps in the lipid melting regime. (*Right*) Current histograms for the two temperatures. At 17°C, two maxima in the histogram can be seen.

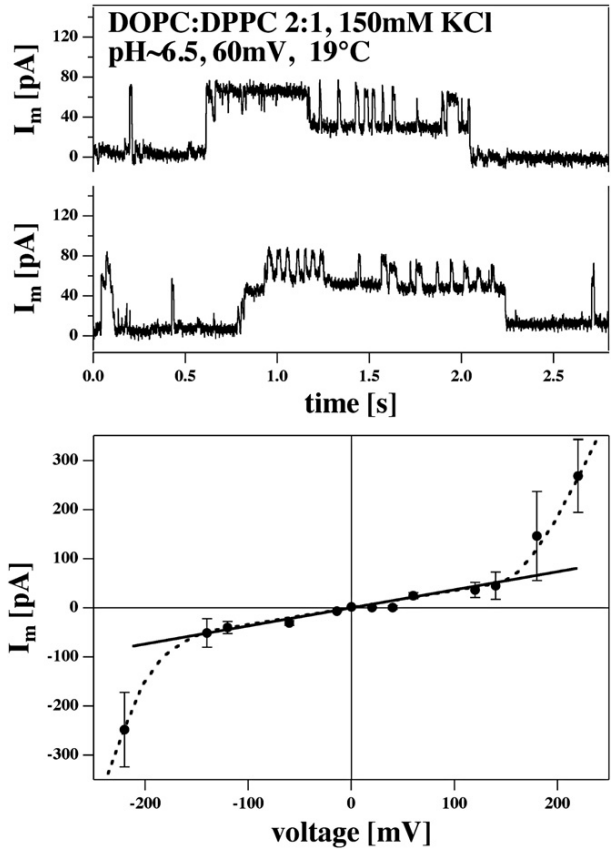

FIGURE 5 Currents and current-voltage relationship for BLMs made of a DOPC/DPPC = 2:1 mixture (150 mM KCl, 19°C, pH ≈ 6.5). The membrane is in its melting regime (see Fig. 6, *left panel*). (*Top*) Current traces at a voltage of 60 mV. One can see up to five current levels with equal distance between adjacent levels. (*Bottom*) Current-voltage relation for the above membranes. The mean amplitude of current events is shown as a function of voltage. It is linear in the range between −150 mV and +150 mV. If $|V|$ is larger than 150 mV, the relationship is nonlinear due in part to several simultaneous open events in the membrane. A total of 328 current traces of 30 s duration was used for this analysis.

compressibility becomes high. In fact, one can see the increased fluctuations in liquids close to their transition in optical experiments. The problem of permeability changes and of pore formation is of a similar nature, since it requires moving lipids into another region of the membrane to create a pore. In particular, the likelihood to form pores or holes in the membrane is closely related to fluctuations in density. The problem can now be posed as follows: How much work must be performed to move a lipid from a membrane segment of dimensions L^2 into another region of similar size?

The work necessary to compress a membrane (i.e., the Helmholtz free energy change) by an area a is a quadratic function of the area that has the form

$$\Delta W(a) = \frac{1}{2} K_{\mathrm{T}}^{\mathrm{A}} \left(\frac{a}{A_0}\right)^2 A_0, \tag{5}$$

where A_0 is the total area of the membrane, a is the size of a defect, and $K_{\mathrm{T}}^{\mathrm{A}}$ is the isothermal area compression modulus (e.g., (8)). The compressibility of a membrane is given by

$$\kappa_{\mathrm{T}}^{\mathrm{A}} = -\frac{1}{A_0}\left(\frac{\partial A}{\partial \Pi}\right)_{\mathrm{T}} \equiv \frac{1}{K_{\mathrm{T}}^{\mathrm{A}}}, \tag{6}$$

where $\kappa_{\mathrm{T}}^{\mathrm{A}}$ is the isothermal area compressibility. The compressibility is also proportional to the area fluctuations (9)

$$\kappa_{\mathrm{T}}^{\mathrm{A}} = \frac{\langle A^2 \rangle - \langle A \rangle^2}{\langle A \rangle kT}, \tag{7}$$

whereas the heat capacity is proportional to the fluctuations in enthalpy (9):

$$c_{\mathrm{p}} = \frac{\langle H^2 \rangle - \langle H \rangle^2}{kT^2}. \tag{8}$$

The empirical finding that, close to transitions, the changes in area and the changes in enthalpy are proportional functions of temperature, i.e., $\Delta A(T) = \gamma_{\mathrm{A}} \Delta H(T)$ (9,37–39), leads to

$$\Delta \kappa_{\mathrm{T}}^{\mathrm{A}} = \frac{\gamma_{\mathrm{A}}^2 T}{A_0} \Delta c_{\mathrm{p}} \tag{9}$$

or

$$\kappa_{\mathrm{T}}^{\mathrm{A}} = \kappa_{\mathrm{T},0}^{\mathrm{A}} + \frac{\gamma_{\mathrm{A}}^2 T}{A_0} \Delta c_{\mathrm{p}}. \tag{10}$$

Nagle and Scott (8) assumed that the permeability can be expressed as a series expansion with respect to the area fluctuations that are also proportional to the lateral compressibility. The resulting permeability obtained by Nagle and Scott is

$$P = a_0 + a_2 \kappa_{\mathrm{T}}^{\mathrm{A}} + \text{higher order terms}, \tag{11}$$

where a_0 and a_2 are constants to be determined from experiment. Using Eq. 10 yields

$$P = c_0 + c_2 \Delta c_{\mathrm{p}}, \tag{12}$$

where c_0 and c_2 are also constants to be determined from experiment. This is a simple expression directly coupled to the calorimetric experiment. In particular, it predicts that the change in permeability is proportional to the excess heat capacity, which is easily measured. This approach relies on area fluctuations and does not involve a molecular model for a pore. In particular, we do not consider a line tension around the pore. The experimental results below will justify this approach.

The results of this section also immediately imply that everything that changes heat capacity profiles will also change the permeability in a coherent and predictable manner. The similarity of this problem to critical opalescence

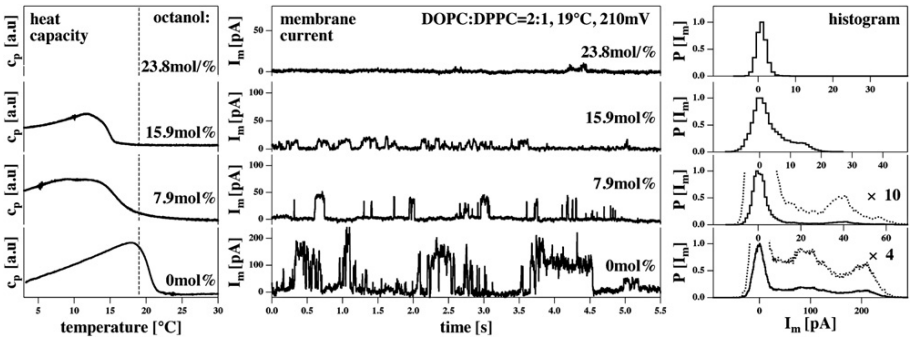

FIGURE 6 Influence of the anesthetic octanol on membrane currents through BLMs made of a DOPC/DPPC = 2:1 mixture (150 mM KCl, 19°C, pH ≈ 6.5) at a voltage of 210 mV. Shown are four different octanol concentrations, 0 mol % (*bottom panels*), 7.9 mol % (*second* from *bottom*), 15.9 mol % (*second* from *top*), and 23.8 mol % (*top panels*) given as mol % of molecules in the membrane. (*Left*) Heat capacity traces for three octanol concentrations (trace for 23.8 mol % not shown). Increasing octanol content leads to a shift of the profiles toward lower temperatures. This effect is known as freezing-point depression (27). In the absence of octanol, the experimental temperature is at the c_p-maximum, whereas it is above the c_p-maximum in the presence of octanol. (*Center*) Representative current traces at the four octanol concentrations. The current amplitudes and the total time in the open state become smaller with increasing octanol concentration. (*Right*) Current histograms showing several peaks. At higher octanol concentration, the peak positions are at lower voltages. At 23.8 mol %, current events disappear completely. Note the different scales of the current axis in the center and the right panel.

implies that it should be possible to detect the critical nature of pore formation in optical experiments.

RESULTS

We have investigated two different aspects of lipid membrane permeability: the macroscopic permeability of lipid vesicles for fluorescence markers and the permeability of planar lipid membranes for ions. Although in the first setup, one obtains an ensemble average over many permeation events, in the second experiment, the permeation events allow us to draw conclusions regarding the possible size of the defects. In particular, we investigate the correlation with anesthetics. We show that such drugs influence the permeability in a coherent and predictable manner.

Permeability of LUV measured by FCS

Fluorescence correlation spectroscopy is a technique with single molecule resolution in which the diffusion constant and particle concentration can easily be determined on the length scale of the microscope focus. Rhodamine 6G fluorescence dyes were entrapped in lipid vesicles of 100-nm diameter. Both vesicles and dyes are smaller than the microscope focus diameter. However, the diffusion constant of the singular dyes is much higher than that of the much larger vesicles. Although the typical dwell time of a single dye molecule in our FCS setup is ~100 μs, the dwell time of a fluorescing vesicle is of ~10 ms. If both single dye molecules and fluorescent vesicles coexist in a solution, the correlation function will show two steps with amplitudes related to the concentrations of dyes in vesicles and free dyes.

Initially, all R6G molecules are trapped in the vesicles. With time, they leak out of the vesicles as shown schematically in Fig. 1 (*left*). This process can be followed in repeated FCS experiments (Fig. 1, *center*), and the relative fraction of dye in vesicles and as free molecules can be deduced from the amplitudes of the steps in the correlation function following the procedure given in Eq. 4. As an example, we show the leakage of R6G out of vesicles made of 95 mol % DPPC and 5 mol % DPPG measured at 39.5°C, which is ~2 K below the heat capacity maximum of the membrane melting profile. Under these conditions, permeation of dyes through the vesicular walls is quite slow. One can see two correlation steps. Although the correlation times remain constant, the relative fraction of slow and fast diffusion species is changing. Fig. 1 (*right*) shows that the progress of leakage for a sample at 36.6°C ($\approx$5 K below the transition maximum) yields a single exponential decay with a time constant of 4800 s and a permeation rate constant of 2.1×10^{-4} s^{-1}.

We recorded the permeation rate constants as a function of temperature and compared them with the heat capacity profile (Fig. 2). It was found that the permeation rate of R6G was, within experimental accuracy, linearly related to the excess heat capacity as predicted by Eq. 12. In the temperature range from 36.5° to 41.4°C, the permeability changed by a factor of 50. Compared with temperatures below the pretransition temperature (<34°C), the change is several orders of magnitude (data not shown). Close to the heat capacity maximum the permeation rate is ~0.01 s^{-1}, which corresponds to a time constant of 100 s. The dwell time of a vesicle in the microscope focus is ~10 ms. To obtain a correlation function of reasonable quality, one needs to record a fluorescence noise trace of at least 10 s. Thus, the permeation rate at heat capacity maximum is close to the resolution limit of our method. Only two data points have been measured above the melting regime. These points are difficult to obtain because, during equilibration of the sample to the experimental temperature, it passes through the phase transition regime and most of the dye leaks out before the start of the experiment. The permeation rates for temperatures above 41.4°C given in Fig. 2 represent the single exponential decay of the remaining fluorescence markers

(of ~10% of the original dye concentration). This slow decay is absent in the data at the transition point. We conclude that the permeability returns to values similar to those below the transition range, in agreement with previous studies. A control experiment with tetramethylrhodamine dextrane (MW $\approx$ 3000 g) at the melting temperature of 41.4°C showed that this large dye remained inside of the vesicles on timescales of several hours (data not shown). This indicates that the vesicles stay intact when passing through the melting regime and do not rupture.

Influence of anesthetics

In 2007, we showed that anesthetics act as freezing-point depressants (27). At critical anesthetic dose (2.6 mol % of anesthetics in the membrane), one obtains a melting point depression of ~0.6°. Since all anesthetics shift the heat capacity profile by the same known value, one expects a predictable change of anesthetics on permeability. In particular, if one measures permeability below the melting temperature of the vesicles, anesthetics should increase the permeability since the melting events are moved toward experimental temperatures. If one repeats the same experiment above the melting temperature, addition of anesthetics should decrease the permeability since the transition events are moved away from experimental temperatures. This was investigated using the anesthetic 1-octanol. Fig. 3 (*right*) shows the effect of the addition of 3.5 mol % percent of octanol (calculated from the total octanol content and a lipid/water partition coefficient of 200 (40)) on the heat capacity profile. It shifts by ~0.9 K to lower temperatures, in agreement with the freezing-point depression relation derived in Heimburg and Jackson (27). Upon addition of octanol to the vesicle dispersion at 37.6°C, the permeation rate increases dramatically (Fig. 3, *left*; the time of octanol addition is indicated by an *arrow*). Dye release for different amounts of octanol is shown (Fig. 3, *center*). The permeation rates are 0.24×10^{-3} s^{-1} in the absence of octanol, 1.19×10^{-3} s^{-1} in the presence of 3.5 mol % octanol, and 19.8×10^{-3} s^{-1} in the presence of 7 mol % octanol. In Fig. 3 (*right*), the permeation rates with and without octanol are compared with the heat capacity changes. At 37.6°C, the permeability increase caused by octanol is approximately fivefold and matches exactly the change of the excess heat capacity caused by octanol at the same temperature.

Permeation of ions through black lipid membranes

It has been shown previously (3,4) that permeation of ions through BLMs is most prominent in the phase transitions regime. Further, conductance changes occur in quantized steps similar to those reported for channel forming proteins or peptides (3,4,13,16–20). To stay closer to room temperature, we used lipid mixtures in the BLM experiments, which differed from those of the FCS experiments. BLMs below the transition are typically not stable. In Fig. 4, we show data recorded on a DOPC/DPPC = 3:1 (mol/mol) mixture (150 mM KCl, 1 mM Tris, pH 7.4). This mixture displays a broad melting profile with a maximum at 17°C (Fig. 4, *left panel*). Above 22°C, the mixture is in the fluid phase. We compared current measurements at 17°C and 30°C (Fig. 4, *center panel*). At 17°C and a transmembrane voltage of 40 mV, one sees discrete current steps with an amplitude of ~35 pA (see histogram in the *right-hand panel*) and typical channel open times of several 10 ms. At 30°C, one does not see any current steps even at higher voltages of 150 mV. This supports the notion that the transition is the regime in which such events can be found. Our observation of well-defined conductance steps indicates that this particular lipid composition is able to form well-defined defects even in the absence of peptides or proteins (e.g., (20)).

Fig. 5 (*top*) shows traces from a DOPC/DPPC = 2:1 (150 mM KCl, 60 mV, pH $\approx$ 6.5, 19°C). This mixture has a heat capacity maximum close to 19°C. The figure shows that one can find traces with at least four equally spaced conductance steps, probably corresponding to several lipid channels opening simultaneously. Such multiple events seem to be more frequent when one is closer to the transition regime or if the voltage is higher. The bottom panel of Fig. 5 shows a current-voltage relationship for the membranes used in the top panel recorded at 19°C. It represents the average current for all events where I_m is larger than zero. It is linear in the regime between -150mV and $+150$ mV. If $|V| >$ 150 mV, the overall conductance increases, probably because of a significant contribution of multiple conductance steps induced by higher voltage. Note that the electrostatic potential is an intensive thermodynamic variable that influences the state of the membrane (see Discussion). From the slope in the linear regime, one can calculate a channel conductance of 300 ± 80 pS. Assuming a pore in the lipid membrane filled with electrolyte (4), one calculates a pore radius of ~0.75 nm, which is practically identical to the diameter of a single lipid. (DPPC has a cross-sectional area of 0.63 nm^2 in the fluid state (9) corresponding to a diameter of ~0.8 nm.) This size is similar to the radii reported for protein channels, e.g., 0.45–0.5 nm for the voltage-gated potassium channel K_v1.2 (41) or 0.3 nm for the acetylcholine receptor (42). The fact that lipid ion channels display larger conductance at high voltage could be considered as a voltage-gating. However, it seems likely that this effect reflects, instead, the influence of voltage on the transition.

In the section above on dye permeation through vesicles, it was shown that anesthetics (octanol) influence permeation because of the influence of anesthetics on the heat capacity, and hence on the lateral compressibility. In Fig. 6 (*left panel*), the heat capacity profiles of DOPC/DPPC = 2:1 membranes are shown in the absence and the presence of 1-octanol. For the DPPC/DPPG = 95:1 membranes in Fig. 3, the melting events are shifted toward lower temperatures. We performed BLM measurements at 19°C, which is

close to the transition maximum. Thus, one expects that adding octanol moves the membranes out of their transition regime and according to Eq. 12, the permeability should decrease. That this is in fact the case is shown in Fig. 6 (*center* and *right*). At 210 mV, the currents in the absence of octanol show two maxima at ~100 and 200 pA. In the presence of 7.9 mol % octanol, the current steps range between 20 and 40 pA, whereas in the presence of 15.9 mol % octanol, the current amplitudes are ~15 pA. At higher octanol concentrations (23.8 mol %), conductance events disappear completely. This reflects the decrease in heat capacity at 19°C induced by increasing octanol concentrations. Visual inspection of the current traces also seems to indicate that the mean open time per channel decreases with increasing octanol content. For each octanol concentration, we recorded ~50–60 traces of 30 s each that all looked similar to the traces shown in Fig. 6. We performed a statistical analysis of all the traces recorded for each condition, and evaluated the percentage of the total time in which no current events were observed. We found 62% closed time in the absence of octanol, 84% closed time for membrane containing 7.9 mol % octanol, 89% closed time for 15.9 mol% octanol, and 93% closed time for 23.8 mol % octanol. Thus, increasing amounts of octanol decrease the overall probability of the membrane to be found in a conducting state. Visual inspection of the current traces also indicates that the mean open time per channel decreases with increasing octanol content.

DISCUSSION

In this article, we investigated the permeability of lipid membranes for dyes and ions using FCS and BLM measurements. In agreement with earlier studies (3,4,7,11), we found that the permeability for both dyes and ions is maximum in the melting regime of the membranes. The FCS experiments showed that the permeation rate is, within experimental error, proportional to the heat capacity of a DPPC/DPPG = 95:5 membrane. This can be understood by the large fluctuations in area near the transition. This leads to a high compressibility and, consequently, the work required to create a pore by thermal fluctuation is small (see Theory). Several degrees below the transition the membrane was practically impermeable to dyes. Using the BLM technique (12), we measured ion currents through lipid pores. The findings are in agreement with the dye permeation experiments. We showed that one finds quantized currents in the melting regime which are absent at higher temperatures. Because of their similarity with protein channel currents, one can consider these events as lipid ion channels. Wunderlich et al. (43) showed that the mean conductance of a membrane of a lipid mixture indeed correlates well with the heat capacity (in their case of a $DC_{15}PC$/DOPC mixture). One may compare the permeation rates measured by FCS and the BLM measurements. The surface of the BLM hole with ~80 μm diameter is ~1.6×10^5 larger than the surface of a 100-nm vesicle. If the mean frequency of pore creation is between 1/s and 100/s (e.g., *traces* in Fig. 5), and assuming that the content of the vesicles empties upon one hole formation, one would assume that the time constant of the dye release from the vesicles is of ~10^3–10^5 s. This is approximately the order of magnitude found in our experiments (where we find between 100 and several 1000 s). This suggests that the permeation process in the BLM and the FCS experiments is the same or very similar. Glaser et al. (44) suggested that, at sufficiently high voltages, stable hydrophilic pores of 0.6–1 nm can exist. This is in agreement with our findings that suggest pore sizes of approximately one lipid cross-section. The ionic radius of K^+ is 0.138 nm, the radius of Cl^- is 0.181 nm, and the size of the dye molecule is ~1 nm. In contrast to protein channels, the number of lipid channels is not fixed. They are merely fluctuating defects in membranes, and their occurrence depends on the state of the membrane as controlled by the intensive thermodynamic variables of the system (e.g., temperature, pressure, electrostatic potential, and the chemical potential of the components). We suggest that, if number and lifetime allow it, such lipid pores may fuse to form pores that are big enough to be permeable to large molecules. If one is precisely at the transition, this may already occur at zero or small voltages. It is known that at high voltages one finds the well-documented phenomenon of electroporation (45). At and above 500 mV, long-lived pores can be produced in biological cell membranes. This effect is used to facilitate the transport of drugs into cancer cells (46). Molecular dynamics simulations suggest that stable pores of nm-size can exist after applying transmembrane voltage pulses (47,48). We have shown here that at voltages above 150 mV the current-voltage relationship becomes nonlinear so that currents are much larger. We further showed the existence of pores of a size sufficient to be permeable for small fluorescence dyes. One may well ask if the quantized currents found at lower voltages and electroporation found at high voltages are, in fact, the same phenomenon, with the difference that the pore sizes are larger at high voltage. This matter requires further investigation. In our experiments, the BLMs typically rupture above 300 mV. It should be noted here that one major disadvantage of the BLM technique is that the Teflon hole is prepainted with 5% hexadecane or decane in pentane. Thus, the membranes contain some residual alkanes that may influence the state of the membrane to a degree that may vary between different experiments. It would be of great interest to develop the Montal-Müller technique such that no additional organic solvent is required—or to repeat these studies with the patch-clamp technique, as for example done in Kaufmann et al. (18).

We have shown above that the presence of a melting transition and the accompanying area fluctuations are necessary for permeation effects. Whatever changes the state of the membrane potentially affects the permeability. Here, we studied in particular the effect of anesthetics on the permeation of dyes in FCS and ions in the BLM technique. We found that, in both techniques, the permeability changes

in agreement with the changes in heat capacity. The lipid ion channels showed smaller conductances in the presence of anesthetics. In a recent article (27), we investigated the effect of anesthetics on membranes that lower the melting point of membranes. Here, we have shown that, below the melting transition, the presence of anesthetics can increase the permeability because the transition temperature is shifted toward the experimental temperature (Fig. 3). If one is above the transition, the presence of anesthetics lowers the permeability because the transition events are moved further away from experimental conditions (Fig. 6). In Heimburg and Jackson (27), we derived the following equation for the difference in free energy between fluid and gel phase of a membrane

$$\Delta G = \Delta H \left(\frac{T_m - T}{T_m} - \frac{RT}{\Delta H} x_A + \gamma_V \Delta p \frac{T}{T_m} + f(\mu_{H^+}) + f(\mu_{Ca^{2+}}) + f(\Psi) + \ldots \right), \quad (13)$$

where ΔH is the transition enthalpy, T_m is the melting temperature, x_A is the molar fraction of anesthetics in the membrane, Δp is the hydrostatic pressure, and γ_V is a parameter describing the relation between volume and enthalpy changes ($\gamma_V = 7.8 \times 10^{-10}$ m^2/N). This equation contains one term describing the effect of temperature, a term for the influence of anesthetics and a further term describing the effect of hydrostatic pressure. For each change in an intensive thermodynamic variable, one can add further terms into this equation; for example, for pH, calcium concentration or voltage, denoted here as $f(\mu_{H^+})$, $f(\mu_{Ca^{2+}})$, and $f(\Psi)$. We suggested in Heimburg and Jackson (27) that whenever the value of the potential ΔG is the same, the anesthetic action is also the same. Similarly, one can state here that whenever the value of ΔG is the same, one expects the same permeability. Changes in different variables may compensate; for example, the pressure and the anesthetics concentration known as pressure reversal of anesthesia (27). Therefore, it is to be expected that the decrease in permeability observed in our BLM measurements would be compensated by hydrostatic pressure. In biological preparations that are found slightly above the transition of their membranes, one would expect an increase in conductance of lipid ion channels with increased pressure. In this context, it is interesting to note that the acetylcholine receptor displays a dependence on hydrostatic pressure, which becomes apparent at 400 bars (49), corresponding to a shift of the transition temperature of ~10 Kelvin to higher temperatures (39). This is the approximate difference of the melting temperature of biological membranes and physiological temperature. One would also expect that an increase in voltage would change the state of membranes because each monolayer of the membrane possesses a quite high dipole potential of ~200–500 mV (e.g., (50)). Antonov et al. (21) showed that increase in voltage increases the chain melting temperature. Here, we found a nonlinear current-voltage relationship (Fig. 5). The increase in conductance at higher voltages observed in our BLM measurements (Fig. 5) is in agreement with Antonov's findings. However, the voltage effect is not well studied. Since the bilayer possesses two monolayers with opposing dipole potentials, the effect of voltage may be different in the two layers. Impurities and proteins (or their chemical potentials) are further intensive variables. We have shown previously that fluctuations in lipid state are especially enhanced at lipid domain boundaries (51) and at protein interfaces (52). This makes domain boundaries and protein-lipid interfaces particularly susceptible for lipid ion channel formation.

Elliott and Haydon (53) found that octanol also increases the tension in the membrane. We find it unlikely that the tension in the fluid membrane itself makes the membrane more permeable other than by its influence on the melting transition. This judgment is based on the coherence of the explanation of permeation events presented in this article. However, we have no independent experimental evidence that rules out the possibility of changes in the membrane tension having some influence on the permeability.

Previously, we have investigated the fluctuation lifetimes of lipid vesicles that are identical to the relaxation timescale after a small perturbation (54,55). We found that relaxation timescales are proportional to the heat capacity. Multilamellar vesicles with very cooperative transitions display relaxation times of up to 30 s at the c_p maximum. Unilamellar vesicles display less cooperative transitions with maximum relaxation times at ~1–2 s. If calorimetric profiles are broader (and the heat capacity is smaller), one instead expects relaxation times near 10–100 ms. E.g., it has been estimated that the relaxation timescale in the c_p maximum of lung surfactant is ~100 ms. This timescale is close to what we find here for the channel lifetimes. It has been discussed before that channel lifetimes are in fact longer when the heat capacity is higher (55). This has been shown in BLMs by Wunderlich et al. (43) showing longer mean open times of the lipid channels close to the c_p-maximum of a $DC_{15}PC$/1,2-dimyristoyl-*sn*-glycero-3-phosphocholine mixture that correlated with the heat capacity changes. This may explain why Antonov et al. (4) found channel lifetimes on the order of seconds at the c_p maximum of DPPC membranes. As mentioned, this is the relaxation timescale for unilamellar DPPC membranes (55). Overall, the channel lifetimes seem to be related to the fluctuation timescales of lipid membranes.

Finally, it is tempting to compare lipid channels with protein channels. It seems that they display very similar signatures both with respect to conductances and to mean channel open times. This is striking and raises the question of whether the physics behind these events is similar. It is remarkable that Na^+ channels and the acetylcholine receptor are affected by octanol in a manner similar to our lipid channels (56,57). The same is true for the effect of ethanol that leads to an increase in channel lifetimes (data not shown) and which has also been reported to have a similar affect on the acetylcholine receptor (58,59). In the literature, the effect of anesthetics on ion channels has led to the notion

that anesthesia acts via a specific binding mechanism to channel proteins, a view that we have opposed in Heimburg and Jackson (27) on thermodynamic grounds. The similarity between protein channel data and lipid membrane conductance deserves to be investigated in greater detail in future studies. At present, the precise connection between the two phenomena must remain an open question. However, it must be concluded that

1. The finding of quantized currents in itself does not prove the activity of a channel protein since lipid membranes show very similar or identical events close to transitions.
2. The effect of drugs on the conduction events does not prove drug binding to a protein, because anesthetics can strongly influence conductance events in the complete absence of proteins because of their effect on the thermodynamics of the membrane.

Thus, an analysis of channel proteins exclusively based on conduction events and their alteration by drugs must be considered logically incomplete. To identify the action of a protein, one needs a clearcut criterion that allows discrimination between lipid and protein ion channels. The readers should feel encouraged to develop such criteria, should they exist.

CONCLUSIONS

We have shown here that lipid membranes are permeable to dyes and ions if one is close to the chain melting regime. The microscopic permeation for ions has been shown to be quantized with conductances and lifetimes similar to those reported for proteins channels. Membrane permeation can be influenced by changes in intensive thermodynamic variables, particularly temperature, voltage, and chemical potential of anesthetic molecules. Other authors have shown that permeation for ions can be influenced by calcium (20,19), pH changes (16,17), and changes in membrane tension (18). The same will be true for an increase of hydrostatic pressure. Thus, it must be concluded that the overall physics of lipid membrane permeation is straightforward and easily understood as a consequence of lateral area fluctuations. Since all biological membranes possess lipid membranes (and membrane proteins), it cannot be conclusively excluded that some of the quantized current events reported in the literature for proteins are in fact due to lipid channels, especially when considering that biological membranes exist in a state close to their melting transitions (5,6). In a recent article, we proposed that the action potential in nerves is related to the phase transition in biomembranes (27). In particular, we have shown that close to such transition one obtains the possibility of solitary piezoelectric pulses. It is interesting to note that, under exactly these conditions, one finds the quantized ion currents through lipid membranes.

We acknowledge discussions with Dr. K. Kaufmann (Göttingen) and his earlier manuscript that has been published in a private edition (see (18)). The BLM cell was built during a bachelor project of H. Krammer, who was a visiting student from the LMU Munich. We further acknowledge the friendly help concerning the BLM setup by Dr. M. F. Schneider and C. Leirer (Augsburg). An article with complementary data on the temperature dependence of lipid channels has recently been submitted by Wunderlich et al. (43). The little calculation in Discussion comparing vesicle permeation rates with pore formation in the BLMs was suggested to us by one of the reviewers. We thank Prof. Andrew D. Jackson for critical proofreading of the manuscript.

Matthias Fidorra was supported by the Villum-Kann-Rasmussen foundation via BioNET.

REFERENCES

1. Hodgkin, A. L., and A. F. Huxley. 1952. A quantitative description of membrane current and its application to conduction and excitation in nerve. *J. Physiol.* 117:500–544.
2. Jansen, M., and A. Blume. 1995. A comparative study of diffusive and osmotic water permeation across bilayers composed of phospholipids with different head groups and fatty acyl chains. *Biophys. J.* 68:997–1008.
3. Antonov, V. F., V. V. Petrov, A. A. Molnar, D. A. Predvoditelev, and A. S. Ivanov. 1980. The appearance of single-ion channels in unmodified lipid bilayer membranes at the phase transition temperature. *Nature.* 283:585–586.
4. Antonov, V. F., A. A. Anosov, V. P. Norik, and E. Y. Smirnova. 2005. Soft perforation of planar bilayer lipid membranes of dipalmitoylphosphatidylcholine at the temperature of the phase transition from the liquid crystalline to gel state. *Eur. Biophys. J.* 34:155–162.
5. Heimburg, T., and A. D. Jackson. 2005. On soliton propagation in biomembranes and nerves. *Proc. Natl. Acad. Sci. USA.* 102:9790–9795.
6. Heimburg, T. 2007. Thermal Biophysics of Membranes. Wiley VCH, Berlin, Germany.
7. Papahadjopoulos, D., K. Jacobson, S. Nir, and T. Isac. 1973. Phase transitions in phospholipid vesicles. fluorescence polarization and permeability measurements concerning the effect of temperature and cholesterol. *Biochim. Biophys. Acta.* 311:330–340.
8. Nagle, J. F., and H. L. Scott. 1978. Lateral compressibility of lipid mono- and bilayers lateral compressibility of lipid mono- and bilayers. Theory of membrane permeability. *Biochim. Biophys. Acta.* 513:236–243.
9. Heimburg, T. 1998. Mechanical aspects of membrane thermodynamics. Estimation of the mechanical properties of lipid membranes close to the chain melting transition from calorimetry. *Biochim. Biophys. Acta.* 1415:147–162.
10. Cruzeiro-Hansson, L., and O. G. Mouritsen. 1988. Passive ion permeability of lipid membranes modeled via lipid-domain interfacial area. *Biochim. Biophys. Acta.* 944:63–72.
11. Corvera, E., O. G. Mouritsen, M. A. Singer, and M. Zuckermann. 1992. The permeability and the effect of acyl-chain length for phospholipid bilayers containing cholesterol: theory and experiment. *Biochim. Biophys. Acta.* 1107:261–270.
12. Montal, M., and P. Müller. 1972. Formation of bimolecular membranes from lipid monolayers and a study of their electrical properties. *Proc. Natl. Acad. Sci. USA.* 69:3561–3566.
13. Yafuso, M., S. J. Kennedy, and A. R. Freeman. 1974. Spontaneous conductance changes, multilevel conductance states and negative differential resistance in oxidized cholesterol black lipid membranes. *J. Membr. Biol.* 17:201–212.
14. Neher, E., and B. Sakmann. 1976. Single-channel currents recorded from membrane of denervated frog muscle fibers. *Nature.* 260: 779–802.
15. Bean, R. C., W. C. Shepherd, H. Chan, and J. Eichner. 1967. Discrete conductance fluctuations in lipid bilayer membranes. *J. Gen. Physiol.* 53:741–757.
16. Kaufmann, K., and I. Silman. 1983. Proton-induced ion channels through lipid bilayer membranes. *Naturwissenschaften.* 70:147–149.
17. Kaufmann, K., and I. Silman. 1983. The induction by protons of ion channels through lipid bilayer membranes. *Biophys. Chem.* 18:89–99.

18. Kaufmann, K., W. Hanke, and A. Corcia. 1989. BOOK 3: Ion Channel Fluctuations in Pure Lipid Bilayer Membranes: Control by Voltage. http://membranes.nbi.dk/Kaufmann/. Caruaru, Brazil.
19. Antonov, V. F., E. V. Shevchenko, E. T. Kozhomkulov, A. A. Molnar, and E. Y. Smirnova. 1985. Capacitive and ionic currents in BLM from phosphatidic acid in Ca^{2+}-induced phase transition. *Biochem. Biophys. Res. Commun.* 133:1098–1103.
20. Gögelein, H., and H. Koepsell. 1984. Channels in planar bilayers made from commercially available lipids. *Pflugers Arch.* 401:433–434.
21. Antonov, V. F., E. Y. Smirnova, and E. V. Shevchenko. 1990. Electric field increases the phase transition temperature in the bilayer membrane of phosphatidic acid. *Chem. Phys. Lipids.* 52:251–257.
22. Boheim, G., W. Hanke, and H. Eibl. 1980. Lipid phase transition in planar bilayer membrane and its effect on carrier- and pore-mediated ion transport. *Proc. Natl. Acad. Sci. USA.* 77:3403–3407.
23. Yoshikawa, K., T. Fujimoto, T. Shimooka, H. Terada, N. Kumazawa, et al. 1988. Electrical oscillation and fluctuations in phospholipid membranes. Phospholipids can form a channel without protein. *Biophys. Chem.* 29:293–299.
24. Woodbury, D. J. 1989. Pure lipid vesicles can induce channel-like conductances in planar bilayers. *J. Membr. Biol.* 109:145–150.
25. Trudell, J. R., D. G. Payan, J. H. Chin, and E. N. Cohen. 1975. The antagonistic effect of an inhalation anesthetic and high pressure on the phase diagram of mixed dipalmitoyl-dimyristoylphosphatidylcholine bilayers. *Proc. Natl. Acad. Sci. USA.* 72:210–213.
26. Kharakoz, D. P. 2001. Phase-transition-driven synaptic exocytosis: a hypothesis and its physiological and evolutionary implications. *Biosci. Rep.* 210:801–830.
27. Heimburg, T., and A. D. Jackson. 2007. The thermodynamics of general anesthesia. *Biophys. J.* 92:3159–3165.
28. Overton, C. E. 1901. Studien über die Narkose. Verlag Gustav Fischer, Jena, Germany. [English translation: 1991. Studies of Narcosis. R. Lipnick, Ed. Chapman and Hall/CRC, Boca Raton, FL.].
29. Hac, A., H. Seeger, M. Fidorra, and T. Heimburg. 2005. Diffusion in two-component lipid membranes—a fluorescence correlation spectroscopy and Monte Carlo simulation study. *Biophys. J.* 88:317–333.
30. Peterson, U., D. A. Mannock, R. N. A. H. Lewis, P. Pohl, R. N. McElhaney, et al. 2002. Origin of membrane dipole potential: contribution of the phospholipid fatty acid chains. *Chem. Phys. Lipids.* 117:19–27.
31. Chanturiya, A. N., G. Basanez, U. Schubert, P. Henklein, J. W. Yewdell, et al. 2004. Pb1-f2, an Influenza A virus-encoded proapoptotic mitochondrial protein, creates variably sized pores in planar lipid membranes. *J. Virol.* 78:6304–6312.
32. Neville, F., M. Cahuzac, and D. Gidalevitz. 2004. The interaction of antimicrobial peptide ll-37 with artificial biomembranes: epifluorescence and impedance spectroscopy approach. *J. Phys. Condens. Matter.* 16:S2413–S2420.
33. Dilger, J. P., and R. Benz. 1985. Optical and electrical properties of thin monoolein lipid bilayers. *J. Membr. Biol.* 85:181–189.
34. Krichevsky, O., and G. Bonnet. 2001. Fluorescence correlation spectroscopy: the technique and its applications. *Rep. Prog. Phys.* 65:251–297.
35. Blicher, A. 2007. Permeability studies of lipid vesicles by fluorescence correlation spectroscopy and Monte Carlo simulations. Master's thesis, University of Copenhagen. http://membranes.nbi.dk/thesis-pdf/2007_Masters_A.Blicher.pdf.
36. Einstein, A. 1910. The theory of the opalescence of homogeneous fluids and liquid mixtures near the critical state [Theorie der Opaleszenz von homogenen Flüssigkeiten und Flüssigkeitsgemischen in der Nähe des kritischen Zustandes]. *Ann. Phys. (Leipzig).* 33:1275–1298.
37. Heimburg, T. 2000. Monte Carlo simulations of lipid bilayers and lipid protein interactions in the light of recent experiment. *Curr. Opin. Colloid Interface Sci.* 5:224–231.
38. Dimova, R., B. Pouligny, and C. Dietrich. 2000. Pretransitional effects in dimyristoylphosphatidylcholine vesicle membranes: optical dynamometry study. *Biophys. J.* 79:340–356.
39. Ebel, H., P. Grabitz, and T. Heimburg. 2001. Enthalpy and volume changes in lipid membranes. I. The proportionality of heat and volume changes in the lipid melting transition and its implication for the elastic constants. *J. Phys. Chem. B.* 105:7353–7360.
40. Jain, M. K., and J. L. V. Wray. 1978. Partition coefficients of alkanols in lipid bilayer/water. *Biochem. Pharmacol.* 275:1294–1295.
41. Treptow, W., and M. Tarek. 2006. Molecular restraints in the permeation pathway of ion channels. *Biophys. J.* 91:L26–L28.
42. Corry, B. 2006. An energy-efficient gating mechanism in the acetylcholine receptor channel suggested by molecular and Brownian dynamics. *Biophys. J.* 90:799–810.
43. Wunderlich, B. C., A. Leirer, U. F. Idzko, V. Keyser, T. Myles, and M. Heimburg Schneider. 2009. Phase state dependent current fluctuations in pure lipid membranes. *Biophys. J.* 96:4592–4597.
44. Glaser, R. W., S. L. Leikin, L. V. Chernomordik, V. F. Pastushenko, and A. I. Sokirko. 1988. Reversible breakdown of lipid bilayers: formation and evolution of pores. *Biochim. Biophys. Acta.* 940:275–287.
45. Freeman, S. A., M. A. Wang, and J. C. Weaver. 1994. Theory of electroporation of planar bilayer membranes: predictions of the aqueous area, change in capacitance, and pore-pore separation. *Biophys. J.* 67:42–56.
46. Neumann, E., S. Kakorin, and K. Tænsing. 1999. Fundamentals of electroporative delivery of drugs and genes. *Bioelectrochem. Bioenerg.* 48:3–16.
47. Tieleman, D. P., H. Leontiadou, A. E. Mark, and S. J. Marrink. 2003. Simulation of pore formation in lipid bilayers by mechanical stress and electric fields. *J. Am. Chem. Soc.* 125:6382–6383.
48. Böckmann, R., R. de Groot, S. Kakorin, E. Neumann, and H. Grubmüller. 2008. Kinetics, statistics, and energetics of lipid membrane electroporation studied by molecular dynamics simulations. *Biophys. J.* 95:1837–1850.
49. Heinemann, S. H., W. Stümer, and F. Conti. 1987. Single acetylcholine receptor channel currents recorded at high hydrostatic pressures. *Proc. Natl. Acad. Sci. USA.* 84:3229–3233.
50. Sehgal, K. C., W. F. Pickard, and C. M. Jackson. 1979. Phospholipid monolayers at the hydrocarbon-electrolyte interface—interrelation of film potential and film pressure. *Biochim. Biophys. Acta.* 552:11–22.
51. Seeger, H., M. Fidorra, and T. Heimburg. 2005. Domain size and fluctuations at domain interfaces in lipid mixtures. *Macromol. Symp.* 219:85–96.
52. Ivanova, V. P., I. M. Makarov, T. E. Schäffer, and T. Heimburg. 2003. Analyzing heat capacity profiles of peptide-containing membranes: cluster formation of gramicidin A. *Biophys. J.* 84:2427–2439.
53. Elliott, J. R., and D. A. Haydon. 1979. The interaction of *n*-octanol with black lipid bilayer membranes. *Biochim. Biophys. Acta.* 557:259–263.
54. Grabitz, P., V. P. Ivanova, and T. Heimburg. 2002. Relaxation kinetics of lipid membranes and its relation to the heat capacity. *Biophys. J.* 82:299–309.
55. Seeger, H. M., M. L. Gudmundsson, and T. Heimburg. 2007. How anesthetics, neurotransmitters, and antibiotics influence the relaxation processes in lipid membranes. *J. Phys. Chem. B.* 111:13858–13866.
56. Zuo, Y., G. L. Aistrup, W. Marszalec, A. Gillespie, L. E. Chavez-Noriega, et al. 2001. Dual action of *n*-alcohols on neuronal nicotinic acetylcholine receptors. *Mol. Pharmacol.* 60:700–711.
57. Horishita, T., and R. A. Harris. 2008. *n*-alcohols inhibit voltage-gated Na^+ channels expressed in *Xenopus* oocytes. *J. Pharmacol. Exp. Ther.* 326:270–277.
58. Forman, S. A., and Q. Zhou. 1999. Novel modulation of a nicotinic receptor channel mutant reveals that the open state is stabilized by ethanol. *Mol. Pharmacol.* 55:102–108.
59. Zuo, Y., K. Nagata, J. Z. Yeh, and T. Narahashi. 2004. Single-channel analyses of ethanol modulation of neuronal nicotinic acetylcholine receptors. *Alcohol. Clin. Exp. Res.* 28:688–696.
60. Overton, E. 1895. On the osmotic properties of living plant and animal cells [Über die osmotischen Eigenschaften der lebenden Pflanzen und Thierzelle]. *Vierteljahrsschr. Naturforsch. Ges. Zürich.* 40:159–201.

View Online

The thermodynamics of lipid ion channel formation in the absence and presence of anesthetics. BLM experiments and simulations†

Katarzyna Wodzinska,‡* Andreas Blicher‡* and Thomas Heimburg

Received 19th May 2009, Accepted 17th June 2009
First published as an Advance Article on the web 23rd July 2009
DOI: 10.1039/b909877a

It is known that lipid membranes become permeable in their melting regime. In conductance measurements on black lipid membranes one finds that conduction takes place *via* quantized events closely resembling those reported for protein ion channels. Here, we present data of ion currents through black lipid membranes in the presence and absence of the anesthetics octanol and ethanol, and compare them to a statistical thermodynamics model using parameters that are obtained from experimental calorimetric data. The conductance steps in pure lipid membrane suggest aqueous pores with the size of approximately one lipid cross-section. We model the permeability by assuming empty lattice sites of the size of one lipid. We find that pore formation in the melting transition regime is facilitated by the increase of the lateral compressibility that expresses itself in the area fluctuations, a process that is related to critical opalescence in two dimensions. Anesthetics alter the permeability by affecting the thermodynamic state of the membrane and by shifting the heat capacity profiles.

Published on 23 July 2009 on http://pubs.rsc.org | doi:10.1039/B909877A
Downloaded by New Copenhagen University on 25 April 2011

1 Introduction

In biology, lipid membranes are typically considered as insulators, which is an important assumption for models related to nerve pulse propagation (*e.g.*, the Hodgkin–Huxley model[1]) and the conduction of ions through proteins. It is known, however, that lipid membranes become permeable in the proximity of membrane melting transitions,[2–4] which creates significant conceptual problems for such models because biological membranes under physiological conditions are in fact often close to such transitions.[5] We have shown in two recent papers that the membrane permeability changes continuously in the transition with a behavior closely resembling the heat capacity anomaly.[6,7] This is both true for permeation of fluorescence dyes[6] and for potassium and sodium chloride[6,7] through black lipid membranes of lipid mixtures in their transition regime. The increased permeability of membranes in transitions has been attributed to the large fluctuations in membrane area generally related to transitions, and to the appearance of domain boundaries.[2,8] The area fluctuations are proportional to the lateral compressibility[9] that also reaches a maximum in the transition regime. Thus, the work necessary to create conducting membrane defects under these conditions is small.[3]

Interestingly, it has been found in microscopic measurements using black lipid membranes or using a patch-clamp that the conductance of ions through pure lipid membranes occurs in quantized steps, suggesting pores of well-defined size.[6,10–15] These events display a similar conductance and typical opening and closing time scales as the conduction events reported for protein ion channels.[16] In a recent paper we found conductance steps suggesting aqueous pores of 0.7 nm, very similar to the size proposed for protein ion channels.[6] Pores of this size have also been proposed on the basis of molecular dynamics simulations.[17]

The obvious question arises how the lipid conduction events can be distinguished from those of proteins. In particular, while lipid membranes can be investigated in the absence of proteins, channel proteins cannot be investigated in the absence of lipid membranes into which they are embedded. A patch pipette has a diameter of about 1 μm while the diameter of a typical membrane protein is of the order of 5 nm. The patch tip area is therefore about 40 000 times larger than the protein, which renders it technically impossible to measure currents through proteins without simultaneously measuring the events in the lipid membrane, too.

Taking the very convincing evidence of a direct coupling between heat capacity and permeability we concluded that everything shifting the heat capacity profile of membrane melting will also alter the membrane permeability.[6] This includes changes in temperature, pressure and pH, but also the presence of anesthetics. The latter molecules have been shown to lower membrane transitions according a freezing point depression law, completely independent of the nature of the anesthetics drug.[18] When measuring in the transition regime, anesthetics therefore lower the permeability, and quantized current events are 'blocked'.[6]

In this paper we show experimental data on quantized currents through black lipid membranes (BLMs) and the effect of anesthetics on the conduction. In comparison to our two earlier recent publications[6,7] we focus here on investigating the origin of the current fluctuations from lateral area fluctuations that are strongly enhanced in transition regimes. We rationalize our findings with a statistical thermodynamics model that takes the area fluctuations of the membranes into account. Statistical thermodynamics models (*e.g.*, 2 state Ising models or 10 state Pink models) in the past have been successfully used to describe cooperative melting events in membranes.[19–25] In transitions, the cooperative

Niels Bohr Institute, University of Copenhagen, Denmark. E-mail: k.wodzinska@gmail.com; ablicher@gmail.com.; theimbu@nbi.dk
† This paper is part of a *Soft Matter* themed issue on Membrane Biophysics. Guest editor: Thomas Heimburg.
‡ K. W. and A. B. contributed equally to this work.

Published on 23 July 2009 on http://pubs.rsc.org | doi:10.1039/B909877A
Downloaded by New Copenhagen University on 25 April 2011

fluctuations lead to domain formation on scales much larger than the individual lipid. On these scales, the lack of molecular detail is not important. For this reason, one cannot deduce molecular pore geometries. In this publication we allow for the formation of pores facilitated by the fluctuations in area without specifying a detailed pore geometry. We demonstrate that this models results in channel statistics similar to the BLM experiment and that this approach explains the effect of anesthetics.

2 Methods

2.1 Materials

Chemicals. Decane and 1-octanol were purchased from Fluka Chemie AG (Deisenhofen, Germany), *N*-hexadecane, chloroform and ethanol were obtained from Merck (Hohenbrunn, Germany), *n*-pentane was provided by BDH (Poole, UK) and potassium chloride from J.T. Baker Analyzed (Deventer, Holland). 1,2-dipalmitoyl-sn-glycero-3- phosphocholine (DPPC) and 1,2-dioleoyl-sn-glycero-3-phosphocholine (DOPC) were purchased from Avanti Polar Lipids (Birmingham, AL) and used without further purification. For all experiments, MilliQ water (18.1 MΩ) was used.

Calorimetry. DSC experiments were performed on a VP-DSC Calorimeter (MicroCal, Nort-hampton, MA, USA) with a scan rate of 5 °C/h. The lipid samples were prepared by pre-dissolving in chloroform, which was first dried under a nitrogen stream and then kept under high vacuum overnight. The dried lipid mixtures were dispersed in MilliQ water to a final concentration of 20 mM. The buffer used was the same as for the BLM experiments. Before filling the calorimeter, the solutions were degassed for 10 min.

Black lipid membranes. Planar bilayers were formed over a round aperture of ~80 μm radius in a Teflon film of 25 μm thickness dividing two compartments of a Teflon chamber embedded in a brass block that could be heated by a circulating water bath. The aperture in the Teflon film was prepainted with 5% hexadecane in pentane. The BLMs were painted with DOPC:DPPC 2:1 lipid solutions in decane/chloroform/methanol 7:2:1 and formed following the method described by Montal and Mueller.[26] The two compartments of the Teflon block were filled with unbuffered 150 mM KCl (pH 6.5). Lipid solution (25 mg/ml) was spread on the buffer surface in each compartment (approx. 3 μl on each side). Ag/AgCl electrodes were placed into both compartments of the chamber. After 15–30 min to allow for the evaporation of the solvent, the water level of the compartments was lowered and raised several times until a bilayer was formed over the hole. The formation of BLMs was controlled visually and by capacitance measurements (with a triangular 100 mV voltage input pulse). For the experiments with octanol, 15% v/v octanol in methanol solution was prepared and added symmetrically on both sides of the Teflon chamber. To calculate the concentration of octanol in the membrane we assumed an octanol partition coefficient between lipid membrane and water of 200.[27] In the experiments with ethanol we used 60 μl and 120 μl of 99% ethanol for a buffer volume of the two compartments of 2 ml. Assuming a ethanol partition coefficient of 0.48 between the membranes and water[28] this corresponds to 9.5 mol% and 19 mol% ethanol in the membrane.

Conductance measurements were performed on an Axopatch 200B amplifier in voltage clamp mode connected to a DigiData 1200 digitizer (both Molecular Devices, Sunnyvale, CA, USA). Current traces were filtered with 1 kHz low-pass Bessel filter and recorded with Clampex 9.2 software (Axon Instruments) on the hard drive of the computer using an AD converter with a time resolution of 0.1 ms. The data was further analyzed with Clampfit 9.2 and low-pass filtered with Bessel (8-pole) filter at a cut-off frequency of 300 Hz. Temperature was controlled by a HAAKE DC30 K20 (Waltham, USA) waterbath and a thermocouple (WSE, Thermocoax).

2.2 Simulating pore formation

Here we introduce a statistical mechanical model for pore formation close to lipid melting transitions in a system with one species of lipid and a second species of molecule (here anesthetics), based on previous work by Ivanova *et al.*[25] We further base our simulations on a theoretical paper by Nagle and Scott[3] that relates pore formation to the lateral compressibility of the membrane. The aim of this work was to rationalize the findings from a paper by Papahadjopoulos *et al.*[2] that has first shown experimentally that membranes are most permeable in their transition. According to Nagle and Scott, the work necessary to compress a membrane (*i.e.*, the Helmholtz free energy change) by an area a is a quadratic function of the area that has the form

$$\Delta W(a) = \frac{1}{2} K_T^A \left(\frac{a}{A_0}\right)^2 \cdot A_0 \tag{1}$$

where A_0 is the total area of the membrane, a is the size of a pore defect and K_T^A is the isothermal area compression modulus (*e.g.*, ref. 3). The compressibility of a membrane is the inverse of the compression modulus given by

$$\kappa_T^A = -\frac{1}{A_0}\left(\frac{\partial A}{\partial \Pi}\right)_T \equiv \frac{1}{K_T^A} \tag{2}$$

Nagle and Scott[3] assumed that the permeability can be expressed as a series expansion with respect to the area fluctuations that are also proportional to the lateral compressibility. The resulting permeability obtained by Nagle and Scott is

$$P = a_0 + a_2 \kappa_T^A + \text{higher order terms} \tag{3}$$

where a_0 and a_2 are constants to be determined from experiment. We have shown previously that close to transitions the lateral compressibility is proportional to the heat capacity:

$$\kappa_T^A = \kappa_{T,0}^A + \frac{\gamma_A^2 \, T}{A_0} \, \Delta c_p \tag{4}$$

Inserting expression 4 into eqn 3 yields

$$P = c_0 + c_2 \Delta c_p \tag{5}$$

where c_0 and c_2 are also constants to be determined from the experiment. This is a simple expression directly coupled to the

 This journal is © The Royal Society of Chemistry 2009

Published on 23 July 2009 on http://pubs.rsc.org | doi:10.1039/B909877A
Downloaded by New Copenhagen University on 25 April 2011

calorimetric experiment. More details can be found in ref. 6. As pointed out in ref. 6, this approach resembles that employed by Einstein to rationalize critical opalescence in lipid mixtures close to a critical point.[29] The Nagle–Scott model[3] combined with eqn 4 as given by eqn 5 suggests a proportional relation of lateral compressibility and pore formation probability. The argument implied in this notion is that one needs to perform work against the lipid matrix to create a hole by compressing the rest of the matrix. This also implies, that the formation of the pore must keep the overall area of the membrane constant, *i.e.*, the area of the membrane does not increase upon the introduction of a pore. Since the compressibility is at a maximum in the transition regime, one expects the highest likelihood of pore formation. Would the formation of a hole in the lipid matrix just increase the overall area one would not find a maximum in conductance in the transition because the membrane is not compressed. One would rather find a stepwise change in conductance from gel to fluid membranes. In a recent publication[6] we have shown experimentally by fluorescence correlation spectroscopy that the permeability of a lipid membrane for a fluorescence dye in fact follows the predictions of the Nagle–Scott model in combination with the proportional relation of compressibility and heat capacity (eqn 3 and 5) within experimental accuracy. Thus, it has been experimentally shown that the pore formation process maintains the membrane area. Therefore, we designed a simulation in which the pore formation process was chosen such that the overall area was maintained.

Fig. 1a and 1b show two different possible pore geometries. They correspond to two pore intermediates found in MD simulations.[17] Fig. 1b also corresponds to the geometry assumed in elasticity theory.[30] In both papers, the pore size was found to be of the order 0.7–1 nm. Fig. 1a corresponds just to a vacancy of diameter of one lipid in which lipid chains are exposed to water with an associated free energy change due to the hydrophobic contact, while the second geometry (Fig. 1b) requires a rearrangement of lipids such that no hydrophobic contact with the water exists. One has, however, a free energy of curvature for the lipids at the interface of the pore. Thus, both geometries consist of a pore with diameter of 0.7 nm and an interfacial free energy. In this work we employ a lattice Ising model where pores are represented by a free lattice site and the pore free energy by the interaction of the pore with the lipids (*cf.*, Fig. 1c). This is a reasonable model for the both pore geometries given in Fig. 1a and b. One should keep in mind that the Ising model does not contain a detailed molecular model for the pore. It contains, however, the measured pore area, and the interfacial free energy of the pore with the lipids. Thus, representing a pore by a vacancy in a lattice does not specify a molecular geometry.

In the simulation, each lipid could be in either gel or fluid state. This model formally corresponds to an Ising model in a field. In the present work we additionally allowed for the formation of pores in the membrane by moving lipids from randomly chosen lattice sites to the edge of the computer matrix. For a given temperature we evaluate the mean number of gel and fluid lipids and the fluctuations in their number, and we determine the number of spontaneously formed pores. A numerical evaluation by means of Monte Carlo simulations was used. To do this one first has to define the various Monte Carlo steps. Whether a given step is accepted or not, depends on difference in the free energy of the old and the new system configuration as given by eqn (1). At its most basic (*i.e.* a one-component system without anesthetics and no pore formation) only one type of step is needed, namely one that allows the lipids to change their state (a "melting step"). As we are using the two-state Ising model as a basis, each lipid is assumed to be in either an ordered (gel) or disordered (fluid) state.[22,25] For the more advanced models (multiple lipid species, anesthetics, pore formation, *etc.*) it is also necessary to include the possibility for any two particles to swap positions (*i.e.*, a "diffusion step"),[31,32] as well as to include a Monte Carlo step which allows for the creation/sealing of a pore. The basic idea behind the pore forming step is the observation that a lipid changes area by approximately 25% when it goes from the fluid

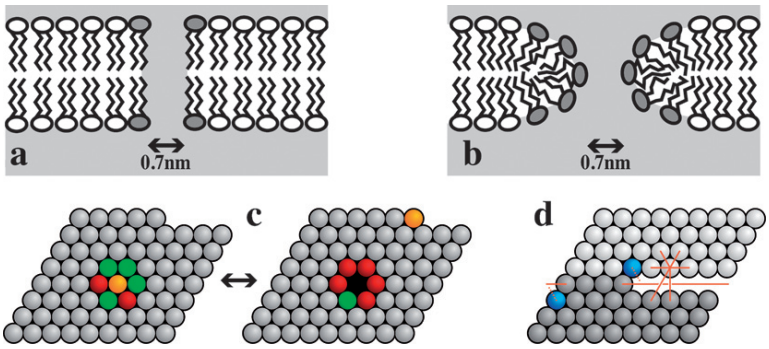

Fig. 1 **a.** The pore modeled by a hole in the membrane of about a lipid diameter with the chains exposed to water. The lipids with altered free energy are displayed with gray headgroups. **b.** The pore modeled with lipid arrangement. The head groups point towards the aqueous pore, but the monolayers display curvature. The lipids with altered free energy are displayed with gray headgroups. **c.** The pore formation step in the lattice Monte Carlo simulation. Green represents fluid state lipids, while the gels are red. The yellow particle can be either a lipid or an anesthetic molecule. In this Monte Carlo step three lipids simultaneously change state while the yellow particle is moved to or from the edge of the lattice. This means that the pore formation step increases the lattice size by one. During this step the overall area of the matrix stays constant (see text). **d.** The dark and light grey regions (bottom and top half) indicate the boundaries of repeating lattices. The definition of the nearest neighbors of the particle moved from the site of the pore to the edge. The red lines indicate the definition of nearest neighbors at the edge. Due to the odd shape of the lattice the blue lattice sites display a different definition of nearest neighborhood (indicated by the dotted red line). Still all lattice sites have 6 nearest neighbors.

View Online

Published on 23 July 2009 on http://pubs.rsc.org | doi:10.1039/B909877A
Downloaded by New Copenhagen University on 25 April 2011

to the gel state. So if three neighboring fluid lipids simultaneously change states, one can create a pore which has an area that is equal to a gel state lipid. Thus this step both conserves the number of lipids and also the area as $A_{before} = 3A_{fluid} = A_{after} = 3A_{gel} + A_{pore}$. In this kind of system a pore has automatically the cross-section of one lipid, which is what is observed in experiments[6] and molecular dynamics simulations.[17]

First pore formation is described. This step can be applied if a matrix site (that is not already a pore) is randomly picked: first the surroundings (nearest neighbors) is checked for lipids in the fluid state. If there are three or more, a pore is temporarily created by changing the three fluids into gels, and moving the "central particle" to the "end" of the lattice, increasing the number of lattice sites by one (see Fig. 1, left and center). In order to obey detailed balance, there must also be a possibility to seal a pore. This can happen when a pore is picked, and it has three or more neighbors which are gel state lipids. If so, the pore is temporarily sealed by changing the three gels to fluids, and moving the "end particle" into the pore, thus reducing the number of lattice sites by one (see Fig. 1). Finally, the proposed change is accepted or rejected using the Glauber algorithm.[33] We used periodic boundary conditions using a special definition of the nearest neighbor lipid environment on the edge (see Fig. 1, right).

Model parameters. There are three parameters which need to be determined if one wants to describe the melting transition of the most basic one-component two-state lipid system, namely the melting enthalpy, ΔH, the melting entropy, ΔS, and the cooperativity parameter, ω_{fg}. The latter parameter describes the interaction between a gel and a fluid lipid and determines the half width of the melting transition. For the model additionally containing anesthetics and pores, another five interaction parameters are needed, namely ω_{af} (anesthetic/fluid), ω_{ag} (anesthetic/gel), ω_{ap} (anesthetic/pore), ω_{pg} (pore/gel), and ω_{pf} (pore/fluid).[24]

With these parameters given the changes in free energy can be calculated as

$$\Delta G = \Delta H - T\Delta S + \Delta N_{fg}\omega_{fg} + \Delta N_{af}\omega_{af} + \Delta N_{ag}\omega_{ag} + \Delta N_{pf}\omega_{pf} + \Delta N_{pg}\omega_{\mathrm{pg}} + \Delta N_{ap}\omega_{\mathrm{ap}} \quad (6)$$

Fortunately, the first three parameters can be obtained from calorimetric experiments,[25] while the remaining three parameters are chosen such that pore formation likelihoods from permeation measurements are well described. Specifically, one can obtain the melting enthalpy and entropy of the lipids from the heat capacity profile of the one-component lipid system: the enthalpy change of the transition is obtained by integrating over the excess heat capacity in the relevant temperature interval. The entropy change can then easily be determined *via* $\Delta S = \Delta H/T_m$, as the transition midpoint, T_m, can be read off the heat capacity profile directly. The cooperativity parameter, ω_{fg}, relates directly to the width of the transition peak, and can consequently be determined by fitting the simulated heat capacity profiles to the experimentally measured one.

The five remaining interaction parameters, ω_{ij}, can be obtained indirectly from various other experiments. We have shown before that most anesthetics generate a freezing point depression that is consistent with ideal solubility in the fluid phase and no solubility in the gel phase.[18] Therefore we chose $\omega_{af} = 0$, and a high value for the anesthetic–gel interaction with $\omega_{ag} = \omega_{fg}$.[25] Determination of the remaining three parameters (ω_{ap}, ω_{pg} and ω_{pf}) can, in principle, be done by comparing the simulated permeability (basically the average number of pores) to the measurements.

Even before doing this, it is possible to predict a number of relations, if we assume that hydrophobic matching is a major determinant of the nearest neighbor interactions. Firstly, if the added anaesthetic is strongly hydrophobic, it seems reasonable to assume that $\omega_{ap} \gg \omega_{fg}$, as the cooperativity parameter, ω_{fg}, is largely determined by the hydrophobic mismatch between a fluid and gel state lipid. Similarly, this should mean that $\omega_{pg} > \omega_{pf}$ for two reasons: (1) the lipid in the gel state would have a larger part of the hydrophobic chains exposed to the water, and (2) the fluid phase is more loosely packed, meaning that defects and spaces between the lipids (*i.e.* pores) would be more likely to appear than in the tightly packed gel phase.

Based on the considerations above, the parameter values used in the simulations were as follows: $\Delta H = 36400$ J/mol, $\Delta S = 115.87$ J/(mol K), $\omega_{fg} = 1326$ J/mol, $\omega_{pf} = 3700$ J/mol, $\omega_{pg} = 6000$ J/mol, $\omega_{pa} = 13\,260$ J/mol, $\omega_{af} = 0.0$ J/mol, and $\omega_{ag} = 1326$ J/mol. The values for ΔH, ΔS and ω_{fg} are identical to those used in ref. 25. As seen in the results section, the average number of pores formed in the BLM experiments is in the range 1–2 in an area of 50 μm^2 corresponding to 10^8 lipid molecules. In our simulations we used a matrix with 10 000 lipids that is 10 000 times smaller than the experimental membrane. Therefore, for the pore formation we opted for a set of pore–lipid interaction parameters which on average generate a similar number of pores as in the experiment requiring smaller pore–lipid interaction parameters as one would expect in a natural membrane. Additionally, it was necessary to disallow direct pore–pore interactions, so as to avoid run-away aggregation of pores and infinite growth of the simulation matrix. The effect on the results should be negligible, as typically the pore density in the simulation was so low as to make pore–pore interactions insignificant. In the experiment collisions of pores are much less likely because of the much larger area, but may occur under stress when the membrane ruptures. The exact appearance of the pores *vs.* temperature profiles will, of course, depend on the choice of parameters. However, for a large range of interaction values, the permeability profile shows a strong peak at the phase transition temperature, and the position of this peak was found to always follow the peak of the heat capacity profile. Typical system sizes were 10^4 particles on a triangular lattice with periodic boundary conditions. The typical simulation was allowed to equilibrate for 2×10^4 to 10^5 Monte Carlo cycles (lattice sweeps) two times, first without pores involved, and then again with pore formation allowed. The actual sampling was then done over another 10^5 to 5×10^5 cycles. Most of the calculated curves presented were in addition averaged over several independent runs.

Our error analysis was performed using the blocking or bunching method described in Flyvbjerg and Petersen.[34] Error bars are not shown for heat capacity and pore numbers. The simulated c_p and pore numbers in Fig. 5, 6 and 8 represent the statistical mean and are not fitted. A detailed analysis can be found in the Masters thesis of A. Blicher.[35]

 This journal is © The Royal Society of Chemistry 2009

Published on 23 July 2009 on http://pubs.rsc.org | doi:10.1039/B909877A
Downloaded by New Copenhagen University on 25 April 2011

Some general consideration about the validity of lattice site simulations. Simulations based on an Ising model are successful for cooperative transitions with correlation length larger than individual lattice sites. Thus, they live on the fact that they don't require molecular detail. Therefore, one might argue that introducing a defect of the size of one lattice site is outside of the scope of such a simulation. This is partially true if one refers to molecular details about pore structure and geometry. It is not true if one attempts to make statements about the likelihood to obtain an area fluctuation of a particular magnitude. A pore in the matrix is most likely not just a hole in the lattice. On the other hand we know that the lipid ion channels display sizes of about one lipid diameter. There is some discussion in the literature about the geometry of such pores. Recent MD simulations suggest that the pore formation process is a formation of some aligned water molecules through the membrane followed by a lipid rearrangement where the lipid head groups point towards the aqueous water pore (*cf.* Fig. 1a and 1b). In our Monte Carlo simulation, the lipid rearrangement would be hidden in the interfacial energy of the hole (*i.e.*, the hole–lipid interaction parameters). The second, important fact is that pore formation occurs by keeping the total area constant. Fluctuations in lipid area of the size of one lipid area, however, are completely within the scope of MC simulations as long as one does not attribute a molecular meaning to the pore geometry.

3 Results

In this paper we investigate pore formation in lipid membranes both experimentally with black lipid membranes (BLM) using the Montal–Mueller technique,[26] and theoretically with Monte Carlo simulations. The goal is to demonstrate that pore formation is related to the heat capacity and the cooperative area fluctuations, respectively, and that anesthetics change the permeability in a coherent manner.

3.1 Black lipid membranes

In the following we show the conduction events through synthetic BLMs. We have chosen to work with lipid mixtures that have their transition events close to room temperature and that display broad heat capacity profiles. The latter makes it easier in experiments to adjust the temperature such that one is very close to the heat capacity maximum.

Fig. 2 shows the current traces for a DOPC:DPPC = 2:1 mixture at 19 °C (150 mM KCl, pH ≈ 6.5) for various transmembrane voltages between −220 mV and +220 mV. The heat capacity profile for this lipid mixture can be found in Fig. 3A (bottom). It displays a c_p-maximum close to 19 °C. In agreement with earlier publications[6,11] (*e.g.*,we find quantized conduction events very similar to those reported for protein ion channels (Fig. 2, bottom) with voltage dependent amplitudes. The amplitudes display a linear dependence on the transmembrane voltage, V_m, between about −150 to +150 mV (Fig. 2, top). At voltages above $|V_m| = 150$ mV, the conductance is found to be higher than expected from the linear relation. The origin of this non-linear current–voltage relationship is not clear but may be related to the influence of voltage on the phase behavior of the lipid membranes. It has been shown by other authors that the position of the melting transition can be influenced by voltage.[36–38] Thus, we suspect that the nonlinear behavior at higher voltages is a consequence of the influence of voltage on the phase transition.

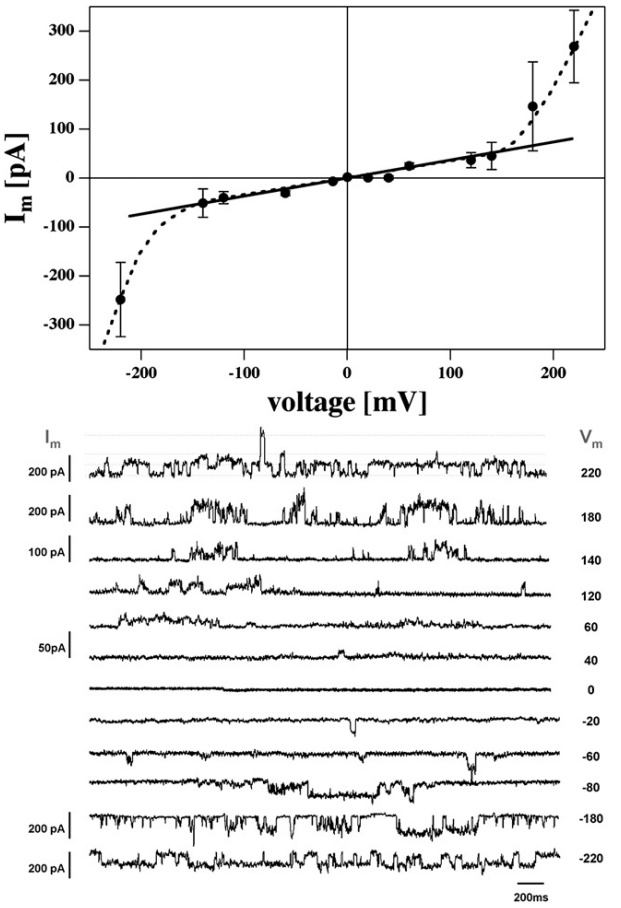

Fig. 2 Bottom: current traces through BLMs of a DOPC:DPPC = 2:1 mixture (150 mM KCl, pH ≈ 6.5 at T = 19 °C) for different voltages. Top: current–voltage relationship for the traces from the bottom panel. One finds a linear current–voltage relationship in the range from −150 mV to +150 mV. At higher voltages the traces become nonlinear. A total of 328 current traces with 30 s each where used for this graph. The current–voltage relationship was adapted from ref. 6.

The effect of anesthetics. Fig. 3 shows the influence of octanol on the permeation of the above membranes measured at 19 °C and 210 mV. The top panels show heat capacity profiles (Fig. 3A), representative current traces (Fig. 3B), current histograms (Fig. 3C) and pore number probability distribution (Fig. 3D) in the presence of 15.9 mol% octanol in the membrane (calculated using an octanol partition coefficient in the membrane of 200).[27] The bottom panels show the respective data in the absence of octanol. One can see that the presence of octanol shifts the calorimetric profiles towards lower temperatures such that one is above the chain melting regime in the presence of octanol and in the transition regime in the absence of octanol. The current traces display smaller current amplitudes and a lower frequency of current events in the presence of octanol. Fig. 3C shows current amplitude histograms obtained

View Online

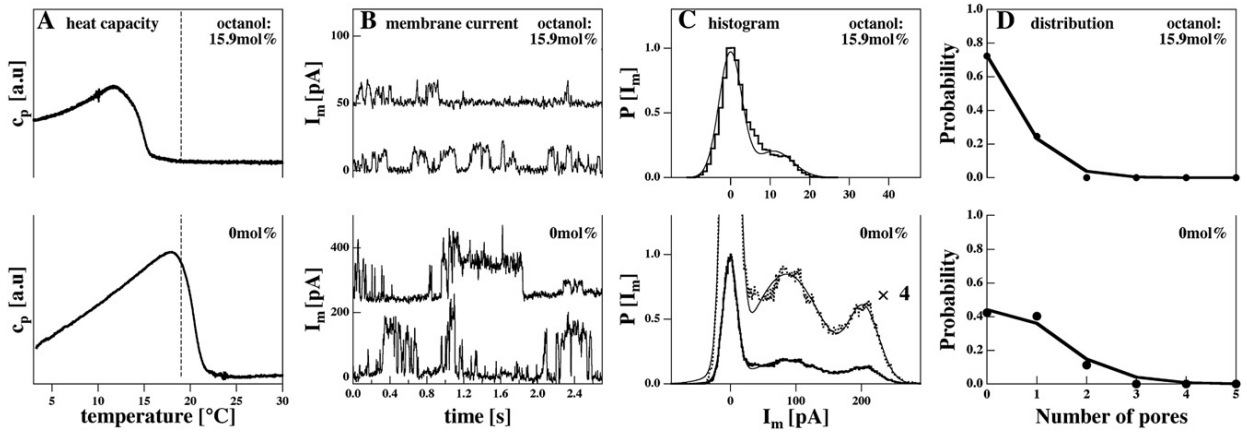

Fig. 3 Experiments on BLMs of a DOPC:DPPC = 2:1 mixture (150 mM KCl, pH ≈ 6.5) in the presence (top) and the absence (bottom) of 15.9 mol% octanol in the membrane. A: Heat capacity profiles. The dashed line indicates experimental temperature. Octanol shifts the calorimetric events towards lower temperatures. In the presence of octanol the experimental temperature above the melting events while it is at the c_p-maximum in the absence of octanol. B: Current traces obtained at T = 19 °C and 210 mV. Two representative traces are given for the two experimental conditions, respectively. Note the different amplitudes of the currents and the altered frequencies of current events. C: Current histograms from the curves in panel B showing one or two current events. D: Analysis of the frequencies of the number of pores. Symbols represent the areas of the peaks in panel C. The solid line represents a best fit to a Poisson distribution.

Downloaded by New Copenhagen University on 25 April 2011
Published on 23 July 2009 on http://pubs.rsc.org | doi:10.1039/B909877A

from the data shown in Fig. 3B. In the absence of octanol one finds at least two current steps corresponding to the two maxima of the histogram that are different from zero. In the presence of 15.9 mol% octanol one finds only one current step with a much lower amplitude. Fig. 3D shows the areas of the current peaks from Fig. 3C (obtained from fitting the peaks with Gaussian profiles). The solid lines are fits to a Poissonian distribution. Such distributions are expected for a low mean number of lipid ion channels.

Fig. 4 shows the corresponding experiments in the presence of ethanol. Ethanol is a very weak anesthetic with a membrane–water partition coefficient of about 0.48[28] (octanol has about 200). Three experiments recorded at V_m = 120 mV are shown, with 0 mol%, 9.5 mol% and 19.5 mol% ethanol in the fluid lipid membrane. Increasing amounts of ethanol shift the melting profile towards lower temperatures. The corresponding current traces show at least two current steps at 39 and 78 pA in the absence of ethanol (note that the voltage is lower than in the octanol experiment in Fig. 3), while there seems to be only one step for 19.5 mol% of around 45 pA. The current histograms suggests that the two current steps seen in the absence of ethanol merge into one in the presence of ethanol. This behavior is different from that of octanol where the overall conductance decreased upon the addition of anesthetics. We did not attempt

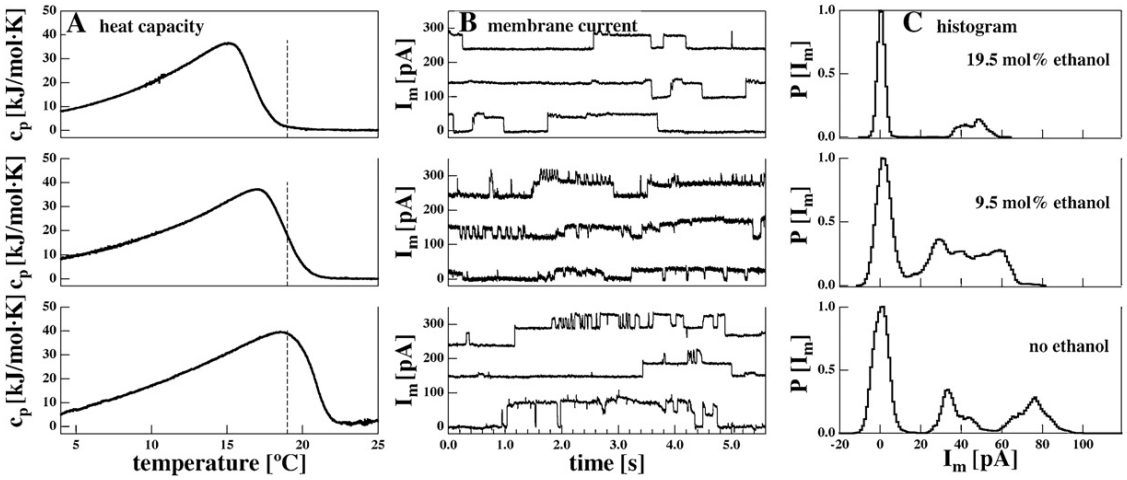

Fig. 4 Experiments on BLMs of a DOPC:DPPC = 2:1 mixture (150 mM KCl, pH ≈ 6.5) in the presence of 19.5 mol% ethanol (top), 9.5 mol% (middle) and no ethanol in the fluid lipid membrane. A: Heat capacity traces. B: Current traces measured at 120 mV. The presence of ethanol seems to generate longer opening times. Three representative traces are given for each experimental condition. C: Histograms of the current events. The behavior is different as in the presence of octanol (Fig. 3). In the absence of ethanol one finds two clearly visible equally spaced current steps of about 39 pA that merges into one peak in the presence of ethanol.

 This journal is © The Royal Society of Chemistry 2009

View Online

Downloaded by New Copenhagen University on 25 April 2011
Published on 23 July 2009 on http://pubs.rsc.org | doi:10.1039/B909877A

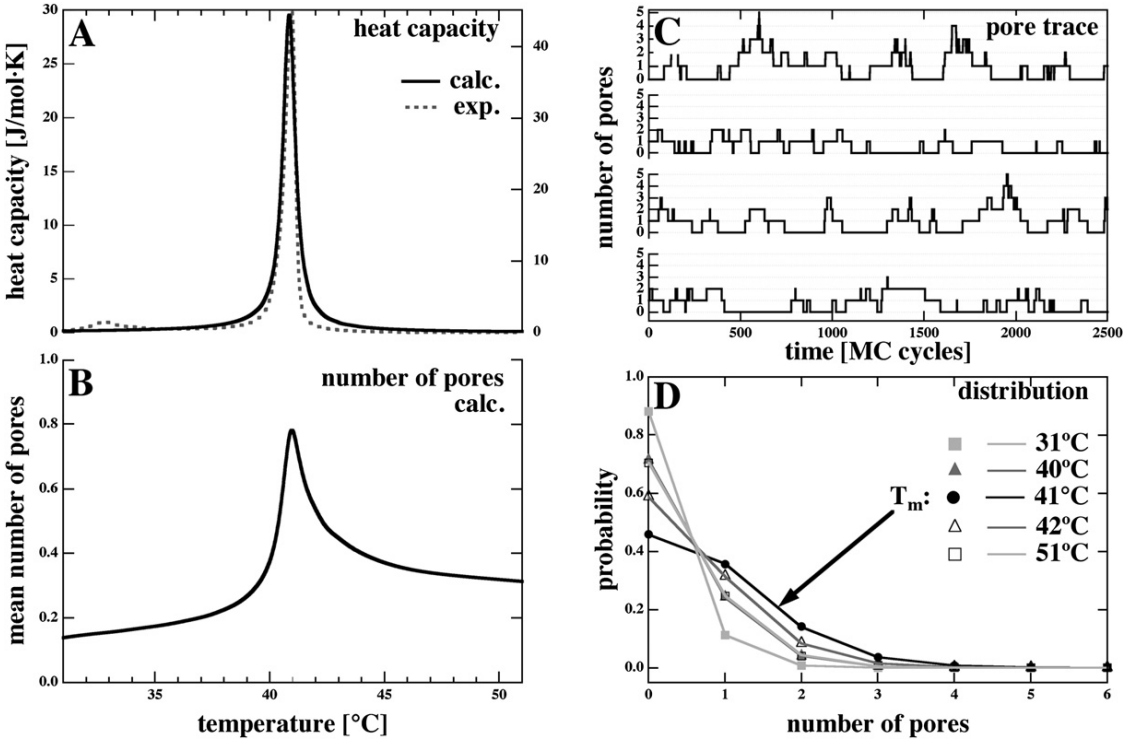

Fig. 5 Monte Carlo simulations of a DPPC membrane. A: calculated heat capacity profile compared to the experimental profile of DPPC large unilamellar vesicles. B: calculated temperature dependence of the membrane permeability (mean number of pores). C: four traces of the number of pores (corresponding to conductance) calculated at the melting temperature, T_m, at 41 °C. D: probability distribution of the number of pores. The symbols originate from the simulation, the solid lines are fits by a Poisson distribution. Simulation parameters are given in the text.

to make a Poisson analysis of the histograms of the ethanol containing membranes since the histograms in the presence of ethanol do not contain evenly spaced conduction levels in the presence of ethanol.

In the discussion section we show that the response of the lipid ion channels to both octanol and ethanol is very similar to that reported for protein ion channels.

3.2 Monte Carlo simulations

In the following we attempt to rationalize the experimental findings obtained from anesthetic-containing membranes by a statistical thermodynamics model that is described in detail in the Materials section. The main postulate in this simulation is to postulate a pore formation process that conserves the overall area of the total membrane. The conservation of area during the pore formation step implies that pores can only form when compressing the area of the lipids. Hence, the pore formation process is linked to the area fluctuations of the lipid matrix. The area fluctuations, however, are proportional to the lateral compressibility. Nagle and Scott[3] argued that the likelihood of finding a pore is proportional to the compressibility. Now it is known that the excess heat capacity of lipid melting is proportional to the compressibility.[9] In section 2.2 we have therefore argued that the likelihood of finding a pore must be intimately related to the heat capacity.[6] Our Monte Carlo model makes use of the considerations of Nagle and Scott.[3]

Fig. 5 shows the results of a simulated DPPC membrane. The simulated heat capacity profiles are compared to an experimental profile of DPPC large unilamellar vesicles in Fig. 5A. The close agreement of the two curves is not accidental but a consequence of using the parameters ΔH, ΔS and the half width of the experimental heat capacity profile. Fig. 5B shows the calculated mean number of pores in the simulation box, which is proportional to the conductance of the membrane. They show that the mean number of simulated pores reaches a maximum close to the transition maximum at 41 °C. This behavior is exactly that found by Blicher *et al.*[6] for dye permeation through large unilamellar vesicle membranes and confirms the concept of Nagle and Scott[3] that makes use of the maximum of the lateral compressibility at T_m. Fig. 5C shows representative traces of the pore number computed at the melting temperature, T_m. These traces strongly resemble those from the BLM experiments (Fig. 2, 3 and 4). Fig. 5D shows the probability distribution of the number of pores for five different temperatures below, at and above the melting temperature. The solid lines in this panel represent Poisson distributions indicating that the calculated behavior matches the experimental one (Fig. 3D, bottom). The Poissonian statistics are expected when pores form independently of each other. The lipid–pore interaction parameters (ω_{pf} and ω_{pg}) are given in the Methods section and have been chosen such that the absolute number of pores is of similar order as in the BLM experiment. Since the simulated matrix has about 10 000 lipids while the black lipid membrane displays a much larger area of about 1.6×10^{10} lipids, the pore–lipid interaction parameters

Downloaded by New Copenhagen University on 25 April 2011
Published on 23 July 2009 on http://pubs.rsc.org | doi:10.1039/B909877A

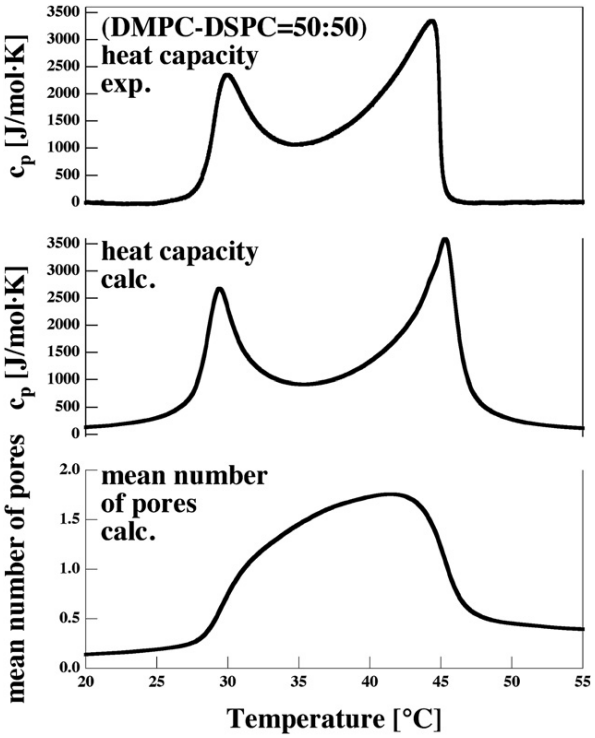

Fig. 6 DMPC–DSPC mixture. Top: experimental heat capacity profile. Middle: calculated heat capacity profile from MC simulation (shown is the statistical mean). Bottom: calculated mean number of pores as a function of temperature. One can recognize that the membrane permeability reaches a maximum in the chain melting regime. Simulation parameters are given in the text.

would have to be about 2–3 times higher if the simulation matrix had the same size as the BLM membrane. With such parameters, however, we would hardly ever see a conduction event in the simulation at a matrix size of 10 000 lipids. Therefore, we have chosen smaller parameters. Qualitatively, however, the behavior of the pore formation rate with a maximum at T_m is maintained when using the smaller model parameters given above.

The above concept also works in mixtures of different lipids with a broad melting peak. Fig. 6 shows the mean number of pores, *i.e.*, the permeation profile, for a DMPC–DSPC = 50:50 lipid mixture. The corresponding experimental and simulated heat capacity profile is shown in the top panels of Fig. 6. The maximum permeability (≡ mean number of pores) is found in the chain melting regime between the two outer c_p maxima.

The effect of anesthetics. The famous Meyer–Overton rule[39] states that the effectiveness of anesthetics is exactly proportional to their solubility in lipid membranes and independent of their chemical nature. Further, anesthetics are known to lower the phase transition temperature of lipid membranes. In a recent paper we have shown that the effect of anesthetics on pure lipid membranes can be well described by the well-known freezing-point depression law $T_m = \frac{RT_m^2}{\Delta H} \cdot x_A$, where x_A is the molar fraction of anesthetics.[18] The derivation of this formula is based on only two assumptions: the anesthetics molecule is ideally soluble in the liquid phase, and that it is insoluble in the solid phase. In our simulation the anesthetics molecules are modeled as resembling lipids that occupy lattice sites. The perfect solubility of anesthetics in the fluid membrane phase can easily be modeled by assuming that the anesthetic–fluid interaction is zero ($\omega_{af} = 0$), while the insolubility in the gel phase means that the anesthetic–gel parameter (ω_{ag}) is very large.

Fig. 7 shows Monte Carlo snapshots for DPPC membranes at seven different temperatures evenly spaced by 2.5 degrees. The three columns are calculated for 0 mol%, 5 mol% and 10 mol% anesthetics, respectively. Here, each anesthetic molecule occupies one lattice site. The melting temperature is again $T_m = 41$ °C. In this figure red and green dots represent gel and fluid lipids, while

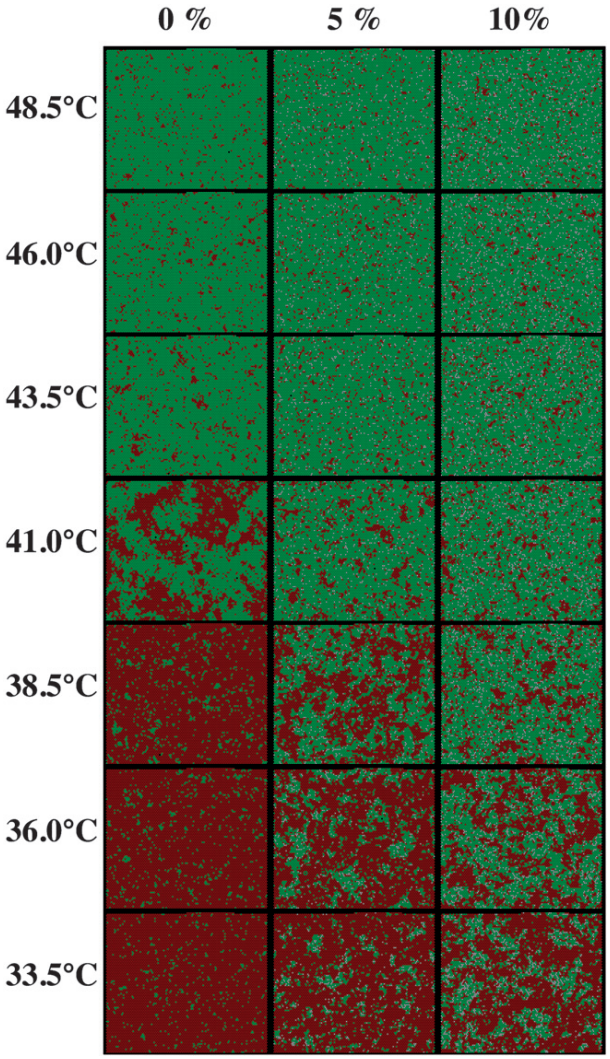

Fig. 7 Simulations of DPPC membranes in the presence of anesthetics as a function of temperature and anesthetics concentration. Left column: Monte Carlo snapshots in the absence of anesthetics. Center column: in the presence of 5 mol% anesthetics. Right column: in the presence of 10 mol% anesthetics. The rows indicate different temperatures between 33.5 °C and 48.5 °C. Gel lipids are given in red, fluid lipids in green, anesthetic molecules in white and pores in black. One can recognize that the presence of anesthetics shifts the melting temperature towards lower temperatures. Simulation parameters are given in the text.

 This journal is © The Royal Society of Chemistry 2009

white dots represent anesthetics molecules and black dots are pores. One can see how the increasing amount of anesthetic lowers the melting events as evident from the lower temperatures where one finds coexistence of red gel domains and green fluid domains. These simulations are further analyzed in Fig. 8. Fig. 8 (top) shows the heat capacity profiles for the simulations in Fig. 7. They are found to be very similar to those found experimentally in the case of DPPC with octanol[18] and show the lowering of the melting temperature in the presence of anesthetics. Note, that the critical anesthetic dose for tadpoles corresponds to 2.6 mol% of anesthetics in the membrane,[18] which is somewhat lower but of same order as the concentrations used in this work. Fig. 8 (middle) shows the corresponding permeation profiles that show a similar shift towards lower temperatures in the presence of anesthetics. Fig. 8 (bottom) shows pore formation traces for three different anesthetics concentrations calculated at 41 °C. These traces correspond to the experimental situation in Fig. 3. The mean number of pores is reduced. Since Monte Carlo simulations are based on equilibrium thermodynamics the time scales of these traces do not correspond to a real time scale. This means that one cannot conclude from the simulation that the mean life time of the pore openings in the presence of anesthetics is longer as in the absence of anesthetics even though the traces seem to suggest that. This is an intrinsic feature of equilibrium statistical thermodynamics simulations that do not contain intrinsic time scales. However, the very procedure assumed for the pore generation process implies that the pore generation process must have a characteristic time scale that is related to the fluctuation life time of the lipid membrane. We have recently shown this to be the case for the pore formation process.[7]

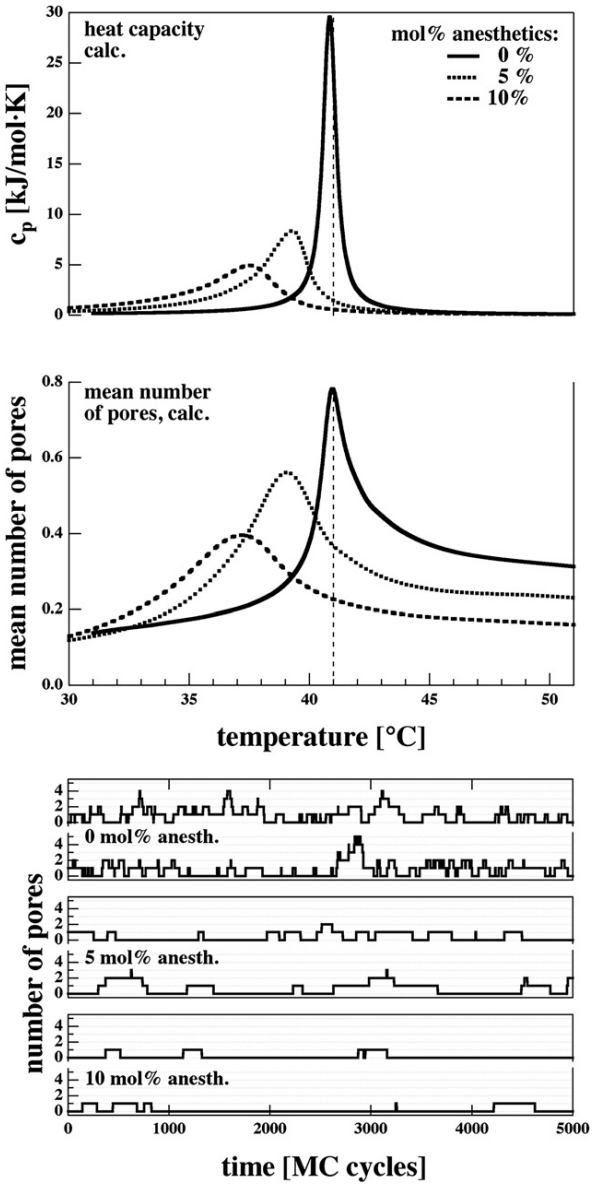

Fig. 8 Monte Carlo Simulation of DPPC membranes in the presence of 0 mol%, 5 mol% and 10 mol% of anesthetics in the membrane. Top: calculated heat capacity profiles show the shift of the melting events towards lower temperatures in agreement with the snapshots in Fig. 7. Middle: the calculated number of pores (corresponding to a permeability) follows the heat capacity profiles. The maximum permeability shifts towards lower temperatures upon addition of anesthetics. Bottom: calculated traces of the number of pores indicate that the number of pore opening events decreases in the presence of anesthetics. Two traces for each anesthetic concentration are given. Simulation parameters are given in the text.

4 Discussion

In this paper we investigate the lipid ion channel formation in pure lipid membranes in the absence and the presence of anesthetics. The goal was to demonstrate the origin of the pore formation from the cooperative area fluctuations. We studied pore formation both experimentally by the Montal–Mueller[26] black lipid membrane technique, and by Monte Carlo simulations. We show that pure lipid membranes in the absence of proteins display conduction events that resemble those seen in the presence of protein ion channels. For this reason we call them lipid ion channels. Such events have been shown before by a number of authors.[6,10–15,40–44] Although there are obviously many reports about such events it is surprising that such behavior is not better known. While the pores in lipid membranes are shown to exist in the absence of proteins, the conduction of ions through proteins cannot be measured in the absence of lipid membranes. Since the events are so similar to the protein ion channel recordings one requires an unambiguous criterion for how to distinguish the events originating from proteins and lipid membranes. To our knowledge, no such criterion exists. Possibly, site-specific mutations of proteins related to changes in channel activity can be considered as an indirect criterion, but this may not be satisfactory because this only demonstrates that the proteins are somewhat involved in the conduction process (*cf.* last paragraph of discussion).

The importance of phase transitions in lipid membranes for the permeability has been pointed out before.[2–4,6,8,11] The cooperative fluctuation in area renders the pore formation more likely because the lateral compressibility is higher. This effect resembles the phenomenon of critical opalescence described by Einstein.[29] He calculated the work to move one molecule from one part of the volume to another in order to obtain the density fluctuations.

Published on 23 July 2009 on http://pubs.rsc.org | doi:10.1039/B909877A
Downloaded by New Copenhagen University on 25 April 2011

View Online

Downloaded by New Copenhagen University on 25 April 2011
Published on 23 July 2009 on http://pubs.rsc.org | doi:10.1039/B909877A

In a similar manner, the increased fluctuations in the membrane render it easier to move lipids such that pores can be created. In the present paper we used this concept to describe the pore formation process by a simple statistical thermodynamics model in which lipids are moved while simultaneously reducing the area of the surrounding lipids. One could also imagine fluctuations on larger length scales leading to the formation of pores of the size of one lipid, *e.g.* by switching 50 fluid and 50 gel lipids into 47 fluid and 53 gel lipids plus one pore. Thus, it may be sufficient to switch three fluid lipids somewhere in the matrix in order to create a hole. On the other hand, both Papahadjopoulos *et al.*[2] and Corvera *et al.*[4] suggested that the pore formation process takes place at domain interfaces which are the regions of largest fluctuation. This is consistent with the finding that the conductance is maximum within the transition range. This is the view we have taken.

Since the change of the intensive thermodynamic variables (*e.g.*, pressure, lateral pressure, chemical potentials of protons, of calcium or of anesthetic drugs) influences the melting behavior of membranes and thus the fluctuations in the membrane, it is straight forward to explore how changes in these variables influence permeability. For instance, it has been shown that voltage influences the phase transition temperature.[37,38] As evident in our measurements, the mean conductance through pores in lipid mixtures is linear in the range between about −150 to +150 mV. For $|V_m| > 150$ mV the current–voltage relation becomes non-linear indicating that high voltage influences the state of the membrane and induces more conduction events. It has further been shown that changes in calcium concentration[41,14] and pH changes[12,13] influence the occurrence of lipid ion channels. Here, we have used the chemical potential of anesthetics in the membrane as a variable. Our present work is a continuation of a recent publication from our group[6] that shows how anesthetics influence the permeation process by influencing the melting process. Here, we have demonstrated this for the case of octanol and ethanol, which both shift transitions to a similar degree when the membrane concentration of the drug is the same. Both drugs lead to a reduction of the overall conductance, but the modes of interaction seem different. A paper by Ly and Longo[45] described the interaction of short chain alcohols (methanol to butanol) on lipid membrane surface tension. The authors concluded that those alcohols are surface active. Thus, the mode of ethanol interaction with membranes may contain other contributions as compared to octanol. The difference of the ethanol influence is visible in the fact that the overall conductance does not change in the same manner as in the presence of octanol. Instead, two conduction steps merge into one. Thus, we focused in our simulations on octanol which displays a very straight-forward mode of action, namely freezing point depression.

Our simulations describe the main feature found in experiments: the relation of the permeability and the heat capacity leading to maximum permeability at the heat capacity maximum. This confirms the main assumption of our study, which is that the cooperative area fluctuations are responsible for the occurrence of the lipid ion channels. It further describes quantitatively the effect of anesthetics on the heat capacity of the membrane. Anesthetics following the Meyer–Overton correlation also generate freezing-point depression (*cf.* ref. 18). The simulation accurately describes this and therefore also describes the influence of anesthetics on the permeation. However, our pore formation model made the simplifying assumption that a pore has the size of one lipid. This is a reasonable approximation since we found in a recent paper that the conductance through the membrane is well described by assuming an aqueous pore of a diameter of 0.7 nm, which is of same order than that of one lipid site. The measurements in the presence of anesthetics show, however, that the pore size itself can vary and that it is different in the presence and absence of octanol and ethanol. This effect is not contained in our simulations. The pore diameter scales with the square root of the current. In the case of octanol the conductance in the presence of 15.9% octanol is about 7 times smaller than in the absence of octanol. This suggests a pore diameter that is about 2.6 times smaller as the pores in pure membranes. However, such calculations should be taken with care as they assume that the pore interior is filled with free water with a viscosity unaffected by the pore interface, which we consider to be unlikely, both for lipid ion channels as for protein channels. If water ordering at the pore interface is taken into account, the real pore radius may be larger, and the difference in the channel conductances may not be proportional to the pore area since interfacial effects will be larger for smaller pores.

The present Monte Carlo simulation is a coarse grain statistical thermodynamics model. Such models have successfully been used to describe cooperative phenomena in membranes.[19–24] Typically, the number of states for each lipid is reduced to two (Ising model) or 10 (Pink model). Naturally, this is only a very approximate description on the molecular scale. The reason why the lattice models work so nicely is that they are designed to describe cooperative behavior of many molecules—in our case the formation of domains and the cooperative fluctuations. Microscopic details of single lipids and pores described here by lattice sites are not expected to be accurate—and also to be of small relevance. As mentioned above, our simulation is designed such that a pore has always the size of one lattice site. The experiment on octanol shows that the pores in the presence of anesthetics are smaller as in the absence (currents at identical voltage are $\approx$ 90 pA in the absence of octanol and only about $\approx$ 15 pA in the presence of 15.9 mol% octanol). Qualitatively, however, the simulation describes the likelihood of pore formation and thereby permeation quite well. In a recent paper we have shown that the permeation of fluorescence dyes through lipid vesicles is within experimental accuracy proportional to the heat capacity.[6] This paper also shows the quantized conduction events in BLMs that could be abolished by addition of octanol. Our simulation reproduces this close relation between heat capacity and conductance—and is consistent with the quantized nature of the conduction process.

It is likely that many other variable changes would influence the occurrence of lipid ion channels, *e.g.*, proteins that associate or insert into membranes but are not pores in themselves. It is known that the band 3 protein of erythrocytes increases the melting temperature of model membranes.[46] Cytochrome b_5, on the other hand lowers transitions.[47] Cytochrome c binds peripherally and increases the transition temperature.[22] Depending on whether the experimental temperature is found below or above the melting temperature, one would expect that the respective proteins can either increase or lower the likelihood

 This journal is © The Royal Society of Chemistry 2009

View Online

of lipid ion channel formation even if the proteins are not known to form ion channels.

The mechanism of anesthesia has been under much debate and is unexplained until today. Until the mid 1970's lipid models were most popular because they can be easily related to the famous Meyer–Overton rule[39] that states that the effectiveness of anesthetics and their partition coefficient are linearly related, independent of the chemical nature of the anesthetic molecules. Ever since the development of the patch clamp methods and the study of protein ion channel events, a lot of attention has been on the binding of anesthetics to receptors. This is due to the finding that ion channel events that have been attributed to proteins are influenced by anesthetics. Unfortunately, such interaction with proteins is not generally in agreement with the Meyer–Overton correlation. The fact that the noble gas xenon acts as an anesthetic is inconsistent with specific binding to a protein. We have shown here and in ref. 6 that the finding of quantized events does not prove the action of a protein. Further, the influence of anesthetics on the conduction events does not prove a specific binding of the anesthetic drug to a receptor. We have shown here that octanol and ethanol influence the channel events even in the complete absence of proteins.

In this context it is tempting to compare the effect of alkanols on protein ion channels with our findings. The influence of octanol on current fluctuations of lipid ion channels can be compared with those of neuronal nicotinic acetylcholine receptor (AChR, see, *e.g.*, ref. 48), which has been used for many years as a model to study the influence of alcohols.[49–55] It has been shown that neuronal activity of nicotinic acetylcholine receptor (AChR) induced channels under the influence of octanol is markedly inhibited,[48] which was observed as a decrease in current fluctuation amplitude from those channels. Ethanol, on the other hand was found not to be neutral for many protein ligand-gated ion channels such as *N*-methyl-D-aspartate (NMDA), serotonin (5-HT(3)), glycine and GABA receptors.[56,57] The inhibitory action of ethanol was also observed in voltage-gated Ca^{2+} channels[58] and very recently also in potassium channels, which were seen as very important targets of ethanol.[59] Similar findings were reported for experiments with AChR channels subjected to 100 mM of ethanol.[60] The above reports demonstrate that the effect of octanol and ethanol on membrane protein receptors is quite similar to that found by us for the effect of these alcohols on lipid ion channels. In this context it is also interesting to note that protein ion channels have been shown to respond to the phase behavior of lipids[61] or to different lipid environments.[62]

Summarizing, one has to conclude that many channel events that have been attributed to particular specific proteins may well originate from membrane fluctuations. The voltage-clamp experiment in itself can not distinguish proteins from lipid events. If the observed currents in fact originated from the lipid membrane, the dependence of the open-probabilities of channels on the various intensive variables as pressure (mechano-sensitive channels), temperature (temperature sensors) and drugs and ions (channel gating) would immediately find an explanation in the well-understood thermodynamics of cooperative membrane events.

References

1 L. Hodgkin and A. F. Huxley, *J. Physiol.*, 1952, **117**, 500–544.
2 D. Papahadjopoulos, K. Jacobson, S. Nir and T. Isac, *Biochim. Biophys. Acta*, 1973, **311**, 330–340.
3 J. F. Nagle and H. L. Scott, *Biochim. Biophys. Acta*, 1978, **513**, 236–243.
4 E. Corvera, O. G. Mouritsen, M. A. Singer and M. Zuckermann, *Biochim. Biophys. Acta*, 1992, **1107**, 261–270.
5 T. Heimburg and A. D. Jackson, *Proc. Natl. Acad. Sci. USA*, 2005, **102**, 9790–9795.
6 A. Blicher, K. Wodzinska, M. Fidorra, M. Winterhalter and T. Heimburg, *Biophys. J.*, 2009, **96**, 4581–4591.
7 B. Wunderlich, C. Leirer, A. Idzko, U. F. Keyser, V. Myles, T. Heimburg and M. Schneider, *Biophys. J.*, 2009, **96**, 4592–4597.
8 L. Cruzeiro-Hansson and O. G. Mouritsen, *Biochim. Biophys. Acta*, 1988, **944**, 63–72.
9 T. Heimburg, *Biochim. Biophys. Acta*, 1998, **1415**, 147–162.
10 M. Yafuso, S. J. Kennedy and A. R. Freeman, *J. Membr. Biol.*, 1974, **17**, 201–212.
11 V. F. Antonov, V. V. Petrov, A. A. Molnar, D. A. Predvoditelev and A. S. Ivanov, *Nature*, 1980, **283**, 585–586.
12 K. Kaufmann and I. Silman, *Naturwissenschaften*, 1983, **70**, 147–149.
13 K. Kaufmann and I. Silman, *Biophys. Chem.*, 1983, **18**, 89–99.
14 V. F. Antonov, E. V. Shevchenko, E. T. Kozhomkulov, A. A. Molnar and E. Y. Smirnova, *Biochem. Biophys. Research Commun.*, 1985, **133**, 1098–1103.
15 V. F. Antonov, A. A. Anosov, V. P. Norik and E. Y. Smirnova, *Eur. Biophys. J.*, 2005, **34**, 155–162.
16 B. Hille, *Ionic channels of excitable membranes*, Cambridge University Press, Cambridge, 1992.
17 R. Böckmann, R. de Groot, S. Kakorin, E. Neumann and H. Grubmüller, *Biophys. J.*, 2008, **95**, 1837–1850.
18 T. Heimburg and A. D. Jackson, *Biophys. J.*, 2007, **92**, 3159–3165.
19 S. Doniach, *J. Chem. Phys.*, 1978, **68**, 4912–4916.
20 O. G. Mouritsen, A. Boothroyd, R. Harris, N. Jan, T. Lookman, L. MacDonald, D. A. Pink and M. J. Zuckermann, *J. Chem. Phys.*, 1983, **79**, 2027–2041.
21 P. Sugar, R. L. Biltonen and N. Mitchard, *Methods Enzymol.*, 1994, **240**, 569–593.
22 T. Heimburg and R. L. Biltonen, *Biophys. J.*, 1996, **70**, 84–96.
23 P. Sugar, T. E. Thompson and R. L. Biltonen, *Biophys. J.*, 1999, **76**, 2099–2110.
24 V. P. Ivanova and T. Heimburg, *Phys. Rev. E*, 2001, **63**, 1914–1925.
25 V. P. Ivanova, I. M. Makarov, T. E. Schäffer and T. Heimburg, *Biophys. J.*, 2003, **84**, 2427–2439.
26 M. Montal and P. Mueller, *Proc. Natl. Acad. Sci. USA*, 1972, **69**(12), 3561–3566.
27 M. K. Jain and J. L. V. Wray, *Biochem. Pharmacol.*, 1978, **275**, 1294–1295.
28 L. L. Firestone, J. C. Miller, and K. W. Miller. In ed. S. H. Roth and K. W. Miller, *Molecular and cellular mechanism of anesthetics*, pp. 455–470. Plenum Press, 1986.
29 A. Einstein, *Ann. Phys. (Leipzig)*, 1910, **33**, 1275–1298.
30 R. W. Glaser, S. L. Leikin, L. V. Chernomordik, V. F. Pastushenko and A. I. Sokirko, *Biochim. Biophys. Acta*, 1988, **940**, 275–287.
31 A. Hac, H. Seeger, M. Fidorra and T. Heimburg, *Biophys. J.*, 2005, **88**, 317–333.
32 H. Seeger, M. Fidorra and T. Heimburg, *Macromol. Symposia*, 2005, **219**, 85–96.
33 R. J. Glauber, *J. Math. Phys.*, 1963, **2**, 294–307.
34 H. Flyvbjerg and H. G. Petersen, *J. Chem. Phys.*, 1989, **91**, 461–466.
35 A. Blicher, *Permeability studies of lipid vesicles by fluorescence correlation spectroscopy and monte carlo simulations Master's thesis*, University of Copenhagen. http://membranes.nbi.dk/thesis-pdf/2007_Masters_A.Blicher.pdf, 2007.
36 W. M. Heckl, A. Miller and H. Möhwald, *Thin Solid Films*, 1988, **159**, 125–132.
37 V. F. Antonov, E. Y. Smirnova and E. V. Shevchenko, *Chem. Phys. Lipids*, 1990, **52**, 251–257.
38 Y. C. Lee and H. M. McConnell, *Biophys. J.*, 1995, **68**, 1740–1751.
39 E. Overton, *Studien über die Narkose*, Verlag Gustav Fischer., 1901. Jena, Germany. English translation: Studies of Narcosis, Chapman and Hall, 1991, R. Lipnick, Ed.
40 G. Boheim, W. Hanke and H. Eibl, *Proc. Natl. Acad. Sci. USA*, 1980, **77**, 3403–3407.
41 H. Gögelein and H. Koepsell, *Pflügers Arch.*, 1984, **401**, 433–434.
42 K. Yoshikawa, T. Fujimoto, T. Shimooka, H. Terada, N. Kumazawa and T. Ishii, *Biophys. Chem.*, 1988, **29**, 293–299.

Published on 23 July 2009 on http://pubs.rsc.org | doi:10.1039/B909877A
Downloaded by New Copenhagen University on 25 April 2011

View Online

43 K. Kaufmann, W. Hanke, A. Corcia *Ion channels*; (http://membranes.nbi.dk/Kaufmann/pdf/Kaufmann book3 ed.pdf), 1989, Caruaru.
44 D. J. Woodbury, *J. Membr. Biol.*, 1989, **109**, 145–150.
45 H. V. Ly and M. L. Longo, *Biophys. J.*, 2004, **87**, 1013–1033.
46 M. R. Morrow, J. H. Davis, F. J. Sharom and M. P. Lamb, *Biochim. Biophys. Acta*, 1986, **858**, 13–20.
47 E. Freire, T. Markello, C. Rigell and P. W. Holloway, *Biochemistry*, 1983, **28**, 5634–5643.
48 Y. Zuo, J. Z. Yeh and T. Narahashi, *Alcoholism Clin. Exp. Res.*, 2004, **28**, 1648–1656.
49 R. J. Bradley, K. Peper and R. Sterz, *Nature*, 1980, **284**, 60–62.
50 R. J. Bradley, R. Sterz and K. Peper, *Brain Res.*, 1984, **295**, 101–112.
51 S. A. Forman, K. W. Miller and G. Yellen, *Mol. Pharmacol.*, 1995, **48**, 574–581.
52 S. A. Forman, *Biophys. J.*, 1997, **72**, 2170–2179.
53 S. A. Forman and Q. Zhou, *Mol. Pharmacol.*, 1999, **55**, 102–108.
54 S. C. Wood, S. A. Forman and K. W. Miller, *Mol. Pharmacol.*, 1991, **39**, 332–338.
55 G. Wu, P. H. Tonner and K. W. Miller, *Mol. Pharmacol.*, 1994, **45**, 102–108.
56 R. A. Harris, W. R. Proctor, S. J. McQuilkin, R. L. Klein, M. P. Mascia, V. Whatley, P. J. Whiting and T. V. Dunwiddie, *Alcoholism Clin. Exp. Res.*, 1995, **19**, 226–232.
57 R. A. Harris, *Alcoholism Clin. Exp. Res.*, 1999, **23**, 1563–1570.
58 D. Mullikin-Kilpatrick and S. N. Treistman, *Eur. J. Pharmacol.*, 1994, **270**, 17–25.
59 M. S. Brodie, A. Scholz, T. M. Weiger and A. M. Dopico, *Alcoholism Clin. Exp. Res.*, 2007, **31**, 1625–1632.
60 Y. Zuo, K. Nagata, J. Z. Yeh and T. Narahashi, *Alcoholism Clin. Exp. Res.*, 2004, **28**, 688–696.
61 B. Cannon, M. Hermansson, S. Györke, P. Somerharju and J. A. Virtanen, *Biophys. J.*, 2003, **85**, 933–942.
62 D. Schmidt, Q.-X. Jiang and R. MacKinnon, *Nature*, 2006, **444**(7120), 775–779.

Published on 23 July 2009 on http://pubs.rsc.org | doi:10.1039/B909877A
Downloaded by New Copenhagen University on 25 April 2011

 This journal is © The Royal Society of Chemistry 2009